STRONG MICROWAVES IN PLASMAS

1993

Volume 2

Institute of Applied Physics
Nizhny Novgorod

RUSSIAN ACADEMY OF SCIENCES
INSTITUTE OF APPLIED PHYSICS

STRONG MICROWAVES IN PLASMAS

PROCEEDINGS
OF THE INTERNATIONAL WORKSHOP
Moscow – Nizhny Novgorod – Moscow,
15 – 22 August 1993

Edited by
A.G. Litvak

In two volumes
Volume 2

Nizhny Novgorod – 1994

Printed in Russia,
Publishing-house «Chuvashia»
Ivan Jakovlev avenue, 13, 428019 Cheboksary

ISBN 5-201-09298-5

NONLINEAR PROCESSES IN PLASMAS (THEORY AND MICROWAVE EXPERIMENT)

PHASE CONJUGATION IN PLASMA BY FOUR WAVE MIXING

Y. Ben-Aryeh
Technion-Israel Institute of Technology, Haifa, Israel

1 Introduction

Four-wave mixing (FWM) and phase conjugation (PC) in plasmas, using the pondermotive force and other nonlinearities, have been extensively studied[1]. Phase conjugation is a process by which we get an exact inversion of the propagation vector $\vec{k}$ and of the phase ϕ for any plane electromagnetic (em) wave. A reflected beam from a phase conjugating medium is tracing back the original beam, so that the process of PC can be considered as "inversion in time" of the original beam.[2]

There are many non-linear optical processes which can be used to generate PC including especially stimulated Brillouin scattering (SBS) and stimulated Raman Scattering (SRS). SBS is produced by Bragg scattering of an em wave from the grating of ion densities produced by an acoustic wave[3]. The possibility of getting PC by exposing the plasma to more than one wave has been studied in various works[4,5]. Especially interesting is the possibility of generating PC reflections in plasma by Brillouin enhanced FWM. In this case two contra-directional strong pump waves are propagating in the plasma. A small signal em beam is incident upon the plasma with its frequency slightly shifted relative to a pump wave, so that the frequency difference is tuned to match a Brillouin resonance (i.e. ion acoustic wave)[6,7]. For SRS a similar process occurs with plasma waves taking the role of acoustic waves[8]. The scattering of the sec-

ond pump from the excited plasma generates, via phase matching conditions, em wave conjugate to the signal.

Plasmas are efficient FWM and PC media, especially at long wavelengths (far infrared), where they have large non-linearities compared to other materials. PC can be used for many applications (e.g. dispersion compensation, plasma diagnostics, etc.)

The present article on FWM in plasmas is developed by studying the effects of the pondermotive driving force, enhanced by Brillouin scattering, for a quasi-neutral plasma in which the Debye length λ_D is much smaller than the laser wavelength λ. The present theory gives results which are in agreement with recent experiments on PC of microwaves in unmagnetized hydrogen plasma[9]. It is also in agreement with theories based on the use of Vlasov equations [10], but it gives another physical insight to the problem and for certain cases it gives more general results.

2 Theory

For simplicity, the em fields in FWM are taken as plane waves with the same polarization

$$E_j = \frac{1}{2}\left[\sum_{j=1}^{4} A_j(r)\exp(-i\omega_j t + i\vec{k}_j\cdot\vec{r}) + c.c.\right] \quad , \qquad (1)$$

where $\hat{k}_1 = -\hat{k}_2$, $\hat{k}_3 = -\hat{k}_4$ and $c.c.$ denotes complex conjugation. Also it is assumed that the amplitudes $A(r)$ are time independent, the two strong pump waves A_1 and A_2 are undepleted, and the four frequencies ω_j have small detunings:

$$\omega_1 = \omega - \Delta\omega'; \quad \omega_2 = \omega + \Delta\omega'; \quad \omega_3 = \omega - \Delta\omega''; \quad \omega_4 = \omega + \Delta\omega'' \quad (2)$$

The present theory is developed under the general conditions of Eq. (2) but later the analysis is specialized to the case $\Delta\omega' = 0$ (i.e. the two pump waves have the same frequency)[11].

For simplicity of discussion a homogeneous fully ionized plasma is assumed. Conventional notation is used: an ion charge is denoted

by Z, ion and electron densities are denoted, respectively, by $n_i = n_0$, $n_e = Zn_0$ and temperatures by T_i and T_e . m and M are the masses of the electron and ion, respectively, and S is the velocity of sound.

The time dependent momentum equation is given by [12,13]

$$(M + Zm)\left[n\frac{\partial \vec{v}}{\partial t} + n(\vec{v}\cdot\vec{\nabla})\vec{v}\right] = -\vec{\nabla}(p_i + p_e) - n\beta\vec{\nabla}\langle|E|^2\rangle \qquad (3)$$

where n is the ion perturbed density, p_i and p_e are the ion and electron pressures, respectively and

$$\beta = \frac{Ze^2}{4m\omega^2} \qquad (4)$$

is the pondermotive constant[12].

Here $\langle\ \rangle$ denotes the time average on time scale of $\frac{1}{\omega}$ so that the pondermotive force which represented by the last term of Eq. (3) remains time dependent on time scales of $\frac{1}{\Delta\omega'}$ and $\frac{1}{\Delta\omega''}$.

The continuity equation is also time dependent

$$\frac{\partial n}{\partial t} + \vec{\nabla}\cdot(n\vec{v}) = 0 \qquad (5)$$

By neglecting terms that are of second or higher order in Δn and $\vec{v}$, Eqs. (3) and (5) can be written as:

$$n_0\frac{\partial \vec{v}}{\partial t} + S^2\vec{\nabla}n = -n_0\beta_0\vec{\nabla}\langle|E|^2\rangle \qquad (6)$$

where $\beta_0 \simeq \frac{\beta}{M}$,

$$\frac{\partial n}{\partial t} + n_0\vec{\nabla}\cdot\vec{v} = 0\ . \qquad (7)$$

In deriving Eq. (6) from Eq. (3) the relation [12,13]

$$\frac{\vec{\nabla}(p_i + p_e)}{M + Zm} \simeq S^2\vec{\nabla}n \qquad (8)$$

is used, where S is the speed of sound. By differentiating Eq. (7) with respect to time and performing the $\vec{\nabla}$ operation on Eq. (6) an ion density wave equation can be obtained

$$\frac{\partial^2 n}{\partial t^2} - S^2 \nabla^2 n = -n_0 \beta_0 \nabla^2 \langle |E|^2 \rangle \ . \tag{9}$$

Substitution of Eq. (1) into the expression for the pondermotive force gives under the approximations of strong undepleted pump waves [14]

$$n_0 \beta_0 \nabla^2 \langle |E|^2 \rangle = -n_0 \beta_0 \left\{ \sum_{j=1}^{4} q_j^2 F_j \exp(-i\Omega_j t + i\vec{q}_j \cdot \vec{r}) + c.c. \right\} \tag{10}$$

$$\vec{q}_1 = \vec{k}_4 - \vec{k}_1 \ ; \ \vec{q}_2 = 2\vec{k}_1; \ \vec{q}_3 = 2\vec{k}_4; \ \vec{q}_4 = \vec{k}_1 - \vec{k}_3 \tag{11}$$

$$\Omega_1 = \Delta\omega' + \Delta\omega"; \ \Omega_2 = -2\Delta\omega'; \ \Omega_3 = -2\Delta\omega"; \ \Omega_4 = \Delta\omega'' - \Delta\omega', \tag{12}$$

$$F_1 = A_1^* A_4 + A_2 A_3^*; \ F_2 = A_1 A_2^*; \ F_3 = A_3^* A_4; \ F_4 = A_1 A_3^* + A_2^* A_4 \ . \tag{13}$$

One should take into account that the acoustic waves have large wavevectors but small frequencies (since $S << c$). In using the phase matching conditions small shifts $\Delta\vec{k}$ in the wavevectors are neglected in the present analysis since they can be compensated by slight charges in the directions of the wavevectors $\vec{k}_j (\Delta\vec{k} << \vec{k}_j)$. This has been explained in a previous work [14] by comparing the enhancement of PC in degenerate FWM in a flowing plasma with that of nondegenerate FWM in the plasma frame of reference.

The phase matching conditions can be used to present the solution of Eq. (9) as [14]:

$$n = n_0 + \Delta n = n_0 + \left[\sum_{j=1}^{4} n_{j0} \exp(-i\Omega_j t + i\vec{q}_j \cdot \vec{r}) + c.c. \right] \tag{14}$$

By the use of Eq. (14) and by the inclusion of damping mechanism $\left[\Omega_j \rightarrow \Omega_j(1-\frac{i\Gamma}{2})\right]$ Eq. (9) can be rewriteen as:

$$\left[\Omega_j(\Omega_j - i\Gamma) - S^2 q_j^2\right] n_{j0} = \beta_0 n_0 q_j^2 F_j \; ; \quad (\Gamma << |\Omega|)$$

$$n_{j0} = -\frac{n_0 \beta_j}{S^2} F_j \; ; \quad \beta_j = \frac{\beta_0}{1 - M_j^2 + i(M_j \Gamma / q_j S)} \; ;$$

$$M_j = \frac{\Omega_j}{q_j S} \tag{15}$$

Resonances with acoustic waves are obtained under the conditions $\Omega_j \simeq q_j S$.

The em wave equation may be written as

$$\nabla^2 E - \frac{\eta^2}{c^2}\frac{\partial^2 E}{\partial t^2} = 0 \; ; \quad \eta^2 = \eta_0^2 - \frac{\Delta n}{n_c} \; ; \quad n_c = \frac{\epsilon_0 m \omega^2}{e^2} \tag{16}$$

where η_0 and η are the zeroth order and the perturbed index of refraction, respectively.

In order to simplify the above equations additional approximations can be made which usually correspond to the conditions under which experiments are made: a) $\Delta\omega' = 0$ (the two pump waves have the same frequency) so that $\Omega_1 = \Omega_4 = -(\frac{1}{2})\Omega_3, \Omega_2 = 0$. b) A resonance is assumed under the condition $\Omega_4 = \Delta\omega'' = q_4 S = |\vec{k}_1 - \vec{k}_3| S$. $\vec{k}_1 - \vec{k}_3$ is the wave vector of the acoustic wave produced by the pump A_1 and the signal A_3 and $\Delta\omega''$ is the frequency of the acoustic wave which for resonance is equal to the frequency shift of the signal relative to the pump. Under this resonance condition

$$\beta_4 = \beta_0 \left(\frac{-iq_4 S}{\Gamma}\right) \tag{17}$$

while $\beta_2 = 0, \; \beta_1 \simeq 0, \; \beta_3 \simeq 0$.

c) the two strong undepleted em waves have constant intensities:

$$A_1^* A_1 = I_1 \; ; \quad A_2^* A_2 = I_2 \; . \tag{18}$$

Substituting Eq.(1) into Eq. (16), using the slowly varying approximation and the phase matching conditions, and by taking into account only the terms that are first on zeroth order in the relatively weak fields A_3 and A_4, we get [14]:

$$\frac{\partial A_3}{\partial \xi_3} = i\gamma\beta_4^* \left[A_1^* A_1 A_3 + A_1 A_2 A_4^*\right],$$
$$\frac{\partial A_4}{\partial \xi_4} = i\gamma\beta_4 \left[A_2^* A_2 A_4 + A_1 A_2 A_3^*\right], \qquad (19)$$

where $\gamma = (kn_0/2\eta_0 n_c S^2)$ and ξ_j is an axis parallel to $\vec{k}_j$.

Substituting

$$A_3 = \tilde{A}_3 \exp\left[i\gamma\beta_4^* A_1^* A_1 \xi_3\right]; \quad A_4 = \tilde{A}_4 \exp\left[i\gamma\beta_4 A_2^* A_2 \xi_4\right]; \qquad (20)$$

and assuming that the two pump waves have equal intensity ($I_1 = I_2 = I$) Eqs. (19) become similar to those derived by other authors [6-7,15-17]:

$$\frac{d\tilde{A}_3}{d\xi_3} = i\kappa' \tilde{A}_4^*; \quad \frac{d\tilde{A}_4}{d\xi_3} = -i\kappa \tilde{A}_3^* \qquad (21)$$

where

$$\kappa = \gamma\beta_4 A_1 A_2; \quad \kappa' = \gamma\beta_4^* A_1 A_2 \qquad (22)$$

Assuming $\tilde{A}_4(L) = A_4(L) = 0$ where L is the length of interaction region we get:

$$\tilde{A}_4(0) = \left(\frac{i\kappa}{\kappa_0}\right) \tan(\kappa_0 L) \tilde{A}_3^*(0) \qquad (23)$$

where $\kappa_0 = \gamma\beta_4 I$ is the complex amplitude of the backward generated field and $A_3(0)$ is the complex amplitude of the input incident field. The phase conjugate intensity reflectivity is given by

$$R = |A_4(0)|^2 / |A_3(0)|^2 = |\tan^2 \kappa_0 L| \; . \qquad (24)$$

For $|\kappa_0 L| << 1$ we get $R = |\kappa_0|^2 L^2$.

3 Discussion

It is interesting to compare the present analysis with the recent analysis made for observations of PC of microwaves in an unmagnetized hydrogen plasma [9]. Simple two-fluid theory was used to calculate the low frequency plasma response to the beating of two transverse em waves[10]. In the limit of small $\frac{m}{M}$ the quasineutral steady-state response for the maximal change in the ion density, under resonance condition, was given according to Ref. 9 [using our notation]:

$$\begin{aligned}\Delta n &= n_0 \left(\frac{m}{2M}\right) \frac{qS}{\Gamma} \left(\frac{e}{m\omega S}\right)^2 \{E_1 E_3 \sin(qr - \Delta\omega t) \\ &\quad + E_2 E_4 \sin[(q + \Delta q)r - \omega t]\} \qquad (25)\end{aligned}$$

By using Eqs. (15) for $j = 4$ and $M_4 = 1$ ($\Omega_4 = \Delta\omega'' = q_4 S = |\vec{k}_1 - \vec{k}_3|S$), $F_4 \simeq (A_1 A_3^* + A_2^* A_4)$ and the value $\beta_0 = \frac{e^2}{4mM\omega^2}$ we get:

$$\begin{aligned}|n_{40}| &= \left(\frac{n_0}{S^2}\right) \left(\frac{e^2}{4mM\omega^2}\right) \left(\frac{q_4 S}{\Gamma}\right) \\ &\quad [\exp(-i\Delta\omega'' t + iq_4 r)(A_1 A_3^* + A_2^* A_4) + c.c.] \qquad (26)\end{aligned}$$

We find that Eq. (25) written with a real notation for the em fields is equivalent to our result represented by Eq. (26) with the complex notation (for the em fields), when we neglect the small shift Δq in Eq. (25) [this approximation was made in the present article by neglecting Δk in Eqs. (10-13) as explained previously]. The use of complex notation for the em fields is essential for obtaining the physical effects of PC. Eq. (25) or (26) is obtained under the resonance condition. The effect of deviation from resonance can be related to the use of the explicit expression for β_4 as given by Eq. (15) for $M_4 \neq 1$, $[\Omega_4 = \Delta\omega'' \neq q_4 S = |\vec{k}_1 - \vec{k}_3|S]$. For deviation from resonance the expression for Δn obtained in our analysis is in complete agreement with the analogeous expressions given in Refs. 9 and 10.

For the signal and the PC reflected beams the equations used in Ref. 9 are similar to Eq. (19) of the present article. The constant

$(g/2)$ of Ref. 9

$$\frac{g}{2} = \left(\frac{1}{8\pi}\right)\left(\frac{n_0}{n_c}\right)\left(\frac{qS}{\Gamma}\right)\left(\frac{e^2}{mc^2}\right)\left(\frac{2\pi c}{\omega M S^2}\right) \tag{27}$$

is equal to the corresponding constant in Eq. (19)

$$|\beta_4\gamma| = \left(\frac{e^2}{4mM\omega^2}\right)\left(\frac{q_4 S}{\Gamma}\right)\left(\frac{\omega}{c}\right)\left(\frac{n_0}{2\eta_0^2 n_c S^2}\right) \tag{28}$$

Since the em amplitudes in the present article are complex (as it should be) the constant of Eq. (28) is larger by a factor 2 relative to that given in Eq. (27) derived [9] for real amplitudes. Here again we have neglected in our analysis small shifts Δk which have been taken into account in Ref. 9. Although the present analysis is specialized to the recent observations of PC in unmagnetized hydrogen plasma it can be easily applied to other cases.

4 References

1. Federice J.F., IEEE Transactions on Plasma Science 1991, **19**, 549 (Includes a detailed list of references).

2. Fisher R.A., Optical Phase Conjugation, New York: Academic, 1985.

3. Zeldovich B.Y., Pilipetsky N.F. and Shkunov V.V., Principles of Phase Conjugation, New York: Springer-Verlag, 1985.

4. Joshi C., Kitagawa Y. and Lal A., International Journal of Nonlinear Optical Physics, 1992, **1**, 1.

5. Federici J.F. and Mansfield D.K., J. Opt. Soc. Am. B, 1986, **3**, 1588.

6. Nebenzahl I., Ron A., Tzach D., and Rostoker N., Phys. Fluids 1988, **31**, 2144.

7. Nebenzahl I., Ron A., and Rostoker N., Phys. Rev. Lett. 1988, **60**, 1030.

8. Lehner T., Physica Scripta, 1989, **39**, 595.

9. Domier C.W. and Luhmann N.C., Phys. Rev. Lett. 1992, **69**, 3499.

10. Williams E., Lininger D., and Goldman M., Phys. Fluids, 1989, **B1**, 1561.

11. Ma J.X., Chen R., and Xu Z., J. Opt. Am. B, 1991, **8**, 1442.

12. Chen F.F., Introduction to Plasma Physics, New York: Plenum, 1984.

13. Ichimaru S., Basic Principles of Plasma Physics, Reading: Benjamin, 1973.

14. Postan A. and Ben-Aryeh Y., J. Opt. Soc. Am. B 1988, **5**, 1379; 1989, **6**, 373.

15. Yariv A. and Pepper D.M., Optics Letters, 1977, **1**, 16.

16. Ben-Aryeh Y. and Postan A., Optics Commun. 1988, **66**, 47; **69**, 87.

17. Bloom D.M. and Bjorklund G.C., Applied Physics Letters, 1977, **31**, 592.

INSTABILITY AND DYNAMICAL CHAOS IN A WEAK NONLINEAR INTERACTION OF WAVES.

V.A.Buts, O.V.Manuylenko, A.P.Tolstoluzhsky
National Science Center
"Kharkov Institute of Physics and Technology",
Kharkov, Ukraine

Introduction

It is well established now that investigation of dynamical systems with complicated, chaotic trajectories in most cases is possible only numerically. There are some well developed asymptotic methods for investigation of regular dynamic, but as to chaotic motion, the analytical criteria for defining of stochastic regions in phase space are of paramount importance because they give an analytical description of a dynamical system in this region by means of statistical physics methods. In the present report we formulate conditions if being fulfilled the dynamics of the wave-to-wave type of coupling turns out to be chaotic. These conditions are verified via the system which describes coupling of high-frequency (HF) and low-frequency (LF) waves in nonlinear media.

Criterion of stochastisity

As known the energy transfer from one wave to others in nonlinear interaction bears the character of an instability. Therefore one may assume that the dynamic of this coupling will be chaotic when parameter $K \equiv 2\Gamma/\delta$ becomes greater then unity, where Γ is the growth

rate of this instability which plays the role of width of a nonlinear resonance, δ is the distance between resonances of different waves. Observe that value of δ usually corresponds to a minimum frequency. Let the wave of amplitude a_1 wave number k_1 and frequency ω_1 decay into two waves (a_2, k_2, ω_2) *and* (a_3, k_3, ω_3) One more wave is assumed to exist with the following parameter (a_4, k_4, ω_4), $k_4 = k_3$, $\omega_4 - \omega_3 = \Delta << \omega_1$. Suppose at first that forth wave do not influence on the decay. Then the amplitudes of three interacting waves change with time according to [1]:

$$\begin{aligned} \dot{a}_1 &= iV_1^* a_2 a_3, \\ \dot{a}_2 &= -iV_1 a_1 a_3^*, \\ \dot{a}_3 &= -iV_1 a_1 a_2^*, \end{aligned} \tag{1}$$

Where V_1 is the matrix element of interaction. On the linear stage ($|a_1|$=const) of decay the amplitude $|a_2|$ and $|a_3|$ growth exponentially with increment $\Gamma = |a_1||V_1|$. The phase $\Phi = 2\Phi_2 + 2\Phi_3$ changes obeys equation of mathematical pendulum:

$$\ddot{\Phi} + (2|a_1||V_1|)^2 \sin\Phi = 0 \tag{2}$$

It is seen from Eq.(2) that the half width of nonlinear resonance equals 4Γ. If we replace third wave by forth wave we obtain that on the linear stage phase $\Psi = 2\Phi_2 + 2\Phi_4 + 2\delta\tau$ satisfies Eq.(2) too, where $\Gamma_2 = |a_1||V_2|$ This means, that the distance between nonlinear resonances is equal to 2δ. Assuming the width of nonlinear resonance for forth wave is small $\Gamma << \Gamma_2$ we obtain the condition of the nonlinear resonance overlapping and, correspondingly, the criterion of stochastic instability: $2\Gamma/\delta > 1$.

Basic equations and results

The formulated above conditions of transition to stochastisity we checked on different physical models. First of all, this is a model described nonlinear coupling of HF and LF waves in nonlinear media with the second order nonlinearity. Assume, that only one LF wave

take part in the interaction in the none dissipative case, one can obtain following equations for coupling modes [2]:

$$i\dot{a}_n = ba_{n-1}exp(i\Delta\tau) + b^*a_{n+1}exp(-i\Delta\tau),$$
$$\ddot{b} + \Omega^2 b = \sum_n a^*_{n-1}a_n exp(-i\Delta\tau), \tag{3}$$

where b - is the complex amplitude of LF wave, a_n - is the complex amplitude of HF wave with number n, $\Delta \equiv \omega_n - \omega_{n-1}$, ω_n frequency of HF wave with number n; Ω -the free frequency of LF oscillations. The set (3) describes a variety of nonlinear processes of wave coupling. It also comprises, in particular, depending on initial conditions, the processes of coupling or decaying, dynamics of a large number of aggregate oscillators. We studied the decay of wave, which is propagated in a magnetized compensated by charge electron beam on the electromagnetic and beam waves; cascading processes at the decay of the HF wave on HF and LF waves in plasma (for example "beat-wave"); the decay of HF electromagnetic wave in magnetized plasmas wave guide on electromagnetic and langmuir waves. Note that due to the presence radial modes in last case, the amplitude of the pumping wave necessary for onset of dynamical chaos may be significantly lower then in the case of an unbounded system. Let us consider the decay of the HF wave (i) in a magnetized plasma on langmuir (p) and HF (s) waves. On the linear stage of the decay, when we can assume, that the amplitude of incident wave is constant, we can obtain from (3) the dispersion relation and growth rate of the decay instability. Then, by means of formulated above criterion we may obtain following condition for arising of the chaotic dynamic of the decay:

$$E_i^2 > \frac{64}{3^{3/2}} 32\pi m_e n_{0p} \frac{\omega_i}{\omega_p} \frac{\omega_s^2}{k_p^2} \frac{k_{pz}}{k_p} \tag{4}$$

where we used standard variables.

The set of equations (3) has been solved numerically for the different values of the amplitude of incident wave. Time-dependent

dynamics of amplitudes of coupling waves, spectra of obtained realizations and auto correlations functions we show in Fig. 1,2. When the condition (4) is not satisfied,the dynamic of the decay is regular (Fig.1)

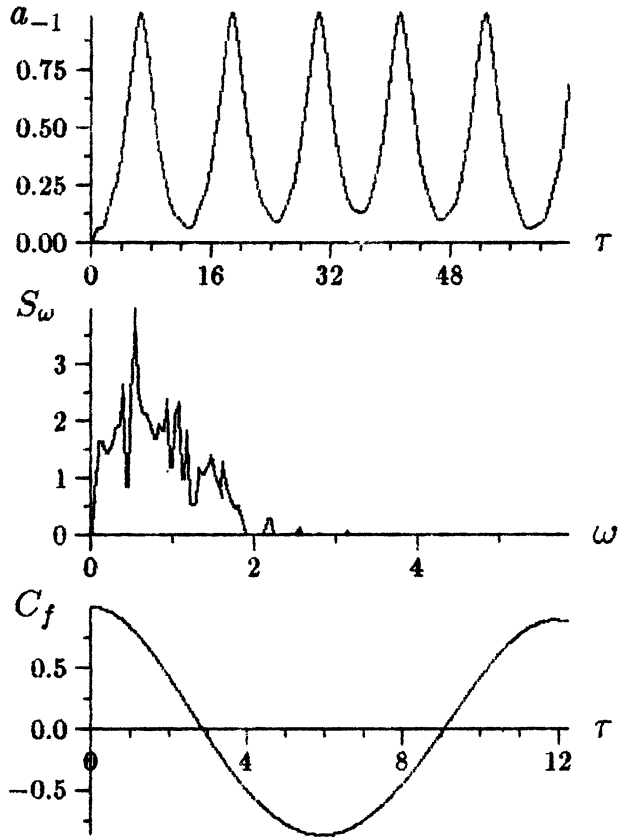

fig.1

In the opposition case the behaviour of the decay is chaotic (Fig.2).

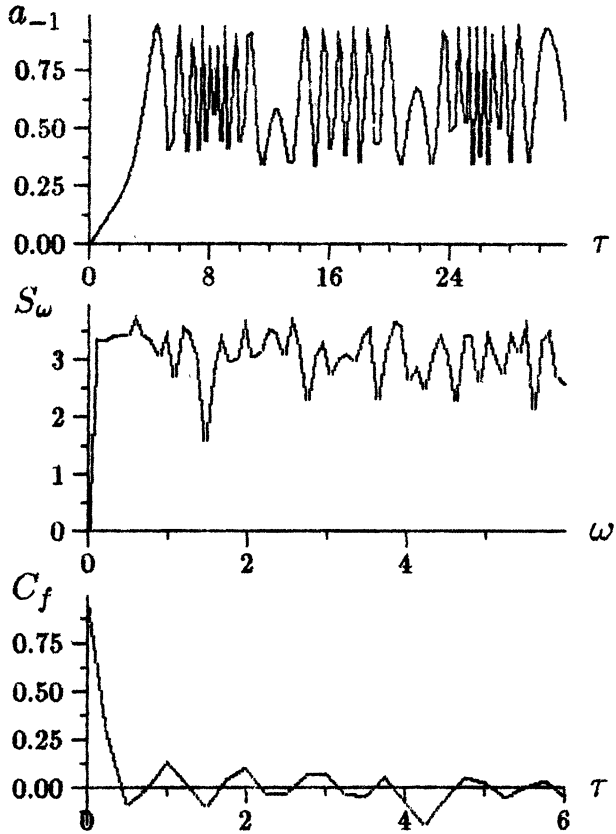

fig.2

Let us consider one of the simplest model of the nonlinear media, which is the aggregate of the nonlinear oscillators. Hamiltonian of such system is:

$$H = \frac{1}{2} \sum_k (\dot{y}_k \dot{y}_{-k} + \omega_k^2 y_k y_{-k}) + \frac{1}{3} \sum_{k_1,k_2,k_3} V_{k_1,k_2,k_3} y_{k_1} y_{k_2} y_{k_3} \delta(k_1 + k_2 + k_3) + \frac{1}{4} \sum_{k_1,k_2,k_3,k_4} V_{k_1,k_2,k_3,k_4} y_{k_1} y_{k_2} y_{k_3} y_{k_4} \delta(k_1 + k_2 + k_3 + k_4) + \dots \quad (5)$$

Let the eigenfreqnences of nearly all oscillators are equidistant and high ($\omega_k = \omega_1 + k\Omega, \omega_1 >> \Omega$) and one among them ($y_0$) has low frequency Ω. In this case the interaction of high-frequency (HF) oscillators has place through the low-frequency (LF) one; coefficients of the matrix of interaction are like each other $V_{k_1,k_2,k_3} = V$ and by physically the process of the oscillators interaction are analogous to cascade process of the decay HF wave on the HF wave and LF, which are described above. Substitution in (5) $y_k = a_k(t)exp(i\omega_k t)$, $y_0 = b(t)$, where a_k, b - amplitudes of HF and LF waves, which have time of the alteration less then period of HF wave, after averaging by high frequency, from the Hamiltonian (5) by taking into account only cubic items one can obtain the set of equations (3). From this result one can conclude that the dynamic of the coupling oscillators with cubic nonlinearity in Hamiltonian may became chaotic when their amplitudes are enough large.

After all we can to do following statement: these are general criterion of the dynamical chaos arising in the systems with cubic items in Hamiltonian. It is necessary to notice that the process of the chaos arising, which has considered above, is main process if basic small parameter are the amplitudes of the coupling modes. If the matrix elements of the interaction are such, that the main items of the Hamiltonian are items of the forth order, then the process of chaos arising will be determined by self-influence effects.

This work was supported by the Ukrainian State Committee of Science and Technology.

References

1. Zaslavskii G.M., Sagdeev R.Z. Introduction in Nonlinear Physics (Russian) M., Nauka publ., 1988.

2. Bakaj A.S. Nuclear fusion, 1970, v.10, p.53-67.

THE POWER LIMITING MECHANISM OF THE PLASMA-BEAM UHF GENERATOR

Yu.P.Bliokh, Ya.B.Fainberg,
V.O.Podobinskii, M.G.Lyubarskii
Kharkov Institute of Physics and Technology,
Kharkov, Ukraine

Introduction

Vacuum slow-wave structures which are used in TWT-generators and amplifiers have a disadvantage, which concerns with surface nature of excited waves. Decreasing of a longitudinal component of a wave electric field from periphery to axis cause diminishing in the coupling coefficient of electron beam with excited wave. It leads in its turn to increment decreasing. This disadvantage is most displayed in the high frequency band.

In this connection the plasma slow-wave structures have a special interest. Slow wave in such structures are space-like and has a maximum of longitudinal electric field on axis of system where, as a rule, the electron beam is propagated. Theoretical and experimental investigations of possibility of using plasma as a medium, where the interaction of charged particles with waves is most efficient are carried out for many years [1,2]. But only in the last decade the attention to this field of physics, namely plasma electronics, strongly increased due to a significant successes in the experiments with charged particles acceleration in plasma and plasma-beam microwave generators and amplifiers design.

We consider in this report the electrodynamic properties of the hybrid plasma-filled slow-wave structures which promise to be very perspective as an element of a plasma-beam microwave generators or amplifiers.

1. The hybrid plasma-filled slow-wave structures.

The simplest plasma slow-wave structure is a metallic waveguid, filled completely up with a plasma. The slow plasma wave in such system is space-like and efficiently interacts with an electron beam. The characteristic disadvantage of the plasma waveguide consists of quasi-longitudinality of the plasma waves. It leads to some difficulties for lead-in and out a microwave energy whithout using the special transforming and matching devices. This disadvantage will be weaker if the plasma fills in only a part of a crossection of a waveguide. In such system the plasma wave field topography provides the marked power flux whithout plasma and facilitates the matching with external waveguide. Exactly such structure was utilized in powerful plasma-beam generator of TWT type described in [3].

The question of matching, injection and extraction of the microwave energy for the hybrid plasma-filled slow-wave structures are almost completely settled by traditional methods of vacuum electronics. These systems consist from a vacuum slow-wave structure with the transit channel filled by plasma. The results of the investigation of such structures are described in [4]. In this article we shall give only a short description of their properties.

If the volume occupyed by plasma is relatively small, the field topography of waves is following: outside the plasma the field structure differs little from the one in the vacuum system. In the plasma channel the field's topography changes radically — the wave becomes space-like and quasi-longitudinal in this region. The main flux of the microwave energy propagates outside of the plasma channel. Thus, for instanse, from hybrid slow-wave structure in form of resonators which are coupled inductively and transit channel filled by plasma, the proprtion between energy fluxes external to the plasma and inside it runs up 10^2 — 10^3.

Such structure of the waves leads to the possibility of using the traditional vacuum devises available for microwave energy extraction. On the other hand, a great increase of the longitudinal component of

electric field in the beam region leads to the increase of the instability increment. In its turn the efficiency of the transformation of a beam energy into a microwaves increases also. Moreover, the neutralization of the beam's space charge allows to use the beams with essentialy greater current. The distance between beam and metallic surface reduces the thermal loads and requirements to the accuracy of beam adjustment.

So, the hybrid slow-wave structures filled by plasma combined the advantages of vacuum and plasma system and in a high degree are free from inherented to them disadvantages.

2. The automodulation plasma density in the presense of powerful UHF fields.

For the realization of advantages UHF plasma devises the homogeneity of plasma density along axis is very essential. It is important in order to maintain the synchronism between the beam and an excited wave. There is specific peculiarity of the plasma structures: their initial uniformity may be disturbed by wave fields. It leads to the change of electrodynamic properties of structure and may limit the utmost attainable power in plasma-beam UHF generators and amplifiers.

Amongst the causes which result in the appearance of inhomogeneities in plasma HF-pressure forses play the essential role. They lead, in particular, to the appearance of the modulation instability, which in case of unbounded warm plasma is well investigated [5]. In reference [6] the mechanism of the increase of larg-scale plasma inhomogeneityes in presence of the powerful waves in the waveguide is explained. It is assumed, that density of the wave energy W is large, i.e. $W \gg nT_e$ (here n, T_e are the plasma density and electron temperature) and the phase velosity V_{ph} is mach smaller than light velosity c. It is assumed also that the group velosity V_g exceeds the ion-sound wave velosity C_s to a marked degree:

$$V_g \gg C_s \tag{1}$$

This condition is natural for devices in which particle accelera-

tion or powerful microwave generation takes place. The mechanism of the arising of large-scale plasma igomogeneities is following. Let the plasma density have in some place a local minimum. Then in the plasma waveguide the slow wave field has in that place a local maximum, although in the warm unbounded plasma it has a local minimum. The HF-pressure's forces in the first case aspire to make a "hole" more deeper and vice versa in the second case. If the HF-pressure forces exceed the forces of the ordinary pressure, the plasma inhomogeneities beginn to increase.

In this paper the mechanism of the inhomogeneity plasma growth, which was described in [6], is cosidered, but now we did not assume, that the waveguide is filled completely with a plasma and the phase velocity is much smaller then c.

For simplicity the plane magnetized plasma waveguide bounded by metallic surfaces $|x| = b$ is considered. The layer $|x| < a$ is filled with plasma which density is n. We assume that the characteristic scale L of plasma inhomogeneity is much larger than wavelength λ. This condition together with inequality (1), which allows to neglect the plasma density variations during the time L/V_g (in this time electromagnetic wave passes through the inhomogeneity region), leads to the law of microwave energy flux conservation:

$$\Pi = \frac{V_{ph}}{2\pi\left(V_{ph}^2/c^2 - 1\right)} \int_a^b \varepsilon(x) E_z^2(x) dx = const \qquad (2)$$

where $\varepsilon = 1 - \omega_p^2/\omega^2$, $\omega_p^2(x) = 4\pi e^2 n(x)/m$.

The influence on the dynamics of plasma density disturbance δn by microwave field inhomogeneities along Z-axis is described by the equation:

$$\frac{\partial^2 \delta n}{\partial t^2} - C_s^2 \frac{\partial^2 \delta n}{\partial z^2} = \frac{ne^2}{4mM\omega^2 a} \frac{\partial^2}{\partial t^2} \delta g \qquad (3)$$

where M is the ion mass, δ_g is the variation of the quantity $g = \int_0^a E_z^2(x) dx$ when the plasma density changes.

Assumptions about large scales of the characteristic time and distance plasma density variations make possible to determine local field

topography and dispersion for different plasma density. These assumptions along with the condidion (2) make possible to reduce the equation (3) to the form

$$\frac{\partial^2 \delta n}{\partial t^2} - C^{*2} \frac{\partial^2 \delta n}{\partial z^2} = 0 \tag{4}$$

where C^* is a modificate velocity of ion sound

$$C^{*2} = C_s^2 (1 + \Pi F) \tag{5}$$

Here F is a complicated function which depends on all parameters of the system (we do not present it here).

As follows from (5), if $F < 0$ then the limiting value of power exists. If the microwave power goes over this limit, then the plasma density ihomogeneouses begin to increase with the time increment $\gamma = |C^*|/L$.

Analysis of the function F for two oscillation modes (plasma and electromagnetic waves) shows that the instability under consideration is possible only if $\omega < \omega_p$. The plasma wave instability is always possible and the limiting power grows if the V_{ph} or ratio b/a increases. The electromagnetic wave instability is possible only in some range of parameters. This range is cutting down when the part of waveguid volume filled with plasma decreases. At that time the limiting power increases.

The rise of plasma density automodulation is one of the possible mechanism of power limiting in the plasma-beam UHF generators. Really, the exitation of the plasma system by an electron beam is resonant by its nature, but the plasma inhomogeneity has influence on the wave velocity and it disturbes the wave-beam synchronism. It leads to decreasing of increment right up to break-down of amplification or generation. Later on the plasma homogeneity will be restored and UHF oscillations grow again. In such a way the low frequency instability arises. Estimations show that in plasma waveguid with cross-section about few cm, plasma dencity $n \sim 10^{11}$ cm^{-3} and electron temperature $T_e \sim 3$ eV the limiting value of power is about 10 kW. If the value of power exceeds this level the plasma density automodulation arises, the UHF oscillation become impulsive and the

average power drops. For inhomogeneities with the scale $\sim$ 10 cm the characteristic time of automodulation growth is $\sim 10^{-5}$ s (it is also the duration of UHF pulses).

Some more once quality of the hybrid plasma-filled structures follows from above-mentioned. Because the part of volume filled with plasma is small, then the connection between dispersion properties of system and plasma density is loosened. It leads to the growth of limiting power value.

Conclusion

The understanding of the above-mentioned instability mechanism allows to increase the maximum power in plasma-beam devices. For this purpose it is necessery to weaken the influence of plasma density on the phase velocity or let pass the main part of UHF power out of plasma. The slow-wave structure which consists of the sequence of connected resonators and plasma-filled channel represents an example of realisation of both methods. Another possibility is to operate with short pulses.

This work was supported by the Ukrainian State Committee of Science and Technology.

References

1. Fainberg Ya.B., Plasma Physics, 1985, V.11, N 11, p.1398–1410.
2. Fainberg Ya.B., Plasma Physics, 1987, V.13, N 5, p.607–625.
3. Kuzelev M.V., Mukhametdzjanof F.Kh, Rabinovitch M.S. et al.,JETPH, 1982, V.83, p.1358–1367.
4. Fainberg Ya.B., Bliokh Yu.P., Lubarskii

STOCHASTIC HEATING OF PLASMAS BY LASER RADIATION

V.A.Buts, K.N.Stepanov
National Science Center
"Kharkov Institute of Physics and Technology",
Kharkov, Ukraine

1 Abstract

A new method for fast heating of plasma is proposed. It is based on the stochastic instability of charged particles motion in the fields of three or more high frequency ($\omega >> \omega_p$) large amplitude electromagnetic waves. The normal (Compton) or anomalous scattering is the elementary mechanism of the resonance interaction between waves and particles in this method. The heating rate for equal power levels may exceed considerably those inherent in other well-known methods.

1. Electromagnetic waves may heat plasma (e.g., in controlled fusion devices) in two regimes. When the wave amplitude is small linear mechanism of the wave energy absorption is at work. The particles gaining the energy from the wave have time to distribute this energy among other particles during the heating period. The deviation of the distribution function from the Maxwellian one is small. Moreover, if the amplitude of the electromagnetic wave is high enough, the beam-plasma like and parametric excitations of natural plasma waves occur resulting in a turbulent plasma heating [1-3].

We propose here a new mechanism of direct heating of plasma particles by strong electromagnetic waves. Interaction between electrons and beat-waves under the Cherenkov resonance condition results in electrons being trapped by beat-waves. These resonances

overlap if their widths are sufficiently large. The consequence of this overlapping is the development of the stochastic instability and the diffusion of particle in energy space. The method proposed here is close to multiwave heating (see ,e.g., [4-5]). In the case considered the nonlinear beat oscillations are similar to those in free electron lasers. Another opportunity exists to heat plasma particles directly with noise electromagnetic fields. Below we will compare stochastic and noise methods of plasma heating and show the first one to be more efficient.

2.Consider a charged particle motion in the field of several $(N+1)$ plane electromagnetic waves $\vec{E} = Re\sum_{n=0}^{N}\vec{E}_n$; $\vec{E}_n = \vec{\mathcal{E}}_n e^{i\Psi_n}$; $\vec{H} = Re\sum_{n=0}^{N}\vec{H}_n$; $\vec{H}_n = c[\vec{k}_n\vec{E}_N]/\omega_n$ where $\Psi_n = \vec{k}_n\vec{r}_n - \omega_n t$.
It is convenient to introduce the following dimensionless variables $\vec{p}_1 = \vec{p}/mc$, $\vec{E}_{n,1} = \vec{E}_n/mc\omega_n$, $\vec{k}_{n,1} = \vec{k}_n c/\omega$, $\tau = \omega_0\tau$, $\vec{r}_1 = \vec{r}\omega_0/c$, $\omega_{n,1} = \omega_n/\omega_0$, $\vec{v}_1 = \vec{v}/c$. In this variables (we omit the subscript "1") the equations of motion assume the form

$$\dot{\vec{p}} = \frac{d\vec{p}}{d\tau} = [Re\sum_{n=0}^{N}\vec{E}_n(\omega_n - \vec{k}_n\dot{\vec{r}}) + Re\sum_{n=0}^{N}\vec{k}_n(\dot{\vec{r}}\vec{E}_n)] \qquad (1)$$

where $\dot{x} \equiv \frac{dx}{d\tau}$.
The wave vectors are assumed to be collinear, the wave amplitudes being small ($|\vec{\mathcal{E}}_n|$) << 1). Then the motion of particle has two temporal scales, the fast one and the slow one.

Averaging over fast motion yields the set of equations for slowly varying quantities:

$$\frac{d\gamma^2}{d\tau} = \sum(\vec{\mathcal{E}}_m\vec{\mathcal{E}}_n)(\omega_m \mp \omega_n)cos\theta_{mn}$$
$$d\theta_{mn}/d\tau = (\vec{k}_m \mp \vec{k}_n)\vec{v} - (\omega_m \mp \omega_n) \qquad (2)$$

where γ is the particle energy, $\theta_{mn} = \Psi_m \mp \Psi_n$ is the beat-wave phase. The summation in the first equation is performed over those pairs of waves whose phase sums θ_{mn} are slowly varying. The upper sign refers to the normal scattering (NS), whereas the lower sign is for the anomalous one (AS) (according to Ref.[6]).

Consider now the simplest option when only three waves are applied, the first $(\omega_1, \vec{k}_1, \vec{\mathcal{E}}_1)$ and second $(\omega_2, \vec{k}_2, \vec{\mathcal{E}}_2)$ ones moving opposite to the zeroth wave $(\omega_0, \vec{k}_0, \vec{\mathcal{E}}_0)$ (NS scheme). Two beat-wave waves $(i = 1, 2)$ arise with phase velocities $\vec{v}_{ph_i} = \Delta\omega_{0_i}/(\vec{k}_0 + \vec{k}_i)$, $\Delta\omega_{0_i} = 1 - \omega_i$.

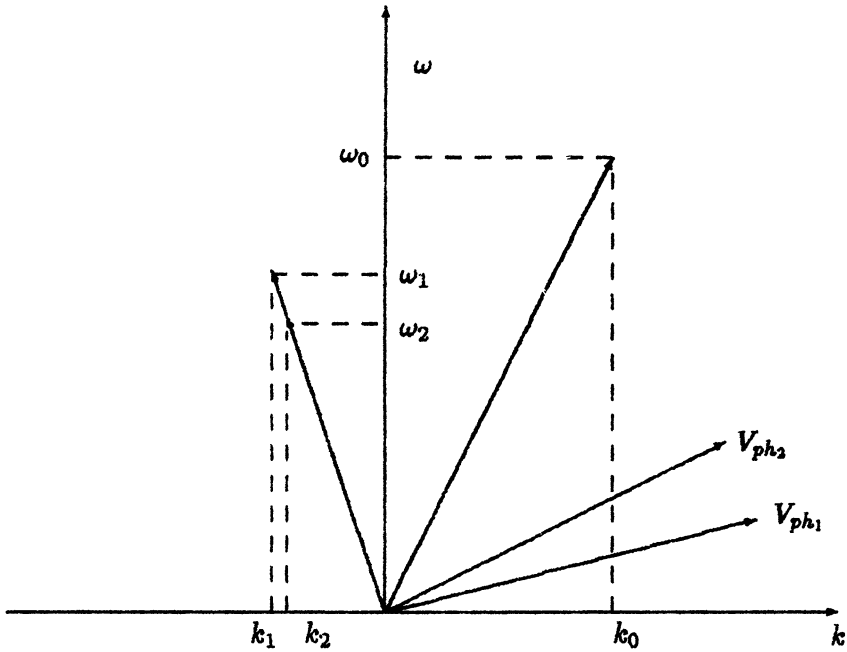

The figure shows the dispersion diagram picturing the beat-wave waves. The condition for the overlapping of nonlinear resonances is the condition for the occurrence of the stochastic instability

$$(v_{ph_2} - v_{ph_1}) \leq \frac{\mathcal{E}_0}{\gamma_0^2 \sqrt{k_0 v_0}} [\sqrt{\mathcal{E}_1 \Delta\omega_{0_1}} + \sqrt{\mathcal{E}_2 \Delta\omega_{0_2}}] \qquad (3)$$

where γ_0, v_0 are the initial energy and velocity values. In this case one can retain in Eq.(2) only the term responsible for the above two beat waves. The phases of these waves may be regarded as random. Then after averaging over random phases and random initial positions of

particles one can obtain the following expression for the mean square of the deviation of energy from its mean value

$$< (\Delta\gamma)^2 > \simeq \frac{\mathcal{E}^4 \Delta\omega^2}{4\gamma_0^2} \tau \qquad (4)$$

where

$$< L > \equiv \frac{1}{2\pi} \int_0^{2\pi} d(\vec{k}\vec{r}_0) \lim_{T\to\infty} \frac{1}{T} \int_{-T}^{T} L dt$$

On deriving Eq.(4) we assumed that $\tau >> \tau_c$, τ_c being the decorrelation time amounting to some periods of the waves. Besides we put for simplicity that $\Delta\omega_{01} \equiv \Delta\omega$, $\mathcal{E}_0 \simeq \mathcal{E}_1 \simeq \mathcal{E}_2 \simeq \mathcal{E}$.

In order that all plasma particles were heated stochastically, the inequally $\Delta v > v_{ph_1}$ should hold. In the nonrelativistic limit this condition is $\mathcal{E} > 0.25\sqrt{\Delta\omega v}$ i.e., moderate laser fields are suffiecient to trap and heat stochastically all plasma electrons.

Let us compare now the efficiency of stochastic heating of particles by coherent fields with that for heating with noise field. Consider a particle moving in a noise field. From the following equation for energy changes

$\frac{d\gamma}{d\tau} = \vec{v}\vec{E}_{noise}$

with the above assumptions one gets easily

$< (\Delta\gamma)^2 >_n = v^2 \mathcal{E}_n^2 \tau$

Let the energies of the coherent and noise fields be equal, i.e., $\mathcal{E}^2_{noise}\delta\omega_{noise} = \mathcal{E}^2\delta\omega$ The spectrum width of the noise field is large, $\delta\omega_{noise} > \omega$, whereas that of the coherent field is narrow $\delta\omega = \omega/Q$, where Q is the quality factor of the optical resonator ($Q \sim 10^6 \div 10^7$). Then the ratio of energy gains of particles in these fields determining the heating efficiency is

$$K \equiv \frac{< (\Delta\gamma)^2 >}{< (\Delta\gamma)^2 >_n} > \frac{\mathcal{E}^2 (\Delta\omega)^2 Q}{4\gamma_0^2 v_0^2} \qquad (5)$$

For the most cases $K >> 1$.

Let us compare the mechanism considered with other ones. There exist two main scenarios of plasma beating with strong electromagnetic waves. In the first scenarii the wave incident on the plasma

excites in it turbulent pulsations of electric and magnetic fields due to parametric processes (decay ones, Raman scattering etc [2]) leading to the turbulent heating. The time of turbulence formation may exceed the time of stochastic heating. Besides, the energy of the incident wave is distribute in a broad spectrum of natural oscillations. In this case, according to Eq.(5), the heating efficiency is less and the heating time is more than the respective values for the stochastic heating. The second scenario is related with Coulomb collisions of particles. The collision frequency ν is proportional to the plasma density and at $n = 10^{12} cm^{-3}$ and $T = 7kev$ it is equal to $\nu = 10^{12} s^{-1}$. If $\omega = 5 \cdot 10^{15} s^{-1}$ and $\mathcal{E} = 0.1$, then the heating of electrons up to $7kev$ will occur during the time $\Delta t_h = 2 \cdot 10^{-14} s^{-1}$, this time being considerably less than the collision time. Thus there exists a domain of plasma and laser radiation parameters in which the stochastic mechanism of heating is more efficient.

Consider now the application of stochastic heating for laser controlled fusion. The stochastic heating of ions is weak because $\tau_h \propto (m_i)^4$. They are heated faster as a result of collisions with hot electrons heated stochastically. Under the action of the laser field with $\mathcal{E} \sim 0.1$, $\omega = 5 \cdot 10^{15} s^{-1}$ plasma electrons with $n = 10^{22} cm^{-3}$ during the time $t < 10^{-13} s$ are heated to $T = 7kev$. The heated electrons transfer its energy to ions during the time $t \sim 10^{-9} s$. During this time the target of the radius $r = 0.1cm$ will have no time to fly off.

Fast heating of electrons will prevent the development of most instabilities because their growth rates Γ are not large $\Gamma \Delta t_h < 1$. In this case the absorbed energy of laser radiation will go efficiency to electrons and ions.

This work was supported by the Ukrainian State Committee of Science and Technology.

References

1. Stepanov K.N. Fizika plazmy, 1983, **9(1)**, 45.

2. Tsitovich V.N. Teoriya turbulentnoii plazmy (in Russian), Moscow,

Atomizdat publ., 1971.

3. Silin V.P. Parametricheskoe vozdejstvie izlucheniya bol'shoii moschnosti na plasmu. (in Russian), Moscow, Nauka publ., 1973.

4. Lihtenberg A., Liberman M. Regular and Stochastic Motion Springer-Verlag. N.-Y., Heidelberg, Berlin

5. QuonB.H., Dundl R.A., Divergilio et al. Phys. Fl. 1985, **28(5)**, 1503.

6. Frank I.M. Uspehi Fiz. Nauk (in Russion), 1979 **129(4)**, 685.

THE EXCITATION OF A PLASMA-FILLED SLOW WAVE RESONATOR BY AN ELECTRON BEAM

V. A. Buts, V. I. Miroshnichenko, V. V. Ognivenko,
I. N. Onishchenko, Yu. A. Turkin
Kharkov Institute of Physics and Technology,
Kharkov, Ukraine

Introduction

The employment of a plasma as an electrodynamic structure element has revealed a number of advantages connected with the peculiarities of plasma-waveguide dispersion characteristics and plasma nonlinearities [1]. A rise in efficiency of powerfull HF-oscillation excitation by an electron beam in plasma-filled slow wave structures [2–4] has been widely discussed [1,5–8], yet the problem is still remained to be unsolved.

The present paper is concerned with the investigation of the evolutionary electrodynamic characteristics changing due to the nonlinearity of the plasma being in strong fields of excited waves. The amplification and generation regimes are considered.

It is known [9] that the beam-wave energy exchange limitation is caused by beam trapping in the wave well. To get over this restriction, the space nonuniform structures with decreasing phase velocity or beam reacceleration are commonly used. It is alluring to find an inherent nonlinear mechanism, which leads to self-maintaining of resonance between the bunch velocity and the phase velocity of the wave [10].

Amplification regime

In the case considered, as a result of nonlinear wave interaction leading to plasma density modulation, a distributive radiation removal from the system is possible, this being equivalent to dissipative energy losses by the excited wave [10]. Therefore, the problem may be investigated using a simple model of the dissipative beam instability, described by a set of nonlinear self-consistent equations for amplitude ε and phase α of the wave and the equations of motion for beam electrons in the following form:

$$\frac{d\varepsilon}{d\zeta} = \frac{1}{2\pi}\int_0^{2\pi} \sin(\tau+\alpha)d\tau_0 - \nu\varepsilon \tag{1}$$

$$\frac{d\alpha}{d\zeta} = \frac{1}{2\pi\varepsilon}\int_0^{2\pi} \cos(\tau+\alpha)d\tau_0 \tag{2}$$

$$\frac{d^2\tau}{d\zeta^2} = -\varepsilon\sin(\tau+\alpha). \tag{3}$$

We have used the dimensionless variables $\tau = -\omega(t - z/v_0)$, $\zeta = æz$, $\varepsilon = E/E_{tr}$. Here $æ = \omega/v_0\,(n_1 v_0/n_0 v_g)^{1/3}$ is the space coefficient of amplification; $E_{tr} = \left[4\pi n_1 m v_0^2\,(n_1 v_0^4/n_0 v_g)^{1/3}\right]^{1/2}$ is the amplitude of trapping; n_1, n_0 are the beam and plasma densities; ω is the wave frequency; v_0 is the beam velocity; v_g is the group velocity; ν is the effective dissipation coefficient.

The main special feature of this problem is the nonlinear self-consistent closeness of the phase velocity (v_{ph}) to the beam velocity ($v_{ph} \approx v_0$), which does not require any particular external steps to be taken. The dependence of the wave phase on its amplitude (2) during the wave evolution is the cause of v_{ph} decrease over the interaction length, while for the dissipativeless case ($\nu = 0$) the average phase velocity remains constant (Fig. 1a). If $\nu \neq 0$, successive phase jumps (decrease and increase in v_{ph}, obeying the bunch beating in the wave well) become nonsymmetrical, because the amplitude is essentially damped during a bounce period. Hence, during the whole trap oscillation v_{ph} is not reestablished, becoming the smaller, the greater is ν (Fig. 1b,c for ν =0.1; 1)

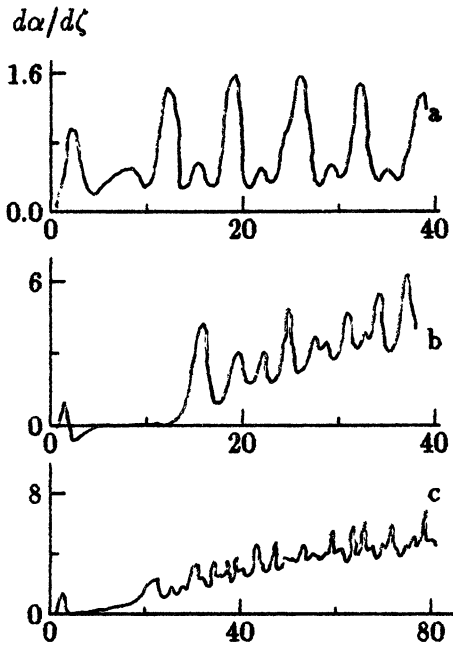

Fig.1

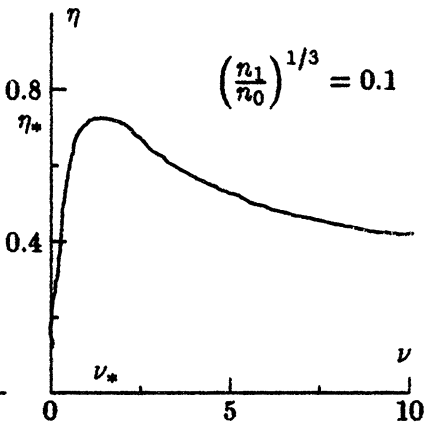

Fig.2

The efficiency $\eta = {}_\Delta W/W_b$ (here ${}_\Delta W$ denotes the beam energy losses over the distance ζ of ${}_\Delta W$ saturation, ${}_\Delta W_b$ is the initial beam energy) as a function of ν is presented in Fig. 2. It is seen that with growing ν the efficiency η rises, reaching its maximum value $\eta_* = 0.72$ for $\nu_* = 1.5$ and further falls down slowly. Phase plane $\left(\tau, \frac{d\tau}{d\eta}\right)$ shows that the beam particles are divided into two groups, namely, trapped and transit particles. The trapped bunch loses its energy the more intensely the greater is ν. The number of trapped particles decreases with ν growth. The competition of these two factors leads to the existence of maximum η_* for the optimum parameter ν_*.

Generation regime

The plasma-filled electrodynamic systems for HF-generators and particle accelerators seem promising owing to the "flexibility" of their

dispersion characteristics. For high power levels, because of the plasma density deformation, they can change their electrodynamic properties so that particle-wave resonance lasts longer than in the vacuum case [10]. To verify these considerations for generating operation, we solve the problem of oscillation excitation by the electron beam in a resonator filled with a plasma, which is being modulated in the HF-potential of the excited waves [11].

Suppose that the longitudinal components of the synchronous and reflected waves have the following form:

$$E_{\pm}(\vec{r},t) = \mathrm{Re}\left\{A_{\pm}(\vec{r},t)\exp\left[-i(\omega t \mp kz)\right]\right\}. \qquad (4)$$

The synchronous E_+-wave, excited by the beam, is in nonlinear interaction with the reflected E_--wave and the low-frequency plasma oscillations. This process is described by a set of Maxwell's equations for the wave fields, the hydrodynamic equations for electrons and ions of the plasma and the equations of motion for the beam electrons. The boundary conditions at the entrance ($z = 0$) and at the exit ($z = L$) of the resonator can be written as

$$\begin{aligned} A_+(z=0,t) &= R_1 A_-(z=0,t) \\ A_-(z=L,t) &= R_2 A_+(z=L,t), \end{aligned} \qquad (5)$$

where $R_{1,2}$ are the reflection coefficients at the resonator ends. Let us consider the static approximation, when the velocities of slow plasma motions are small comparing with the ion thermal velocity, e.g., $\left|\partial^2\delta n/\partial t^2\right| \ll c_s^2\left|\partial^2\delta n/\partial z^2\right|$, here δn is the plasma modulation, c_s is the sound velocity. After averaging over HF-oscillations and using the dimensionless variables $\zeta = æz$, $\tau = \omega(t - z/v_0)$, $\theta = \omega t_l(z,t_0) - kz$, $a,b \equiv |e|A_{\pm}\omega/\left[m_0 v_0 (æ v_0)^2\right]$, $v_{\pm} = \lambda\dfrac{v_g/v_0}{1 \mp v_g/v_0}$, $\omega = \dfrac{(v_z - v_0)}{\lambda v_0}$, $\lambda \equiv \dfrac{æ v_0}{\omega}$, $æ = \dfrac{\omega_b}{v_0}\left[2\dfrac{v_p v_0}{c^2}\dfrac{g}{4\pi}\lambda\right]^{1/2}$, $\sigma = \dfrac{\omega_p^2}{8\omega k c^2}\dfrac{v_0^3}{c_s^2}\dfrac{m}{M}\left(\dfrac{æ v_0}{\omega}\right)^4\lambda$, g — beam-wave coupling coefficient, $\theta_0 = \theta(z=0)$, we obtain the following set of self-consistent nonlinear equations

$$\left(\frac{\partial}{\partial\tau} + v_+\frac{\partial}{\partial\zeta}\right)a = i\sigma|b|^2 a + \frac{1}{2\pi}\int_0^{2\pi} d\theta_0 e^{i\theta} \qquad (6)$$

$$\left(\frac{\partial}{\partial\tau} - v_- \frac{\partial}{\partial\zeta}\right) b = i\sigma|a|^2 b \tag{7}$$

$$\frac{d\omega}{d\zeta} = \mathrm{Re}\left(ae^{i\theta}\right), \quad \frac{d\theta}{d\zeta} = \omega. \tag{8}$$

Here the group velocity of the synchronous wave is supposed to be positive $v_g > 0$ (travelling wave tube). For the backward-wave oscillator it is necessary to replace v_g by $-v_g$ and $A_+ \rightleftharpoons A_-$.

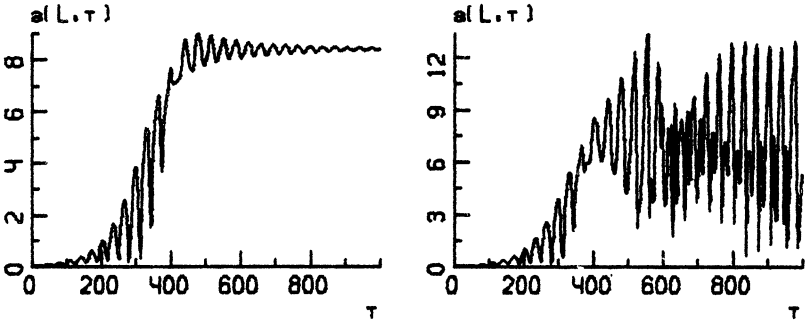

a b

Fig. 3.

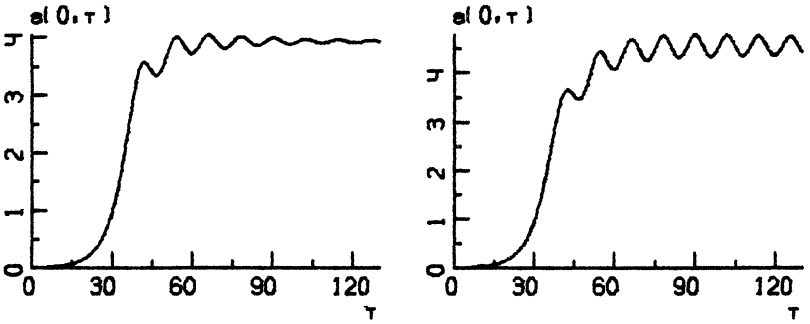

a b

Fig. 4.

Equations (6–8) were solved numerically for the following parameters: $a_0 = b_0 = 0.01$, $L = 2$, $R_1 = 1$, $R_2 = 0.3$. The temporal

evolution of the synchronous wave amplitude $a(\tau)$ for the amplifier (TWT) ($v_g/v_0 = 0.1$, $\lambda = 1$, $\sigma = 0.005$) and for the oscillator (BWO) ($v_g/v_0 = 0.8$, $\lambda = 0.5$, $\sigma = 0.03$) are presented in the Fig. 3 and Fig. 4, correspondingly (a — vacuum case, $\sigma = 0$; b — plasma case, $\sigma \neq 0$). It is seen that the straight and reflected waves coupling due to the plasma modulation leads to more complicated temporal behaviour $a(\tau)$ approximately at the same power level. The threshoulds of multiperiodic and stochastic modulations are lowering with plasma filling. A slight power enhancement is noticed for BWO. The further investigations will persue the quantitative coincidance of the numerical results with experiments [1–4] for the experimental parameters.

This work was supported by the Ukrainian State Committee of Science and Technology.

References

1. Fainberg Ya. B. et al, Dokl. Akademii Nauk Ukrainy. Ser. A. 1990, **11**, 55. (In Russ.)
2. Tkach Yu. V. et al, Fizika Plasmy, 1975, **1**, 81. (In Russ.)
3. Carmel Y. et al, Phys. Rev. Lett., 1989, **62**, 2389.
4. Perevodchikov V. I. et al,Proc. 9-th Int. Conf. on High Power Particle Beams, Washington, 1992, PD–19
5. Fainberg Ya. B. et al, Lektsii po ehlecktron. i radioph.,Saratov University publ., 1992, 66. (In Russ.)
6. Batskih G. I. et al, Proc. 8-th Int. Conf. on High Power Particle Beams, Novosibirsk, 1990, **2**, 1173.
7. Lin A. T., Chen L., Phys. Rev. Lett., 1989, **63(26)**, 2808.
8. Lou W. R. et al, Phys. Rev. Lett., 1991, **67(18)**, 2481.
9. Onishchenko I. N. et al, Pis'ma v ZhETF, 1970, **12**, 407.
10. Balakirev V. A. et al, Plasma, Laser, Collect. Accelerators (Accelsem 92), Kharkov, Ukraine, 6–9 Oct., 1992.
11. Bottom M., Amiram Ron., Phys. Rev. Lett., 1991, **66(19)**, 2468.

WAVE - BEAM INTERACTION IN THE PRESENCE OF INHOMOGENEOUS STATIC MAGNETIC AND ELECTRIC FIELDS

G.M.Fraiman and I.Yu.Kostyukov
Institute of Applied Physics, Russian Academy of Sciences,
Nizhny Novgorod, Russia

1 Introduction

The influence of perturbation on dynamic system motion being the solution of the integrable problem, is the traditional problem of hamiltonian mechanics [1–7]. In canonical action-angle variables, this task can be formulated as follows. Let us consider the time-dependent hamiltonian system with N degrees of freedom, given by Hamiltonian: $H(\mathbf{I},\boldsymbol{\Theta},t) = H_0(\mathbf{I},t) + H_\sim(\mathbf{I},\boldsymbol{\Theta},t)$, with initial condition: $I_i(t=0) = I_i^0$, $\Theta_i(t=0) = \Theta_i^0$. Here, $H_0(\mathbf{I},t)$ is the Hamiltonian of the unperturbed problem and $H_\sim(\mathbf{I},\boldsymbol{\Theta},t)$ is the perturbation, being the 2π - periodical function of angle variables $\Theta_1,\ldots,\Theta_N$. In the unperturbed problem ($\mu = 0$), all action variables are the first integrals. The problem is to calculate the variations of the action variables during evolution of the system.

In application to celestial mechanics a number of methods to take into account the perturbation were suggested. (The analysis of the methods is given by Poincare [1]). However, they have serious defects, related to the existence in the solutions of the "secular" term, infinitely increasing in time (the so-called problem of small denominators). To formally overcome the divergence new methods of perturbation

(the Poincare method [1], the averaging method [2,3] and the others [4-7]) were developed. Usually, the smallness parameter of the perturbation theory is μ. Despite the fact that the solution obtained by means of these methods are the formally divergent series they can describe the real system motion good enough under some conditions (which determined by the intense of the perturbation and required accuracy). Many problems have been investigated with the help of the methods (variation of adiabatic invariants [3], etc.).

Unlike the traditional problems of classical mechanics, for the problem of collective phenomena physics (interaction between a beam of charged particles and HF field etc.) the solution obtained for one particle must be averaged over all particles. It will be seen further that in the problem of interaction between the charged particle beam and HF field, the averaged variation of one of the action variables corresponds to the variation energy of the beam and the averaging over the particle ensemble corresponds to the averaging over all initial angle variables. The action-variable variations averaged over all Θ_i^0 to the first order in μ equal zero and the second order of perturbation theory corresponding to the usual methods is difficult enough for analytic analysis (the multiple integrals, etc. [5,7,8]). Therefore, it is important to develop a method, allowing us to obtain a more convenient form of averaged variation to the second order in μ.

In this paper we shall derive general relations within the framework of hamiltonian mechanics and discuss their possible applications to the plasma physics problems. Since they have the hamiltonian nature, the range of their use is wider than we discuss here.

In the first section, the some expressions of classic mechanics are adduced (the relative integral invariants, the Lagrange bracket and so on). Taking these expressions as basis the general relations for the action variables variation averaged over all Θ_i^0 to the second order in μ are obtained. The form of the relations is compact and physically clearer for the analysis. It is shown that obtained expressions are the generalization of relation between the factors in Fokker-Planck-Kolmogorov equation known in stochastic dynamics. In the one - dimensional case, the limits of validity of the relations are found.

In the second section, the one - dimensional problems are discussed. The expressions for the problem of interaction between a charge particle beam and HF field in the presence of a static field are derived. The results are generalized for the nonlinear field regime (consideration of the ponderomotive force action). The known and new problems of beam-plasma interaction are solved.

In the third section, the obtained results are applied to analyze the many - dimensional problem: the interaction between the charge particle beam and microwave in the presence of an inhomogeneous magnetostatic field. It is shown that the inhomogeneity of the magnetic field can change not only the rate of microwave absorption but the sign of the effect. It means that the HF field can be pumped by the beam due to the action of the inhomogeneity of the magnetic field.

2 General Expressions

Let us consider the dynamic system with N degrees of freedom, having the Hamiltonian $H(\mathbf{I}, \mathbf{\Theta}, t)$. The evolution of the system described by the Hamiltonian equations:

$$\frac{dI_i}{dt} = -\frac{\partial H}{\partial \Theta_i}, \qquad \frac{d\Theta_i}{dt} = \frac{\partial H}{\partial I_i}, \qquad i = 1, \ldots, N. \tag{1}$$

The initial condition are added to Eq. (1) :

$$I_i(t=0) = I_i^0, \ \Theta_i(t=0) = \Theta_i^0. \tag{2}$$

On the other hand, the hierarchy of the Poincare invariants can be taken as a basis for the Hamiltonian system theory [4]. For the first time, these invariants of various dimension were investigated by Poincare [1]. He showed that some quantities that he called relative

integral invariants do not vary during the time t:

$$\oint_{\partial\sigma_1} \sum_{i=1}^{N} I_i d\Theta_i = const,$$

$$\oint_{\partial\sigma_2} \sum_{i,j=1,i\neq j}^{N} I_i I_j d\Theta_i d\Theta_j = const, \quad \dots \quad , \tag{3}$$

$$\oint_{\partial\sigma_N} I_1 I_2 \dots I_N d\Theta_1 d\Theta_2 \dots d\Theta_N = const.$$

It is integrated through the corresponding "fluid " hypersurfaces at a certain moment of the time. The first invariant corresponds to conservation of the vector **I** circulation along the fluid closed line $\partial\sigma_1$ consisting of the particles moving according to the equations (1) and (2) and the equation for the last N-th invariant expresses the well-known Luiville theorem of the conservation of phase volume bounded by the arbitrary closed surface $\partial\sigma_N$.

The main idea of the present paper may be formulated as follows. The Poincare invariants give quantity averaged over this hypersurface. Therefore, we can hope that if we choose a good hypersurface and the averaging quantity, we can obtain the relation, which will useful for physical applications. To obtain this relation for an arbitrary function of the canonical variables we should use the differential form of Equation (3). In the general case, the connection between the integral invariants and the differential forms was shown by, e.g, Arnold [4]. However, in our case it is more convenient to use a more concrete method, in which the differential form of Eqs. (3) is the corresponding expression of the jacobian of the transition from the initial variables $\mathbf{I}^0, \mathbf{\Theta}^0$ to the variables $\mathbf{I}, \mathbf{\Theta}$.

For the first integrable invariant we have the known relations of the Lagrangian brackets:

$$\{I_i^0, \Theta_j^0\} \equiv \sum_{k=1}^{N} det \left\{ \frac{I_k, \Theta_k}{I_i^0, \Theta_j^0} \right\} = \delta_{ij}, \tag{4}$$

$$\{I_i^0 I_j^0\} = 0, \tag{5}$$

$$\{\Theta_i^0 \Theta_j^0\} = 0. \tag{6}$$

For the N-th integral invariant we have the well-known consequence from the Louiville theorem: the jacobian of the transit from the initial variables to the $\mathbf{I}, \boldsymbol{\Theta}$ variables $\mathbf{I}^0, \boldsymbol{\Theta}^0$ is equal unity:

$$det \left\{ \frac{I_1, \Theta_1, \ldots, I_N, \Theta_N}{I_1^0, \Theta_j^0, \ldots, I_N^0, \Theta_N^0} \right\} = 1. \tag{7}$$

Let us derive the expressions of the action variables variation defined by Eqs.(1) and (2) and averaged over all initial angle variables:

$$\Delta I \equiv \frac{1}{(2\pi)^N} \int_0^{2\pi} \ldots \int_0^{2\pi} [I(\mathbf{I}^0, \boldsymbol{\Theta}^0, t) - I^0] d\Theta_1^0 \ldots d\Theta_N^0. \tag{8}$$

Here and further, $<< \ldots >>$ means the averaging over the all initial angle variables. We assume, that there is an infinite set of the dynamic system, having the equal volume of the action variables and evenly distributed in the all angle variables at the initial time moment $t = 0$. Due to the periodicity with respect to $\boldsymbol{\Theta}^0$, the solution of problem (1), (2) at an arbitrary time moment t can be written in the following form:

$$I_i \equiv I_i^0 + \Delta I_i + I_i^{\sim}, \quad \Theta_i \equiv \Theta_i^0 + \Delta\Theta_i + \Theta_i^{\sim}. \tag{9}$$

In definition $<< \mathbf{I}^{\sim} >> = << \boldsymbol{\Theta}^{\sim} >> = 0$ averaged over all Θ_i^0.

Because the derivation of expression for ΔI is unwieldy it is given in Appendix A. Here, we give the final result:

$$<< \Delta I_i >> = \frac{1}{2} \sum_{j=1}^{N} \frac{\partial}{\partial I_j^0} << I_j^{\sim} I_i^{\sim} >> . \tag{10}$$

For the present, we can define the limits of applicability of this relations only in the unidimensional case. To find these limits we shall now obtain an exact relation. Let us multiply equation (7) by

an arbitrary function $\frac{\partial^N}{\partial I_1 \dots \partial I_N} f(\mathbf{I}, \Theta)$, then, average it over Θ^0 and integrate it over $\mathbf{I}^0$. As a result, we get:

$$<< \int^{I_1^0} \dots \int^{I_N^0} \frac{\partial^N}{\partial I_1 \dots \partial I_N} f(\mathbf{I}, \Theta) dI_1^0 \dots dI_N^0 >>=$$

$$<< \int^{I_1^0} det \left\{ \frac{I_1, \Theta_1, \dots, I_N, \Theta_N}{I_1^0, \Theta_j^0, \dots, I_N^0, \Theta_N^0} \right\} \frac{\partial^N}{\partial I_1 \dots \partial I_N} f(\mathbf{I}, \Theta) dI_1^0 \dots dI_N^0 >> . \tag{11}$$

Using the Green-Stocks-Poincare theorem [4], we integrate the right part of Eq. (11) over $\mathbf{I}$ and Θ. Then we differentiate the obtained expressions over $\mathbf{I}^0$ and as a result we get:

$$<< \frac{\partial^N}{\partial I_1 \dots \partial I_N} f(\mathbf{I}, \Theta) >>=$$

$$= \frac{\partial^N}{\partial I_1^0 \dots \partial I_N^0} << f(\mathbf{I}, \Theta) det \left\{ \frac{\Theta_1, \dots, \Theta_N}{\Theta_1^0, \dots, \Theta_N^0} \right\} >> . \tag{12}$$

In the unidimensional case, having substituted $f(\mathbf{I}, \Theta)$ for $\frac{I^{m+1}}{m+1}$ we obtain the following relations between the moments $< I^m >$ and $< I^{m+1} >$ ($< \dots >$ we denote the averaging over Θ^0):

$$< I^m >= \frac{1}{m+1} \frac{\partial}{\partial I^0} < I^{m+1} \frac{\partial \Theta}{\partial \Theta^0} > . \tag{13}$$

By means of Eq. (13) it may be shown that there exists the following relation between $I^{\sim}$ and ΔI:

$$\Delta I = -exp \left(-\frac{I^{\sim}}{A} \frac{\partial}{\partial I^0} \right) \times \frac{I^{\sim}}{A}, \qquad A = \frac{\partial}{\partial I^0} (I^0 + \Delta I). \tag{14}$$

Let us assume again that $I^{\sim}$ is small. Then, using the theory of perturbation and expanding in a series according to $I^{\sim}$ in Eq.(14) we

can write ΔI as function of $I^{\sim}$. We find with an accuracy to $(I^{\sim})^5$:

$$\Delta I = \frac{1}{2}\frac{\partial < (I^{\sim})^2 >}{\partial I^0} - \frac{1}{6}\frac{\partial^2 < (I^{\sim})^3 >}{\partial (I^0)^2} + \frac{1}{24}\frac{\partial^3 < (I^{\sim})^4 >}{\partial (I^0)^3}$$

$$- \frac{1}{8}\frac{\partial^3}{\partial (I^0)^3} < (I^{\sim})^2 >^2 + \frac{1}{8}\frac{\partial}{\partial I^0}\left(\frac{\partial}{\partial I^0} < (I^{\sim})^2 >\right)^2 + O((I^{\sim})^5) \tag{15}$$

Therefore, in the one-dimensional case the relation (10) is correct with an accuracy to $\frac{1}{6}\frac{\partial^2}{\partial (I^0)^2} < (I^{\sim})^3 >$.

We would like to discuss the connection with the known results. An expression similar to Eq. (10) was known in stochastic dynamics [6,7]. In this case, the evolution of the dynamic system by means of the distribution function $F(\mathbf{I},t)$ is given by Fokker - Planck - Kolmogorov equation:

$$\frac{\partial F}{\partial t} = -\frac{\partial}{\partial I_i} A_i F + \frac{1}{2}\frac{\partial^2}{\partial I_i \partial I_j} B_{ij} F,$$

$$A_i = \frac{1}{T} << \delta I_i >>, \qquad B_{ij} = \frac{1}{T} << \delta I_i \delta I_j >>, \tag{16}$$

where $\delta\mathbf{I}$ is the variation $\mathbf{I}$ during T. If the dynamic system is hamiltonian, the equilibrium state is constant $F(\mathbf{I},t) = const$. The following expressions follow from this fact:

$$< \delta I >= \frac{1}{2}\frac{\partial}{\partial I} < (\delta I)^2 >, \qquad \delta I = I - I^0. \tag{17}$$

Another derivation given by Landau is based on expanding in Tailor series according to the interaction time and consequently it is correct at a small interaction time [7]. It is seen from Eq. (15) that the limit of applicability is determined by the smallness of the action variable variation and therefore it is not necessary the chaotic behavior of the motion and the smallness of the interaction time. Essentially, our result is that the nature of these relations is pure dynamical and, therefore, the range of their application is greatly extended besides stochastic dynamics, to the regular mechanics.

To use formula (10) in physic application we have to give $\mathbf{I}^{\sim}$ the concrete form. Let us assume that the Hamiltonian consist of integrable part $H_0(\mathbf{I},t)$ describing the unperturbed motion and the perturbation $H_{\sim}(\mathbf{I},\mathbf{\Theta},t)$: $H(\mathbf{I},\mathbf{\Theta},t) = H_0(\mathbf{I},t) + H_{\sim}(\mathbf{I},\mathbf{\Theta},t)$. Thus, the problems of searching for the action variation averaged over the entrance phases is reduced to relation (10), in which the value of the oscillatory part is found in the first approximation:

$$I_i^{\sim} = -\int_0^t \frac{\partial H_{\sim}(\mathbf{I}^0, \psi_i^0(\mathbf{I}^0,\xi) + \mathbf{\Theta}_i^0, \xi)}{\partial \mathbf{\Theta}_i^0}\, d\xi, \quad \psi_i^0 = \int_0^t \frac{\partial H_0(\mathbf{I}^0,\xi)}{\partial I_i^0}\, d\xi, \tag{18}$$

It is the main result to use in the next section for the analysis of the beam-plasma interaction problem.

Eqs. (10) and (18) can be generalized to consider "averaged" ponderomotive force. In this case, the oscillatory action component in Eq.(10) is found in the first order of the perturbation theory along the trajectory defined by the effective Hamiltonian:

$$H_0^{eff}(\mathbf{I},t) = H_0(\mathbf{I},t) + \frac{1}{2}\frac{\partial}{\partial I_i} \sum_{\mathbf{m}=-\infty}^{+\infty} \frac{H_{\mathbf{m}}^{\sim} H_{\mathbf{m}}^{\sim} m_i}{q_{\mathbf{m}}}, \; q_{\mathbf{m}} = \sum_{i=1}^{N} m_i \omega_i,$$

$$H_{\sim}(\mathbf{I},\mathbf{\Theta},t) = \sum_{m=-\infty}^{+\infty} H_{\mathbf{m}}^{\sim}(\mathbf{I},t) e^{i\mathbf{m}\mathbf{\Theta}}, \quad \omega_i = \frac{\partial H_0(\mathbf{I},t)}{\partial I_i}, \tag{19}$$

where $\mathbf{m}\mathbf{\Theta} = m_1\Theta_1 + \ldots + m_N\Theta_N$, m_i is the integer over which is summed.

3 The Application to the One - Dimensional Problems

3.1 The Finite Motion

We shall consider the problem of the interaction between weak varying electric field and the charged particles oscillating in potential well.

The particle motion is described by equation:

$$m\frac{d^2x}{dt^2} + \frac{dU}{dx} = -eE_{\sim}(x,t) = e\frac{\partial V(x,t)}{\partial x}, \tag{20}$$

where q is particle charge, m is particle mass, $U(x)$ is potential of the static field, $E(x,t)$ is varying electric field. The motion of the system is given by the Hamiltonian

$$H = \frac{p^2}{2m} + U(x) - eV(x,t). \tag{21}$$

Let us make transition to new canonical angle-action variables, I and Θ,:

$$\begin{aligned} I(\mathcal{E}) &= \frac{1}{\pi}\int_{x_{ref1}}^{x_{ref2}} \sqrt{\frac{2\mathcal{E} - 2U(x)}{m}}\, dx, \qquad \mathcal{E} = \frac{p^2}{2m} + U(x), \\ \Theta + \Theta^0 &= \frac{\partial}{\partial I}\int^x \sqrt{\frac{2\mathcal{E}(I) - 2U(x)}{m}}\, dx, \quad \Theta(t=0) = 0, \end{aligned} \tag{22}$$

where x_{ref1} and x_{ref2} is the coordinates of the reflection points, Θ and Θ^0 is the current and initial phases of the oscillations. As a result of the transformation the Hamiltonian acquires the following form:

$$H = \mathcal{E}(I) - eV(x(I, \Theta + \Theta^0), t). \tag{23}$$

We assume that the particles are evenly distributed in initial phases of the oscillations. Then, according to expressions (10) and (18), we find the variation of the action variable I averaged over the initial phase of the oscillations:

$$< \Delta I >= \frac{e^2}{2}\frac{\partial}{\partial I_0} < \left(\int_{-\infty}^{+\infty} \frac{\partial V(x(I_0, \omega_0(I)t + \Theta^0), t)}{\partial \Theta^0}\, dt\right)^2 >, \qquad \omega_0(I) = d\mathcal{E}/dI. \tag{24}$$

Using the relationship (22) of energy $\mathcal{E}$ to action variables I and periodic dependence of the coordinate x on the oscillation phase Θ

$x(I,\Theta,t) = x(I,\Theta+2\pi,t)$, we find:

$$< \Delta\mathcal{E} >= 4\pi^2 e^2 \sum_{k=1}^{+\infty} k\omega_0(\mathcal{E}) \frac{d}{d\mathcal{E}} k\omega_0(\mathcal{E}) |V_k(\mathcal{E},\omega_0(\mathcal{E})|^2,$$

$$V(x(\mathcal{E},\omega_0(\mathcal{E})t),t) = \sum_{k=-\infty}^{+\infty} \int_{-\infty}^{+\infty} V_k(\mathcal{E},\omega)\, exp(ik\omega_0(\mathcal{E})t + i\omega t) d\omega. \tag{25}$$

The expression (25) completely coincides with the expression, obtained by A.V.Gaponov *et. al.* [9]. The relation was used by these authors to analyse the induced radiation of excited oscillations and to apply in HF electronics. They have shown that the possibility of induced radiation (absorption) is defined by the relation of the natural oscillation frequency to the energy of the natural oscillations and the form of the spectrum of the varying force.

3.2 The Infinite Motion

However, if we consider interaction between the transit (not trapped) charged particles and HF forces in the presence of the static field, it is difficult to introduce canonical angle-action variables because the infinite motion of the particles takes place along coordinate, being parallel to the velocity of the particles. In this case, it is more convenient to go to description, within which this coordinate plays a role of the time and the time is a canonical variable. To do it we make the transformation described further.

Let us assume that $H(\mathbf{p},\mathbf{q},t)$ is the Hamiltonian of a system with N degrees of freedom and the periodical function of the time t, q_n is the coordinate along which the infinite motion takes place. Taking H and t into the set of the canonical variables we broad the phase space up to $N+1$ degrees of freedom: $q_{n+1} \equiv t$, $p_{n+1} \equiv -H$. As result we have the following Hamiltonian: $H_1(\mathbf{p},\mathbf{q},p_{n+1},q_{n+1},t) \equiv H(\mathbf{p},\mathbf{q},q_{n+1},t) + p_{n+1}$.

Then we reduce the phase space down to N degrees of freedom. Then p_n is a new Hamiltonian: $H \equiv p_n(p_1,q_1,\ldots,p_{n-1},q_{n-1},p_{n+1},q_{n+1},q_n)$, q_n is new time: $t \equiv q_n$. We also assume: $p_n \equiv p_{n+1} - H_1$,

$q_n \equiv q_{n+1}$. We thus have the Hamilonian, in which the coordinate describing the infinite motion plays a role of the time t and the time t is one of the canonical variables.

As an example, we shall now find the work of the HF forces $qE(x)e^{i\omega t}$ on the beam of charged particles in the presence of the static field. The Hamiltonian of this system is the same as in the previous task. However, in this case, we consider transit (not trapped) particles. Making the procedure, describing above, we go to a new Hamiltonian:

$$H = \sqrt{2m\omega(\mathcal{E} - U(x))} + eE_{\sim}(x)\cos(\Theta + \Theta^0). \tag{26}$$

In obtained Hamiltonian, the coordinate x plays the role of the time t and the particle energy in the static field, $\mathcal{E} = \frac{p^2}{2m} + U(x)$, and the normalized time, $\omega t = \Theta + \Theta^0$, is the canonical conjugate variables. Here, $\Theta^0 = \omega t(x = 0)$ is the input phase. The beam particle is evenly distributed in Θ^0, if the beam is not bunched. Then, using relations (10), (18) and assuming that the action of the HF force is weak, we can obtain the beam particle energy variation averaged over the input phases Θ^0 along the route of length L per particle [10]:

$$< \Delta\mathcal{E} >=< \mathcal{E}(L, \varphi_0, \mathcal{E}_0) - \mathcal{E}_0 >= \frac{1}{4}\frac{\partial}{\partial \mathcal{E}_0}|I_{\sim}|^2,$$

$$I_{\sim} = \int_0^L eE_{\sim}(x)e^{i\Theta_0(\mathcal{E}_0, x)}dx, \tag{27}$$

$$\Theta_0(\mathcal{E}_0, x) = \omega\int_0^x \frac{dx}{V(\mathcal{E}_0, x)}, \quad \mathcal{E}_0 = \frac{mV^2}{2} + U(x).$$

According to Eq. (18) the Eq. (27) can be generalized for the nonlinear field regime. In the calculation of $\Theta_0(\mathcal{E}, x)$ it suffices to take into account the averaged ponderomotive force. I.e. $V(\mathcal{E}_0, x)$ may be determined from the following energy conservation law:

$$\mathcal{E}_0 = \frac{mV^2}{2} + U(x) + \frac{e^2E_{\sim}^2}{4m\omega^2}. \tag{28}$$

For an arbitrary beam energy distribution function $f(\mathcal{E}_0)$ the dissipating power is expressed through:

$$Q = \int_{-\infty}^{+\infty} \frac{1}{2m} n_b < \Delta\mathcal{E}(\mathcal{E}_0) > f(\mathcal{E}_0) d\mathcal{E}_0. \qquad (29)$$

It is seen from Eq. (29) that sign of Q depends on the sign of $\Delta\mathcal{E}$.

The application condition of Eqs. (27) is the weakness of the beam bunching due to the action of the HF force. It means the following. An electron travels a distance without the action of HF force. The transit time is changed under the effect of the HF force. Then, Eqs. (27) are correct when the periodic component of this transit time variation is much smaller than a period of the HF force.

3.3 A Problem of Beam - Plasma Interaction

The interaction between a charge particle beam and HF field in the presence of an inhomogeneous static field in general case has not been considered analytically. This is due to the following fact. Usually, the expression for the beam current is obtained from Vlasov equation by means of the perturbation theory and it is the double integral. Consequently, the expression for beam work is the triple integral that is very difficult for analytic analysis [8]. However, as we show in Eqs. (27), this expression can be transposed to a more compact form, where it is necessary to take only one integral $I_\sim$. Moreover, since it is proportional to the derivative of $|I_\sim|^2$ with respect to the initial energy $\mathcal{E}_0$ the search of dumping (pumping) zones reduce to the search of increasing (decreasing) region of $|I_\sim(\mathcal{E}_0)|^2$. It allows us to analyze the beam-plasma interaction problem in more detail.

It has been shown in experiments [10, 11] that clusters of Langmuir oscillations with a monotonically decaying spatial Fourier spectrum can be easily excited by electron beams both in the layers adjacent to an electrode and in the region of plasma resonance. At the same time, it is well known that in the framework of the traditional model of Landau damping of plasma waves, the similar fields damp due to the interaction with beams having an arbitrary distribution function. Indeed, when a monoenergetic electron beam with

the initial velocity V passes through an HF field cluster $E(x,t) = E_{\sim}(x)\sin(\omega t)$, time-averaged work at the beam is described by the relation:

$$< \Delta\mathcal{E} >= -\frac{e^2\omega}{4mV^3}\frac{\partial}{\partial k}|E_k|^2, \quad k = \frac{\omega}{V}, \quad E_k = \int_{-\infty}^{+\infty} E_{\sim}(x)e^{ikx}dx, \tag{30}$$

where n_b is electron beam density, $< \Delta I >$ is time-averaged energy gain. This value is positive for the fields with a monotonically decreasing Fourier spectrum.

According to Eqs. (30), a stationary Langmuir soliton cannot be pumped by a monoenergetic beam with arbitrary energy [12]. The presence of the static electric field in the layers adjacent to an electrode which slows down or accelerates electrons is the most prominent feature by which the interaction of electron beams and HF clusters differs from the Landau model. The similar distinction of the interaction of the electron beams and Langmuir soliton in a cavern. This permits one to expect that even when the structure of a HF field is constant, electrons may give up their energy, since due to the presence of the static field, the time of their existence in the retarding phase can increase.

Using Eqs.(27) we will analyze the problem of interaction of the beam having the velocity V and the stationary Langmuir soliton. Unlike the previous problem where the electrons had no initial energy ($I_0 = 0$), in this case the beam electrons travel to the interaction region with some initial velocity ($V \neq 0$). Note that if in (27) we have:

$$E_{\sim}(x) = \frac{E_0}{ch(k_0x)}, \quad U(x) = \frac{U_0}{ch^2(k_0x)}, \tag{31}$$

then we can obtain an analytical result:

$$< \Delta I >= \frac{\pi^2}{4} A \frac{\partial}{\partial V} \frac{1}{ch^2\left(\frac{\pi}{2k_0} \frac{\omega}{V} \right)} \times$$

$$\times \begin{cases} \cos^2 \left[\frac{1}{2k_0} \frac{\omega}{V} arcch \left(\frac{V^2 - V_\sim^2}{V^2 + V_\sim^2} \right) \right], & \frac{V}{V_\sim} \geq 1, \\ \sin^2 \left[\frac{1}{2k_0} \frac{\omega}{V} arcch \left(\frac{V_\sim^2 - V^2}{V^2 + V_\sim^2} \right) \right], & \frac{V}{V_\sim} < 1, \end{cases} \tag{32}$$

$$A = \frac{(eE_0/k_0)^2}{mV}, \quad \frac{mV_\sim^2}{2} = U_0.$$

For the running soliton we have: $E_\sim(x) = E_0 \exp ikx/ch(k_0\xi)$, $U(x) = U_0/ch^2(k_0\xi)$, $\xi = x - V_{gr}t$ when: $k_0 \gg k$, $V \gg V_\sim$ one should substitute ω for $\omega - kV_{gr}$, V for $V - V_{gr}$ and ω/V for $\omega/V - k$ in Eq.(32).

The first relation in set (32) corresponds to the transit beams of electrons, the second one corresponds to the reflected ones. It is readily seen from here that if $U_0 = 0$, i.e. the potential energy of the static field specified by the conditions of quasineutrality is compensated by the potential of the averaged motion, we have ordinary Landau damping of a stationary soliton [12]. In the general case ($U_0 \neq 0$) the asymptotic formula of Landau damping can be applied for beams with the energies:

$$\frac{mV^2}{2} \gg \sqrt{\frac{U_0 m\omega^2}{k_0^2}}. \tag{33}$$

For the beams with the energy satisfying the inverse inequality, there exist generation zones alternating with absorption zones (see Fig.). In this case, the width of the zones diminishes, while the increment maximum (in our approximation) increases without restriction as the beam energy approaches U_0 (the minimal energy corresponding to the transit regime).

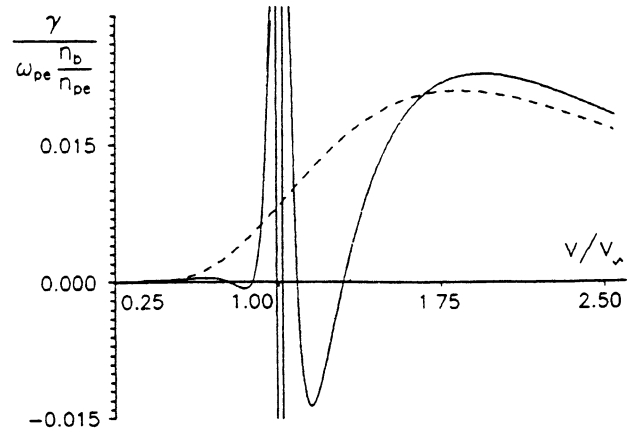

Fig. (a) The normalized increment of the stationary soliton pumping $\gamma[\omega_{pe}(n_b/n_0)]^{-1}$ a function of the normalized beam velocity $V/V_{\sim} \equiv \sqrt{mV^2/2eU_0}$, at $k_0 r_{de} \simeq 0.38$ (a solid line). (b) The same dependence for the stationary soliton in the absence of the static field $U_0 = 0$ (a dashed line)

The boundary between the generation zone and the absorption zone $I_0 \simeq kT_e$ does not depend on spatial width of the soliton. Therefore the distribution function of plasma electrons is deformed at $I_0 \simeq kT_e$ during relaxation of strong langmuir turbulence.

We would like to emphasize that unlike the Cherenkov pumping mechanism of the moving soliton [12], which is realized for sufficiently epithermal electrons, qualitatively new effects (the possibility to pump solitons) are achieved at low beam energies.

4 Example of the Many-Dimensional Problem

In this section we shall use expressions (10) and (18) for the study of a many-dimensional problem. Particularly, we shall consider the interaction between a beam of charged particles and an HF field in the presence of a smoothly inhomogeneous magnetostatic field. In detail the problem are discussed in paper [14] of this book. Here we present the main results.

Let us suppose that a charged particle beam propagates through the region of the inhomogeneous magnetostatic and the HF fields. The motion of a particle in electromagnetic fields is given by the Hamiltonian:

$$H = c\sqrt{\left(\mathbf{p} - \frac{q}{c}\,\mathbf{A}\right)^2 + m_0^2 c^2}, \tag{34}$$

where c is velocity of light, m_0 is the particle's mass of rest, q is charge of the particle and $\mathbf{A} = \mathbf{A}^0 + \mathbf{A}^{\sim}$ is the vector potential of the electromagnetic field. In our problem $\mathbf{A}^0$ is the vector potential of the magnetostatic field, $\mathbf{A}^{\sim} = \dfrac{qE^0(z)}{c}\, Re\{\mathbf{x}_0 + i\mathbf{y}_0 e^{i\omega t}\}$ is the vector potential of the HF field.

Let the "guiding center" of a "Larmor circle" move along the force lines of the magnetic field. Reducing the Hamiltonian to the necessary form [13, 14] and using relations (10) and (18) we can obtain the mean variation of the beam energy per particle in drift approximation:

$$< \Delta\mathcal{E} >= \frac{1}{16} \sum_{l=-\infty}^{+\infty} \left(\frac{\partial}{\partial \mathcal{E}^0} + l \frac{\partial}{\partial \mathcal{E}_\perp^0} \right) |F_1|^2 + |F_2|^2 \,,$$

$$F = \int_0^L qE_\perp^0(x) \frac{V_\perp(\mathcal{E}_\perp^0, x)}{V_\parallel(\mathcal{E}^0, \mathcal{E}_\perp^0, x)}\, e^{i\Theta_0(\mathcal{E}^0, \mathcal{E}_\perp^0, x)} dx,$$

$$F_2 = \int_0^L qE_\parallel^0(x) e^{i\Theta_0(\mathcal{E}^0, \mathcal{E}_\perp^0, x)} dx, \tag{35}$$

$$\Theta_0(\mathcal{E}_0, x) = \int_0^x \frac{\omega - \omega_B(\xi)}{V_\parallel(\mathcal{E}^0, \mathcal{E}_\perp^0, \xi)}\, d\xi,$$

$$V_\parallel(\mathcal{E}^0, \mathcal{E}_\perp^0, x) = \sqrt{\frac{2}{m}\left(\mathcal{E}_0 - \frac{\omega_B(x)}{\omega}\,\mathcal{E}_\perp^0\right)},$$

$$V_\perp(\mathcal{E}_\perp^0, x) = \sqrt{\frac{2}{m}\left(\frac{\omega_B(x)}{\omega}\,\mathcal{E}_\perp^0\right)},$$

where $E_{\|}^0$ and $E_{\perp}^0$ are longitudinal and tranverse (relative to the magnetic field lines) components of HF field.

More detailed analysis of expressions (34) is given in [14]. Here we adduce the main conclusions.

By analogy with the unidimensional case the term $\frac{\omega_B(z)}{\omega}\,\mathcal{E}_{\perp}^0$ plays the role of "effective" potential energy. The resonance points $\omega = \omega_B(z)$ give the main contribution in the integral F. If there is one resonance point and the beam particle pass it once, the HF oscillations always damp due to the interaction with the electron beam. In order to form the generation zones of the HF field the beam particles must pass several reflection points. It is possible if the magnetostatic field has the nonmonotonic spatial profile or the beam is reflected at "magnetic mirror" for the case with the monotonic spatial profile of the magnetic field. Thus, the nonlocal nature of the beam-wave interaction plays a important role in the energy exchange.

5 Conclusions

Two main results presented here seem , in our opinion, most advanageous for application. The first is that one can write down a compact expression for the time-averaged effect variation which is calculated through perturbations of the first order. The second is that the relations obtained are of the purely dynamic origin independent of whether the arising representation of the (9) type is a dynamic or stochastic one. The main consequence of these relations exemplified by the problems considered is the possibility to control the process of energy exchange of particles with HF fields by means of introducing static fields into the interaction zone.

However, it should be noted that a number of the points interesting applications remained beyond the scope of our consideration. To some extent this is caused by the fact that application of some relations (of the (12) type in the multi-dimensional problem) is not yet completely clear. On the other hand, one can make a note of some clear problems that have not been solved yet, though. That is, first of all, the quasi-linear theory of particle beam interaction with

many clusters with static fields and ponderomotive forces taken into account. Another group of questions is connected with application of the results obtained to wave interactions, etc.

In a more general aspect we are of the opinion that the research should go on to investigation of the possibility to obtain useful generally physical results based on the Poincare's invariants for Hamiltonian systems.

Appendix A

Let us assume that $\mathbf{I}^{\sim}$, $\Theta^{\sim}$ and their derivatives are small. Then we can develop the theory of perturbation. For convenience, we multiply $\mathbf{I}^{\sim}$, $\Theta^{\sim}$ by factor μ which will equal unity in the final results. Using the relations for the Lagrange brackets (4–6) we can obtain some useful expressions.

1) We average Eq. (4) over all Θ_i^0. As a result we obtain:

$$\Delta I_i = -\mu^2 \sum_{j=1}^{N} << I_j^{\sim} \frac{\partial \Theta_j^{\sim}}{\partial \Theta_i^0} >> . \tag{36}$$

2) We multiply Eq. (4) by $I \sim_k$ and average over all Θ_i^0:

$$\begin{aligned} &<< I_k^{\sim} \frac{\partial I_i^{\sim}}{\partial I_j^0} >> + << I_k^{\sim} \frac{\partial \Theta_j^{\sim}}{\partial \Theta_i} >> + \\ &+ \sum_{m=1, m \neq k}^{N} \frac{\partial \Delta \Theta_m}{\partial I_j^0} << I_k^{\sim} \frac{\partial I_m^{\sim}}{\partial \Theta_i^0} >> + O(\mu) = 0. \end{aligned} \tag{37}$$

3) We multiply Eq. (4) on $\Theta_k^{\sim}$ and average over all Θ_i^0:

$$<< \Theta_n^{\sim} \frac{\partial I_j^{\sim}}{\partial \Theta_i^0} >> - << \Theta_n^{\sim} \frac{\partial I_i^{\sim}}{\partial I_j} >> + O(\mu) = 0. \tag{38}$$

4) We average Eq. (6) over all Θ_i^0:

$$\frac{\partial \Delta \Theta_j}{\partial I_i^0} - \frac{\partial \Delta \Theta_j}{\partial I_i^0} + O(\mu^2) = 0. \tag{39}$$

5) We multiply Eq. (5) on $I_k^{\sim}$ and average over all Θ_i^0:

$$<< I_k^{\sim} \frac{\partial I_j^{\sim}}{\partial \Theta_i^0} >> + << I_k^{\sim} \frac{\partial I_i^{\sim}}{\partial \Theta_j^0} >> + O(\mu) = 0. \qquad (40)$$

Inserting Eq. (36) into Eq. (35) we find:

$$\Delta I_i = \mu^2 \sum_{j=1}^{N} << I_j^{\sim} \frac{\partial I_i^{\sim}}{\partial I_j^0} >> +$$

$$+\mu^2 \sum_{j=1}^{N} \sum_{m=1, m\neq k}^{N} \frac{\partial \Delta \Theta_m}{\partial I_j^0} << I_j^{\sim} \frac{\partial I_m^{\sim}}{\partial \Theta_i^0} >> + O(\mu). \qquad (41)$$

Using Eqs. (36) and (37) expression (41) can be reduced to the following form:

$$\Delta I_i = \frac{1}{2}\mu^2 \frac{\partial I_i^{\sim}}{\partial I_j^0} << I_j^{\sim} I_i^{\sim} >> + \frac{1}{2}\mu^2 \sum_{j=1}^{N} \sum_{m=1, m\neq i}^{N} \frac{\partial \Delta \Theta_m}{\partial I_j^0} \times$$

$$<< I_i^{\sim} \frac{\partial I_m^{\sim}}{\partial \Theta_j^0} >> + \frac{1}{2}\mu^2 \sum_{j=1}^{N} \sum_{m=1, m\neq j}^{N} \frac{\partial \Delta \Theta_m}{\partial I_j^0} << I_j^{\sim} \frac{\partial I_m^{\sim}}{\partial \Theta_i^0} >> + O(\mu^3) \qquad (42)$$

The next to last addendum in Eq. (42) can be transported to the form:

$$\frac{1}{2}\mu^2 \sum_{j=1}^{N} \sum_{m=1, m\neq i}^{N} \frac{\partial \Delta \Theta_m}{\partial I_j^0} \left(<< I_i^{\sim} \frac{\partial I_m^{\sim}}{\partial \Theta_j^0} >> - << I_i^{\sim} \frac{\partial I_m^{\sim}}{\partial \Theta_j^0} >> \right) +$$

$$\frac{1}{2}\mu^2 \sum_{m=1, m\neq i}^{N} \frac{\partial \Delta \Theta_m}{\partial I_i^0} << I_i^{\sim} \frac{\partial I_m^{\sim}}{\partial \Theta_i^0} >> . \qquad (43)$$

Then, according to Eq. (39) this addendum is term of order $O(\mu^4)$. Similarly, it can be shown from Eq. (39) that the last addendum in Eq. (42) is the term of the order $O(\mu^3)$. Finally we have:

$$<< \Delta I_i >> = \frac{1}{2}\mu^2 \sum_{j=1}^{N} \frac{\partial}{\partial I_j^0} << I_j^{\sim} I_i^{\sim} >> + O(\mu^3). \qquad (44)$$

Appendix B

Let us consider the following form:

$$H = H_0(\mathbf{I},t) + H_\sim(\mathbf{I},\Theta,t),$$

$$H_\sim(\mathbf{I},\Theta,t) = \sum_{m=-\infty}^{+\infty} H^\sim_{\mathbf{m}}(\mathbf{I},t)e^{i\mathbf{m}\Theta}, \tag{45}$$

where $\mathbf{m}\Theta = m_1\Theta_1 + \ldots + m_N\Theta_N$ and n is the integer, over which summation is taken. As usual, we introduce a small factor μ before $H_\sim$, which will equal 1 in final results. Let us develop the formal theory of perturbation [7]. We make transition to new canonical variables $\mathbf{P},\mathbf{Q}$ by means of generating function:

$$S(\mathbf{P},\Theta,t) = \mathbf{P}\Theta + \mu S_1(\mathbf{P},\Theta,t),$$

$$S_1(\mathbf{P},\Theta,t) = i\sum_{\mathbf{m}=-\infty}^{+\infty} \frac{H^\sim_{\mathbf{m}}(\mathbf{I},t)}{q_{\mathbf{m}}}\, e^{i\mathbf{m}\Theta}, \quad \omega_i = \frac{\partial H_0(\mathbf{P},t)}{\partial P_i}, \tag{46}$$

$$q_{\mathbf{m}} = \sum_{i=1}^{N} m_i\omega_i.$$

The old action variables are defined by the relations:

$$I_i = P_i + \mu\frac{\partial S_1(\mathbf{P},\Theta,t)}{\partial\Theta_i}, \quad Q_i = \Theta_i + \mu\frac{\partial S_1(\mathbf{P},\Theta,t)}{\partial I_i}. \tag{47}$$

The old canonical variables to accuracy in μ^2 are given by equations:

$$I_i = P_i + \mu\frac{\partial S_1(\mathbf{P},\mathbf{Q},t)}{\partial Q_i} - \mu^2\frac{\partial^2 S_1}{\partial Q_i\partial Q_j}\frac{\partial S_1}{\partial I_j} + O(\mu^3),$$

$$Q_i = \Theta_i - \mu\frac{\partial S_1(\mathbf{P},\mathbf{Q},t)}{\partial I_i} + \mu^2\frac{\partial^2 S_1}{\partial I_i\partial Q_j}\frac{\partial S_1}{\partial I_j} + O(\mu^3). \tag{48}$$

Let us find the Hamiltonian in the new canonical variables $\mathbf{P},\mathbf{Q}$. We get:

$$\bar{\mathrm{H}}(\mathbf{P},\mathbf{Q},t) = H(\mathbf{I}(\mathbf{P},\mathbf{Q},t),\Theta(\mathbf{P},\mathbf{Q}),t) + \mu\frac{\partial S_1}{\partial t}. \tag{49}$$

Expanding the right part of Eq. (49) in series according to μ we have a new Hamiltonian:

$$\bar{\mathrm{H}}(\mathbf{P},\mathbf{Q},t) = \bar{\mathrm{H}}_0(\mathbf{P},t) + \bar{\mathrm{H}}_{\sim}(\mathbf{P},\mathbf{Q},t),$$

$$\bar{\mathrm{H}}_0(\mathbf{P},t) = H_0(\mathbf{P},t) + \frac{1}{2}\frac{\partial}{\partial P_i}\sum_{\mathbf{m}=-\infty}^{+\infty}\frac{H_{\mathbf{m}}^{\sim}H_{\mathbf{m}}^{\sim}m_i}{q_{\mathbf{m}}} + O(\mu^3), \tag{50}$$

$$\bar{\mathrm{H}}_{\sim}(\mathbf{P},\mathbf{Q},t) = \sum_{\mathbf{m}=-\infty}^{+\infty}\frac{e^{i\mathbf{m}\Theta}}{q_{\mathbf{m}}}\frac{\partial}{\partial t}H_{\mathbf{m}}^{\sim}.$$

Let us apply to $\bar{\mathrm{H}}(\mathbf{P},\mathbf{Q},t)$ Eqs. (10,18) to obtain the variation $\mathbf{P}$ averaged over all Q_i^0:

$$<< \Delta I_i >>= \frac{1}{2}\frac{\partial}{\partial I_j^0} << I_j^{\sim} I_i^{\sim} >>,$$

$$I_i^{\sim} = -\int_0^t \frac{\partial H_{\sim}(\mathbf{I}^0,\psi_i^0(\mathbf{I}^0,\xi)+\Theta_i^0,\xi)}{\partial\Theta_i^0}\,d\xi, \quad \psi_i^0 = \int_0^t \frac{\partial\bar{\mathrm{H}}_0(\mathbf{P}^0,\xi)}{\partial P_i^0}\,d\xi. \tag{51}$$

Integrating by parts $\mathbf{P}^{\sim}$ and taking into account the relations between $\mathbf{P}$ and $\mathbf{I}$, finally we have:

$$\psi_i^0 = \int_0^t \frac{\partial H_0^{eff}(\mathbf{P}^0,\xi)}{\partial P_i^0}\,d\xi,$$

$$H_0^{eff}(\mathbf{I},t) = \bar{\mathrm{H}}_0(\mathbf{I},t) = H_0(\mathbf{I},t) + \frac{1}{2}\frac{\partial}{\partial I_i}\sum_{\mathbf{m}=-\infty}^{+\infty}\frac{H_{\mathbf{m}}^{\sim}H_{\mathbf{m}}^{\sim}m_i}{q_{\mathbf{m}}}. \tag{52}$$

In this case, ψ_i^0 is found along the trajectory defined by the effective Hamiltonian $H_0^{eff}(\mathbf{I},t)$. It is seen from Eq. (51) that H_0^{eff} go into infinity under resonance condition $q_{\mathbf{m}} = 0$.

Our research was supported by RBSF Grant No. 93-02-837 to the Institute of Applied Physics.

References

1. H.Poincare, Les Methodes Nouvelles de la Mecanique Celeste, Paris, Gauthier-Villars, 1892.
2. N.N.Bogolyubov, Yu.A.Mitropolskiy, Asymptotic methods of nonlinear oscillation theory, M.: Nauka, 1974.
3. M.D.Kruskal, Nucl.Fusion, 1962, Suppl., Pt.2, p.775.
4. V.I.Arnold, Mathematical methods of Classic Mechanics, M.: Nauka, 1977.
5. G.E.O.Giacaglia, Perturbation methods in Nonlinear Systems, N.Y., Springer-Verlag, 1971.
6. G.M.Zaslavsky, R.Z.Sagdeev, Introduction into Nonlinear Physics: from Pendulum to Turbulence and Chaos, M.: Nauka, 1989.
7. A.J.Lichtenberg, M.A.Lieberman, Regular and Stochastic Motion, Springer-Verlag, 1983.
8. V.D.Shafranov, Problems of Plasma Theory, M.: Gosatomizdat, 1963, V.3, p.3.
9. A.V.Gaponov, M.I.Petelin and V.K.Yulpatov, *Sov. Izv. Vyz., Radiofizika*, **10**, 1414, (1967).
10. G.M.Fraiman and I.Yu.Kostyukov, *Physica Scripta*, **V47**, 221, (1993).
11. Yu.Ya.Brodsky, S.I.Nechuev, Ya.Z.Slutsker, A.M.Feigin, G.M.Fraiman, *Sov. Fizika Plazmy*, **15** , 1187, (1989).
12. R.L.Stenzel, *Rev. Phys. Lett.*, **60** , 704, (1988).
13. L.I.Rudakov, *Dokl. Akad. Nauk SSSR*, **207**, 821, (1972).
14. G.M.Fraiman and I.Yu.Kostyukov, Influence of inhomogeneity of magnetic field on the cyclotron damping of plasma waves, in this book.

Frequency self-conversion of focused electromagnetic pulse producing gas ionization

V.B.Gildenburg, V.I.Pozdnyakova, I.A.Shereshevskii
Institute of Applied Physics RAS
Nizhny Novgorod Russia

The frequency of powerful electromagnetic radiation producing ionization of the medium along its propagation path, has to increase continuously due to the temporal growth of the produced plasma density [1-3]. This effect being of great interest for directed transmission and spectral conversion of intense radiation of various frequency bands was initially evaluated [4-6] and observed [7,8] only for the case of a small frequency perturbation. More general theoretical analysis predicting great ($\sim$ 100%) frequency a self-upshift on the basis of spatio-temporal geometric optics or exact solution of wave equation was carried out within the framework of a one-dimensional model [3,9,10] assuming plane wave packets with a field amplitude unchanged along a wave front. In order to elucidate the role of the front limiting and transverse focusing of the ionizing radiation, we carried out numerical simulation of two- dimensional pulse evolution. The pulse was supposed to be focused by a lens or a mirror and to have the gaussian intensity profile at the entrance into ionizable gas region.

Initial equations and approximations. Pulse electric field $\vec{E} = \vec{y}_0 E(x,z,t)$ was described by the two-dimensional wave equation

$$\frac{\partial^2 E}{\partial x^2} + \frac{\partial^2 E}{\partial z^2} - \frac{1}{c^2}\frac{\partial^2 E}{\partial t^2} = \frac{4\pi e^2}{mc^2} NE \qquad (1)$$

Here N is free electron density, e and m are the charge and the mass of the electron respectively, c is the light velocity, t is the time, x and z are transverse and longitudinal (in relation to the pulse propagation direction) Decart coordinates respectively; electric field is perpendicular to the plane (x,z). As the main mechanism of gas breakdown, we consider the direct (tunnel) ionization of atoms by the wave electric field. The conditions of the ionization rate $\partial N/\partial t$ is instantaneously following the field variations $E(x,z,t)$ was assumed to be fulfilled

$$W \gg I,\ \gamma \gg \omega \tag{2}$$

where $W = e^2E^2/4m\omega^2$ is the averaged oscillatory motion energy of the free electron in the field with a characteristic frequency ω, $I = h\gamma$ is the potential of atom ionization, γ is the proper frequency of the bound electron in atom, h is the Planck constant. This conditions permit us to use the known static expression for the ionization rate $\partial N/\partial t$ [11,12] at each moment of time

$$\frac{\partial N}{\partial t} = \gamma N_m \exp\left(-\frac{E_a}{\mid E(x,z,t) \mid}\right) \tag{3}$$

where $E_a = 4(2mI^3)^{1/2}/3he$ is characteristic atomic field, N_m is the gas atom density that is supposed to be constant.

At time moment $t = 0$, the following initial conditions were set:

$$N = 0,\ E = F(x,z),\ \partial E/\partial t = G(x,z) \tag{4}$$

The functions $F(x,z), G(x,z)$ were chosen so that the wave packet, at the absence of ionization ($\gamma = 0$), moves in $+z$ direction, forming in some time $t = t_0$ the focused pulse of finite length l with the center at the point $x = z = 0$ and with Gaussian transverse profile:

$$E(x,z,t_0) = A(x,z) = \begin{cases} E_0 \sin kz \exp\left(-\frac{x^2}{2x_0^2}\right), & \text{if } \mid z \mid < l/2 \\ 0, & \text{otherwise} \end{cases} \tag{5}$$

Here E_0 is the maximum field amplitude, x_0 is the minimal effective transverse dimension of the pulse, $k = \omega_0/c$, ω_0 is the initial

(undisturbed) carrier frequency. The functions $F(x,z)$, $G(x,z)$ were found, on the ground of the time reversibility of the field equation solution in vacuum, by the numerical integration of equation 1 with $N \equiv 0$ at the initial conditions:

$$E(x,z,-t_0) = 2A(x,z),\ \partial E/\partial t(x,z,-t_0) = 0. \qquad (6)$$

In the solution obtained, we then cut off the part representing the pulse propagating in $+z$ direction and changed the sign of the time derivative $\partial E/\partial t$ at $t = 0$. At the boundaries of calculation interval ($z = \pm z_1, x = \pm x_1$) the boundary conditions were set to correspond to the periodical continuation of the solution.

Some results of numerical integration of the equation sistem 1, 3 are presented, in dimensionless variables $x \to kx$, $z \to kz$, $t \to \omega_0 t$, $E \to E/E_a$, $N \to N/N_c$ ($N_c = m\omega_0^2/4\pi e^2$), by Figs. 1 - 3 for the parameter values: $E_m = E_0/E_a = 0.5$, $kl = 6\pi$, $kx_0 = 6$, $kz_1 = 120$, $kx_1 = 60$, $\omega_0 t_0 = 60$, $\gamma_m = \gamma N_m/\omega_0 N_c = 5$. Figs.1 and 2 show the spatial distributions of the field and the electron density at different time moments; Fig. 3 shows the time spectrum of the field at the point $x = 0$, $z = 25$. The main conclusions from the results obtained are as follows:

1. We demonstrated by numerical simulations the effect of a frequency self-up-conversion for the focused (two-dimensional) electromagnetic pulse. The maximal frequency up-shift achieves, in our simulations, approximately 50% .

2. We found the specific plasma distribution in the ionization wave accompanying the focused wave packet. The maximum of plasma density in this wave was near the critical value N_c defined by the initial pulse frequency.

3. We found that the frequency self-conversion in a focused pulse is accompanied by distortion of its regular wave front and transverse structure. Probably, this distortion increases for more sharp focusing of the pulse and higher ionization rate.

This work was fulfilled with financial support of the Russian Foundation of Fundamental Investigations, project 93-02-843.

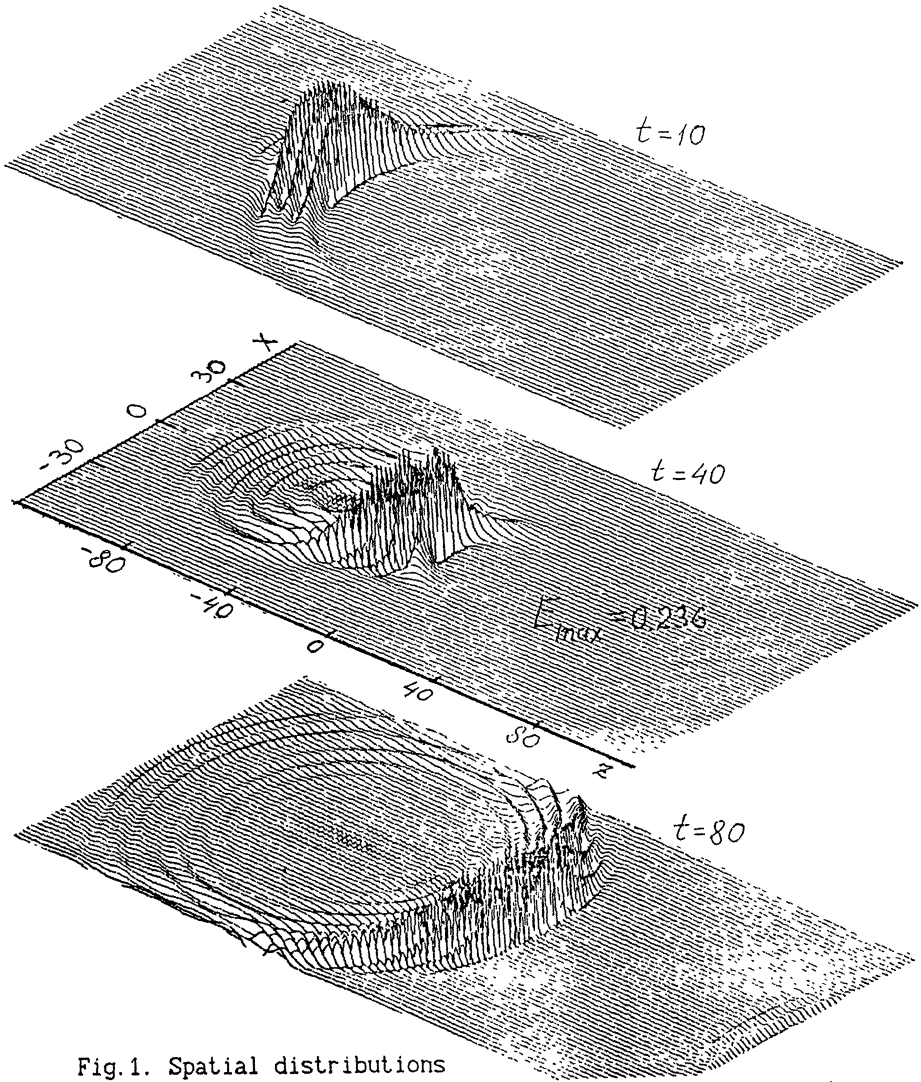

Fig. 1. Spatial distributions of the wave electric field at different time moments

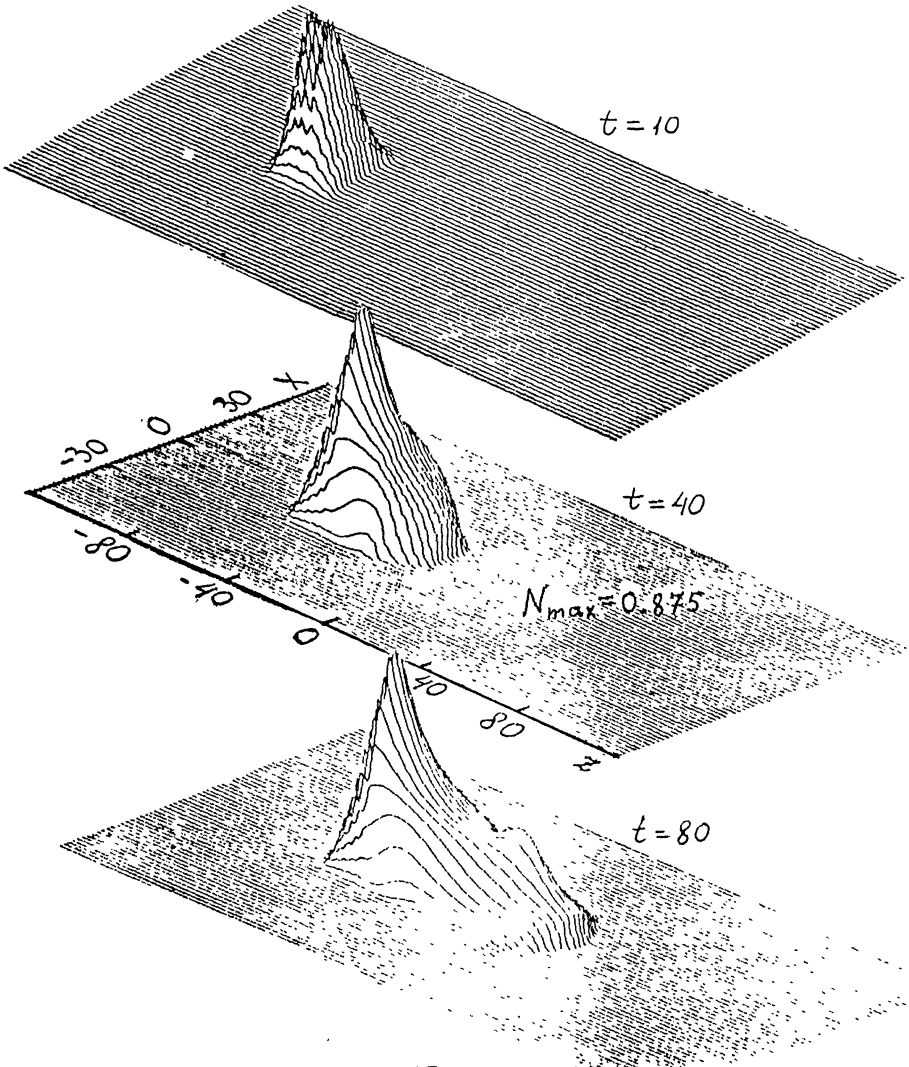

Fig.2. Plasma density distributions in the breakdown wave

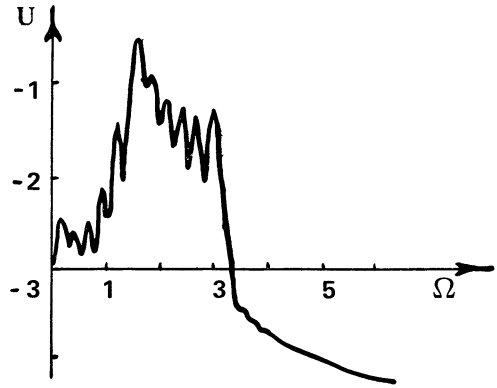

Fig. 3. Time spektrum of the field E_ω at the point $x = 0$, $z = 0$, $U = \log(E_\omega / E_0)$; $\Omega = \omega / \omega_0$

References

1. N.S.Stepanov. Izv. VUZ-ov, Radiofizika, v.19, p.960, 1976.
2. Y.A.Kravtsov and Y.I.Orlov. Geometrical optics of nonhomogeneous media. Moscow: Nauka, 1980.
3. V.B.Gildenburg, A.V.Kim, V.A.Krupnov et al. IEEE Trans. on Plasma Science, v.21, N 1, p.34, 1993.
4. E.Yablonovitch. Phys.Rev., v.10, p.1888, 1974.
5. P.B.Corcum. IEEE J. Quant. Electron., v.QE-21, p.216, 1985.
6. V.T.Platonenko and V.D.Taranukhin. Izv.Akad.Nauk SSSR, ser. Fizika, v.50, p.786, 1986.
7. S.P.Kuo, Y.S.Zhang, and A.Ren. Phys.Lett.A, v.150, p.92, 1990.
8. W.M.Wood, C.W.Siders, and M.C.Downer. Phys.Rev.Lett., v.67, p.3523, 1991.
9. V.B.Gildenburg, V.A.Krupnov, and V.E.Semenov. Pis'ma Zh.Tekh. Fiz., v.14, p.1695, 1988 [Sov.Tech.Phys.lett., v.14, p.738, 1988].
10. V.B.Gildenburg, A.V.Kim, and A.M.Sergeev. Pis'ma Zh.Eksp. Teor. Fis., v.51, p.91, 1990 [JETP Lett., v.51, p.104, 1990].
11. L.D.Landau and E.M.Lifshitz. Quantum mechanics, 3rd ed., Oxford: Pergamon, 1977.
12. L.V.Keldysh. Zh.Exp.Teor.Fis., v.47, p.1945, 1964 [Sov.Phys. JETP, v.20, p.1307, 1965].

EXPERIMENTAL INVESTIGATION OF MILLIMETER WAVE PHASE CONJUGATION VIA FOUR-WAVE MIXING IN NONLINEAR MEDIA

N.A. Bogatov, M.S. Gitlin, S.V. Golubev,
A.G. Litvak, A.G. Luchinin
Institute of Applied Physics RAS, Nizhny Novgorod, Russia
G.S. Nusinovich
University of Maryland, College Park, MD 20742, USA

An interest has recently arisen for investigations of phase conjugation (PC) via millimeter wave degenerate four-wave mixing (DFWM) in nonlinear media [1,2]. Possible application of millimeter wave PC is real-time correction of image distortions caused by deformations and manufacture imperfections of antennas, atmospheric refraction and scattering by earth surface, etc. The process of PC via DFWM in inertial nonlinear media can be easily understood in analogy with real-time holography [3,4]. DFWM implies that two quasi-plane counter-propagating pump waves (forward pump wave f and backward pump wave b) and the third, signal wave s of identical frequencies interact within a nonlinear medium and generate the wave c phase-conjugate to the signal wave. This method of phase correction is widely used in optics [3,4]. Besides compensation of phase distortions in transparent inhomogeneous media, DFWM can be used for amplification and generation of millimeter waves, control of spatio-temporal structure of wave fields, interferometry, nonlinear spectroscopy, etc. [3,4].

In spite of practical importance of realizing DFWM on the real-

time scale, four-wave mixing has not been yet experimentally demonstrated in the millimeter wave region. The most complicated problem is the search for, or creation of a suitable nonlinear medium. In papers [1,5] artificial Kerr media were proposed as nonlinear media for microwave and millimeter wave DFWM. Phase conjugation of centimeter waves in such nonlinear media was later demonstrated in [6]. Unfortunately, artificial nonlinear media have slow response time ($\geq 1s$), therefore, generally they cannot be used for PC of centimeter or millimeter waves on the real-time scale.

We proposed to use for DFWM of millimeter waves the gases, whose mechanism of nonlinearity is caused by power saturation of the rotational transition of dipole molecules [2,7]. Such nonlinear media are most efficient in the short millimeter and submillimeter region, where dipole molecules have strong rotational absorption lines. Advantageous features of such nonlinear media are their being easy to produce, convenient to use, and fast response time.

Among the gases with strong absorption lines in the millimeter wave region, one of the most convenient gases for experimental investigation of DFWM is carbonyl sulphide (OCS). A linear molecule of OCS has relatively low chemical activity, and has a simple rotational spectrum [8]. When gas pressure is $P > 1$ Torr, rotational lines of OCS are homogeneously broadened. The profile of the spectral line in this case is described by the Lorentz function g, whose width, when the gas is affected by a sufficiently strong and near to the resonance electromagnetic field, is determined both by collisions of molecules, and power saturation [8,9]:

$$g\,(\nu-\nu_0,\ I/I_{sat}) = \frac{T_2}{\pi}\left[4\pi^2 T_2^2(\nu-\nu_0)^2 + (1+I/I_{sat})\right]^{-1}\ , \qquad (1)$$

where ν is radiation frequency, ν_0 is resonance frequency of the rotational transition, I is intensity of the electromagnetic radiation, and I_{sat} is saturation intensity of the rotational transition, equal to [9]

$$I_{sat} = \frac{3\,\varepsilon_0 c}{4}\ \frac{\hbar^2(2J''+1)(2J''+3)}{T_1 T_2\,\mu^2(J''+1)^2}\ ; \qquad (2)$$

here T_2 and T_1 are transverse and longitudinal relaxation times, respectively (T_1 and T_2 are in direct proportion to temperature of the gas T and in inverse proportion to pressure P [8,10]), J'' is rotational quantum number in the lower state, μ is dipole momentum of the OCS molecule, and ε_0 is dielectric susceptability of vacuum. In the range from 150 to 200 GHz the weak-field absorption coefficient at the center of rotational lines of OCS α_0 at gas temperature $T \approx 200$K is from 0.02 to 0.05cm^{-1} [8]; it permits one to experimentally realize the situation, when optical thickness of the gas at resonance frequencies of rotational transitions is sufficiently high: $\alpha_0 L \geq 1$.

Resonant DFWM in saturable-absorbing media under the condition of homogeneous line broadening was theoretically investigated in [11,12,13,14]. It has been shown that when $\alpha_0 L \sim 1$ the maximal phase-conjugate reflectivity is $R_c \sim 1\%$, and the maximum of reflection is achieved when input intensities of the pump waves I_0 are approximately equal to I_{sat}, and when radiation frequency is tuned to the center of the rotational line, $(\nu - \nu_0) < \Delta\nu_L = (2\pi T_2)^{-1}$.

In order to observe and investigate DFWM of millimeter waves in OCS an experimental set-up was made, whose scheme is given in Fig. 1. A gyrotron with pulsed magnetic field [15] produced by a water-cooled solenoid was used as a source of powerful millimeter wave radiation ($\lambda < 2$ mm). Gyrotron pulse duration was 40μs, pulse repetition rate, 0.1 Hz. Radiation power at the frequency corresponding to the center of the chosen rotational line, was 30kW. Gyrotron radiation was converted into a quasi-Gaussian beam with a parabolic reflector and a diaphragm *D1* made of a millimeter wave absorber.

Metal mirror *M1* was used to direct the pump wave into a metal vacuum chamber (with internal diameter 18 cm and length $L_{ch} =$ 30cm) through a plane-parallel quartz window. The polished surface of the chamber back wall served as a plane mirror *M2* ($R = 100\%$) set perpendicularly to the incident pump beam and was to form the backward pump beam. The chamber was filled with gaseous OCS, whose pressure within the chamber was measured with mechanical and oil pressure gauges. The chamber was placed in a thermostat and cooled with dry ice to the temperature $\approx$ 200K to increase resonance absorp-

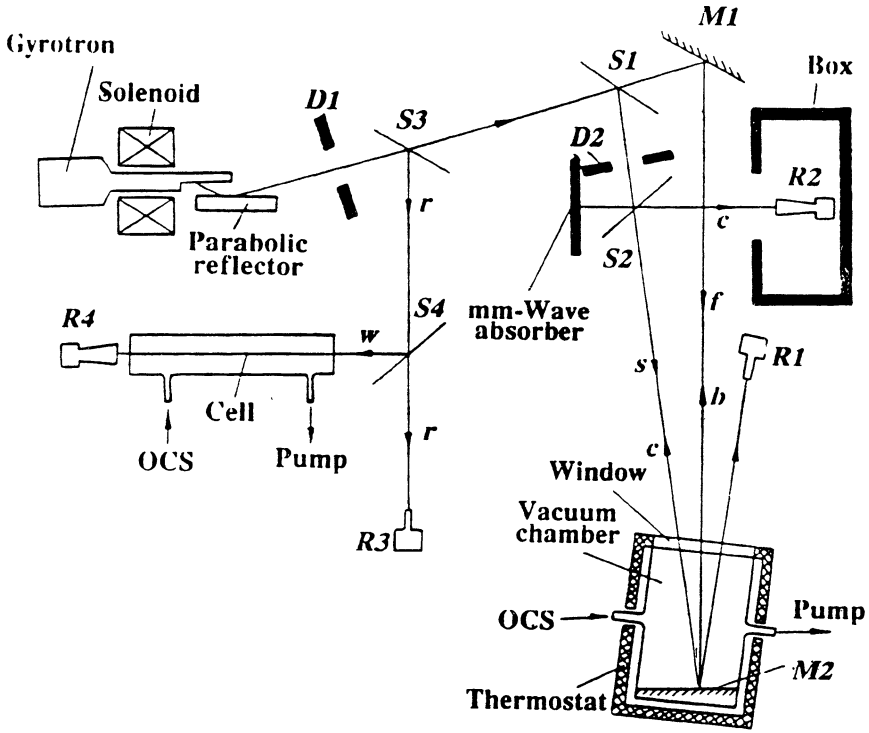

Figure 1: Experimental set-up

tion. Signal beam s was directed into the chamber at the angle 6° to the pump beam f. The signal beam was formed by means of beam splitter $S1$ (a plane-parallel quartz plate with reflection coefficient 50%), and diaphragm $D2$, 60mm in diameter. Within the chamber, at the boundary of the gaseous meduim, the ratio of intensities at the maximums of the pump and signal beams was approximately 1.5, and their widths (full-widths half-maximums) were 7.5 and 6.5 cm, respectively. Optical axes of the signal and pump beams were crossed at the surface of mirror *M2*, hence the length of the wave interaction volume was approximately equal to the doubled length of the vacuum chamber: $L \approx 2L_{ch} = 60$cm. After double pass through the chamber, the signal wave reached receiving system *R1*. The reflected wave resulting from DFWM in gas, was directed to receiving system *R2* by plane-parallel quartz plate *S2* with reflection coefficient 15%; system *R2* was placed in a box made of a millimeter wave absorber. Beam r was branched from the main beam with a mylar-film beam splitter *S3* (reflection coefficient 7%). It was directed to receiving system *R3* and used to control the regime of gyrotron operation and radiation power in each pulse. Beam r was split with a mylar-film beam splitter *S4* (reflection coefficient 7%) and the obtained beam w passed through a cylindrical quartz cell filled with OCS at the temperature 300K, and then reached receiving system *R4*. The internal diameter of this cell was 8cm, and length $L_c = 40$ cm. Since power saturation of the rotational transition in OCS does not occur when the weak beam w propagates through the gas in the cell, this beam was used to measure the radiation frequency detuning from the center of the rotational line. As receiving systems *R1*, *R2*, *R3*, *R4*, we used mm-wave packaged diodes, at whose input there was set either a section of a rectangular waveguide for the two-millimeter region (*R1*, *R3*) or a horn rectangular antenna (*R2*, *R4*), in dependence on the intensity of the received wave.

The wavelength of gyrotron radiation measured with the Michelson interferometer, proved to be 1.65 ± 0.04 mm. The rotational transition $J' = 15 \leftarrow J'' = 14$ whose resonance frequency is $\nu_0 = 182.43$GHz [8] is the closest by its frequency. For this rotational

transition line-center saturation intensity is easy to evaluate using Eq. (2); it is $I_{sat} \approx 2(PT_0/(P_0T))^2$, where I_{sat} is measured in W/cm^2; P in Torr, and T in K; $P_0 = 1$Torr, and $T_0 = 300$K. Under the experimental conditions, a pump wave intensity in the center of the beam did not exceed 300W/cm^2, therefore, noticeable saturation ($I/I_{sat} \geq 1$) of the rotational transition at $T = 200$K is possible only at $P \leq 10$Torr. Under this condition, collision halfwidth of the rotational line $\Delta\nu_L$ ($\Delta\nu_L$(MHz) $\approx 6PT_0/(P_0T)$ [8]) does not exceed 100 MHz, hence, for the condition $(\nu - \nu_0) \ll \Delta\nu_L$ to be valid, gyrotron radiation frequency tuning to the center of the spectral line with precision $\leq$ 30MHz is necessary. Such tuning was performed by selecting an approriate gyrotron cavity from a set of cavities with slightly different diameters, and by smooth frequency tuning by changing the value of magnetic field produced by the solenoid. Detuning $\delta\nu = \nu - \nu_0$ was determined by the dependence on the gas transmissivity in the cell $T_w = I_w/I_{w_0}$ for weak beam w on the gas pressure. Its intensity at the cell input was $I_{w_0} \approx 1W/\text{cm}^2$, therefore a line broadening caused by power saturation of the rotational transition by this beam at $P > 1$Torr can be neglected. In this case, according to Eq.(1) and the Bouguer-Lambert-Beer law, dependence T_w on the gas pressure has the following form:

$$T_w = \frac{I_w(P)}{I_{w_0}} = \exp\left[-\alpha_0\, L_c \left(1 + \left(\frac{\delta\nu P_0}{\Delta\nu_1\, P}\right)^2\right)^{-1}\right], \qquad (3)$$

where $\Delta\nu_1$(MHz) $\approx 6T/T_0$. From Eq. (3) it is easy to find that the function

$$Y = \left\{-\left[1 + \frac{\alpha_0 L_c}{\ln T_w}\right]\right\}^{-1/2}$$

depends linearly on the gas pressure: $Y(P) = \Delta\nu_1 \cdot P/\delta\nu \cdot P_0$. Therefore, using the dependence $T_w(P)$ given in Fig. 2 one can determine the tangent of the angle between the straight line $Y(P)$ and the horizontal axis P, and hence, find that detuning $\delta\nu$ in our experiments is about 15 MHz.

To verify that saturation influences propagation of intensive radiation with the frequency near to the OCS rotational transition frequency, we measured the pressure dependence of the signal beam transmissivity $T_s = I_s(P)/I_{s0}$ through the gas filling the vacuum chamber. The intensity of the signal wave at the entrance to the gas medium, I_{s0}, was two orders of magnitude larger than that of the beam w. The pump beam in this series of experiments was blocked by an absorbing screen behind mirror *M1*. The experimental results for two values of the gas temperature (200 K and 300 K) are given in Fig. 2. It is difficult to precisely determine the value of I_{sat} by the experimental dependences because of low accuracy of measurements of absolute values of I_{s0}, as well as of the complex structure of the field within the chamber, caused by interference of two counterpropagating and partially overlapped beams. However, these results give the opportunity to evaluate gas pressure P_{sat}, under which saturation parameter $I_{s0}/I_{sat}(P)$ equals 1. At the temperature of 200 K P_{sat} is about 10 Torr.

Measurements of transmissivity of the signal beam through the vacuum chamber at $P \gg P_{sat}$ permit us to determine double-path optical thickness of the gas at the center of the unsaturated rotational transition $\alpha_0 L$, which was equal, at $T = 200\text{K}$, 1.9 ± 0.1, and at $T = 300\text{K}$, 0.85 ± 0.05.

If the signal and pump beams were directed into the vacuum chamber simultaneously, then at pressures lower than 30Torr ($T = 200\text{K}$), movable receiving system *R2* detected a reflected wave formed by DFWM in gas. The optical path from the chamber window to the receiving system *R2* was ≈ 1.5 m. With the aid of this moving receiver we found that the reflected beam propagating towards the signal beam had horizontal width less than 5cm, their maximums coincided with experimental accuracy of $\approx$ 2cm. The fact that the reflected wave was produced by DFWM in gas was confirmed, besides the opposite direction of propagation, by disappearance of this wave when either of the two beams incidents at the gas was blocked, either by the signal beam, or the pump beam. To measure absolute value of the phase-conjugate reflectivity, receiving system *R2* was calibrated

with the aid of a mylar film mirror with thickness 10μm. During calibration this mirror was set in the place of the chamber perpendicularly to the optical axis of the signal beam, and its reflection coefficient was 0.2%.

Dependence of the phase-conjugate reflectivity, R_c on gas pressure at the temperature $T = 200$K ($\alpha_0 L = 1.9$) was experimentally investigated. The results of these measurements are presented in Fig. 3.

The reflection was maximal, with the pressure close to P_{sat}, under which the saturation parameter is optimal, and approximately equals 1. Figure 3 shows also theoretical dependence of $0.2R_c$ on relative pressure P/P_m; this dependence was derived from calculations given in [12] of the reflectivity via DFWM in a two-level saturable-absorber on the saturation parameter $I_0/I_{sat} = (P_m/P)^2$, for the case of $\alpha_0 L = 2$. Coefficient $P_m \approx 7$Torr was chosen such that positions of R_c maximums at theoretical and experimental graphs would coincide. Maximal R_c by DFWM in gas was about 0.4%. In accord with calculations in [12], when $\alpha_0 L = 2$, maximal reflectivity is $\approx 2\%$. Difference between experimental and theoretical value of the maximal reflectivity is caused, apparently, by the fact that real pump waves had limited widths, and were not plane waves, as it was assumed in [11,12,13,14].

Note that the response time of saturable-absorbing gaseous media is determined by the relaxation time of population difference of rotational levels T_1 of OCS molecules. In our case this time is less than 10^{-8}s. Due to this, such nonlinear media can be used as PC mirrors in resonators of powerful short-pulse millimeter wave generators, e.g., for FELs.

In the millimeter wave region the majority of applications of PC devices require $R_c \sim 100\%$. At short millimeter waves such a growth in R_c in saturable-absorbing gases may be provided by the increase in $\alpha_0 L$ [3]. It is possible to significantly increase both L and α_0, first realizing the DFWM in oversized waveguides [3] and second, using the gases whose linear molecules have a large dipole momentum (BrCN, ClCN, etc.) [8].

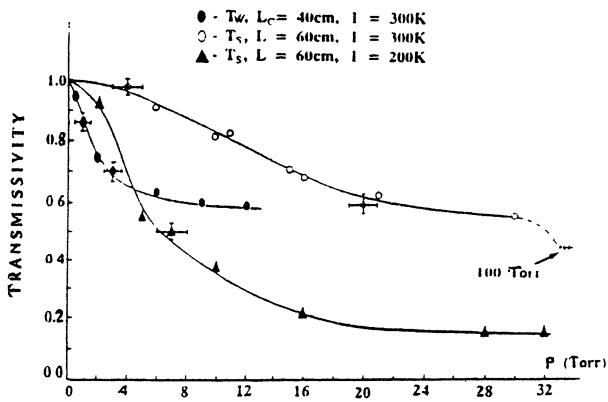

Figure 2: Dependence of transmissivity of radiation with the frequency close to the resonance frequency of the rotational transition $15 \leftarrow 14$, on the gas pressure, T_w–transmissivity of the weak beam w through gas in the quartz cell, T_s–transmissivity of the signal beam s through gas in the vacuum chamber; $I_{w0}/I_{s0} \simeq 10^{-2}$.

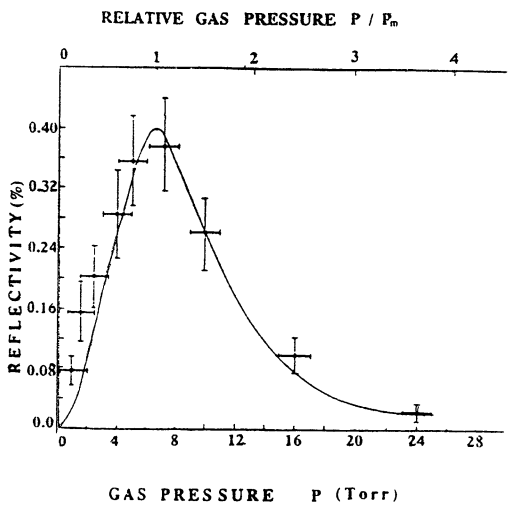

Figure 3: Dependences of phase-conjugate reflectivity on the gas pressure. The solid line shows the results of calculations of reflectivity $0.2R_c$ vs. relative pressure P/P_m.

However, such nonlinear gas media are not applicable for DFWM of the main part of millimeter wave region ($\lambda > 3$ mm), where dipole molecules have no strong rotational absorption lines. These considerations make it necessary to search for other types of nonlinear media for DFWM of middle and long millimeter waves.

In 1979 it was proposed in [16] to use completely ionized plasma (CIP) as a nonlinear media for DFWM, and showed that they become more efficient at longer wave lengths. Theoretical [17,18,19,20] and experimental [21,22,23] grounds of DFWM and nearly degenerate four-wave mixing (FWM) in CIP have been recently developed. It was shown that there are two regimes of nonlinear wave mixing in completely ionized plasmas: the first is the regime of the ponderomotive force [16] and the second is that of the thermal force [17]. The experiments [22,23] showed that CIP is a rather promising medium for centimeter wave FWM. For efficient FWM of millimeter waves it is required to use plasma with high density ($n_e \geq 10^{11}\text{cm}^{-3}$) and low electron temperature ($T_e \lesssim 1eV$) [18]. Generation of completely ionized homogeneous plasma with such parameters in the large volume ($\sim 10^3\text{cm}^3$) is a rather complicated problem. Recently we proposed to use nonequilibrium weakly ionized plasmas (WIP) as a nonlinear media for millimeter wave FWM[1], whose mechanism of nonlinearity is caused by dependence of its kinetic coefficient (generation and losses rates of charged particles, their mobility, diffusion coefficient, etc.) on electron temperature [25]. Such plasma media are easier to create and utilize than CIP, and they can have fast response time, which is determined, in dependence on the nonlinearity mechanism, by the characteristic relaxation time of electron energy distribution function or electron density. Weakly ionized plasma can be generated by millimeter waves itself or sustained by external ionization courses (visible or UV radiation, electron beam, glow and arc discharge, etc.). The first method of weakly ionized plasma generation is called a self-sustained gas discharge in the millimeter wave beams

[1]In paper [24] it was considered theoretically the possibility to use equilibrium weakly ionized plasma with dominant ionization nonlinearity for PC via DFWM in broad range from the infrared to the microwaves.

(SMWD) [26,27,28], and the second one is a non-self-sustained gas discharge in the millimeter wave beams (NSMWD) [29,30]. The use of a SMWD for millimeter wave DFWM is rather attractive because it does not require to create plasma preliminary. However, nonlinear media of such a type have several disadvantages. The dependence of the electron density on the electric field intensity in a SMWD has as a rule a "threshold character". This requires first of all the use of rather powerful pump waves whose intensity should exceed the "threshold one" [26,27] and, secondly, this imposes strict demands on the quality of pump beams (they should have practically constant intensity within their apertures). Besides, it is difficult to realize a quasistationary regime of DFWM in a SMWD, since the plasma density gratings break due to small-scale ionization instabilities [26,27]. It was supposed that a rather promising nonlinear medium for DFWM of millimeter waves can be the plasma of a nonequilibrium non-self-sustained discharge [25,31], since the use of external gas ionization permits one to produce large volume homogeneous plasma with high electron density and to realize the stable quasi stationary discharge. Due to the low electron temperature in NSMWD high nonlinearity of its high-frequency susceptibility can take place under small absolute changes of T_e and, consequently, efficient DFWM is possible with low intensity of millimeter waves.

Recently we started to develop the methods of creation of nonlinear media on the basis of nonequilibrium weakly ionized plasma [32]. In this work we consider as an example of a nonlinear medium the plasma of the non-self-sustained millimeter wave discharge in nitrogen with an admixture of oxygen, which is sustained by an external source of ionizing UV radiation, and we use this example to consider the mechanism of plasma nonlinearity connected with the dependence of the electron-ion recombination rate on electron temperature. We found the value of nonlinear high-frequency susceptability and estimated efficiency of degenerate FWM of millimeter radiation.

To evaluate nonlinear high-frequency susceptability of photoionized N_2/O_2 mixture we performed an experimental investigation of the dependence of electron density n_e on the amplitude of the wave's

electric field E_a. The scheme of the experimental set-up is shown in Fig. 4.

As a source of millimeter wave radiation with wavelength ≈ 7 mm we used a pulse gyrotron (pulse duration 40 μs). The gas was ionized in the focus region of the millimeter wave beam by means of UV radiation of an open spark discharge (pulse duration ≈ 200 μs). Electron density was determined from absorption of weak diagnostic microwave radiation with wavelength 3 cm that was propagating through the plasma along a two-wire (Lecher) line. Figure 5 shows the dependence of electron density on the density-normalized effective electric field E_e/N (here N is molecule density,

$$E_e = E_a/[2(1+\omega^2/\nu_m^2)]^{1/2}$$

is the effective electric field amplitude, ν_m is the effective transport frequency of the elastic electron-molecule collisions, and ω is circular frequency of the electromagnetic field) measured under partial pressure 215 Torr of nitrogen and 3 Torr, of oxygen. The observed variation of electron density with growth of E_e/N can be connected only with the decrease of the electron loss rate, since ionization by an electron impact plays an important role only under the value of the field that is close to the breakthrough one ($E_e/N \geq 30$ Td) [29,33]. For the value $E_e/N \leq 20$ Td and low densities of molecular oxygen ($\leq 10^{17}$ cm^{-3}), the main mechanism of electron losses is dissociative recombination of electrons and ions N_4^+, O_4^+, $N_2O_2^+$. The solid line in Fig. 5 represents the results of calculation $n_e(E_e/N)/n_e^o$, where n_e^o is density of electrons produced by the UV source in the absence of the millimeter wave; the calculation was performed using the dependences of the rate coefficient of dissociative recombination on T_e [34] and characteristic energy kT_e/e on E_e/N [35]. That part of dependence $n_e(E_e/N)$ at $0.1 \leq E_e/N \leq 5$ Td, where the variation of electron density with growth of E_e/N is sufficiently fast, can be approximated by the power law:

$$n_e(E_e/N) = n_e^o \left[\frac{E_e/N}{(E_e/N)_o}\right]^p , \qquad (4)$$

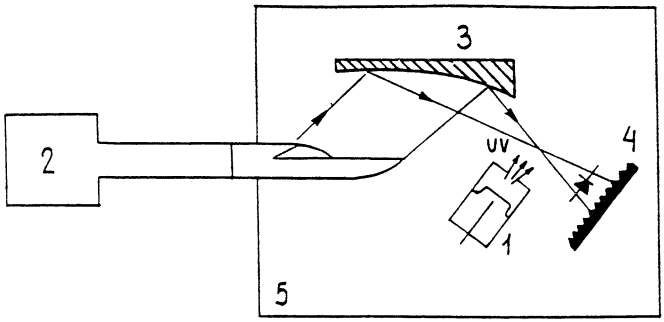

Figure 4: Scheme of the experimental set-up. 1—source of UV radiation, 2—gyrotron; 3—parabolic reflector, 4—millimeter wave absorbing screen, 5—vacuum chamber

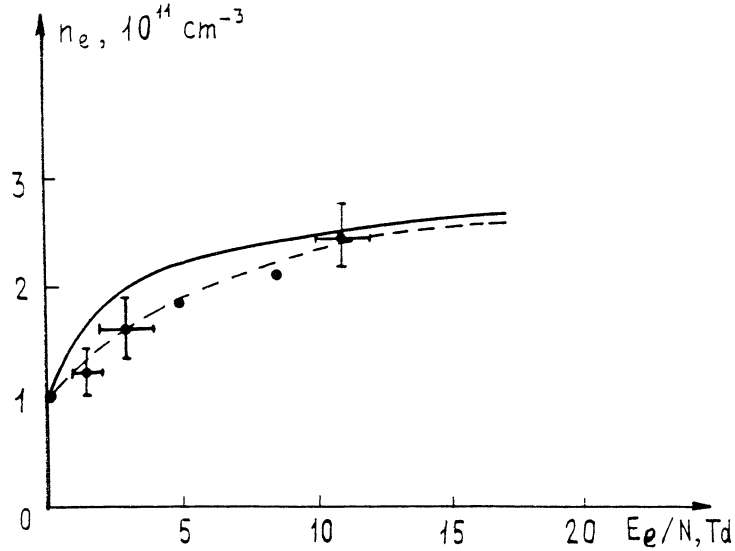

Figure 5: The dependence of electron density in a non-self-sustained mm wave discharge in N_2/ O_2 mixture on E_e/N.

where $(E_e/N)_o = 0.1$ Td, $p = 0.2$—0.25.

In this region $0.1 \leq E_e/N \leq 5$ Td the amplitude of nonlinear plasma polarization is

$$P^{NL} = \chi(|E|)E = \chi^{NL}|E|^p E; \qquad (5)$$

here χ^{NL} is nonlinear susceptability of plasma equal to

$$\chi^{NL} = \frac{n_e^o(1+i\nu_m/\omega)}{4\pi n_c(1+\nu_m^2/\omega^2)}\left[(E_e/N)_o N\sqrt{2(1+\omega^2/\nu_m^2)}\right]^{-p}, \qquad (6)$$

where $n_c = 4\pi e^2/m\omega^2$ is critical plasma density. Estimates based on relation (6) show that under the conditions of our experiments at the frequency 40 GHz nonlinear susceptability of photoionized N_2/ O_2 mixture is $|\chi^{NL}| \sim 10^{-4}$ esu.

In the case of the same linear polarization of interacting waves under condition $\omega \gg \nu_m$ within the approximation of equal and constant intensities of plane pump waves ($I_f = I_b = I = \text{const}$) the stationary PC reflection coefficient from a plasma slab with length L equals [36]

$$R = \tan^2 \beta L, \text{ where } \beta = \frac{\omega}{c} p \frac{\Gamma(\frac{p+1}{2})\sqrt{\pi}}{\Gamma(\frac{p}{2}+1)}(4I)^{p/2}\chi^{NL}; \qquad (7)$$

here Γ is the gamma-function. This relation yields that PC reflectivity of the wave with frequency 40 GHz from a photoionized N_2/O_2 slab with length 50 cm under gas pressure $\sim$ 10 Torr, initial density of electrons $n_e^o \approx 10^{11}$ cm^{-3} and intensity of pump beams $I = 15$ W/ cm^2 can be ≈ 10 %.

Response time of such a nonlinear medium is determined by the time of electron-ion recombination, which at $n_e \approx 10^{11}$ cm^{-3} is approximately equal 30 μs.

A higher electron density as compared to the discharge in N_2/ O_2 mixture can be achieved in the volume $> 10^3$ cm^3 if main gas is seeded with the vapor of a low-ionization-potential species. For millimeter wave DFWM seems very promising of using photoionization and photoresonant methods of plasma creation. In photoioniza-

tion plasma charged particles are generated by straight or step-by-step photoionization of readily ionized organic seeds, such as N,N-dimethylaniline, acetone, naphthalene, tri-n-propylamine, tetrakis-dimethylaminoethylene (TMAE), etc [37,38,39]. Sources of ionizing UV radiation can be corona or spark discharges, as well as flash lamps filled with an inert gas. Photoresonant plasma is created in vapors of metals with low ionization potential (Cs, Na, K, Hg, etc.) irradiated by resonant radiation [40,41]. The source of resonant radiation is a discharge in vapor of the same metal. Generation of charged particles in the photoresonant plasma occurs under associative, Penning or cascade ionization of the atoms of alkaline metal. These methods of plasma generation make it possible to increase the electron density up to 10^{12} cm^{-3}. At the same time, in such plasmas the electron temperature has a rather low value ($T_e < 0.3$ eV). Thus, for long millimeter waves phase conjugate reflectivity of such nonlinear media can attain the value of the order of 100%, when the pump wave intensity is of the order of 10 W/ cm^2.

References

1. Mansfield D.K., Federici J.F., Int. J. of Infrared and Millimeter Waves, 1988, v. 9, 419.
2. Bogatov N.A., Gitlin M.S., Litvak A.G. et al., Phys. Rev. Lett., 1992, v.69, 3635.
3. Optical Phase Conjugation. Ed. R.A. Fisher. New York: Academic Press, 1983.
4. Zeldovich B.Ya., Pilipetsky N.F., Shkunov V.V. Principle of Phase Conjugation. Heidelberg: Springer-Verlag, 1985.
5. Bobbs B., Shin R., Fetterman H.R., Ho W.W., App. Phys. Lett., 1988, v. 52, 4.
6. Shin R., Fetterman H.R., Ho W.W. et al., Phys. Rev. Lett., 1990, v. 65, 579.
7. Bogatov N.A., Gitlin M.S., Litvak A.G. et al., Proc. Intern. Workshop Strong Microwaves in Plasmas. Ed. A.Litvak. Suzdal, Russia, 1990, Nizhny Novgorod: IAP, 1991, v.2, 520

8. Gordy W., Cook R.L. Microwave Molecular Spectra. New York: Wiley, 1984.
9. Pantell R.H., Puthoff H.E. Fundamentals of Quantum Electronics. New York: Wiley, 1969.
10. Mäder H., Z. Naturforsch., 1979. v. 34a. 1170.
11. Brown W.P., J. Opt. Soc. Am., 1983, v. 73, 629.
12. Gruneisen M.T., Gaeta A.L., Boyd R.W., J. Opt. Soc. Am. B., 1985, v. 2, 1117.
13. Betin A.A., Dyatlov A.J., Kulagina S.N. et al., Sov. J.Quantum Electron., 1986, v. 16, 1304.
14. Abrams R.L., Lind R.C., Opt. Lett., 1978, v. 2, 94.
15. Flyagin V.A., Luchinin A.G., Nusinovich G.S., Int. J. of Infrared and Millimeter Waves, 1983, v. 4, 629.
16. Steel D.G., Lam J.F., Optics Letters, 1979, v.4, 11, 363.
17. Federici J.F., Mansfield D.K., JOSA B, 1986, v. 3, 1588.
18. Nebenzahl I., Ron A., Tzach D., Rostoker N., Phys. Fluids., 1988. v.31, 2144.
19. Postan A., Ben-Aryeh Y., J. Opt. Soc. Am. B., 1988, v. 5, 1379.
20. Goldman M.V., Williams E.A., Phys. Fluids B., 1991, v. 3, 751.
21. Kistagama Y., Savage R.L.,Jr., and Joshi C., Phys. Rev. Lett., 1989, v.62, 151.
22. Lehner T., Phys. Scripta., 1989, v.39, 595.
23. Domier C.W., Luhmann N.C.,Jr, Phys. Rev. Lett., 1992, v.69, 3499.
24. Federici J.F., Valeo E.J., Phys. Rev. A., 1991, v.44, 5158.
25. Bogatov N.A., Gitlin M.S., Golubev S.V., et al., Proc. Intern. Workshop Strong Microwaves in Plasmas. Ed. A.Litvak. Suzdal, Russia, 1990, Nizhny Novgorod: IAP, 1991, v.1, 413.
26. Vikharev A.L., Gil'denburg V.B., Golubev S.V. et al, Sov. Phys. JETP, 1988, v.67, 724.
27. Vikharev A.L., Gil'denburg V.B., Kim A.V. et al., HF Discharge in Wave Fields (in Russian). Ed. A.Litvak. Gorky: Inst. of Appl.Phys., 1988, p.41.
28. Vikharev A.L., Gil'denburg V.B., Ivanov O.A. et al., Fizika plasmy (in Russian), 1984, v.10, 165.

29. Bogatov N.A., Golubev S.V., Zorin V.G., Pis ma v ZhTF (in Russian), 1984, v.10, 271.
30. Gritsinin S.I., Kossyi I.A., Silakov V.P. et al., ZhTF (in Russian), 1977. v.57, 681.
31. Bogatov N.A., Gitlin M.S. and Golubev S.V., Proc. 20th Intern. Conf. on Phenomena in Ionized Gases, Ed. V. Palleschi and M. Vaselli. Pisa, Istituto di Fisica Atomica e Molecole, 1991, 1174.
32. Bogatov N.A., Gitlin M.S., Golubev S.V., Pis'ma v Zhurnal Tekhncheskoi Fiziki, (in Russian), 1992, v.18, 89.
33. Golubev S.V., Gritsinin S.I., Zorin V.G. et al. HF Discharge in Wave Fields (in Russian). Ed. A.Litvak. Gorky: Inst. of Appl.Phys., 1988, p.136.
34. Mitchell J.B.A., Phys. Reports, 1990, v.186, 217.
35. Dutton J., J. Phys. Chem. Ref. Data, 1975, v.4, 577.
36. Bogatov N.A., Gitlin M.S., Golubev S.V., Preprint N301, Nizhny Novgorod: Inst. Appl. Phys., 1991.
37. Levine J.S., Javan A., Appl. Phys. Lett., 1973, v.4, 55.
38. Kosinskaya I.V., Polozova L.P., Siretskaya T.V. et al., Zhurnal Prikladnoi Spektroskopii (in Russian), 1979, v.31, 536.
39. Stalder K.R., Vidmar R.J., Eckstrom D.J., J. Appl. Phys., 1992, v.72, 5089.
40. Klucharev A.N., Yanson M.L. Elementary processes in the plasma of the alkaline metals (in Russian), Moscow: Energoatomizdat, 1988.
41. Beterov I.M., Eletskii A.V., Smirnov B.M., Uspekhi Fizicheskikh Nauk (in Russian), 1988, v.155, 265.

Hamilton approach to the problem of Langumuir collapse

V.V. Gushchin, V.V. Gulenko
Department of Physics and Technology, Kharkov State University, 4, Svobody sq., 310077, Kharkov, Ukraine (CIS)

The hamilton formalism is shown to be very productive for the studies of wave collapses. It allows to consequently take into account the higher order nonlinearities, which may be very significant in the collapse dynamics.

The phenomenon of the waves self compression belongs to the number of general nonlinear effects which are appropriate to the waves of an arbitrary nature. In many cases this process continues until some energy dissipation mechanism switches on, i.e. wave collapse takes place [1]. In spite of the fact that main investigations of this phenomenon are concentrated in plasma physics [2 - 4] its universality testifies the following. The nonlinear stage of the soliton instability, the object which is being actively studied in different areas of modern theoretical physics, may lead to the development of the wave collapse [1].

Alongside with a significant generally theoretical interest to the fundamental phenomenon such as the singularity formation under the evolution of the wave perturbation in nonlinear dispersive media, it is also significant for numerous applicatious. Particularly, in a plasma, the wave collapse should be realized through different oscillation branches, defining the fate of the plasma turbulence. It exerts the significant influence on the character of the charged particles relaxation, plasma heating and on the anomalous transfer process both in laboratory and spase plasmas [2 - 5].

The Langmuir waves colapse has been studied most of all. It is enough to say that there are more than ten reviews which are devoted to this subject. The general qualitative picture of the collapse which is now more or less generally accepted, is presented now in the following way [2 - 5]. As a result of the development of a modulational instability in a plasma the cavernas (the region with a lowered density) filled by the oscilations are formed. The process of the caverna comression quickly goes to the automodel regime and the shape of the caverna attains the universal, significally flattened form. Under the process of compression the energy of oscillations which are contained in a caverna, conserves. When the minimal shape of the caverna becomes comparable with the Debye radius, the Landau damping becomes significant and the oscilations, contained in a caverna are "burned" accelerating the plasma electrons. As a result the energy is transferred to a small group of accelerated particles and the caverna which becomed empty is compressed, giving rise to the short-wave sound.

The main results which confirm such scenario are obtained in the framework of Zakharov equations [2]. However, these equations do not take into account many nonlinesr effects of higher order: electron nonlinearity, variations of the wave dispersion law, intstability saturation, hydrodynamic ion nonlinearities e.t.c. Their significance increases with the caverna compression and according to the estimates [6], all nonlinearities are to be taken into account simultaneously, and this fact makes the equations considerably more complicated. But the successive and coordinated taking into account of all the effects pursuing the aim of obtaning the simple enough "improved" dynamical equations, adequatevely describing the final stage of the collapse, seems impossible [7]. This wide-spread opinion and the limited possibilities of the analitycal solution even of Zakharov equations, lead to a necessity of numerical simulation of the problem. And this necessity is growing with the development of the computer technique.

Among the great number of the papers in this area we point out only the most advanced according to our point of view. At first, it is three-dimensional modelling of the last stage of the Langmuir cav-

erna evolution using the particles method in the framework of the kinetic description of plasma [7]. Secondly, the calculation of the three-dimensional strong Langmuir turbulence in the framework of Zakharov equations, which are supplied by dissipative terms, without the simplifuing assumption about the spatial symmetry of the problem [8]. The clear picture of the collapse is obtained in the paper [7] and in the paper [8] the strong Langmuir turbulence was shown to be supported by the nucleation effect [9] - the effect of arising of new cavernas instead of buried ones due to a catching of plasmons in the density pits, which are remained after a burying of the caverna of the previous generation.

In spite of all advantages of the numerical approach, which is of a principal importance in the theory of wave collapses, it is necessary to point out that the given calculations have mainly demonstraited character. The obtained results convincingly testify about the tendencies of the compression but remain a lot of questions. However, in the paper [7] the main deepening of the ion density pit was shown happen after the reaching of the RF field maximum. This fact probably seems to correspond to qualitative views about the impact of ions inertia in the three-dimensional case, which is capable to "compress" the caverna until the Landau damping is switched on, even under the arising of additional nonlinear mechanisms. But this qualitative view is based on the estimates which use the automodel solutions oif Zakharov equations. It is not obvious that additional nonlinearities do not change the form of the automodel solutions. It is known [6] that even a weak modification of Zakharov model, e.g. the nonlinearity saturation taking into account, leads to a possibility of existance of the stable cavitons. Secondly, the large minimal size of the caverna ($\sim$ 16 r_{de}), corresponding with the observed in laboratory experiments [10] is explained by a possible modification of the wave-particle interaction by the strong nonlinearity ($W/nT \sim 3$). But such a big exceeding of the energy density of the waves over the threschold of the modulational instability contains a danger for the caverna compression as a whole. It is obvious that it is necessary to study the dependence of the modulational increment on the per-

turbations wavelenght with higher order nonliarities and to establish the reasons of arising of such a strong damping. Due to the fact that the collapsed caverna is an elementary cell of the Langmuir turbulence, it is natural that the results of [8] have the limited range of applicability.

Therefor, the reached up to now level of understanding of the collapse dynamics is not satisfactory enough due to the fact that in general case one can not avoid the queation about the influence of higher nonlinearities on the collapse dynamics. The numerous attempts of Zakharov model variation are not satisfactory due to nonobvious assumptions or to one-dimensionless of the approach. The electron nonlinearities are the exclusions. Their taking into account and investigations are the most successive [11, 12]. However, the fact of their being insignificant probably gives a possibility to neglect the another nonlinearities.

The generalization of Zakharov equations by taking into account additional nonlinearities turns out to be the best using the Hamiltonian formalism. Really, in the framework of the latter formalism one can successively take into account all nonlinearities, and the obtained equations are formally simple and are applicable for the waves of an arbitrary physical nature. It is necessary to underline that the commonly used hamiltonian formalism [13, 14] needs in organization of general variants of canonical transforms and of transition to the normal variables. Only after this it gave the possibility to obtain the "improved" dynamical equations which have the following form

$$\frac{\partial a_k}{\partial t} + i\omega_k a_k = -i\frac{\delta \tilde{H}_{int}}{\delta a_k^*}; \qquad \frac{\partial b_k}{\partial t} + i\Omega_k b_k = -i\frac{\delta \tilde{H}_{int}}{\delta b_k^*}; \qquad (1)$$

$$\tilde{H}_{int} = \tilde{H}_3 + \tilde{H}_4 + \tilde{H}_5 + \tilde{H}_6;$$

Here $a_k \equiv a(\vec{k},t)$, $b_k \equiv b(\vec{k},t)$, $\omega_k \equiv \omega(\vec{k})$, $\Omega_k \equiv \Omega(\vec{k})$ are the complex amplitudes and dispersion laws of high-frequency (HF) and low-frequency (LF) waves respectively, and $\tilde{H}_{int}$ is a reduced interaction hamiltonian. Omitting the details due to a limited volume, let us only recall the main results (see the details in the papers [15, 16]).

The equations (1), written in the impulse $(\vec{k},\omega)$ represantation,

one can write in the coordinatee $(\vec{r}, t)$ representation, using the reverse Fourier transform. They are significally more complicated, but in the limiting cases they are transformed into all well-known equations studied in the Langmuir collapse problem. Precisely, they are transformed into Kuznetsov [11], Zakharov, statistical approximation equation and the nonlinear Shrodinger equation [2].

The estimates in the framework of equations (1) show that in $\tilde{H}_6$ there are the terms which are significant even when $W/n_0T_e < 1$, $kr_{de} < 1$, while the electron nonlinearities are significant only for $W/nT \sim kr_{de} \sim 1$.

In the framework of the analysis of the linear stage of the instability the influence of higher nonlinearities on the instability increment is established.

Introducing the positively defined value $I \equiv \int |\frac{\partial a_k}{\partial \vec{k}}|^2 d\vec{k}$ one can write the Talanov theorem in $\vec{k}$ representation with higher nonlinearities taking into account. But the interpretation of the results in this case is less obvious.

Higher nonlinearities forbid the existence of well known automodel solutions. And the search of new ones needs additional efforts.

Under the analysis of the stationary solutions, using Helder inequalities, one can prove that the hamiltonian is limited from below for the fixed plasmon number. This fact allows to make a conclusion about a possibility of existence of stable solutions.

The enumerated results prove the significant impact of higher nonlinearities on the collapse dynamics. But more deep understanding of the problem needs further investigations.

References

[1] Zakharov V.E., Usp.Fis.Nauk 1988, **155**, 529 (in Russian).

[2] Zakharov V.E. in Basic Plasma Physics,ed.Galeev A.A. and Sudan R.: Moscow: Energoatomizdat, 1984, v.2, p.79 (in Russian).

[3] Shapiro V.D. and Shevchenko V.I. ibid. p.119.

[4] Goldman M.V. Rev.Mod.Phys. 1984, **56**, 709.

[5] Gorev V.V., Kingsep A.S. and Rudakov L.I. Sov.Radiophysics 1976, **19**, 691.

[6] Dyachenko A.I., Zakharov V.V., Rubenchik A.M., Sagdeev R.Z. and Svets V.F. Zh.E.T.F. 1988, **94**, 591.

[7] Zakharov V.E., Pushkarev A.I., Rubenchik A.M. and Sagdeev R.Z. Zh.E.T.F. 1989, **96**, 591.

[8] Robinson P.A.,Newman D.L. and Goldman M.V. Phys.Rev.Lett. 1988, **61**, 702.

[9] Doolen G.D., DuBouis D.F. and Rose H.A. Phys.Rev.Lett. 1985, **54**, 804.

[10] Wong A.Y. and Cheung P.Y. Phys.Fluids, 1985, **28**, 1538.

[11] Kuznetsov E.A. Sov.Physica Plasmy, 1976, **2**, 327.

[12] Malkin V.M. Zh.E.T.F. 1986, **90**, 59.

[13] Zakharov V.E. and Kuznetsov E.A. Sov.Sci.Rev. 1984, **4**, 170.

[14] Zakharov V.E., Musher S.L., and Rubenchik A.M. Phys.Reports. 1985, **129**, 285.

[15] Gulenko V.V. and Gushchin V.V. Doklady Acad.Sci.Ukraine 1994, N3, N4, N5.

[16] Gulenko V.V. and Gushchin V.V. Ukr.Fiz.Zh. 1994, 39, N4.

DETECTION OF HF SIGNAL BY THE PLANAR PLASMA LAYER

A.Kingsep
RRC Kurchatov Institute, Moscow, Russia

J.Kalda
Institute of Cybernetics, Tallinn, Estonia

In this paper, effect of nonlinear detection will be considered, conditioned by the range of phenomena that may be studied within the framework of electron magnetohydrodynamics (EMH [1]).

It is known that the hierarchy of the relaxation time scales

$$\tau_{ee}/\tau_{ii}/\tau_{ei}^{(E)} = 1/(M/m)^{1/2}/(M/m) \qquad (1)$$

provides the conditions of applicability for two-fluid MHD. This treatment, in turn, under the following conditions:

$$c_s, v_A \ll j/ne \ll v_{Te}, v_{Ae}, \qquad (2)$$

$$c/\omega_{pi} \gg a \gg c/\omega_{pe}, \qquad (3)$$

and, what is especially important just in our case,

$$\omega_{pi}, \omega_{Bi} \ll \partial/\partial t \ll \omega_{pe}, \omega_{Be} \qquad (4)$$

may be reduced to the basic EMH equation of the magnetic field freezing in the electron current flow

$$\partial B/\partial t + \mathrm{curl}[j/ne, B] = -(c/\sigma)\mathrm{curl}\ j \qquad (5)$$

(All the terms are conventional but a, that is the space scale of the problem). In homogeneous plasmas and by the field lines being straight, Eq.(5) degenerates to the ordinary equation of a field diffusion, i.e., in the case of HF irradiation of a plasma layer, nothing but skin-effect may exist. If, however, the field curvature or possible density gradient are taken into account, all the situation changes drastically. In the last case, e.g., Eq.(5) transforms into the following one:

$$\partial B/\partial t + (c/8\pi e)[\nabla B^2, \nabla(n^{-1})] = (c^2/4\pi\sigma)\nabla^2 B, \qquad (6)$$

which, in turn, for the traditional quasi-plane skin problem

($\partial/\partial x, \partial/\partial y \ll \partial/\partial z$) becomes reduced to the Burgers equation

$$\partial B/\partial t + æB(\partial B/\partial z) = D\partial^2 B/\partial z^2 \qquad (7)$$

where $æ = (c/4\pi e)(\partial n^{-1}/\partial x)$ and $D = c^2/4\pi\sigma$. Its solution (not less exact than that of the diffusion equation) reveals different properties depending upon the sign of æ. Taking the most simple boundary/temporal condition, $B(z = 0) = B_0\theta(t)$, and $æ < 0$ (that means that nonlinear field transport begins to compete with diffusive transport), one can readily obtain by $t \to \infty$ the field profile 'locked' near the plasma surface

$$B = B_0(1 - æB_0 z/2D) \qquad (8)$$

while in the opposite case $æ > 0$ the magnetic field penetrates into a plasma in the form of EMH shock:

$$B = (B_0/2)[1 - \tanh(æB_0/4D)(z - ut)] \qquad (9)$$

where $u = æB_0/2$ (see Ref.[2]).

The temporal/boundary condition used is the most typical of pulsed plasmas.It is interesting, however, to examine the skin problem in traditional form, i.e., using the conditions

$$B_{(z=0)} = B_0 \cos \omega t \qquad (10)$$

or

$$B_{(z=0)} = B_0\theta(t)\cos \omega t. \qquad (11)$$

It becomes moreover of interest, because EMH effects conditioned by ∇n or ∇T may really join the game while studying skin phenomena.

The nonlinearity of EMH skin problem may be characterised by the dimensionless parameter β determined as a ratio of the nonlinear space scale $\delta_{eff} = D/æB_0$ and the linear skin depth $\delta_{sk} = (2D/\omega)^{1/2}$:

$$\beta \equiv 2^{1/2}\delta_{eff}/\delta_{sk} = (\nu_{eff}\omega)^{1/2}/(\nu_{Ae}\partial_x \ln n)$$

where ν_{eff} is the effective collision frequency.

As it is well known, the linear skin problem based on a linear diffusion equation is invariant with respect to the change of the field sign. There is, however, no such invariance for the Burgers equation. That is just the reason of importance of the topology of $(\nabla n, B, e_z)$ triplet. In a planar geometry, within the limits of applicability of Burgers equation (7) the field of definite orientation (let us define it as $B > 0$) is effectively transported into a plasma depth while the field of opposite orientation (we define it as $B < 0$) tends to be locked near the plasma surface. Hence, there is a reason to believe that this problem has no steady solution at all. Indeed, the pulses of positive field should periodically penetrate into a forbidden region, as a result, the positive magnetic flux and the field energy have to be accumulated within a plasma volume. Respectively, in a steady problem [see Eq.(10)] one should assume that the periodic solution is accompanied by the non-zero, positive and constant in time magnetic field by $z \to \infty$. These speculations will be reinforced by the exact solutions. In spite of being nonlinear, Burgers equation is exactly integrable by means of the substitution

$$B = (2D/\varkappa)\partial \ln|\varphi|/\partial z \qquad (12)$$

transforming Eq.(7) into the conventional diffusive equation

$$\partial\varphi/\partial t = D\partial^2\varphi/\partial z^2.$$

Averaging Eq.(7) along the period $2\pi/\omega$ and then integrating it twice over z we have

$$B_{(z=\infty)} = (\varkappa/2D)\int_0^\infty (\langle B^2\rangle - B^2_{(z=\infty)})dz > 0. \qquad (13)$$

We set $B_{(z=\infty)} = \alpha B_0$, $0 < \alpha < 1$. Let us try to find the function $\varphi(z)$ We note that the periodic behavior of B in time does not mean

the same for φ. Solving the diffusion equation for φ by $z \to \infty$ one can obtain $\varphi \propto \exp(\alpha^2\omega t/4\beta^2)$. Respectively, taking an arbitrary z we could assume the following form for exact solution:

$$\varphi = \tilde{\varphi} \exp(\alpha^2\omega t/4\beta^2) \tag{14}$$

where $\tilde{\varphi}$ is assumed to be periodic in time. This function could be found in a form of Fourier series:

$$\tilde{\varphi} = \sum_{n=-\infty}^{+\infty} \tilde{\varphi}_n \exp[-(A_n/4\beta)(\omega/D)^{1/2}z - in\omega t] \tag{15}$$

$$A_n = 2(\alpha^2 - 4\beta^2 n i t)^{1/2}, \quad Re\, A_n > 0, \quad \tilde{\varphi}_{-n} = \tilde{\varphi}_n^*.$$

Using Eq.(15) we can rewrite Eq.(10) in form:

$$A_n = \psi_{n+1} + \psi_n^{-1}, \quad \psi_n \equiv \tilde{\varphi}_n / \tilde{\varphi}_{n-1} < 1. \tag{16}$$

Taking into account that $\tilde{\varphi}$ is a real function defined independent of an arbitrary numerical factor, we can put $\tilde{\varphi}_n = 1$. Then we find from Eq.(16):

$$\psi_n = 1/(A_n - 1/(A_{n+1} - 1/(A_{n+2} - \ldots)). \tag{17}$$

So, we can obtain the general term of Eq.(15) series:

$$\tilde{\varphi}_n = \prod_{m=1}^{n} 1/(A_m - 1/(A_{m+1} - \ldots) \tag{18}$$

An important result from Eqs.(16) and (18):

$$\alpha = Re\, 1/(A_1 - 1/(A_2 - 1/A_3 - \ldots)). \tag{19}$$

Eq.(19) allows to find $\alpha(\beta)$ function and then, in a result, the general solution as well:

$$B = -(2D/æ)\partial_z \ln\{\exp(-\alpha æ B_0 z/2D) + \tag{20}$$

$$+ 2Re\sum_{n=1}^{\infty} \tilde{\varphi}_n \exp[-(A_n/4\beta)(\omega/D)^{1/2}z - in\omega t]\}$$

closed by Eqs.(18,19). In a general case, i.e., for arbitrary quantity of β, the result may be presented only in form of Fourier series and continuous fractions. It turns out, however, to be very simple and obvious in both limits of the quasi-linearity and strong nonlinearity. First, in the weakly nonlinear limit, $\beta \gg 1$,

one can calculate $\alpha = 2^{-5/2}\beta^{-1}$, so that

$$B = \begin{cases} B_0 \exp(-z/\delta_{sk}) \cos(z/\delta_{sk} - \omega t), & z \ll \delta_{sk} \ln \beta \\ B_0/(2^{5/2}\beta), & z \gg \delta_{sk} \ln \beta \end{cases} \qquad (21)$$

Thus, in this limit the classic skin solution turns out to be expanded into the plasma depth by the plateau of the small amplitude and of the permanent sign.

The strongly nonlinear limit, $\beta \ll 1$, is hardly less obvious. In this case it is more convenient to start immediately from Eq.(7). Let us consider the penetration of the negative field pulse. The characteristic time of the formation of the steady profile (8) is $\tau \approx \beta^2/\omega \ll \omega^{-1}$. That means that the penetrating negative field 'follows' the boundary condition forming near the plasma surface the oscillating profile

$$B \cong B_0 \cos \omega t / [1 + (\varkappa z/2D) B_0 \cos \omega t]$$

with a scale of the width $\delta_{eff} \approx \delta_{sk}\beta$ and of the penetration depth $\delta \approx \delta_{sk}$. Then let us repeat the proof of Eq.(13) but integrating over $z > \delta_{sk}$. In that region only positive half periods give some input. On the other hand, here we may neglect the diffusive term in Eq.(7). So, we obtain

$$B^2_{(z=\infty)} \cong \langle B^2 \theta(B) \rangle_{(z=0)}$$

and the final result for the boundary condition (10) is

$$B_{(z=\infty)} = B_0/2. \qquad (22)$$

Thus, we have obtained very interesting effect, i.e., nonlinear detection of the oscillating signal by the plasma layer.

Similar scenario may be developed using (11) boundary condition. To be short, we restrict ourselves by formulating the results. In the strongly nonlinear limit, $\beta \ll 1$, the solution coincides with that of quasi-steady problem by z less than some $z_0(t)$. By $z > z_0(t)$, we have $B(z,t) = 0$. The quantity $z_0(t)$ may be

estimated taking the integral of Eq.(7) over z and over t,

$$\int_0^{z_0} B_1(z,t)dz \cong (\varkappa/2)\int_0^t [B^2\theta(B)]_{(z=0)}dt \qquad (23)$$

where $B_1(z,t)$ is the solution of the quasi-steady problem, $B_1(z,t) \to B_0/2$ by $z,t \to \infty$. Roughly $z_0(t)$ may be estimated from the argument in Eq.(9): $z_0(t) \approx u(B_0)t$. In the weakly nonlinear limit, $\beta \gg 1$, all the estimates are worth to be done only in the region $z > \delta_{sk}\ln\beta$ where the nonlinearity is essential. As a very good model, the solution may be used, found using the following boundary condition, $B_{(z=0)} = \alpha B_0\theta(t)$, which results in the effective depth of the penetration

$$z_0 \cong 2^{-5/2}\beta^{-1}\varkappa B_0 t. \qquad (24)$$

Eq.(24) presents the width of the broadening plateau.

In conclusion, we should emphasise that within the framework of the non-trivial EMH theory 'classic' skin effect does not exist. The field translated to the infinity inside the conducting medium has the definite sign (i.e., some kind of nonlinear detection occurs). It travels in a form of shock wave and may be as high in amplitude as one half of the boundary oscillating field. In addition, we note that the result represented in form of continuous fractions is a rarity in physics.

References

1.Kingsep A.S., Chukbar K.V. and Yan'kov V.V., 1987, Voprosy Teorii Plazmy, ed, B.B. Kadomtsev, V.16 (Moscow: Energoizdat) [Reviews of Plasma Physics, V.16, 1990, (NY: Consultants Bureau) pp 243-91].

2.Kingsep A.S., Mokhov Yu.V. and Chukbar K.V., 1984, Fizika Plazmy [Sov.Journ.Plasma Phys.], 10, 854-9.

INFLUENCE OF INHOMOGENEITY OF MAGNETIC FIELD ON THE CYCLOTRON DAMPING OF PLASMA WAVES.

G.M.Fraiman and I.Yu.Kostyukov
Institute of Applied Physics, Russian Academy of Sciences,
Nizhny Novgorod, Russia

In this report we shall apply the general results for multi-dimensional systems (see paper [1] in this book) to study the interaction between a beam of charged particles and microwaves in the presence of smoothly inhomogeneous magnetostatic field.

Let us assume that the scalar potential $V_0(z)$ on the axis z smoothly depends on coordinate z. Then we can write the vector potential within the paraxial approximation: $A(r,z) = \frac{rB_0(z)}{2} + O(\nu^2)$, where $B_0(z) = \frac{dV_0(z)}{dz}$ is the magnetostatic field intensity on the axis z, $\nu \sim \frac{1}{B_0}\frac{dB_0}{dz}$ is the small parameter, characterizing the magnetostatic field inhomogeneity.

The cylindrical coordinate system is not suitable. It is better to introduce an orthogonal coordinate system, which is connected with the lines of force of the magnetic field [2]. This is the system, whose coordinate curves in the η, ξ plane are formed by the lines of force and the curves perpendicular to them. The transformation from the old coordinates (z,r,φ) to the new coordinates (η,ξ,φ) will be defined by the relations:

$$rA^0(r,z) = \xi, \quad V(r,z) = V(\eta). \tag{1}$$

In our problem the linear polarized electromagnetic wave propagates at the angle α to the axis z:

$$A_r^{\sim} = \frac{cE_0(z)\cos\alpha}{\omega}\sin\varphi\sin[k\sin\alpha z + k\sin\alpha r\cos\varphi - \omega t],$$

$$A_\varphi^{\sim} = \frac{cE_0(z)\sin\alpha}{\omega}\cos\varphi\sin[k\sin\alpha z + k\sin\alpha r\cos\varphi - \omega t],$$

$$A_z^{\sim} = \frac{cE_0(z)\sin\alpha}{\omega}\sin[k\sin\alpha z + k\sin\alpha r\cos\varphi - \omega t].$$

We assume that the wave intensity is weak. (It is convenient to place the parameter μ before $\mathbf{A}^{\sim}$ which will be assume as equal 1 in the final results.)

The motion of a particle in magnetostatic and microwaves is given by the Hamiltonian:

$$H = c\sqrt{\left(\mathbf{p} - \frac{q}{c}\mathbf{A}\right)^2 + m_0^2c^2}, \tag{2}$$

where c is velocity of light, m_0 is the particle's mass of rest, q is charge of the particle and $\mathbf{A} = \mathbf{A}_0 + \mu\mathbf{A}^{\sim}$ is the vector potential of the electromagnetic field.

Following the procedure in section 3.2 of [1] let us go to a new Hamiltonian, in which η plays a role of the time t and t, $-H$ is a new canonical variables:

$$H_1(p_\xi, \xi, p_\varphi, \varphi, -H, t, \eta) = p_\eta(p_\xi, \xi, p_\varphi, \varphi, -H, t, \eta). \tag{3}$$

Then we make transition to new canonical variables by means of canonical transformation. We get the following relations between the old canonical variables $p_\xi, \xi, p_\varphi, \varphi, -H, t$ and new canonical variables $M, \varphi_1, \Pi, \varphi_2, I, \Theta$:

$$\xi^2 = \Pi + M + 2\sqrt{\Pi M}\sin(\varphi_1 + \varphi_2), \quad p_\xi^2\xi^2 = 4M\Pi\cos^2(\varphi_1 + \varphi_2),$$
$$\phi = arctan\left\{\frac{\sqrt{2M}\cos\varphi_1 + \sqrt{2\Pi}\sin\varphi_2}{\sqrt{2M}\sin\varphi_1 + \sqrt{2\Pi}\cos\varphi_2}\right\}, \quad p_\phi = \Pi - M,$$
$$H = \mathcal{E} = \omega I, \quad \Theta = \omega t. \tag{4}$$

Analysis of the canonical transformation gives the following significance of the new quantities: M is magnetic moment, Π is drift

moment, φ_1 is angle of gyromagnetic rotation, φ_2 is angle of rotation about the z axis, $H = \mathcal{E} = \omega I$ is particle energy, $\Theta = \omega t$ is the normalized time.

As a result of canonical transformation, the new Hamiltonian is, to order of μ and ν^2:

$$H(M,\varphi_1,\Pi,\varphi_2,I,\Theta,\eta) = H_0(M,I,\eta) + \mu H_1^{\sim}(M,\varphi_1,\Pi,\varphi_2,I,\Theta,\eta) + \\ + \nu^2 H_2^{\sim}(M,\varphi_1,\Pi,\varphi_2,\eta),$$

$$H_0(M,I,\eta) = \sqrt{\frac{\omega^2 I^2}{c^2} - m_0^2 c^2 - 2\omega_B(\eta) m_0 M}, \quad \omega_B(\eta) = \frac{qB_0(\eta)}{m_0 c}. \tag{5}$$

We write $H_1^{\sim}(M,\varphi_1,\Pi,\varphi_2,I,\Theta,\eta)$ for cases $\Pi \gg M$ and $\Pi \ll M$:

$$H_1^{\sim} = \frac{qE_0(z)}{\omega} \sin[k\sin\alpha z + k\sin\alpha r\cos\varphi - \Theta] \times \\ \times \left\{ \frac{2\sqrt{2\omega_B(z) m_0 M}}{H_0(I,M,\eta)} \frac{m_0 c^2}{I} \frac{\omega_B(z)}{\omega} \cos\alpha\cos\varphi_1 + \sin\alpha \right\}. \tag{6}$$

The beam of charged particles propagates through the region of the inhomogeneous magnetostatic and the HF fields $\eta > 0$. If the beam is not modulated, the beam particle is evenly distributed in initial angle variables $\Theta^0 = \Theta(\eta = 0)$, $\varphi_1^0 = \varphi_1(\eta = 0)$. Then, using relations (10) and (18) in Ref [1] we can obtain the beam mean variations of the action variables per particle.

Unlike one-dimensional case, now we have two small parameters μ and ν. Since the general problem of particle motion in inhomogeneous magnetic field is nonintegrable, there is new small parameter ν conditioned by the inhomogeneity of the magnetostatic field. The moments M, Π vary as effect of the HF field and the inhomogeneity of the magnetostatic field. If the electromagnetic waves is absent the averaged variations of M, Π is the averaged variations of the adiabatic invariants due to the inhomogeneity of the magnetic field. Since $H_2^{\sim}$ does not depend on Θ, the particle energy varies only due to the action of the HF field. We are interested in the energy exchange between the beam and the microwave and, therefore, one finds the

averaged variation of the beam energy per particle:

$$< \Delta\mathcal{E} >= \frac{1}{16} \sum_{l=-\infty}^{+\infty} \left(\frac{\partial}{\partial \mathcal{E}^0} + l \frac{\partial}{\partial \mathcal{E}_\perp^0} \right) |F_1|^2 + |F_2|^2 ,$$

$$F_1 = \int_0^L qE_0(x) \cos\alpha \frac{\sqrt{\frac{\omega_B(x)}{\omega} \mathcal{E}_\perp^0}}{H_0(\mathcal{E}^0, \mathcal{E}^0{}_\perp, x)} \frac{m_0 c^2}{\mathcal{E}_0} l \times$$
$$\times [J_{l+1}(a(x, \mathcal{E}_\perp^0)) + J_{l-1}(a(x, \mathcal{E}_\perp^0))] e^{i\Theta_0(\mathcal{E}^0, \mathcal{E}_\perp^0, x)} dx,$$

$$F_2 = \int_0^L qE_0(x) \sin\alpha J_{l+1}(a(x, \mathcal{E}_\perp^0)) e^{i\Theta_0(\mathcal{E}^0, \mathcal{E}_\perp^0, x)} dx,$$

$$a(x, \mathcal{E}_\perp^0) = k \cos\alpha \sqrt{\frac{2\mathcal{E}_\perp^0}{\omega \omega_B(x) m_0}},$$

$$\Theta_0(\mathcal{E}_0, x) = ik \sin\alpha x - i \sin\varphi_2^0 a(x, \omega\Pi_0/\mathcal{E}_\perp^0) -$$
$$-\omega \{ \frac{\partial}{\partial \mathcal{E}^0} - l \frac{\partial}{\partial \mathcal{E}_\perp^0} \} \int_0^x H_0(\mathcal{E}^0, \mathcal{E}_\perp^0, \xi) d\xi,$$

$$H_0(\mathcal{E}^0, \mathcal{E}_\perp^0, x) = \sqrt{\frac{(\mathcal{E}^0)^2}{c^2} - m_0^2 c^2 - m_0 \frac{\omega_B(x)}{\omega} \mathcal{E}_\perp^0}, \quad \mathcal{E}_\perp^0 = \omega M_0. \tag{7}$$

To understand some qualitative aspects of interaction between the beam of the charged particles and the HF field in the presence of the inhomogeneous magnetostatic field let us consider expression (7) in the nonrelativistic case and with $k = 0$, $\alpha = 0$. Then, we have:

$$< \Delta\mathcal{E} >= \frac{1}{16} \left\{ \frac{\partial}{\partial \mathcal{E}^0} - \frac{\partial}{\partial \mathcal{E}_\perp^0} \right\} |F|^2,$$

$$F = \int_0^L qE_0(x) \frac{V_\perp(\mathcal{E}_\perp^0, x)}{V_\parallel(\mathcal{E}^0, \mathcal{E}_\perp^0, x)} e^{i\Theta_0(\mathcal{E}^0, \mathcal{E}_\perp^0, x)} dx,$$

$$\Theta_0(\mathcal{E}_0, x) = \int_0^x \frac{\omega - \omega_B(\xi)}{V_\parallel(\mathcal{E}^0, \mathcal{E}_\perp^0, \xi)} d\xi,$$

$$V_{\parallel}(\mathcal{E}^0, \mathcal{E}_{\perp}^0, x) = \sqrt{\frac{2}{m}\left(\mathcal{E}_0 - \frac{\omega_B(x)}{\omega}\,\mathcal{E}_{\perp}^0\right)},$$
$$V_{\perp}(\mathcal{E}_{\perp}^0, x) = \sqrt{\frac{2}{m}\left(\frac{\omega_B(x)}{\omega}\,\mathcal{E}_{\perp}^0\right)}. \tag{8}$$

Substituting $\mathcal{E}_{\perp}^0$ for $\mathcal{E}^0 - \mathcal{E}_{\parallel}$, we reduce equations (8) to a more convenient form:

$$<< \Delta\mathcal{E} > 4 >= \frac{1}{16}\,\frac{\partial}{\partial\mathcal{E}^0}\,|F|^2\,. \tag{9}$$

Thus, generation (absorption) zones correspond to increase (decrease) region of the function $|F|^2$ of $\mathcal{E}_0$ at $\mathcal{E}_{\parallel}^0 = const$. It is seen from (8) that the resonance points $\omega = \omega_B(z)$ give the main contribution in the integral F.

We shall consider some examples of the interaction monoenergetic electron beam and HF field $E_0 e^{i\omega t}$ in the presence of the inhomogeneous magnetic field. If the magnetic field has linear spatial profile $\omega_B(z) = \omega_B^0 \frac{z}{l}$ and the size of the resonance zones $L_r = \left[\frac{d\omega_b/dz}{V_{\parallel}(z)}\right]^{-1/2}$ is much smaller than L_f the scale length of the HF field, we obtain:

$$<< \Delta x >>= \pi\frac{c}{l\omega}\left(\frac{qE_0 l}{2m_0c^2}\right)^2 \frac{\partial}{\partial x_0}\,\frac{x_0(x_0 - z_0)}{\sqrt{x_0^2(2z_0 - x_0) - 1}}\,,$$
$$x_0 = \frac{\mathcal{E}^0}{m_0c^2}\,, \qquad y_0 = \frac{\mathcal{E}_{\perp}^0}{m_0c^2}\,, \qquad z_0 = x_0 - y_0. \tag{10}$$

Since Δx is positive for $x_0 > z_0 > 1$ in this case, the HF oscillations always damp due to the interaction with the electron beam.

In order to form the generation zones of the electromagnetic waves, the beam particles must pass several reflection points. It is possible in the case of $k = 0$, if the magnetostatic field has the nonmonotonic spatial profile or the beam is reflected from a "magnetic mirror" for the case with the monotonic spatial profile of the magnetic field.

We consider again the examples with the conservative magnetic field, having the linear spatial profile, but we take into account now

the reflection of the beam particles. In this example the beam particle pass the reflection point twice. Let us assume that $L_r \ll L_d \ll L_f$, where L_d is the distance, which the beam particles transit between resonance points. Then according to (8) and (9), the averaged energy variation per particle is given by:

$$<< \Delta x >>= \pi \frac{c}{l\omega} \left(\frac{qE_0 l}{m_0 c^2} \right)^2 \frac{\partial}{\partial x_0} \frac{x_0(x_0 - z_0)}{\sqrt{x_0(2z_0 - x_0) - 1}} \sin^2 \psi(x_0),$$
$$\psi(x_0) = \frac{l\omega}{c} \left(\sqrt{x_0(2z_0 - x_0) - 1}(x_0^2 - 2x_0 + 2z_0 - 1) \right). \tag{11}$$

It follows from (11) that there are generation zones alternating with the absorption zones.

Physically, the mechanism of formation of the generation zones in these examples is like the principle of operation of gyroklystron (the example with "magnetic mirrors" corresponds to a reflective gyroklystron). Thus, the nonlocal nature of the beam-waves interaction plays an important role in the energy exchange.

Our research was supported by RBSF Grant No.93-02-837 to the Institute of Applied Physics.

References

1. G.M.Fraiman and I.Yu.Kostyukov *Wave - Beam interaction in the presence of inhomogeneous static magnetic and electric field*, in this book .

2.J.Lacina, *Czech.J.Phys.*,**B13**,401,(1963).

RADIATION OF WHISTLER RANGE WAVES IN IONOSPHERE AND MAGNETOSPHERE PLASMA

A.V.Kostrov, A.A.Shaikin, A.I.Smirnov and T.M.Zaboronkova

Institute of Applied Physics, Nizhny Novgorod, Russia

For "active" experiments in space rather actual are the problems on the efficiency of whistler electromagnetic (e.m.) waves radiation by antennas locating on artificial Earth's satellites and on their further propagation in ionosphere and magnetosphere plasma. Predicting the results of such expensive works is an important task. Its successful solution requires the preliminary laboratory modeling and thorough theoretical calculation. In IAP RAS already several years laboratory studies of electrodynamic characteristics of road and loop antennas, locating in magnetoactive plasma, have been performed by the similarity parameter of the corresponding Earth ionosphere and magnetosphere. The given communication deals with the analysis of the results of this activity.

1. The experiments were carried out in a vacuum chamber containing the magnetized plasma column of 150 cm length and 60 cm diameter. The parameters of our laboratory experiment were chosen such as to model the operation of magnetic and electric antennas on board a spaceship in whistler frequency range in space plasma ($\omega_{lh} << \omega << \omega_{ce} << \omega_{pe}$, where ω_{lh}- is the low hybrid frequency, ω - radiation frequency, ω_{ce} and ω_{pe} are electron cyclotron and plasma frequency).

Using the similarity relation one could model on the experimental setup the radiation of the antennas on board the satellite in the fre-

quency range from 10 kH to 100 kH at height from 150 km to 2000 km. For experiments in space of importance is determination of the part of the antenna radiation power which goes directly to the whistler waves. Note that the studied frequency range is characterized by the open (non-closed) surface of wave vectors (Fig.1). Depending on the value of the wave vector projection (k) transverse to the magnetic field, three characteristic wave types are singled out: a) whistler wave ($kc << \omega_{pe}$), b) conic refraction($kc \sim \omega_{pe}$),c) quasielectrostatic ($kc >> \omega_{pe}$). Such classification reflects essential differences in the polarization and refraction properties of these spatial harmonics.

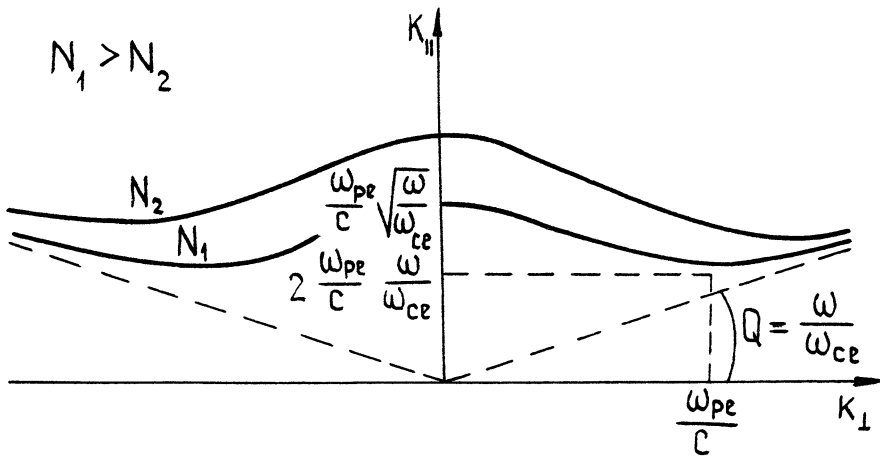

Fig. 1

The research were focussed on the investigation of radiating sources, the space-time structure of the field and nonlinear phenomena in plasma.

2. The structure of electromagnetic fields excited in magnetoactive plasma by loops and roads has been the subject of a great many experimental and theoretical investigations [1]. Unlike these efforts,

our purpose was to not only state the evidence of this or that physical effect, but to closely follow a gradual process of a radiation pattern development and, specifically, to find out the influence of various factors (geometrical size, power, etc.) on radiation efficiency of a certain spatial harmonic. Even for low powers the fields of loop and road antennas in a magnetoactive plasma in the whisitle range differ qualitatively from the vacuum fields both far off and in close proximity to a radiation source . This fact is accounted for by specific dispersion characteristics of a magnetoactive plasma, in particular, by the surface form of wave vectors of extraordinarily polarized plane waves (Fig.1).

It should be noted that vacuum notions of far and near fields of antenna as well as Fresnel and Fraungofer diffraction zones can not be directly applied to magnetoactive plasma. These notions need to be specified and partly reconsidered. For example, a wave field structure typical of a far (Fraungofer) zone is formed here at different distances from the antenna for the whistler waves and the conic-refraction waves, while quasistatic ("near" according to vacuum terminology) fields can extend to large, compared to a whistler wave-length, distances, forming the so called resonance cone with the angle ω / ω_{ce} .

Radiation fields produced by elementary dipole antennas are concentrated mainly in a cone with its aperture $\alpha < \omega$ /ω_{ce}, whose central axis is directed strictly along the magnetic field. In the immediate neighborhood of this axis, beginning from distances $\geq \lambda_{wh} = (2\pi c/\omega_{pe})\sqrt{\omega_{ce}/\omega}$ they are superposition of modes propogating along the magnetic field: a whistler wave with a quasi-plane phase front and a quasi-standing (in the plane transverse to the magnetic field) mode consisting of the cone refraction waves. The last mode has a period of transverse structure close to $\pi c/\omega_{pe}$, and a propogating constant along the magnetic field is equal to $2\omega_{pe}\omega/c\omega_{ce}$.

Fig.2 gives the measurement results for a electric field excited by a road antenna near the Z axis of symmetry (the road is perpendicular to the magnetic field). The radiation efficiency and the radiation pattern are largely affected by the geometrical size of antennas. It

was found out experimentally that antennas of small electric size d ($\omega_{pe}d << c$) mainly radiate quasipotential waves propagating along resonance surface, while those of large electric size ($\omega_{pe}d > c$) produce whistler and conic-refraction waves [3]. With higher powers delivered to antennas the structure of fields starts to change, which is caused by formation of wave-guiding channels owing to a thermodiffusion process.

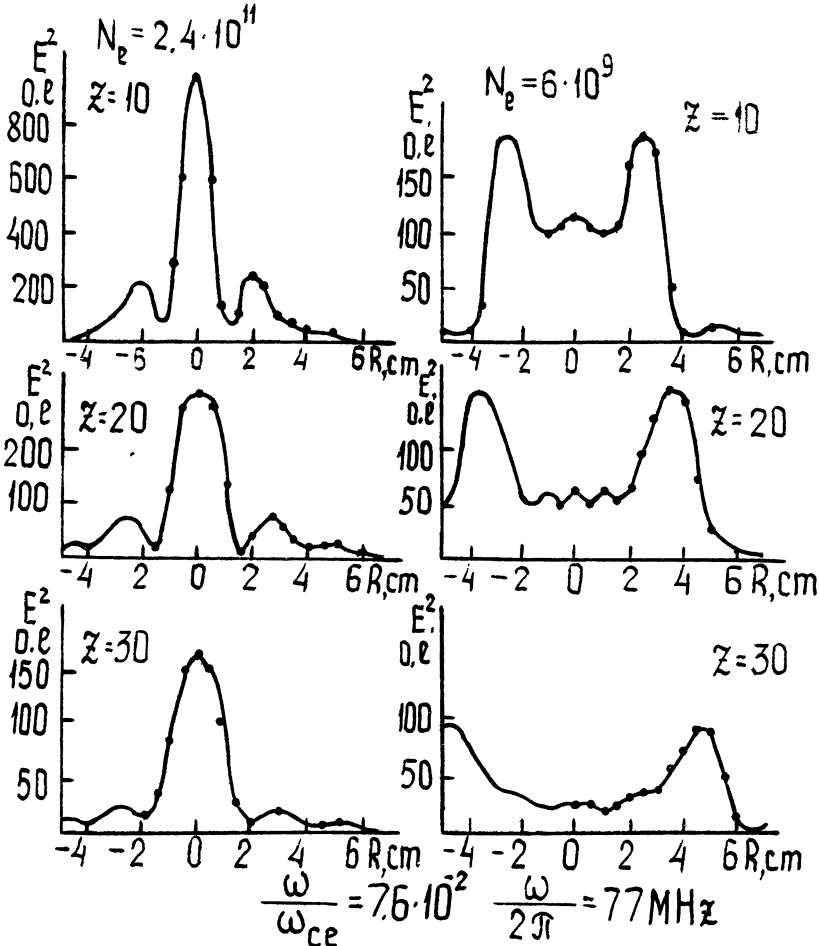

Fig. 2

3.It is shown that nonuniform distribution of plasma density near the radiators causes the variation of directivity diagrams of radiation and the value of radiation resistance with respect to a uniform plasma.The inhomogeneous structure along the magnetic field may be formed as a result of the nonlinear interaction between the electromagnetic field and surrounding plasma .The channel with nonmonotonous low of plasma density variation transversely to the external magnetic field in whistler frequency range occurs in magnetoactive plasma near the radiators as a result of electron heating by the quasistatic field of the antenna and thermal-diffusion- driven redistribution of the plasma it products.

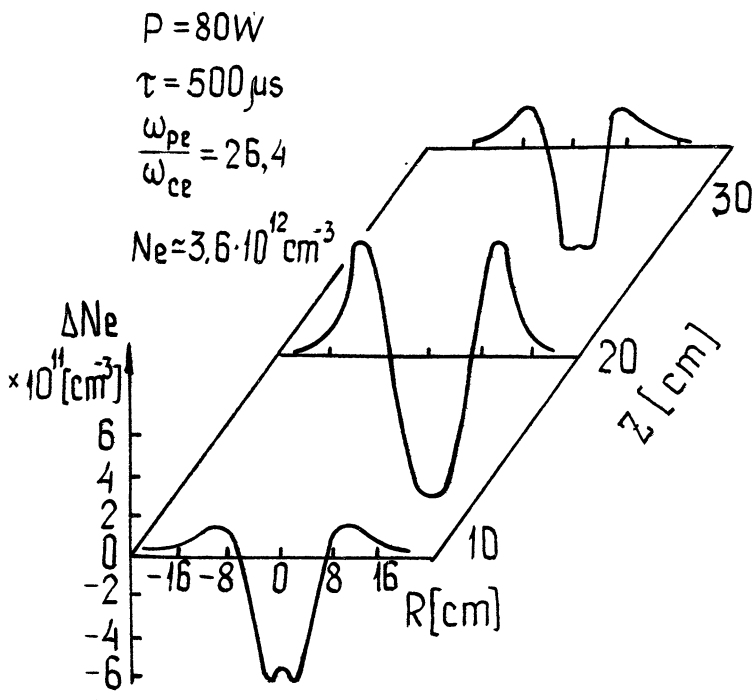

Fig. 3

In the laboratory experiment as a source of whistler waves the loop antenna was used (1 sm. diameter).The distribution of the plasma density perturbations N at time t=500msec is shown in Fig 3.The wave propagation of two independent modes in the whistler range has been detected in such plasma formation. To explain the experimental results,the strict theoretical analysis has been made of the field structures in this channel.It is established,that the field of waves of conic refraction is concentrated in the central part of the channel with decreased plasma density relative to the back-ground and the field of proper whistler wave [2] is concentrated in a ring layer around the central part with an increased density. Therefore,taking into consideration such nonuniform distribution of plasma density,that takes place near the radiator at nonlinear power levels P fed to the antenna can be of importance.It can lead to the increase of the relative contribution of the proper whistler and waves of conic refraction to the total radiation power and also to the variation of the radiation resistance and therefore to the variation of the optimum conditions of matching antenna operation.

References

1. Stenzel R.L.. *Radio Sci.*,1976, **11**, 1045; *Fhys.Fluids*, **19**, 857.

2. Zaboronkova T.M., Kostrov A.V. et al. *Sov. Phys.JETP*,1992, **75**,625.

3. Kondrat'ev I.G., Kudrin A.V., and Zaboronkova T.M. *Radio Sci.*,1992, **27**, 315.

ON MODULATED INSTABILITY OF ELECTROMAGNETIC WAVES IN PLASMAS

S.V. Vladimirov and V.S. Krivitsky
General Physics Institute, 117942 Moscow, Russia

We consider a strongly collisional plasma, where the effective collision frequency ν_{eff} is not only much larger than the characteristic frequency $\Delta\omega$ of the modulational perturbations, but also is larger in the presence of significantly stronger inequality:

$$|\Delta\omega| \ll \nu_{\text{eff}}^{(\text{eq})} = \frac{m_e}{m_i}\nu_{\text{eff}}. \tag{1}$$

Here, $m_{e(i)}$ is the electron (ion) mass. The characteristic frequency $\nu_{\text{eff}}^{(\text{eq})}$ defines the time of equalization of the electron and ion temperatures; thus the inequality (1) means that for the time of modulational instability development (or for the period of modulations) the electron and ion temperatures have time to equalize each other. This problem arises, for instance, when investigating plasma heating by strong laser radiation, which is relevant for inertial confinement fusion schemes [1,2].

We start our investigation with the hydrodynamic equations that can be obtained from the kinetic equation with Landau collision integral [3,4]. We consider that, in general, among all the characteristic frequencies of the problem, only the frequencies of the modulated perturbations are in the hydrodynamical regime $|\Delta\omega| \ll \nu_{\text{eff}}$. The other frequencies correspond to the regime of rare collisions. In calculating the latter quantities, we use a collisionless approximation. Thus we

have the following equations for the electron (ion) $\mathbf{v}^{(e,i)}$ velocities:

$$m_{e,i}n_{e,i}(\partial_t + \mathbf{v}^{(e,i)} \cdot \nabla)v_j^{(e,i)} = -\nabla_j n_{e,i}T_{e,i} - \nabla_l \pi_{lj}^{(e,i)} \mp en_{e,i}(E_j + [\mathbf{v}^{(e,i)} \times \mathbf{B}]_j/c) \pm R_j, \quad (2)$$

where we assume that the ions have the charge e. The equations (2) are completed by the continuity equations for the electrons and ions as well as the equations of thermal balance

$$3n_{e,i}(\partial_t + \mathbf{v}^{(e,i)} \cdot \nabla)T_{e,i}/2 + n_{e,i}T_{e,i}\nabla \cdot \mathbf{v}^{(e,i)} = -\nabla \cdot \mathbf{q}^{(e,i)} - \pi_{lj}^{(e,i)}\nabla v_l^{(e,i)} + Q_{e,i}. \quad (3)$$

In Eqs.(2) the terms containing ∇nT describe the contribution from the pressure of electron and ion gases; $\pi_{lj}^{(e,i)}$ are the tensors of electron and ion viscosity:

$$\pi_{lj}^{(e)} = -0.73\frac{n_e T_e}{\nu_e}w_{lj}^{(e)}, \quad \pi_{lj}^{(i)} = -0.96\frac{n_i T_i}{\nu_i}w_{lj}^{(i)}, \quad (4)$$

where $w_{lj}^{(e,i)} = \nabla_j v_l^{(e,i)} + \nabla_l v_j^{(e,i)} - \frac{2}{3}\delta_{lj}\nabla \cdot \mathbf{v}^{(e,i)}$. Furthermore, $\mathbf{R}$ is the friction forse between the electrons and ions:

$$\mathbf{R} = \mathbf{R}_\mathbf{u} + \mathbf{R}_T = -0.51n_e m_e \nu_e \mathbf{u} - 0.71n_e\nabla T_e, \quad (5)$$

where the forse of relative friction $\mathbf{R}_\mathbf{u}$ is defined for $\omega \ll \nu_e$ (we have $\nu_{\text{eff}} \simeq \nu_e$ in the case considered; let us note that if $\omega \gg \nu_e$ holds, then $\mathbf{R}_\mathbf{u} \simeq -n_e m_e \nu_e \mathbf{u}$, but in this case some questions arise on applicability of the hydrodynamical description). Finally, $\mathbf{q}^{(e,i)}$ in Eqs.(3) is the heat flux:

$$\mathbf{q}^{(e)} = 0.71n_e T_e \mathbf{u} - 3.16\frac{n_e T_e}{m_e \nu_e}\nabla T_e, \quad \mathbf{q}^{(i)} = -3.9\frac{n_i T_i}{m_i \nu_i}\nabla T_i, \quad (6)$$

and

$$Q_e = -\mathbf{R} \cdot \mathbf{u} - Q_i, \quad Q_i = 3\frac{m_e}{m_i}n_e\nu_e(T_e - T_i) \quad (7)$$

are the heating powers.

We solve the above equations by expanding in powers of the electric field $\mathbf{E}$. To investigate modulational instability, we have to take

into consideration terms up to the third order in the fields, as well as interactions through virtual waves (which are perturbations of the pump electric field on the beat frequency $\Delta\omega$ and in general also the double frequency $2\omega_0$). As a result, for the Fourier component

$$\mathbf{j}_{\mathbf{k}\omega} = \int \mathbf{j}(\mathbf{r},t)\exp(i\omega t - i\mathbf{k}\cdot\mathbf{r})d\mathbf{r}dt/(2\pi)^4 \tag{8}$$

of the high-frequency plasma current density of the third order, we obtain the following expression containing only the high-frequency fields

$$\begin{aligned}\mathbf{j}^{(3),HF}_{\mathbf{k}\omega} = \int \Sigma^{eff}_{ijlm}(\mathbf{k},\omega;\mathbf{k}_1,\omega_1;\mathbf{k}_2,\omega_2;\mathbf{k}_3,\omega_3)\times \\ E^{HF}_{\mathbf{k}_1\omega_1,j}E^{HF}_{\mathbf{k}_2\omega_2,l}E^{*HF}_{\mathbf{k}_3\omega_3,m}\delta(\mathbf{k}-\mathbf{k}_1-\mathbf{k}_2-\mathbf{k}_3)\times \\ \delta(\omega-\omega_1-\omega_2-\omega_3)d\mathbf{k}_1d\mathbf{k}_2d\mathbf{k}_3d\omega_1d\omega_2d\omega_3,\end{aligned} \tag{9}$$

where $*$ denotes complex conjugate.

The effective nonlinear third-order plasma response is equal to

$$\Sigma^{eff}_{ijlm} \simeq \frac{n_0e^4}{5m_e^2T_e}\frac{\nu_e\delta_{ij}\delta_{lm}}{\Delta\omega\omega_1\omega_2\omega_3}\frac{\Delta\mathbf{k}^2v_s^2}{\Delta\omega^2-\Delta\mathbf{k}^2v_s^2}, \tag{10}$$

where n_0 is the unperturbed electron density, $\Delta\mathbf{k} = \mathbf{k}-\mathbf{k}_1 = \mathbf{k}_2+\mathbf{k}_3$, $\Delta\omega = \omega-\omega_1 = \omega_2+\omega_3$, and $v_s = (10T_e/3m_i)^{1/2}$ is the speed of sound (under the assumption (1)). We note that the expression $\Delta\omega^2-\Delta\mathbf{k}^2v_s^2$ in the denominator of the right hand side of (10) is incorrect when $\Delta\omega^2 \sim \Delta\mathbf{k}^2v_s^2$; for this case we have to proceed with another expression. To find the characteristic times of the modulated instability development, we have to substitute (8)-(10) into the equation for the high-frequency wave field:

$$\left(\varepsilon^t_{\mathbf{k}\omega} - \frac{\mathbf{k}^2c^2}{\omega^2}\right)E^{HF}_{\mathbf{k}\omega,i} = -\frac{4\pi i}{\omega}j^{(3),HF}_{\mathbf{k}\omega,i}, \tag{11}$$

where $\varepsilon^t_{\mathbf{k}\omega}$ is the usual (linear) transverse dielectric permittivity of a plasma.

Then we proceed with the following ansatz

$$\mathbf{E}_{\mathbf{k}\omega} = \mathbf{E}_0\delta(\mathbf{k}-\mathbf{k}_0)\delta(\omega-\omega_0) + \delta\mathbf{E}_{\mathbf{k}\omega}, \tag{12}$$

where $\delta\mathbf{E}_{\mathbf{k}\omega}$ is the modulated perturbation of the pump fields $\mathbf{E}_0$, $|\delta\mathbf{E}_{\mathbf{k}\omega}| \ll |\mathbf{E}_0|$.

After linearising the corresponding equation for $\delta\mathbf{E}_{\mathbf{k}\omega}$, and using an analogous procedure for the complex conjugate fields $\mathbf{E}^*$, we have the following dispersion equation for the modulational instability (the analogous equation was obtained in [5-7]):

$$1 = \Sigma_0|\mathbf{E}_0|^2\left[\frac{|\mathbf{k}_0\times(\Delta\mathbf{k}+\mathbf{k}_0)|^2/\mathbf{k}_0^2|\Delta\mathbf{k}+\mathbf{k}_0|^2}{(\varepsilon^t_{\Delta k+k_0}-(\Delta\mathbf{k}+\mathbf{k}_0)^2c^2/(\Delta\omega+\omega_0)^2}\right]+$$
$$\Sigma_0|\mathbf{E}_0|^2\left[\frac{|\mathbf{k}_0\cdot(\Delta\mathbf{k}-\mathbf{k}_0)|^2/\mathbf{k}_0^2|\Delta\mathbf{k}-\mathbf{k}_0|^2}{(\varepsilon^t_{\Delta k-k_0}-(\Delta\mathbf{k}-\mathbf{k}_0)^2c^2/(\Delta\omega-\omega_0)}\right], \qquad (13)$$

where $\varepsilon^t_{\Delta k\pm k_0}$ is the linear high frequency transversal dielectric permittivity of a plasma, and E_0 is the electromagnetic pump field (we assume the plasma is strongly underdense: $\omega_0 \gg \omega_{pe}$, where $\omega_{pe} = (4\pi n_0 e^2/m_e)^{1/2}$ is the electron plasma frequency). The factor Σ_0 in Eq.(13) is

$$\Sigma_0 = \frac{i}{5}\frac{\omega_{pe}^4}{\omega_0^4}\frac{1}{4\pi n_0 T_e}\frac{\nu_e|\Delta\mathbf{k}|^2v_s^2}{\Delta\omega[(\Delta\omega)^2-|\Delta\mathbf{k}|^2v_s^2]}. \qquad (14)$$

For the electromagnetic pump the instability is supersonic. Its rate is

$$\gamma^{\text{mod}} = \frac{1}{2}\nu_e\left(\frac{|\Delta\mathbf{k}|v_s}{\nu_e}\right)^{\frac{2}{3}}\left[\frac{1}{5}\frac{\omega_{pe}^4}{\omega_0^4}\frac{|\mathbf{E}_0|^2}{4\pi n_0T_e}\right]^{\frac{1}{3}} \qquad (15)$$

The instability rate is increased on the entire interval of the allowed values of $|\Delta\mathbf{k}|$, whose maximum is also given by the diffusion condition. We have

$$\gamma^{\text{mod}}_{\text{max}} = \nu_e\frac{v_s}{v_{Te}}\left(\frac{1}{5}\frac{\omega_{pe}^4}{\omega_0^4}\frac{|\mathbf{E}_0|^2}{4\pi n_0T_e}\right)^{\frac{1}{2}} \qquad (16)$$

By deriving (16) we have used an assumption $|\Delta\mathbf{k}| > \omega_{pe}^3\nu_e/\omega_0^3c$, which gives the minimum value for the wave vector of the modulated perturbations. So the following threshold arise:

$$\frac{|\mathbf{E}_0|^2}{20\pi n_0T_e} > \max\left\{\left(\frac{\omega_{pe}}{\omega_0}\right)^2\left(\frac{v_{Te}}{c}\right)^2, \left(\frac{3m_i}{10m_e}\right)^2\left(\frac{v_{Te}}{c}\right)^4\left(\frac{\omega_{pe}}{\omega_0}\right)^8\right\}. \qquad (17)$$

It is worth comparing the modulated instability rate and threshold with other nonlinear processes taking place in strongly underdense laser plasmas. The most effective nonlinear process there is stimulated Raman backscattering (SRS) [1,2]. Its rate is

$$\gamma^{\mathrm{SRS}} = \omega_{pe} \left(\frac{\omega_{pe}}{\omega_0} \frac{|\mathbf{E}_0|^2}{4\pi n_0 m_e c^2} \right)^{\frac{1}{2}}, \tag{18}$$

as well as the threshold

$$\gamma^{\mathrm{SRS}} > \frac{1}{2} \left(\frac{\omega_{pe}}{\omega_0} \right)^2 \nu_{\mathrm{eff}}. \tag{19}$$

Comparing (16) and (18), we have

$$\frac{\gamma^{\mathrm{mod}}}{\gamma^{\mathrm{SRS}}} = \frac{10 m_e}{3 m_i} \frac{\nu_e}{\omega_{pe}} \left(\frac{\omega_{pe}^3}{\omega_0^3} \frac{c^2}{v_{Te}^2} \right)^{\frac{1}{2}} \tag{20}$$

For the typical laser plasma parameters ($\omega_0 \sim 10^{15}$rad/sec, $\omega_{pe} \sim 10^{14}$rad/sec, $\nu_e \sim 10^{12}$rad/sec, $v_{Te}/c \sim 10^{-2} - 10^{-1}$), the rate of the modulational instability is always less than the γ^{SRS}. But we note that the SRS is a resonant process occuring only in localized regions of the (inhomogeneous) plasma corona determined by corresponding energy and momentum matching conditions. The modulational instability is a nonresonant process (like filamentation of the laser light), and consequently no matching conditions are to be satisfied. Moreover if we compare the thresholds of the modulational instability and the SRS, we find $\gamma_{\mathrm{thr}}^{\mathrm{mod}}/\gamma_{\mathrm{thr}}^{\mathrm{SRS}} \sim 10^5 (v_{Te}/c)^4$, this can be much less than unity, depending on plasma temperature. Thus the modulational instability can occur when the SRS is "switched off".

The considered case of relatively small instability rates (because of condition (1)) is useful to establish the instability threshold. It is also interesting to examine the case of larger rates, when inequality opposite to (1) takes place (but $|\Delta\omega| \ll \nu_{\mathrm{eff}}$).

References

1. Kruer W.L. Physics of Laser Plasma Interactions. Redwood Sity, CA: Addison-Wesley, 1988).

2. Campbell E.M., Phys. Fluids B, 1992, **4**, 3781.
3. Braginskii S.I. Reviews of Plasma Physics (Ed. M.A.Leontovich). N.Y.: Consultants Bureau, 1965, 205.
4. Tsytovich V.N. Theory of Turbulent Plasma. N.Y.: Consultants Bureau, 1977.
5. Stenflo L., Physica Scripta, 1990 **T30**, 166.
6. Stenflo L., J. Atm. Terr. Physics, 1990, **52**, 6.
7. Vladimirov S.V. and Krivitsky V.S., Phys. Rev. E, 1993, **47**, R1471.

STIMULATED SCATTERING OF UPHYBRID PLASMA WAVE BY RELATIVISTIC ELECTRON BEAM

V. I. Miroshnichenko, Ya. B. Fainberg, A. E. Volkov
Kharkov Institute of Physics and Technology,
Kharkov, Ukraine

There has been a great deal of interest in recent years in the possibility of using a powerful Langmuir wave, exited in a plasma, as an effective undulator for lasing, based on the stimulated coherent scattering of the wave by a relativistic electron beam [1-3]. This interest has been caused by the several following factors. As it is well known [4], the wavelengths λ_s of the stimulated coherent radiation resulting from a spatially periodic magnetostatic field of an undulator (wiggler) is determined by the following approximation formula:

$$\lambda_s = \lambda_\omega/2\gamma^2, \quad \gamma = (1-\beta^2)^{-1/2}, \quad \beta = v/c. \tag{1}$$

where λ_ω is the space period of the magnetostatic field, γ is the relativistic factor($\gamma = E/mc^2$, E is the electron beam energy)

The construction of undulators with the periods λ_ω smaller than several centimeters and sufficiently powerful magnetic fields presents some technical difficulties. It was suggested in [1-3] to use a powerful plasma wave as an undulator for promotion towards the range of shorter wave lengths.

The plasma wavelengths can be significantly smaller in comparison with the space periods of conventional undulators used in free electron lasers (FEL's).

Among the attractive features of using the plasma wave as an undulator for FEL we shall mention the following:

1. It is possible to transmit significantly higher currents through the plasma then through vacuum, consequently, using of plasma opens the way for enhancing short wavelengths radiation. The transmitted electron beam can be focused by the plasma in this case.

2. The electric field strengths attained with plasma waves are as high as the intensities of conventional magnetostatic undulator fields, or may be superior in their action on relativistic beam electrons.

3. Undulators with wavelengths ranging from $1cm$ to tens of μm can be created by varying the plasma density in a wide range and by exiting intense Langmuir waves in plasma.

4. The employment of various waves excited in the plasma extends the set of elementary effects that can be used for short wavelength radiation generation (the possibility of existing of collective effects based on the anomalous scattering effects may realized because the plasma waves can be slowed down ($v_{ph} < c$) [5]. The interaction of the REB with plasma whose density periodically changes in spaces offers possibility of using the elementary effect of the parametric Cherenkov radiation in the collective regime [6].

The stimulated coherent scattering of an extraordinary electromagnetic wave excited in a magnetized plasma by a REB to generate a short wavelengths radiation has been investigated in [7].

It is of great interest to study the possibilities of using various waves that can be excited in a plasma as effective undulators for generating short wavelength radiation. On this regard, we investigate here the possibility of employing the uphybrid wave in a magnetized plasma as an undulator. As it is known [8], the uphybrid plasma wave frequency in the case of a slow phase velocity and the perpendicular direction of propagation to the uniform magnetic field is given by the following expression:

$$\omega_3 \simeq \sqrt{\omega_{pe}^2 + \omega_{He}^2} \qquad (2)$$

where $\omega_{pe} = (4\pi e n_0^2/m)^{1/2}$ is the electron plasma freqnency,$\omega_{He} = eH_0/mc$ electron cyclotron frequency.

The occurring dependence of the wave frequency on the magnetic field strength provides for one more channel to change the pump wave

frequency and, consequently, to control the frequency tuning of the short wave length radiation that can be produced due to stimulated scattering of the wave by relativistic beam electron.

Let us consider the stimulated coherent scattering of the uphybrid plasma wave propagating normally to the direction of the beam motion and to the uniform magnetic field H_0. We shall analyze the efficiency of short wavelength radiation that propagates along the beam using the model of three-wave interaction.Suppose that the electric field strength of incident and scattered waves are directed along the x-axis.For the validity of this assumption we shall be interested in the case of great frequency upshifting of the scattered wave, so the influence of the uniform magnetic field on the dispersion characteristics can be ignored.On describing the process of scattering we assume that the electric field strengths of the waves participating in the three-wave interaction have the following form:

$$\vec{\mathcal{E}}_i(\vec{r},t) = Re\vec{E}_i(z)exp[i(\vec{k}_i\vec{r} - \omega_i t)], \quad (i = 1,2,3) \tag{3}$$

where the indices 1,2,3 belong, respectively, to the scattered HF wave, the wave of HF beam charge density and the uphybrid pump wave. Following the standard procedure we shall suppose that the phase synchronism between the wavevectors and the frequencies which provides the effective energy exchange between the interacting waves is achieved under the conditions

$$\vec{k}_1 = \vec{k}_2 + \vec{k}_3; \qquad \omega_1 = \omega_2 + \omega_3. \tag{4}$$

Applying the standard methods one can derive the general dispersion equation to discribe the initial linear stage of the stimulated coherent scattering of the wave under study by the relativistic beam electrons. The nonlinear dispersion equation can be written in the general form, if we take into account the above-made assumptions and ignore the beam electron effect on the dispersion of the scattered wave:

$$(\vec{n}_1^2 - \varepsilon_1)\varepsilon_1[\varepsilon_2 - \frac{\omega_1^2\delta_1^2}{\omega_b^2\delta_2^2} + \frac{\omega_b^2(\varepsilon_2 - 1)\beta^2\vec{n}_{21}^2}{\gamma\omega_2^2\delta_2^2(\vec{n}_2^2 - \varepsilon_2)}] =$$

$$\frac{\omega_b^2\beta_B'^2\varepsilon_2}{4\omega_1^2\delta_2^2\gamma}[\vec{n}_{21}^2 + \gamma^2(n_{2z} - \beta)^2]\{(\vec{n}_1'\vec{e}_3')^2 - 1 - \tag{5}$$

$$-(\varepsilon_1 - 1)[((\vec{n}_1'\vec{e}_{31}')\beta\gamma + \frac{e_{3z}'}{\gamma\delta_1})^2 + \vec{e}_{31}'^2]]$$

where the following notation is used:

$$\begin{aligned}
\vec{\beta}_{31}' &= \beta_B'\vec{e}_{31}' = \beta_B(\vec{e}_{31} + \frac{\beta\vec{n}_{31}}{\delta_3}e_{3z}), \quad \beta_{3z}' = \beta_B'\vec{e}_z' = \beta_B'\frac{e_{3z}}{\gamma\delta_3}; \\
\frac{c\vec{k}_i}{\omega_i} &= \vec{n}_i \quad (i = 1,2,3), \quad \vec{n}_{31}' = \frac{\vec{n}_{31}}{\gamma\delta_3}, \quad n_{3z}' = \frac{n_{3z} - \beta}{\gamma\delta_3}, \qquad (6) \\
\delta_i &= 1 - \beta n_{iz}, \quad \varepsilon_i = 1 - \frac{\omega_{pe}^2}{\omega_i^2}, \quad \omega_b^2 = \frac{4\pi e^2 n_b}{m}, \\
\vec{\beta}_i &= \frac{e\vec{E}_i}{mc\omega_i}, \quad \beta = \frac{v}{c}, \quad \gamma = (1 - \beta^2)^{-1/2}
\end{aligned}$$

The conditions of phase synchronism (4) together with the condition of resonance interaction of the beam electrons with the combination wave

$$\omega_2 - k_{2z}v \simeq 0 \qquad (7)$$

allow us to get the following expression for the scattered wave frequency

$$\omega_1 = 2\gamma^2\omega_3(1 - v\cos\theta_3/v_{ph}), \quad v_{ph} = \omega_3/k_3, \quad k_{3z} = k_3\cos\theta_3 \qquad (8)$$

If the pump uphybrid wave propagates normally to the beam motion $\theta_3 = \pi/2$, we may obtain the following expression for the scattered wave frequency

$$\omega_1 = 2\gamma^2\omega_3 \qquad (9)$$

where ω_3 is given by expression (2) in the case of a strong slowing down of the uphybrid wave.

For chosen configuration of fields of the pump wave, the scattered wave and combination wave eq. (5) can be rewritten in a simpler form:

$$(c^2k_2^2 - \omega_1^2 + \omega_{pe}^2)[1 - \frac{\omega_{pe}^2}{\omega_2^2} - \frac{\omega_{b\|}^2}{(\omega_2 - k_{2z}v)^2}] = \qquad (10)$$
$$-\frac{\omega_{b\|}^2\beta_B^2[c^2k_{2z}/\gamma^2 + c^2k_{21}^2]}{4(\omega_2 - k_{2z}v)^2}$$

The gain coefficients of the scattered electromagnetic wave amplitude for different scattering regimes can be determined from the dispersion equation (10). If the uphybrid wave amplitudes are large enough and the electron beam current density is small, the so-called regime of "modified" decay scattering (or Compton scattering) takes place, which is characterized by the following gain coefficient:

$$Imk_{1z} = (\sqrt{3}/4c)(\omega_{b\|}^2 \beta_B^2 \omega_3)^{1/3} \tag{11}$$

In this case, the forces of HF frequency Coulomb repulsion are negligible as compared to the ponderomotive potential forces, so the beam electrons have no time to make any vibrations due to the force of Coulomb repulsion.

If the electron beam density is high enough, and the oscillations of beam electrons caused by HF beam bunching are essential, then Raman regime of scattering is realized and the gain coefficient is determined by the expression:

$$Im\delta k_1 z = (\beta_B/4c)(\omega_{b\|}\omega_3)^{1/2}, \quad \beta_B = eE_3/mc\omega_3 \tag{12}$$

We now estimate the possible value of the parameter β_B which is essential for the determnation of the gain coefficients. Assuming the complete electron density modulation of the plasma to be achievable and using the Poisson equation, we obtain:

$$\beta_B = \omega_{pe}^2/\omega_3^2 n_x \tag{13}$$

where $n_x = ck_{3x}/\omega_3$ is the refractive index of the uphybrid wave. It follows from (13) that the suitable β_B values should be chosen for moderately slowed down waves rather than for very slow waves. We give the expression for the refractive index of the uphybrid wave as a function of frequency:

$$n_x^2(\omega) = \frac{\omega^4 - 2(\omega_{pe}^2 + \omega_{He})^2) + \omega_{pe}^4}{\omega^2[\omega^2 - (\omega_{pe}^2 + \omega_{He})]} \tag{14}$$

The appropriate choice of the pump wave frequency in the interval ω_{pe} and $\sqrt{\omega_{pe}^2 + \omega_{He}^2}$ can provide the suitable values of the refractive

index n_x. The wave frequency ω_3 will be determined in this case by (14) for given n_x value.

So we come to the conclusion that the uphybrid wave can be used as an effective plasma undulator. The parameters of the undulator depend on both the plasma density and the applied magnetic field H_0. This latter can be varied to tune the scattered wave frequency or to prolong the beam wave interaction for obtaining a higher efficiency.

This work was supported by the Ukrainian State Committee of Science and Technology.

References

1. Balakirev V..,Miroshnichenko V.I., Ognivenko V.V. Ukr. Fiz. J.,1985, **30(12)**,1802

2. Balakirev V..,Miroshnichenko V.I., Fainberg Ya.B. Fizika Plazmy, 1986, **12(8)**,983.

3. C.Joshi, T.Katsouleas, J.M.Dawson, Y.T.Yan, and J.M.Slater. IEEE, J. Quantumn Electronics, 1987, **OE-23(9)**, 1571.

4. T.C. Marshall. Free-Electron Lasers (Russ. transl), Moscow, Mir publ., 1987.

5. Frank I.M. Yadernaya fizika, 1968, **7(5)**, 1100.

6. Fainberg Ya.B., Khizhnyak N.A. JETP, 1957, **32**, 883.

7. Miroshnichenko V.I., Fainberg Ya.B. Plazmennaya Electronika, Kiev, Naukova Dumka publ., 1989, 228.

8. Akhiezer A.I., et al. Elektrodynamika plazmy, Moscow, Nauka publ., 1974.

ON MODULATIONAL INTERACTION OF LOWER–HYBRID DRIFT WAVES

S.I.Popel (a), I.E.Rumanov (b), V.N.Tsytovich (c)
(a) Institute for Dynamics of Geospheres, Moscow, Russia
(b) Moscow Physical-Technical Inst., Dolgoprudny, Russia
(c) General Physics Institute, Moscow, Russia

For many physical and astrophysical problems connected with the investigation of inhomogeneous plasma in the presence of an external magnetic field one should study the evolution in a plasma of oscillations excited as a result of the development of the so–called lower–hybrid drift (LHD) instability (see [1–4]). This instability has been applied to explain the mechanism for the anomalous transport of particles, momentum, and energy in both space and laboratory plasmas (e.g., this instability has been proposed as a mechanism to provide anomalous resistivity for reconnection events in the Earth's magnetosphere [3,5], it has been studied to explain anomalous sheath broadening in theta pinch implosions [6], etc.). Further, the consideration of the LHD waves (i.e. the waves excited as a result of the LHD instability development) is important when describing the wave turbulence, which arises when an ionized cloud expands into background plasma. Such a situation has, in particular, occurred in the experiment carried out by the Active Magnetospheric Particle Tracer Explorers (AMPTE), which involved the release of barium atoms in the solar wind (see [4]).

The most important nonlinear process for the oscillations excited as a result of the LHD instability initiated by an electron current is the modulational interaction (see [3,4]). The modulational interaction of the LHD waves determines the saturation mechanism for the LHD instability, which is associated with the cascade of waves

with high phase velocities along the external magnetic field $\mathbf{B}_0$ to waves with phase velocities along $\mathbf{B}_0$ close to the electron thermal velocity. Use of such a saturation mechanism permits to obtain the effective frequency of electron collisions in inhomogeneous plasmas. The consideration of the modulational instability (MI) of the LHD waves [4] for the case of the AMPTE release experiment is essential for the explanation of the magnetic structures, particles spectra, and the magnitude of electric field amplitude observed in the experiment.

The MI of the LHD waves has been studying previously only in particular cases [3] and for specific situations (*e.g.*, for the conditions of the AMPTE barium release experiment [4]), the consideration of the MI of the LHD waves having been carried out on the basis of the hydrodynamical equations. Here we consider the MI of the LHD waves on the basis of general kinetic approach that enables us to carry out more complete and detailed investigation of the LHD wave MI. We demonstrate that the situation is possible when the nonlinear response defining the character of the LHD MI is determined by the inhomogeneity effects (such a situation has not been analyzed previously). We consider the case, when the LHD waves are excited as a result of the kinetic current–driven LHD instability (see also [3]). This case corresponds to the inequality $|\omega| \ll |\mathbf{k}| v_{Ti}$, where ω, $\mathbf{k}$ are respectively the frequency and the wavenumber of LHD wave, $v_{Ti(e)}$ is the ion (electron) thermal velocity. We assume that the following conditions are valid: $\omega_{Bi} \ll \omega \ll \omega_{Be}$;

$$\left| \frac{1}{k_x} \frac{d}{dx} \ln n_0 \right| \ll 1, \tag{1}$$

where n_0 is the unperturbed plasma density; $\omega_{Be(i)}$ is the electron (ion) gyrofrequency; the axes *Ox, Oy, Oz* are chosen respectively in the directions of the plasma inhomogeneity, the electron current, and the external magnetic field.

When the conditions

$$\omega_{Bi} \ll \omega \ll \omega_{Be}, \quad |\mathbf{k}_\perp| v_{Te}/\omega_{Be} \ll 1, \quad |k_\parallel| v_{Te}/|\omega - k_y u_{ey}| \ll 1,$$
$$\omega \ll |\mathbf{k}| v_{Ti}, \quad \omega_{pe} \ll |\mathbf{k}| c, \quad |\kappa_B| \ll |\kappa_n| \tag{2}$$

and

$$|\cos\theta| = |k_\parallel|/|\mathbf{k}| \ll |k_y\kappa_n/|\mathbf{k}|^2(\mathcal{A}(\mathbf{k}))^{1/2}| \tag{3}$$

(where $\mathcal{A}(\mathbf{k}) = (\omega_{Be}/\omega_{pe})^2 + (1 + |\mathbf{k}|^2 r_{L_*}^2)/|\mathbf{k}|^2 r_{L_*}^2$, $r_{L_*}^2 = T_i/m_e\omega_{Be}^2$, $\kappa_n = (1/n_0)(dn_0/dx)$, $\kappa_B = (1/|\mathbf{B_0}|)(d|\mathbf{B_0}|/dx)$, u_{ey} is the electron drift velocity, c is the speed of light, $T_{e(i)}$ is the electron (ion) temperature, $\omega_{pe(i)}$ is the electron (ion) plasma frequency, $m_{e(i)}$ is the electron (ion) mass) are valid, the linear dispersion equation for the LHD waves has the following solution:

$$\omega_{\mathbf{k}} = k_y u_{ey} + \frac{k_y\kappa_n}{\mathbf{k}^2}\frac{\omega_{Be}}{\mathcal{A}(\mathbf{k})} + i\gamma_{\mathbf{k}}, \tag{4}$$

$$\gamma_{\mathbf{k}} = -\left(\frac{\pi}{2}\right)^{1/2}\frac{k_y\kappa_n\omega_{Be}}{\mathbf{k}^2\mathcal{A}^2(\mathbf{k})}\frac{\mathrm{Re}\omega_{\mathbf{k}}}{|\mathbf{k}|v_{Ti}\mathbf{k}^2 r_{L_*}^2}. \tag{5}$$

The values (4) and (5) are respectively the frequency and the growth rate of the LH drift waves. In the considered situation the LH drift instability develops when u_{ey} exceeds its threshold value:

$$u_{ey} > |\kappa_n|\omega_{Be}/|\mathbf{k}|^2\mathcal{A}(\mathbf{k}) \tag{6}$$

and $k_y\kappa_n < 0$.

The conditions (2) and (3) are supposed to be valid below.

The condition (1) allows us to investigate the LHD wave MI by standard way [7,8]. We derive the equation of the third order in field strength for the LHD waves in inhomogeneous plasma. This equation is derived by using the kinetic equations for electrons and ions and the Poisson equation; perturbations of the distribution function expand in a set of terms over powers of the LHD wave electric field $\mathbf{E}$, which up to the cubic terms are expressed through the LHD wave fields and unperturbed (both electron and ion) distribution function. Further, we distinguish in the obtained equation positive and negative-frequency parts of the LHD wave fields: E_k^+, E_k^- (where $\mathbf{E}_k = \mathbf{k}E_k/|\mathbf{k}|$ defined as follows: $E_k\exp[i\int k_x(x)dx] \approx E_k\exp[ik_x(x)x]$ is the Fourier component of the LHD electric field; $k = \{\omega, \mathbf{k}\}$; E_k^+, E_k^- correspond

to $\omega > 0$, $\omega < 0$ respectively), and introduce the virtual fields E_k^v on the low frequency $\Delta\omega \ll \omega_{LH} = \omega_{pi}(1+\omega_{pe}^2/\omega_{Be}^2)^{-1/2}$. Finally we obtain the equation containing the wave fields $E_k^{\pm}$ only:

$$\varepsilon_k E_k^+ = 2\int \Sigma^{\rm eff}_{k,k_1,k_2,k_3} E_{k_1}^+ E_{k_2}^+ E_{k_3}^- \delta(k-k_1-k_2-k_3)dk_1dk_2dk_3, \quad (7)$$

where $\delta(k) = \delta(\omega)\delta(\mathbf{k})$, $\varepsilon_k = \varepsilon(\omega,\mathbf{k})$ is the linear dielectric function for the inhomogeneous plasma;

$$\Sigma^{\rm eff}_{kk_1k_2k_3} = -\frac{e^2(\Delta\mathbf{k})^2\varepsilon^{(i)}_{\Delta k}}{2m_e^2|\mathbf{k}||\mathbf{k_1}||\mathbf{k_2}||\mathbf{k_3}|\varepsilon_{\Delta k}}$$
$$\times\left\{\frac{k_{2\|}k_{3\|}}{\delta^2} - \frac{(\mathbf{k}_{2\perp}\cdot\mathbf{k}_{3\perp})}{\omega_{Be}^2} - \frac{i(\mathbf{k}_{2\perp}\times\mathbf{k}_{3\perp})_\|}{\omega_{Be}\delta}\right\}$$
$$\times\left\{(\varepsilon^{(e)}_{\Delta k}-1)\left(\frac{k_\| k_{1\|}}{\delta^2} - \frac{(\mathbf{k}_\perp\cdot\mathbf{k}_{1\perp})}{\omega_{Be}^2}\right.\right.$$
$$\left.\left. + \frac{i(\mathbf{k}_\perp\times\mathbf{k}_{1\perp})_\|}{\omega_{Be}\delta}\right) + (\tilde{\varepsilon}^{(e)}_{\Delta k}-1)\frac{k_{1y}\kappa_n}{\omega_{Be}\delta}\right\}. \quad (8)$$

Here $-e$ is the electron charge; $\Delta k = k - k_1$; $\varepsilon^{(e,i)}_{\Delta k}$ is the electron (ion) part of the dielectric function; $\tilde{\varepsilon}^{(e)}_{\Delta k}$ is the electron dielectric function for homogeneous plasma (the smallness of the parameter $|\kappa_n|v_{Te}/\omega_{Be} \ll 1$ has been used), $\delta = \omega - k_y u_{ey}$; the subscripts $\|$, $\perp$ denote respectively the vector component parallel and perpendicular to the external magnetic field. The expressions (7) and (8) are derived when $|\delta| \approx |\delta_1| \approx |\delta_2| \approx |\delta_3| \gg |\Delta\delta|$. Here $\delta_i = \omega_i - k_{iy}u_{ey}$, $i = 1,2,3$, $\Delta\delta = \delta - \delta_1$.

The dispersion equation for the LHD MI is derived from the equations obtained by such a way (as a solvability condition of a system of two equations for modulational perturbations $\delta E_k^{\pm}$). The dispersion equation has the following form:

$$1 = -2|E_0|^2\left(\frac{\Sigma^{\rm eff}_{\Delta k+k_0,k_0,\Delta k+k_0,-k_0}}{\varepsilon_{\Delta k+k_0}} + \frac{\Sigma^{\rm eff}_{\Delta k-k_0,-k_0,\Delta k-k_0,k_0}}{\varepsilon_{\Delta k-k_0}}\right), \quad (9)$$

where E_0 is the amplitude of the pump wave.

The investigation of the dispersion equation demonstrates that the LHD wave MI develops only when the wavenumber of the modulational perturbation $|\Delta\mathbf{k}|$ is less or of the order of that of the pump wave $|\mathbf{k}_0|$. The MI effect is maximum, when $\Delta\mathbf{k} \perp \mathbf{k}_0$. If the inequality $|\Delta\mathbf{k}| \ll |\kappa_n|$ is valid, then the nonlinear response defining the character of the MI is determined by the inhomogeneity effects. In this case the maximum value (for a fixed $|\Delta\mathbf{k}| \ll |\kappa_n|$) of the MI growth rate is attained for the pump levels

$$\frac{|E_0|^2}{4\pi n_0 T_i} \gg \max\left\{ \frac{\omega_{Be}|\mathbf{k}_0|v_{Ti}}{\omega_{pe}^2}; \right.$$
$$\left. \frac{\omega_{Be}^2}{\omega_{pe}^2}\frac{|\kappa_n^3 k_{0y}^3|v_{Te}^6}{\omega_{Be}^4|\Delta\mathbf{k}|^2 v_{Ti}^2}\frac{|\mathbf{k}_0|}{|\Delta\mathbf{k}|}; \frac{\omega_{Be}^2}{\omega_{pe}^2}\frac{\omega_{Be}^2}{\kappa_n^2 v_{Ti}^2}\frac{|\mathbf{k}_0|}{|\kappa_n|}\frac{|\Delta\mathbf{k}|^3}{|k_{0y}|^3}\frac{m_e^3}{m_i^3} \right\}$$

and has the following form

$$\gamma_{max}(|\Delta\mathbf{k}|) \sim \left(\frac{|E_0|^2}{4\pi n_0 T_i}\frac{\omega_{pe}^2}{\omega_{Be}}|\Delta\mathbf{k}|^2 v_{Ti}^2 \frac{|\Delta\mathbf{k}|}{|\mathbf{k}_0|} \right)^{1/3}. \qquad (10)$$

For larger values of $|\Delta\mathbf{k}|(\gg |\kappa_n|)$ the maximum rate of the modulational instability is:

$$\gamma_{max}(|\Delta\mathbf{k}|) = \left(\frac{|E_0|^2}{4\pi n_0 T_i}\frac{\omega_{pe}^2}{\omega_{Be}}|\Delta\mathbf{k}|^2 v_{Ti}^2 \frac{|\Delta\mathbf{k}|^2}{|k_{0y}\kappa_n|} \right)^{1/3}. \qquad (11)$$

The development of the modulational instability with this rate is possible for

$$\frac{|E_0|^2}{4\pi n_0 T_i} \gg \max\left\{ \frac{\omega_{Be} v_{Ti}|\kappa_n k_{0y}|}{\omega_{pe}^2|\Delta\mathbf{k}|}; \right.$$
$$\left. \frac{\omega_{Be}^2}{\omega_{pe}^2}\frac{\kappa_n^4 v_{Te}^4}{\omega_{Be}^4}\frac{v_{Te}^2}{v_{Ti}^2}\frac{k_{0y}^4}{|\Delta\mathbf{k}|^4}; \frac{\omega_{Be}^2}{\omega_{pe}^2}\frac{\omega_{Be}^2}{\kappa_n^2 v_{Ti}^2}\frac{|\Delta\mathbf{k}|^2}{k_{0y}^2}\frac{m_e^3}{m_i^3} \right\}.$$

Thus the influence of the plasma inhomogeneity results in appearance of the additional characteristic parameter of the problem (in comparison with the homogeneous situation), namely the inverse length of plasma inhomogeneity κ_n. The character of the modulational instability of the LHD waves essentially depends on the relationship between this parameter and the length of the wavevector of modulational perturbations. Note also that the LHD wave MI can develop sufficiently effective only when the length of the wavevector of modulational perturbations $\Delta\mathbf{k}$ is less or of the order of that of the pump wave $\mathbf{k}_0$ (in contrast to the well–investigated cases of the LH waves in homogeneous plasmas [7] and Langmuir waves [8], where the MI develops effectively for both $|\Delta\mathbf{k}| \ll |\mathbf{k}_0|$ and $|\Delta\mathbf{k}| \gg |\mathbf{k}_0|$).

References

1. Krall N.A. and Liewer P.C., Phys. Rev. A, 1971, **4**, 2094.
2. Mikhailovsky A.B. Theory of Plasma Instabilities, Vol.2. New York — London: Consultants Bureau, 1974.
3. Sotnikov V.I., Shapiro V.D., and Shevchenko V.I., Physica D, 1981, **2**, 170.
4. Bingham R., Shapiro V.D., Tsytovich V.N., et al., Phys. Fluids B, 1991, **3**, 1728.
5. Huba J.D., Gladd N.T., and Papadopoulos K., J. Geophys. Res., 1978, **83**, 5217.
6. Davis W., DeSilva A.W., Dove W., et al., in *Plasma Physics and Controlled Nuclear Fusion Research* (IAEA, Vienna, 1971), Vol.III, p.289.
7. Tsytovich V.N., Vladimirov S.V., Popel S.I., Phys. Scripta, 1992, **46**, 65.
8. Rudakov L.I., Tsytovich V.N., Phys. Reports, 1978, **40C**, 1.

ON THE BEAM INSTABILITY IN A PLASMA IN THE PRESENCE OF THE ION–SOUND TURBULENCE

S.I.Popel
Institute for Dynamics of Geospheres, Moscow, Russia

For many physical problems (solar bursts, plasma heating by an electron beam, etc.) the interaction of the electron beams with the non–isothermal plasma

$$T_i \ll T_e \tag{1}$$

(where T_i, T_e are respectively the ion and electron temperatures) is a problem of interest. In the situation (1) the ion–sound turbulence can essentially influence the electron beam dynamics. For example, the presence in a plasma of the intesive ion–sound oscillations can result [1] in the stabilization of the beam instability as a consequence of the nonlinear absorbtion of the Langmuir waves. Further, the presence of the ion–sound waves can lead to acceleration of the electrons of a beam [2,3] and to the stabilization of the beam instability [4] due to the nonlinear interaction of the resonant and non–resonant (with the beam) waves (the plasma–maser effect). However, the radiative–resonant interactions (RRIs) [5,6] of the ion–sound waves and plasma electrons can also result in the acceleration of electrons. In the present paper we consider the influence of the RRIs of the ion–sound waves and electrons upon the beam instability development.

Let us consider the one–dimensional nonrelativistic electron beam with the concentration n_b propagating in a plasma, in which the ion–sound waves with the spectrum $W^s_{\mathbf{k}}$ (where $W^s = \int W^s_{\mathbf{k}} d\mathbf{k}$ is the

(beam) of the distribution function and also the growth rate caused by the RRIs of the Langmuir waves and electrons (see [7,8]), then the stabilization of the beam instability occurs. In the case

$$n_b/n \geq (\alpha/4\pi)(\Delta v/c)^2 \tag{8}$$

the stabilization of the beam instability caused by the RRIs of the ion–sound waves and electrons occurs when

$$\left(\frac{n_b}{n}\right)^2 \ll \alpha \frac{m}{M} k_0 r_{De} \frac{W^s}{nT_e} \left(\frac{v_{Te}}{c}\right)^2 \left(\frac{\Delta v}{v_1}\right)^4 \tag{9}$$

(here k_0 is the characteristic value of k in the ion–sound wave spectrum). In the case

$$n_b/n < (\alpha/4\pi)(\Delta v/c)^2 \tag{10}$$

the stabilization of the beam instability occurs when

$$\frac{\alpha}{16\pi^2} \left(\frac{v_1}{v_{Te}}\right)^2 \left(\frac{v_1}{c}\right)^2 \frac{M}{m} \frac{1}{k_0 r_{De}} \frac{nT_e}{W^s} \ll 1. \tag{11}$$

Let us compare the rate of the electron energy change caused by the RRIs and those caused by the plasma–maser effect and the quasilinear interaction. The rate of the electron kinetic energy change caused by the RRIs is

$$\begin{aligned} < \dot{\varepsilon}^{Rad} > &\sim \int (\varepsilon_p - mc^2) Q_{\mathbf{p}} d\mathbf{p} \\ &\sim \alpha \frac{W^s}{nT_e} k_0 r_{De} nmv_s^2 \omega_{pe}. \end{aligned} \tag{12}$$

The conditions under which $< \dot{\varepsilon}^{Rad} >$ exceeds respectively $< \dot{\varepsilon}^{Nl} >$, the rate of the electron energy change caused by the plasma-maser effect (see [3]), and $| < \dot{\varepsilon}^{Ql} > |$, the electron energy change caused by the quasilinear interaction, are the following:

$$R_{\mathbf{p}',\mathbf{p}} \approx \frac{2c^2}{p\varepsilon_p(pc+\varepsilon_p)}\left(1+\frac{(\mathbf{p}'\cdot\mathbf{p})}{p^2}\right.$$
$$\left.+\frac{p'^2}{p^2}-\frac{1}{2}\frac{[\mathbf{p}'\times\mathbf{p}]^2\varepsilon_p}{p^4(cp+\varepsilon_p)}\right); \tag{4}$$

$\varepsilon_p = (p^2c^2+m^2c^4)^{1/2}$; $\hat{I}^{se}_{\mathbf{p}}$ is a quasilinear operator corresponding to the interaction of the ion–sound waves and electrons; $\int \Phi_{\mathbf{p}} d\mathbf{p} = n+n_b$. The calculation of $Q_{\mathbf{p}}$ under the assumptions that the distribution function $\Phi_{\mathbf{p}}$ is Maxwellian for $p \le mv_{Te}$ and the ion charge is e gives:

$$Q_{\mathbf{p}} \approx \frac{\alpha}{3}\left(\frac{2}{\pi}\right)^{1/2}\left(\frac{m}{M}\right)^{1/2}\frac{nv_s}{p^3}\frac{3pc+2\varepsilon_p}{\varepsilon_p(cp+\varepsilon_p)^2}$$
$$\times m^2v_{Te}^2c^2\int_0^\infty dkk^3\frac{W_k^s}{nT_e}. \tag{5}$$

where $v_s = (T_e/M)^{1/2}$. The term $\hat{I}^{se}_{\mathbf{p}}\Phi_{\mathbf{p}}$ in the equation for $\partial\Phi_{\mathbf{p}}/\partial t$ is negligible comparing with $Q_{\mathbf{p}}$ if the following conditions are fulfilled:

$$n_b/n \ll \alpha(v_1/c)^2(\Delta v/v_{Te})^3, \tag{6}$$
$$v \gg v_{Te}[2\ln\{2[\ln(3\pi c^2/4\alpha v_{Te}^2)]$$
$$\times(c/v_{Te})^2(3\pi/4\alpha)\}]^{1/2}. \tag{7}$$

Below we suppose that the conditions (6)–(7) are valid.

Thus (see (5)) the RRIs of the ion–sound waves and electrons result in the generation of the fast particles with the isotropic distribution $\Phi_{\mathbf{p}}^{Rad} = Q_{\mathbf{p}}t$. It is known (see, e.g., [1]) that the Langmuir wave growth rate corresponding to the isotropic distribution function is negative (the waves are damped). If at the time less than the characteristic time of the beam instability development the contribution to the Langmuir wave growth rate from the isotropic part of the distribution function $\Phi_{\mathbf{p}}^{Rad}$ exceeds that from the anisotropic part

energy density of the ion–sound waves) are excited. The spectrum $W^s_{\mathbf{k}}$ is supposed to be contained in the range of the wavevectors $\mathbf{k}$ obeying the following condition:

$$\frac{2}{3}\sqrt{\frac{m}{M}} + \frac{2v_{Te}}{v_1} < kr_{De} \ll 1, \tag{2}$$

where m, M are respectively the electron and ion masses, $v_{Te} = (T_e/m)^{1/2}$, v_1 is the lowest velocity of the beam particles ($v_1 \ll v_{Te}$), $k = |\mathbf{k}|$, $r_{De} = (T_e/4\pi ne^2)^{1/2}$, $-e$ is the electron charge, n is the plasma electron concentration ($n \gg n_b$). The left inequality (2) implies that the decay interactions of the Langmuir waves (excited as a result of the beam instability) and the ion–sound waves are forbidden, while the right inequality (2) allows us not to take into account the process of the induced scattering corresponding to the following resonance condition: $\omega^l_{\mathbf{q}} \pm \omega^s_{\mathbf{k}} = (\mathbf{q} \pm \mathbf{k}) \cdot \mathbf{v}$ (see [1]), where $\mathbf{v}$ is the velocity of the plasma particle, $\mathbf{q}$, $\mathbf{k}$ are respectively the wavevectors of the Langmuir and ion–sound waves; $\omega^l_{\mathbf{q}}$, $\omega^s_{\mathbf{k}}$ are respectively the frequencies of the Langmuir and ion–sound waves. We will assume that the spectrum of the ion–sound waves is isotropic, and the condition of the kinetic description of the beam instability $\Delta v/v_2 \gg (n_b/n)^{1/3}$ is valid. Here $\Delta v = v_2 - v_1$, v_2 is the largest velocity of the beam particles. The external magnetic field is supposed to be absent.

The dynamics of the electron distribution function $\Phi_{\mathbf{p}}$ (including the distributions both of the beam electrons and the plasma electrons) is described by the equations, in which the quasilinear interactions and the RRIs are taken into account (see [5,6]). The most contribution to the equation for $\partial\Phi_{\mathbf{p}}/\partial t$ (among the terms corresponding to the RRIs of the ion–sound waves and electrons) for the case $p \equiv |\mathbf{p}| \gg mv_{Te}$ is made by the following term:

$$Q_{\mathbf{p}} = \pi\alpha \int d\mathbf{p}' R_{\mathbf{p}',\mathbf{p}} \hat{I}^{se}_{\mathbf{p}'} \Phi_{\mathbf{p}'}/(2\pi)^3, \tag{3}$$

where $\alpha = e^2/\hbar c \approx 1/137$; c is the speed of light; $\hbar$ is the Planck's constant; $R_{\mathbf{p}',\mathbf{p}}$ is a certain function of $\mathbf{p}'$ and $\mathbf{p}$ (see [5,6]), and its expansion in the parameters p'/p and p'/mc up to the second order in p' is:

$$\left(\frac{n_b}{n}\right)^2 \ll \alpha \frac{m}{M} k_0 r_{De} \frac{\Delta v}{v_1} \left(\frac{\Delta v}{v_{Te}}\right)^2; \quad (13)$$

$$\left(\frac{n_b}{n}\right)^2 \ll \alpha \frac{m}{M} k_0 r_{De} \frac{W^s}{nT_e} \left(\frac{v_{Te}}{v_1}\right)^2 \left(\frac{\Delta v}{v_1}\right). \quad (14)$$

Thus the RRIs of the ion–sound waves and electrons can result in the stabilization of the beam instability. The conditions (13) and (14) are valid when the conditions for the stabilization of the beam instability ((8)–(9) or (10)–(11)) are fulfilled. However there is the range of parameters (W^s/nT_e, k_0, Δv, v_1, n_b, n, T_e) when the conditions for the stabilization of the beam instability are not fulfilled, but the conditions (13) and/or (14) are valid. In this case generation of fast electrons caused by the RRIs of the ion–sound waves and electrons is the essential process which should be taken into account when describing the beam instability development.

References

1. Tsytovich V.N. Nonlinear Effects in Plasma. New York: Plenum, 1970.
2. Krivitsky V.S. and Vladimirov S.V., J. Plasma Phys., 1991, **46**, 209; *ibid.*, 1991, **46**, 219.
3. Vladimirov S.V. and Krivitsky V.S., Sov. Phys. — Lebedev Inst. Reports, 1990, No.1, 53 [Kratkie Soobshcheniya po Fizike. FIAN, 1990, No.1, 37].
4. Popel S.I., Vladimirov S.V., and Yu M.Y., Phys. Scripta, 1993, **47**, 239.
5. Tsytovich V.N., Phys. Reports, 1989, **178**, 261.
6. Popel S.I., Sov. J. Plasma Phys., 1993, **19**, No.1 [Fiz. Plazmy, 1993, **19**, 60].
7. Popel S.I. and Tsytovich V.N., Sov. Phys. — Lebedev Inst. Reports., 1990, No.4, 29 [Kratkie Soobshcheniya po Fizike. FIAN, 1990, No.4, 22].
8. Popel S.I. and Tsytovich V.N., Sov. Tech. Phys. Lett., 1990, **16**, 602 [Pis'ma Zh. Techn. Phys., 1990, **16**, No.16, 7].

BEAM INSTABILITY DEVELOPMENT AND THE PLASMA-MASER EFFECT

S.I. Popel, S.V. Vladimirov, and M.Y. Yu
Institute for Dynamics of Geospheres, Moscow, Russia
General Physics Institute, Moscow, Russia
Ruhr-University Bochum, Germany

The evolution of waves in turbulent plasmas, in which a large number of degrees of freedom is excited, can often be determined by the nonlinear interactions of the waves. Among them the nonlinear interaction of resonant waves with the non-resonant ones can be important (see, *e.g.*, [1,2]). The non-resonant waves are those for which both the Cherenkov resonance condition

$$\omega - \mathbf{k} \cdot \mathbf{v} = 0 \tag{1}$$

and the scattering (off the second type of waves, namely the resonant waves) condition

$$\omega - \Omega - (\mathbf{k} - \mathbf{q}) \cdot \mathbf{v} = 0 \tag{2}$$

are not satisfied, while the resonant waves are those for which the condition (1) is satisfied. Here ω and Ω are the frequencies of the considered waves, $\mathbf{k}$ and $\mathbf{q}$ are the corresponding wavenumbers, and $\mathbf{v}$ is the velocity of a plasma particle. The effect of the nonlinear interactions of the resonant and non-resonant waves is called the plasma-maser effect (see, *e.g.*, [2]).

In the present paper, we investigate the nonlinear evolution of the resonant waves accounting for their interaction with the non–resonant waves. We obtain a general expression for the nonlinear growth rate of the resonant waves. We consider influence of the plasma–maser effect on the beam instability development.

The electron distribution function f satisfies the collisionless kinetic equation

$$\frac{\partial f}{\partial t} + \mathbf{v} \cdot \frac{\partial f}{\partial \mathbf{r}} + e\mathbf{E} \cdot \frac{\partial f}{\partial \mathbf{p}} = 0 \tag{3}$$

where the electron charge is $e = -|e|$. Let us define the regular part Φ of the distribution function by

$$\Phi = < f >, \tag{4}$$

where the angular brackets $<>$ denote averaging over a statistical ensemble. For the sake of simplicity, we assume that all fields are longitudinal. The electric field $\mathbf{E}$ is then governed by the Poisson's equation

$$\nabla \cdot \mathbf{E} = 4\pi e \int \delta f d\mathbf{p}/(2\pi)^3, \tag{5}$$

where δf is the fluctuating part of the distribution function. We shall represent it by an expansion in powers of the turbulent field $\mathbf{E}$

$$\delta f = \sum_{l=1}^{\infty} \delta f^{(l)}, \tag{6}$$

where $\delta f^{(l)} \propto |E|^l$. We have normalized the distribution function f by

$$n = \int \frac{d\mathbf{p}}{(2\pi)^3} f, \tag{7}$$

where n is the concentration of plasma electrons.

We now introduce the correlation function of the Fourier components of the electric fields by

$$< E_{\omega,\mathbf{k};i} E_{\omega',\mathbf{k}';j} >= |E_{\omega,\mathbf{k}}|^2 \delta(\omega + \omega') \delta(\mathbf{k} + \mathbf{k}') k_i k_j / |\mathbf{k}|^2, \tag{8}$$

where

$$E_{\omega,\mathbf{k}} = \int E(t,\mathbf{r}) \exp(i\omega t - i\mathbf{k} \cdot \mathbf{r}) dt d\mathbf{r}/(2\pi)^4 = \mathbf{k} E_{\omega,\mathbf{k}}/|\mathbf{k}|. \tag{9}$$

Here, for the frequency and wavenumber of the Fourier components of the resonant waves, we use the notations ω and $\mathbf{k}$, while for those

of the non–resonant waves we use Ω and $\mathbf{q}$. The last factors in Eqs.(9) and (10) demonstrate the longitudinal character of the waves.

We are interested in the nonlinear contribution to the dielectric function (of the resonant waves) proportional to $|E_{\Omega,\mathbf{q}}|^2 E_{\omega,\mathbf{k}}$. This can come from coupling $(\delta f^{(2)})^2$ as well as from $\delta f^{(3)}$. The contribution of the second order (in the fields) terms to the imaginary part of the nonlinear dielectric permittivity of the resonant waves is

$$\mathrm{Im}\delta\varepsilon^{\mathrm{pol}}(\omega,\mathbf{k}) = -\frac{16\pi^2 e^6}{|\mathbf{k}|^2}\int \frac{d\Omega d\mathbf{q}}{|\mathbf{q}|^2}\frac{|E_{\Omega,\mathbf{q}}|^2}{|\mathbf{k}-\mathbf{q}|^2\varepsilon^L(\omega-\Omega,k-q)}$$
$$\times\mathrm{Im}[S(\omega,\mathbf{k};\Omega,\mathbf{q};\omega-\Omega,\mathbf{k}-\mathbf{q})S(\omega-\Omega,\mathbf{k}-\mathbf{q};\omega,\mathbf{k};-\Omega,-\mathbf{q})] \quad (10)$$

where the (symmetrized over the last two indices) second order plasma response is

$$S(\omega,\mathbf{k};\omega_1,\mathbf{k}_1;\omega_2,\mathbf{k}_2) = \int \frac{d\mathbf{p}}{(2\pi)^3}\frac{1}{\omega-\mathbf{k}\cdot\mathbf{v}+i0}$$
$$\times\left\{\left(\mathbf{k}_1\cdot\frac{\partial}{\partial\mathbf{p}}\right)\frac{1}{\omega_2-\mathbf{k}_2\cdot\mathbf{v}+i0}\left(\mathbf{k}_2\cdot\frac{\partial}{\partial\mathbf{p}}\right)\right.$$
$$\left.+\left(\mathbf{k}_2\cdot\frac{\partial}{\partial\mathbf{p}}\right)\frac{1}{\omega_1-\mathbf{k}_1\cdot\mathbf{v}+i0}\left(\mathbf{k}_1\cdot\frac{\partial}{\partial\mathbf{p}}\right)\right\}\Phi. \quad (11)$$

In Eq.(11), only for the resonant waves the imaginary parts of the denominators are to be taken into account (the scattering condition (2) is not satisfied here). The contribution of the resonant waves to the imaginary part of the nonlinear dielectric permittivity by the third order terms is

$$\mathrm{Im}\delta\varepsilon^{(3)}(\omega,\mathbf{k}) = \mathrm{Im}\left\{\frac{4\pi^2 e^4}{|\mathbf{k}|^2}\int\frac{d\mathbf{p}}{(2\pi)^3}\frac{d\Omega d\mathbf{q}}{|\mathbf{q}|^2}\frac{|E_{\Omega,\mathbf{q}}|^2}{\omega-\mathbf{k}\cdot\mathbf{v}+i0}\right.$$
$$\times\left(\mathbf{q}\cdot\frac{\partial}{\partial\mathbf{p}}\right)\frac{1}{\omega-\Omega-(\mathbf{k}-\mathbf{q})\cdot\mathbf{v}}\left[\mathbf{k}\cdot\frac{\partial}{\partial\mathbf{p}}\right)\frac{1}{\Omega-\mathbf{q}\cdot\mathbf{v}}\left(\mathbf{q}\cdot\frac{\partial}{\partial\mathbf{p}}\right)$$
$$\left.-\left(\mathbf{q}\cdot\frac{\partial}{\partial\mathbf{p}}\right)\frac{1}{\omega-\mathbf{k}\cdot\mathbf{v}+i0}\left(\mathbf{k}\cdot\frac{\partial}{\partial\mathbf{p}}\right)\right]\Phi\Big\}. \quad (12)$$

We can simplify this equation by a standard method [2,3]. In particular, we expand the denominator $[\omega - \Omega - (\mathbf{k}-\mathbf{q})\cdot\mathbf{v}]^{-1}$ by $[\omega - \Omega - (\mathbf{k}-\mathbf{q})\cdot\mathbf{v}]^{-1} = -(\Omega - \mathbf{q}\cdot\mathbf{v})^{-1}\{1 + [(\omega - \mathbf{k}\cdot\mathbf{v})/(\Omega - \mathbf{q}\cdot\mathbf{v})] + [(\omega - \mathbf{k}\cdot\mathbf{v})/(\Omega - \mathbf{q}\cdot\mathbf{v})]^2 + ...\}$ and use the sign symmetry of Ω and $\mathbf{q}$. Finally, we have

$$\mathrm{Im}\delta\varepsilon^{(3)}(\omega,\mathbf{k}) = -\frac{2\pi^2 e^4}{|\mathbf{k}|^2}\int \frac{d\mathbf{p}}{(2\pi)^3}\frac{d\Omega d\mathbf{q}}{|\mathbf{q}|^2}|E_{\Omega,\mathbf{q}}|^2\delta(\omega - \mathbf{k}\cdot\mathbf{v})$$
$$\times\left[\left(\mathbf{q}\cdot\frac{\partial}{\partial\mathbf{p}}\right)\ \frac{2}{(\Omega - \mathbf{q}\cdot\mathbf{v})}\left(\mathbf{k}\cdot\frac{\partial}{\partial\mathbf{p}}\right)\frac{1}{(\Omega - \mathbf{q}\cdot\mathbf{v})}\left(\mathbf{q}\cdot\frac{\partial}{\partial\mathbf{p}}\right)\right.$$
$$-\left(\mathbf{q}\cdot\frac{\partial}{\partial\mathbf{p}}\right)\frac{1}{(\Omega - \mathbf{q}\cdot\mathbf{v})^2}\left(\mathbf{k}\cdot\frac{\partial}{\partial\mathbf{p}}\right)\left(\mathbf{q}\cdot\frac{\partial}{\partial\mathbf{p}}\right)$$
$$\left.+2\left(\frac{\mathbf{k}\cdot\mathbf{q}}{m_e}\right)^2\frac{2}{(\Omega - \mathbf{q}\cdot\mathbf{v})^4}\left(\mathbf{q}\cdot\frac{\partial}{\partial\mathbf{p}}\right)\Phi\right]. \qquad (13)$$

Using the expressions (10) and (13), one can easily obtain the corresponding rates describing the evolution of the resonant waves

$$\gamma^{nl} = -\left.\frac{(\mathrm{Im}\delta\varepsilon^{\mathrm{pol}} + \mathrm{Im}\delta\varepsilon^{(3)})}{\partial\varepsilon^L/\partial\omega}\right|_{\omega=\omega(\mathbf{k})}, \qquad (14)$$

where ε^L is the linear dielectric permittivity, $\omega(\mathbf{k})$ is the linear frequency (*i.e.*, the solution of $\varepsilon^L(\omega,\mathbf{k}) = 0$) of the resonant waves.

When the constant particle distributions are maintained (*i.e.* the system is open), the contribution to the growth rate of the resonant waves caused by the plasma–maser mechanism is determined by the expression (14). If the particle distributions are not constant then the effects of nonstationarity of the system can be important when describing the evolution of waves in plasmas (*e.g.* the contribution of the effects of nonstationarity to the growth rate of the non–resonant waves is of the order of the "direct third–order" contribution to the nonlinear growth rate of these waves (see [2,3]). However, for the closed systems (in which the (slow) variation of the plasma parameters is governed by the well–known quasilinear equation (see, *e.g.*, [4])

the effects of the system's nonstationarity do not make a contribution to the plasma–maser mechanism for the evolution of the resonant waves (see [5]), in contrast to the evolution of the non–resonant waves (see [2,3]).

The plasma–maser effect can significantly influence the evolution of resonant waves. For example, such a situation can arise when the one–dimensional beam of fast electrons propagates through a plasma [6] in the presence of the ion–sound waves. In this case, the resonant (with the beam particles) are Langmuir waves, while the non–resonant are the ion–sound waves. The plasma–maser effect can [6], in particular, result in the stabilization of the beam instability for the beams which are not symmetrical with respect to the axis $v = v_0$ and if the following conditions are satisfied: $\partial\Phi^{(b)}/\partial v > 0$, $\partial^3\Phi^{(b)}/\partial v^3 < 0$, for $v_1 < v < v_0$, and $\partial\Phi^{(b)}/\partial v < 0$, $\partial^3\Phi^{(b)}/\partial v^3 \leq 0$, for $v_0 < v < v_2$, where v_1 and v_2 are the minimum and maximum speeds of the beam particles, respectively. The following conditions should also be valid

$$\frac{n_b}{n} << \left(\frac{v_0}{v_{Te}}\right)^2 \left(\frac{m_e}{m_i}\right)^{1/2} \left(\frac{q_s v_{Te}}{\omega_{pe}}\right)^3, \quad 1 << \left(\frac{W^s}{nT_e}\right)\left(\frac{v_{Te}^4}{v_0^2 \Delta v^2}\right). \tag{15}$$

Here n_b is the concentration of the beam particles, q_s and W_s are the characteristic wavevector and the energy density of the ion–sound waves, respectively, ω_{pe} is the electron plasma frequency, T_e is the electron temperature, $v_{Te} = (T_e/m_e)^{1/2}$, $\Delta v = v_2 - v_1$. When the conditions (16) are valid, the effect of nonlinear interaction of the resonant and non–resonant waves dominates over that of quasilinear interaction.

In conclusion, the effect of the plasma–maser type nonlinear mechanism on the resonant waves can result in new phenomena which are absent in the more familiar nonlinearities, such as decays and/or induced scattering, as well as quasilinear interactions.

References

1. Tsytovich V.N., Stenflo L., Wilhelmsson H. Phys. Scripta, **11**, 251 (1975).
2. Krivitsky V.S., Tsytovich V.N., Vladimirov S.V. Phys. Reports, **218**, 141 (1992).
3. Isakov S.B., Krivitsky V.S., Tsytovich V.N. Sov. Phys. JETP, **63**, 545 (1986).
4. Tsytovich V.N. Theory of Turbulent Plasma. N.Y.: Consultants Bureau, 1977.
5. Vladimirov S.V., Yu M.Y., Popel S.I. Contrib. Plasma Phys. **33**, 1 (1993).
6. Popel S.I., Vladimirov S.V., Yu M.Y. Phys. Scripta. **47**, 239 (1993).

PARAMETRIC INSTABILITIES DURING THE EXPERIMENT ON ION BERNSTEIN WAVE HEATING OF TOKAMAK PLASMA

R. Cesario
Associazione EURATOM-ENEA sulla Fusione,
Centro Ricerche Energia, Frascati
C.P.65 - 00044 Frascati, Rome, Italy

Abstract

Parametric instabilities in the scenario of the ion Bernstein wave (IBW) plasma heating experiment are investigated. The theoretical analysis shows that the RF power threshold of the instabilities is very low when the plasma density near the antenna meets the condition: $2\omega_{pi} < \omega_0 << \omega_{pe}$. The threshold becomes very high, >>1MW, and is determined by the convective losses due to the plasma inhomogeneity when the plasma density near the antenna is sufficiently high so as $0.5 \leq \omega_{pi} / \omega_0 < 1$. According to the theory, the parametric instability activity should increase if the plasma is moved away from the antenna, creating a low-density electron plasma wave "gap" region. This hypothesis is in agreement with the behaviour of the parametric instability obtained during the IBW experiment on PBX-M. This result shows that the observed parametric instability activity can be explained in terms of the plasma inhomogeneity convective model. It was also demonstrated that, by controlling the plasma position relative to the antenna, parametric instability activity can be controlled at a low level.

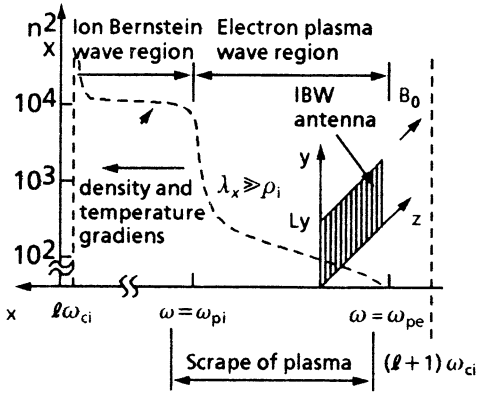

Fig.1 Linear wave dispersion relation solved in the slab plasma model for the IBW plasma heating scenario. n_x: component of the refractive index perpendicular to the toroidal magnetic field. I: ion-cyclotron harmonic number.

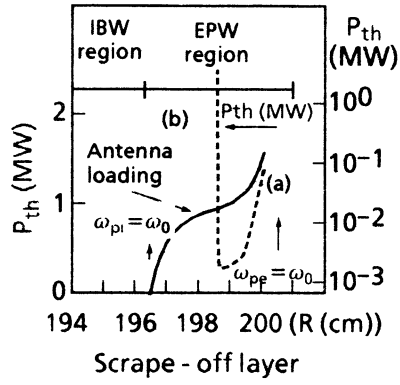

Fig.2 RF power convective threshold due to the effects of the finite extent of the pump wave and the plasma inhomogeneity (curve a) and antenna loading calculations (curve b)

1 Analogies between plasma ion heating by ion Bernstein waves and by lower hybrid waves

The ion Bernstein wave (IBW) heating of tokamak plasmas is an additional RF heating experiment in the range of ion-cyclotron frequencies, which is performed by launching a slow electron plasma wave (Fig.1)..The same kind of wave is launched in the lower hybrid (LH) ion heating experiment, during which strong parametric instabilities have been observed, without any evidence of heating of the bulk plasma [1].

Strong parametric instabilities from the plasma edge, without any evidence of RF heating of the bulk plasma have also been found in the recent Doublet III-D IBW plasma heating experiment [2]. These results suggest that the strong activity of the parametric instabilities inhibits the

propagation of the launched electron plasma wave beyond the scrape-off layer.

2 Analysis of parametric instabilities in the ion Bernstein wave heating scenario

In the homogeneous plasma approximation, the parametric dispersion relation is [3,4]

$$\varepsilon(\omega,\mathbf{k}) - \frac{\mu^{-}(\omega_o,\mathbf{k}_1,\mathbf{k}_0,\mathbf{E}_0)}{\varepsilon(\omega_1,\mathbf{k}_1)} - \frac{\mu^{+}(\omega_0,\mathbf{k}_2,\mathbf{k}_0,\mathbf{E}_0)}{\varepsilon\omega_2,\mathbf{k}_2} = 0,$$

where $(\omega_0,\mathbf{k}_0)$ refers to the pump wave, $(\omega_{1,2},\mathbf{k}_{1,2})$ to the sidebands and $(\omega,\mathbf{k})$ to the low-frequency wave; ε is the dielectric function and $\mu^{-,+}$ are the wave coupling coefficients. The total momentum and energy of the coupled waves must be conserved.

The highest growth rate of the parametric instabilities has been found in the layer:

$$2\omega_{pi} < \omega_0 << \omega_{pe}$$

This condition can be met in the scrape-off plasma of the IBW and LH ion heating experiments. The pump and sideband waves are electron pump waves; the driving mode is an ion cyclotron damped mode.

The RF power threshold of the parametric instability can be estimated by considering the convective losses due to the plasma inhomogeneity and the finite extent of the wave-propagation region, which limit the parametric-instability growth [4]. The WKB equations of the decay waves in an inhomogeneous slab plasma can be solved [5]:

$$\left(\frac{\partial}{\partial t}+\mathrm{v}_{g1}x\frac{\partial}{\partial x}+\Gamma_1\right)\Phi_1(x,t)=-i\frac{\alpha_1}{\dfrac{\partial\varepsilon R(\omega_1,\mathbf{k}_1)}{\partial\omega_1}}\Phi(x,t)\mathrm{e}^{i\int M_x dx}.$$

$$\left[\varepsilon(\omega,\mathbf{k})+i\frac{\partial\varepsilon(\omega,\mathbf{k})}{\partial\omega}\quad\frac{\partial}{\partial t}+\frac{\partial\varepsilon(\omega,\mathbf{k})}{\partial k_x}\quad\frac{\partial}{\partial x}\right]\Phi(x,t)\mathrm{e}^{i\int M_x dx},$$

where Φ_1 is the sideband potential, Γ_1 the linear damping, v_{g1} the group velocity component along the direction of the inhomogeneity gradient x, M_x the component of the mismatching wave vector M, and α, α_1 are the wave-coupling coefficients.

The parametric instability originating at x=0 must conserve the momentum of the waves, i.e. $M=\mathbf{k}_1-\mathbf{k}+\mathbf{k}_0=0$. The growth rate is given by

$$\gamma=-\Gamma_1+\frac{\mathrm{Im}\dfrac{\alpha\alpha(\omega_0,\mathbf{k}_1,\mathbf{k}_0,\mathbf{E}_0)}{\varepsilon(\omega,\mathbf{k})}}{\dfrac{\partial\varepsilon R(\omega_1,\mathbf{k}_1)}{\partial\omega_1}}.$$

For a steady-state interaction $\partial/\partial t=0$.

Far from the interaction region x=0, the potential of the sideband is

$$\Phi_1(x)\approx\Phi_1(0)\mathrm{e}^{A\pi},$$

where

$$A = \frac{\gamma}{\left.\frac{dM_x}{dx}\right|_{x=0} v_{g1x} \frac{\partial \varepsilon R(\omega,\mathbf{k})}{\partial \mathbf{k}_x} \frac{1}{\varepsilon|_m(\omega,\mathbf{k})}}$$

is the convective amplification factor. The instability can grow and becomes significant if $A>1$.

The theoretical analysis shows that the RF power threshold of parametric instabilities depends mainly on the plasma density near the antenna (see Fig. 2):

- High density: $1>\omega_{pi}/\omega_0 \geq 0.5$ $P_{th}>>1$MW. In this case, the convective losses due to plasma inhomogeneity are dominant.
- Low density: $2\omega_{pi}<\omega_0<<\omega_{pi}/\omega_{pe}$ $P_{th}\leq 10$kW In this case, a wider region of propagation, the EPW, reduces the convective losses due to the plasma inhomogeneity. We have considered the parameters of the IBW experiment on PBX-M.

To test the theoretical prediction on PBX-M, the plasma position was varied during the IBW pulse, while monitoring the parametric instabilities. When the plasma edge was moved about 2cm near the antenna, parametric instability activity was very low (≤50dB of the pump wave) (Fig.3). When the plasma edge was moved about 2cm away from the antenna, parametric instability activity increased greatly (>20dB of the pump wave) (Fig. 4). The Langmuir probe measurements showed that the scrape-off plasma density varied by moving the plasma column, giving strong variations in the convective losses due to the plasma inhomogeneity.

3 Conclusions

The strong dependence of parametric instability activity on the plasma position can be attributed to the convective losses due to plasma inhomogeneity, which increase strongly when the plasma density near the antenna is sufficiently high ($0.5\leq\omega_{pi}/\omega_0<1$).

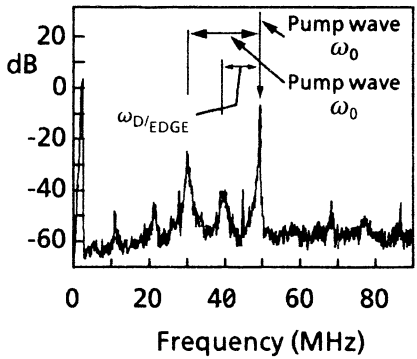

Fig.3 Frequency spectrum of parametric instabilities observed when the plasma column is shifted 2cm from the antenna (relative to nominal position), for $P_{r.f}$=100kW Main plasma parameters: I_p=100kA, B_t=14G, line-averaged density=1×10^{13}cm^{-3}, deuterium plasma.

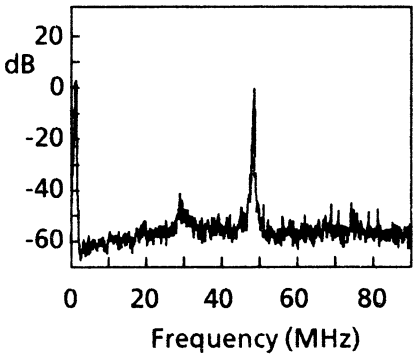

Fig.4 Parametric instability frequency spectrum observed in the same conditions as shown in Fig.3, but plasma column shifted about 2cm close to the antenna (relative to nominal position).

The distance between the antenna and plasma must be small so as not to create a significantly wide layer of electron-plasma-wave propagation. This condition was found during the PBX experiment, while the contrary occurred in the LH ion-heating experiments and probably during the DIII-D IBW experiment.

References

1. Cesario R., Cardinali A., Nucl. Fusion, 1989, 27 n.10, 1709 and references therein.
2. Pinsker R., et al., Proc. 9th Topic. Conf. RF Power in Plasmas, Charleston (American Inst. of Phys. New York, 1991).
3. Porkolab M., Phys. Fluids 1977, 2058.
4. Liu C.S. and Tripathi, V., 1985, Phys Reports.
5. Cardinali A., Cesario R., De Marco F., Sauter O., RF EPS Conf Brussels.

DEVELOPMENT OF HIGH-POWER MICROWAVE SOURCES

ON THE OPTIMAL CHOICE OF MICROWAVE SYSTEMS FOR DRIVING TeV LINEAR COLLIDERS

V.L. Granatstein and G.S. Nusinovich
Laboratory for Plasma Research
University of Maryland, College Park, MD 20742

1 Introduction

An optimum microwave system for driving future linear colliders implies a choice of its parameters which makes this system the most efficient and the least expensive. Among many of the proposed concepts for TeV-class colliders, there is a general tendency to choose a shorter wavelength than in current linacs since this results in an opportunity of increasing the accelerating gradient, and therefore, reducing the length of the linac, and correspondingly, the cost of the whole system. Below, we shall analyze this tendency with a view toward optimizing the microwave pulse duration and the accelerating gradient in a structure.

2 Optimal Pulse Duration

The efficiency of a microwave system may be defined as

$$\eta = \eta_a \cdot \eta_v \cdot \eta_c \tag{1}$$

where η_a is the efficiency of the microwave amplifier, η_v is the efficiency of the high voltage supplies and η_c is the efficiency of a circuit for microwave pulse compression. For a microwave pulse duration,

τ, on the order of microseconds we may assume that the efficiency of the amplifier, η_a, does not depend on τ. The efficiency of a high voltage supply consisting of a line type modulator and a high voltage transformer depends most of all on the rise and fall times. This is so because a microwave source usually operates only during the flat top portion of the voltage pulse, and therefore, the energy spent during voltage rise and fall times is wasted. Let us denote the duration of the flat top by T_0 and the duration of the rise and fall times by T_R. According to [1] T_R relates to T_0 as $T_R = \alpha\sqrt{T_0}$ where the coefficient α is proportional to turns ratio of the pulse transformer. Correspondingly, the efficiency of the high voltage supply can be defined by a simple formula

$$\eta_v = \frac{T_0}{T_0 + T_R} = \frac{T_0}{T_0 + \alpha\sqrt{T_0}}. \tag{2}$$

To define η_c we will consider a binary pulse compression scheme [2] with the given efficiency of one stage of compression, $\eta_c^{(1)}$. Then,

$$\eta_c = \left[\eta_c^{(1)}\right]^{N_s}, \tag{3}$$

where N_s is a number of stages which are necessary to match the microwave pulse duration, τ, with the filling time of the accelerating structure, τ_f:

$$N_s = \log_2\left(\frac{\tau}{\tau_f}\right). \tag{4}$$

Below we will assume that the microwave pulse duration, τ, is approximately equal to the duration of the flat top of voltage pulse, T_0; i.e., $\tau = T_0$ because the risetime of the microwave radiation is typically rather small (e.g., at frequencies above 10 GHz for microwave tubes with a Q-factor of several hundred it is less than 10 nsec). The filling time of the accelerating structure consisting of a chain of pill-box resonators, τ_f, is proportional to the characteristic structure time, Q/ω:

$$\tau_f = q\frac{Q}{\omega} \tag{5}$$

where Q is determined mainly by ohmic losses of microwave power in a resonator, and $\omega = 2\pi f$ is the angular frequency of the microwave

signal, and a typical value of the coefficient q is about 3. For a structure consisting of a chain of pill-box resonators operating with TM_{0n0} modes,

$$Q \simeq Q_{\mathrm{OHM}} \simeq \frac{a}{\delta_{sk}} \cdot \frac{h/a}{1+h/a} \simeq \frac{4.71 \cdot 10^8}{f^{1/2}} \nu_{0n} \frac{h/a}{1+h/a}. \qquad (6)$$

Here a and h are the resonator radius and length, respectively, and δ_{sk} is the skin depth. The radius a and the wavelength $\lambda = c/f$ are related as $a = \nu_{0n}\lambda/2\pi$ where ν_{0n} is the n-th root of equation $J_0(\nu) = 0$ (i.e., $\nu_{01} = 2.4$, $\nu_{02} = 5.52$, etc.) The last expression in Eq. (6) is written for a copper structure, and f is given in Hz. (mks units are used throughout this paper except when otherwise noted).

So, combining η_v with η_c we come to the combined efficiency

$$\eta_{\mathrm{comb}} = \eta_v \cdot \eta_c = \frac{T_0}{T_0 + \alpha\sqrt{T_0}} \left[\eta_c^{(1)}\right]^{\log_2(T_0/\tau_f)}, \qquad (7)$$

which has its maximum when the normalized value $y = \sqrt{T_0}/\alpha$ is equal to

$$y_{\mathrm{opt}} = -1 - \frac{\ell n 2}{2\ell n \eta_c^{(1)}}. \qquad (8)$$

The corresponding optimal pulse duration (flat top of the high voltage pulse) is

$$T_{\mathrm{opt}} = T_R \cdot y_{\mathrm{opt}} \qquad (9)$$

and the maximum combined efficiency is

$$\eta_{\mathrm{comb}}^{\mathrm{max}} \simeq \frac{y_{\mathrm{opt}}}{y_{\mathrm{opt}}+1} \cdot \left[\eta_c^{(1)}\right]^{N_s}. \qquad (10)$$

For example, for the efficiency of one stage of the compression system $\eta_c^{(1)} = 0.9$, $y_{\mathrm{opt}} \simeq 2.289$ that gives $T_{\mathrm{opt}} \simeq 2.289\ T_R$ and $\eta_{\mathrm{comb}}^{\mathrm{max}} \approx 0.7 \cdot 0.9^{N_s}$; for $\eta_c^{(1)} = 0.95$, $y_{\mathrm{opt}} \cong 6$ corresponding to $T_{\mathrm{opt}} \simeq 6\ T_R$ and $\eta_{\mathrm{comb}}^{\mathrm{max}} \approx 0.85 \cdot 0.95^{N_s}$. Clearly, as $\eta_c^{(1)}$ becomes larger, it pays to make the microwave pulse longer and pass it through more stages of pulse compression.

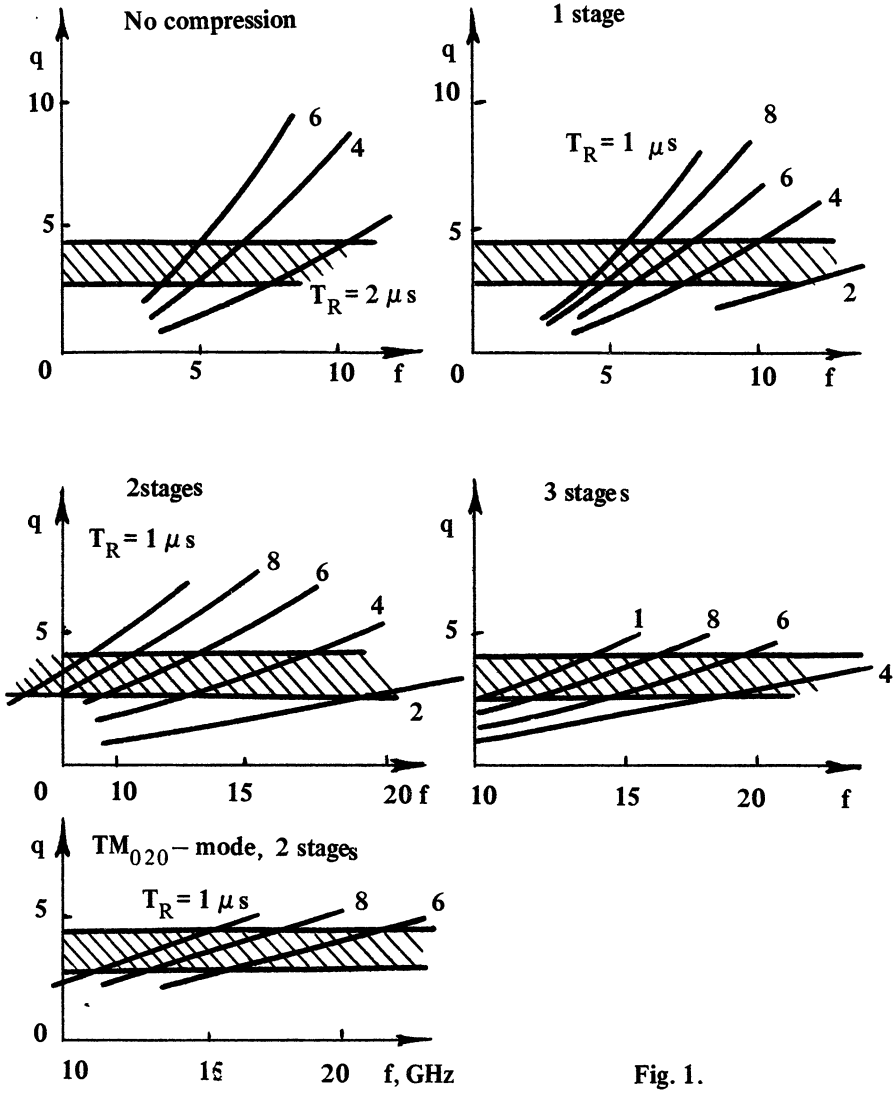
No compression
q
10
5
0
6
4
$T_R = 2\ \mu s$
5
10
f
1 stage
8
$T_R = 1\ \mu s$
6
4
2
2stages
8
6
4
2
15
20 f
3 stages
1
8
6
4
20
TM$_{020}$ – mode, 2 stages
16
20
f, GHz

Fig. 1.

To define a number of required stages in a pulse compression scheme it is necessary to analyze the formula

$$N_s = \log_2 \left(\frac{y_{\text{opt}} \cdot T_R}{\tau_f} \right). \tag{11}$$

Using Eqs. (5), (6) we may interpret this formula as the definition of the coefficient q which defines an excess of the filling time, τ_f, over the typical structure time, Q/ω, for a given number of compression stages:

$$q = \frac{2\pi y_{\text{opt}}}{Q \cdot 2^{N_s}} \, f \, T_R. \tag{12}$$

Taking into account the frequency dependence of Q given by Eq. (6) one can see that $q \sim f^{3/2}$. Therefore, to keep a reasonable value of q, the increase in operating frequency must be accompanied by an increase in the number of compression stages, N_s. Note, that at a high frequency and a moderate number of stages, $N_s \lesssim 4$, it might be also possible to operate with higher order modes (such as TM_{020}, TM_{030}, etc.) that will correspond to reasonable values of q and can mitigate some problems caused by miniaturization of the structure at short wavelengths. The frequency scaling of the coefficient q, given by Eq. (12), for different values of the voltage rise time, T_R, and number of compression stages, N_s, is illustrated by Fig. 1. The data shown in Fig. 1 correspond to the efficiency of one stage of pulse compression, $\eta_c^{(1)} = 0.9$, and the relation between resonator length and radius $h = 2a$. The hatched area is the region of reasonable values of q (from 2.5 to 4). On the bottom of Fig. 1 there is shown a case of operation in the TM_{020} mode with 2-stage pulse compression. From comparison of these pictures it follows, for instance, that if the microwave source operates at 20 GHz and the voltage rise time is 0.5 μsec, to get a reasonable value of q, one has either to use a 3-stage compression scheme for operation in the TM_{010} mode or a 2-stage scheme for operation in the TM_{020} mode. Note that near the axis all these symmetric modes have the same transverse distribution of the microwave field.

3 Optimal Accelerating Gradient and Number of Tubes

It is well known (see, e.g. [3]) that the cost of an RF linear collider is minimum when the cost of accelerator which does not include the cost associated with RF drivers is approximately equal to the cost of the RF system; viz.,

$$C_L L = C_T N_T. \tag{13}$$

Here C_L is the cost per unit length of accelerator, L is its length, C_T is the cost of one tube including all high voltage, pulse compression and microwave transmission technique, and N_T is the total number of tubes. The number of tubes may be found as the ratio of microwave energy stored in all the accelerator structures

$$W = \frac{\pi}{18} 10^{-9} J_1^2(\nu_{0n}) a^2 L E_0^2$$

to the microwave energy delivered from one tube $W_T = T_0 P \eta_c$ (P is the peak output power); i.e.,

$$N_T = \frac{10^7}{8\pi} \cdot \frac{\nu_{0n}^2 J_1^2(\nu_{0n})}{f^2} \cdot \frac{L E_0^2}{T_0 P \eta_c}. \tag{14}$$

Correspondingly, the optimum accelerating gradient, as follows from Eqs. (13), (14) is equal to

$$E_{0,\mathrm{opt}} = \left(0.8\pi \frac{C_L}{C_T} \cdot \frac{T_0 P \eta_c}{\nu_{0n}^2 J_1^2(\nu_{0n})} \right)^{1/2} 10^{-3} f, \tag{15}$$

where C_L is in \$/m, C_T in \$. In Eqs. (13), (14) the length of a linac, L, is, obviously, equal to the ratio of a particle final energy, W_f to the accelerating gradient. So, for $E_0 = E_{\mathrm{opt}}$ the optimum number of tubes is

$$N_T^{\mathrm{opt}} = \frac{0.63 W_f}{f} \left(\frac{C_L}{C_T} \cdot \frac{\nu_{0n}^2 J_1^2(\nu_{0n})}{T_0 P \eta_c} \right)^{1/2} 10^3. \tag{16}$$

Equations (15), (16) show that when it is possible to keep the microwave tube power level constant the increase in both the operating

frequency and the microwave pulse duration is very beneficial because the total cost will scale as $1/fT_0^{1/2}$. The latter effect, the increase in pulse duration, however, must be accompanied with an increase in pulse compression that reduces the compression efficiency, η_c. Note, that in comparing the parameters required for operation with different modes of the accelerating structure it is also necessary to take into account a corresponding difference in the number of compression stages.

The number of microwave tubes required to drive a linear collider with a given final energy has previously been proposed [4] as a figure of merit when comparing different types of microwave tubes as candidates for this application. In line with Eq. (16), recent microwave amplifier experiments with amplifier voltage < 1 MV were compared for minimum values of the quantity $f^{-1}(\tau P \eta_c)^{-1/2}$; the best results to date have been achieved in gyroklystron amplifiers at 19.7 GHz [5] and 'conventional' klystorn amplifiers at 11.4 GHz [6].

4 Consideration of Two Concepts

Consider two concepts for 0.5 TeV linacs with microwave equipment based on the most advanced amplifiers, klystrons and gyroklystrons. Suppose that both of these tubes in the future will be able to produce 100 MW output power with efficiency of 40% and cost 200 K$ each; the klystrons will operate at 11.4 GHz and the gyroklystrons at 17.1 GHz (the corresponding programs are in progress, c.f. [6,7]). Let the voltage rise time be 0.5 μsec, the one stage compression efficiency be $\eta_c^{(1)} = 90\%$, the cost of a linac per unit length be $C_L = 25$ K$/m, and the ratio between resonator length and radius be $h/a = 2$.

Using these values, one can easily find from Eqs. (12), (6) that for a klystron system with no pulse compression the coefficient q is 3.69 and with one stage of compression $q = 1.845$ (in the latter case, a significant amount of microwave power will not be introduced into the accelerating structure during the short fill time). In the case of gyroklystrons one can either use again the same TM_{010} mode with one stage of compression to obtain $q = 3.35$ or try to operate at the

Table 1

Microwave Sources	Operating mode, # of stages	$E_{0,\mathrm{opt}}$ $\times 10^{-6}$	L (m)	C_T $\times 10^{-6}$ (\$)	N_T^{opt}	f_{rep} (Hz) for P_{av}=50 MW	η (%)
Klystrons	TM_{010}, $N_s = 0$	54.6	9157	458	1144	104	28
at 11.4 GHz	TM_{010}, $N_s = 1$	51.8	9652	483	1205	219	25.2
Gyroklystrons	TM_{010}, $N_s = 1$	77.2	6477	324	808	180	25.2
at 17.1 GHz	TM_{020}, $N_s = 0$	54.2	9225	461	1152	130	28

TM_{020} mode with no pulse compression (the corresponding value of q is 2.92). We have taken these four versions as possible options and calculated the corresponding accelerating gradients, length of linac, total cost, total efficiency, averaged microwave power dissipated in walls of a linac structure, and the number of microwave tubes required for one linac. These calculations are summarized in Table 1.

From this table it follows that under the assumptions made, the most beneficial concept is the system operating in the TM_{010} mode and based on 17 GHz gyroklystrons. Of course, a more careful analysis of the cost of microwave system components is strongly desirable as well as detailed consideration of microwave tubes' capabilities in different frequency ranges. Below, we will consider only the basic features of frequency scaling of klystrons and gyroklystrons.

5 Frequency Scaling of Klystrons and Gyroklystrons

5.1 Klystrons

The efficiency of klystrons is a strong function of the microperveance of an electron gun, $\mu K = \left[I/V^{3/2}\right] \cdot 10^6$. The data given in reference [1] allows one to approximate this dependence by the simple formula

$$\eta_a = 0.2(4 - \mu K). \tag{17}$$

Correspondingly, the radiated microwave power may be defined as

$$P = \eta_a V I = 0.2 \cdot 10^{-6} V^{5/2}(4 - \mu K) \cdot \mu K. \tag{18}$$

From these equations it follows that the maximum output power can be achieved at $\mu K = 2$ with an efficiency of 40%. At this value of μK the power depends on voltage as $P = 0.8 \cdot V^{5/2} \cdot 10^{-6}$.

As the wavelength shortens, achievable klystron output power drops, at least, as fast as λ^2. Note that wavelength shortening leads also to degradation in beam quality. Due to this in the best klystron experiment at $f = 11.4$ GHz, only 21.7% efficiency has been achieved

to date [6], and that value of η_a is lower than predicted by Eq. (17) (in the experiment [6], a 1.75 microperveance electron beam was used).

5.2 Gyroklystrons

Magnetron-type thermionic electron guns which are widely used in gyroklystrons (GKLs) produce, typically, a temperature limited electron beam current. Due to this, the space charge effects are not as important for GKL electron beams as for klystrons. We note, for example, the design of a relativistic GKL, 500 kV electron gun with moderate velocity spread over a wide range of electron current from 0 to 800 A [8]. When the quality of such a beam is not too sensitive to beam current the highly efficient operation of GKLs may be realized at different current values if the Q-factor of the output resonator is properly matched.

When the operating mode is fixed, the output power of GKLs, as well as klystrons, scales with the wavelength as λ^2. This scaling follows from the definition of microwave power radiated from the interaction volume, $P_{\rm rad} = (\omega/Q)W$ if stored energy is assumed to scale as λ^3 and Q is independent of wavelength. Here the Q-factor is determined, mainly, by diffractive losses of the radiation. As follows from the power balance equation, $P_{\rm rad} = P$, the microwave power extracted from the beam, $P = \eta V I$, must scale in the same manner. In the latter equation, the maximum efficiency of GKLs, η, does not depend on λ over a wide range of wavelengths. Consider the electron beam current scaling, assuming that the spread in radial coordinates of electron beamlets, R_{el}, is restricted ($\Delta R_{el} \ll \lambda$) in order to avoid the deteriorating effect of radial inhomogeneity of the electromagnetic field on the efficiency of interaction. Then, for magnetron-type electron guns with adiabatic compression of the beam between the cathode and the resonator we get the beam current scaling law $I \sim \lambda^{4/3}/\sin\varphi$, where φ is the angle between the cathode surface and a magnetic line of force. This gives us the scaling law for P: $P \sim V\lambda^{4/3}/\sin\varphi$.

From there it follows that to match P to $P_{\rm rad}$ one can increasing the angle φ as the wavelength shortens and/or reduce the operating

voltage. Both of these tendencies are favorable because at large φ electron beams are quasi-laminar in the gun region and that reduces the influence of space charge effects on the beam quality while reduction of voltage makes a microwave system less expensive. On the other hand, we may fix the angle φ and the operating voltage, and then try to increase the radiated power by reducing the diffractive Q-factor as $Q_{\rm dif} \sim \lambda^{2/3}$ due to corresponding changes in coefficients of radiation reflection from the end of the output cavity. In this case the radiated power will scale as $P_{\rm rad} \sim \lambda^{4/3}$.

Note that the scaling discussed above is valid when the operating mode is fixed. If the frequency increase is accompanied with transition to operation at higher modes in the output resonator (TE_{021}, TE_{031}, etc.), as is common in gyrotrons, the limiting level of radiated power can be almost independent on the wavelength.

6 Discussion

We have considered above some possibilities for optimizing the parameters of microwave systems for driving future linear colliders at high frequencies. Results obtained show that typical optimal values of the accelerating gradient are well below the breakdown limit, and are quite acceptable with respect to dark current. The optimal parameters given in Table 1 also correspond to acceptable levels of average microwave power dissipated in a linac structure, and to quite moderate heating of a structure wall during one pulse (the temperature increase of a copper wall is less than 40° for all cases contained in Table 1).

From the analysis, it follows that operation at high modes in the linac might be expedient only at high frequencies when the typical resonator filltime for a TM_{010}-mode is much shorter than the duration of the microwave pulse, and therefore, a pulse compression by a very large factor is required. The reasons for operation at these frequencies must be studied taking into account transverse wakefield effects. If necessary, well developed methods for suppression of high order modes can be inverted and used for their selective excitation.

Although our consideration was restricted to some specific examples the method used can be applied for parameter optimization in any other microwave system. Our optimization based on the choice of 100 MW microwave sources in the frequency range between 10 and 20 GHz is motivated by recent progress in experiments with 11.4 GHz klystrons [6] and 19.7 GHz gyroklystrons operating at the second cyclotron harmonic [5,9] where, respectively, output powers of 51 MW with 21.7% efficiency and 29 MW with 27% efficiency have been demonstrated. We estimate that the use of depressed collectors [10] can enhance the efficiency of such microwave tubes, at least, to 40%.

Acknowledgements

This work was supported by the U.S. Department of Energy.

References

1. Wilson P.B., Invited Talk at the APS Meeting, Washington, DS, April 1992.

2. Farkas Z.D., Spalek G. and Wilson P.B., SLAC -PUB-4911, March 1989.

3. Mondelli A., Proc. 1991 Particle Accelerator Conference, 1991, 5, 3261.

4. Granatstein V.L. and Nusinovich G.S., Proc. 1993 Particle Accelerator Conference (to be published).

5. Lawson W., et al., Phys. Rev. Lett., 1993, 71, 456.

6. Caryotakis G., ECFA Workshop on e^+e^- Linear Colliders, Garmish-Partenkirchen, July 1992.

7. Lawson W., et al., Proc. of the 1993 Particle Accelerator Conference (to be published).

8. Lawson W. and Spesht V., IEEE Trans. on Electron Devices, 1993, 40, 1322.

9. Calamt J., et al., Proc. of the 1993 Particle Accelerator Conference (to be published).

10. Singh A., et al., Int. J. Electronics, 1992, 72, 1153.

GYROKLYSTRONS—MILLIMETER WAVE AMPLIFIERS OF THE HIGHEST POWER

I.I.Antakov, A.V.Gaponov, E.V.Zasypkin,
E.V.Sokolov, and V.K.Yulpatov
Institute of Applied Physics,Nizhny Novgorod, Russia

L.A.Aksenova, A.P.Keyer, V.S.Musatov,
V.E.Myasnikov, and L.G.Popov
R & D Company "Tory", Moscow, Russia

B.A.Levitan, and A.A.Tolkachev
Radiophysical Research Institute, Moscow, Russia

Introduction

The possibility of creation of the gyroklystron attracted a great attention just after first successful experiments with gyrotrons. The gyroklystron was offered in 1966 by A.V. Gaponov, A.L. Goldenberg, V.K. Yulpatov [1] and independently by J.L. Hirshfield and J.M. Wachtel [2]. In 1967 efficiency of the klystron mechanism of electron bunching in cyclotron resonance masers was demonstrated—electron efficiency about 70% was achieved in a gyroklystron operating in the fundamental TE-mode.

The initial experiments with gyroklystrons were planned at X-band . However, well-known advantages of the mechanism of stimulated cyclotron radiation of Cherenkov and transition radiation used in "classical" electron O-type devices gave a hope of obtaining high power level and efficiency also at the millimeter and submillimeter wavelengths. This circumstance was reflected in the first inventions connected with gyroklystrons [4] filed as patent applications in 1967.

1 X-band experiments

Up to the middle of the 70s the characteristics of gyroklystrons were investigated at X-band [5] .These studies have been performed :

- to verify the gyroklystron amplifier concept in more detail;
- to confirm a predicted possibility of achievement in this devices high efficiency, gain and , simultaneously,acceptable for practice width of frequency bandwidth;
- to examine the possibility of using the oversized cavities in gyroklystron to produce a large output power.

The characteristics of several versions of X-band gyroklystrons are presented in Table 1.

Table 1

PARAMETERS				
Frequency	9.17 GHz	9.25 GHz	15.2 GHz	15.8 GHz
Number of cavities	2	3	3	3
Mode	TE_{111}	TE_{011}	TE_{011}	TE_{021}
Output Power	0.65 kW	4.0 kW	50 kW	160 kW
Efficiency	70%	50%	50%	40%
Power Gain	22 dB	20 dB	30 dB	30 dB
Bandwidth	0.3%	1.0%	0.5%	0.5%
Beam Voltage	16 kV	16 kV	40 kV	40 kV
Pulse Duration	CW	100 μs	100 μs	100 μs

The highest efficiency of about 70% have been achieved in double-cavity gyroklystron at low power level. In multicavity gyroklystrons with operating mode TE011 the output power of 50 kW, efficiency of 50% , gain of 30 dB and half-maximum bandwidth of about 1% have

been measured. The largest output power of about 160 kW have been attained in gyroklystron operating in the TE_{021} mode of the oversized open cavity.These results are in agreement with the notion that a gyroklystron having the characteristics suitable for practical applications can compete by the level of its otput power with an ordinary high-power klystron and TWA of the O-type in the middle part of X-band and becomes more and more advantageous as the operating frequency grows.

2 Ka-band experiments

To the begining of 80s a great experience of developing gyroklystron modifications was accumulated. It served as a basis for elaboration of a millimeter wave gyroklystron amplifier with output power closed to the power of gyrotrons. The efforts in solving this problem were strongly stimulated by the interest of designers of radars to amplifiers operating at Ka-band with the output pulse power of several hundreds kilowatts.

The goal of joint programme of IAP and "Tory" Company was a creation of gyroklystron for millimetre radar operating in pulsed regime at frequency 35 GHz with output power of about 1 MW and bandwidth at half-maximum of 1%. The additional requirement consisted in the restriction of the beam voltage by the value of 80 kV.

At the first stage a scaling of a three-cavity gyroklystron with operating mode TE_{011} (third version in Table 1) from X-band to Ka-band has been performed.This tube has been elaborated for pulsed operation at frequency 35 GHz with output power of 200–250 kW and half-power bandwidth of about 1–1.5%.

A schematic view of the overall sistem is shown in Fig.1. The triode magnetron injection gun was used to produce an electron beam with a beam voltage 50 KV and a current up to 15 A.This gun typically operated with the anode voltage of 5 kV, pulse duration of 100 μs and repetition frequency of 50 Hz.

The HF circuit consisted of three circular cavities operating in the TE_{011} mode at the fundamental cyclotron frequency. The parameters

of the cavities were as follows:

Lengths $L_1 = 1.1\lambda$ $L_2 = 1.2\lambda$ $L_3 = 1.4\lambda$

Q-factors $Q_1 = 350$ $Q_2 = 400$ $Q_3 = 700$

These cavities were separated by radiation free drift spaces. The drive signal was introduced to the input cavity through a rectangular waveguide connected with the cavity by a sistem of longitudinal coupling slots.

Figure 2 shows the measured dependencies of the output power and efficiency on beam current .The maximum output power of about 230 kW with efficiency 32% occured at a beam voltage 50 kV and a current 14 A. The maximum efficiency of 34 output power of about 200 kW.

Figure 3 shows output power and gain as functions of input power. Large-signal gain of 40 dB and small-signal gain of about 45 dB have been observed .

Figure 4 indicates the dependencies of output power and phase of output signal on frequency mistuning $(f - f_0)$, where f_0 corresponds to the maximum of the output power. The measured width of half-maximum bandwidth achieved value of about 500 MHz (it suits $\simeq$ 1.5%). The phase characteristic of the output signal was close to the linear one.

At the second stage we elaborated and created a 35-GHz powerful pulsed gyroklystron with operating mode TE_{021} capable of producing the output power closed to the desired value of 1 MW.

This tube utilized a diode magnetron injection gun to produce a hollow annular electron flow with a current up to 45 A and voltage up to 75 kV.In order to determine an appropriate electrode shape the detailed computer simulation of the electron motion through the gun and compression region has been performed.The diameter of the cathode was 50 mm, the diameter of the beam in the interaction region was about 16 mm. It means that electron beam is injected into the second radial maximum of the cavity RF field. The required dc

magnetic field in the RF circuit was obtained with help of a superconductive magnet. A room temperature coil wound up from water cooled copper tube and centered over the cathode was used to control the beam's velocity ratio.

The RF circuit included two oversized cylindrical cavities operating in the TE_{021} mode at the fundamental cyclotron frequency . The parameters of the cavities (lengths, Q-factors, cold frequencies) and drift space length were calculated at the basis of existing theory of gyroklystron [1]. The length and quality factor of the input cavity were 1.2λ (λ is the operating wavelength) and 100, respectively. The length of the output cavity was 1.5λ and its Q-factor was 250.The input power was supplied by a 100 μs, 10 kW mechanically tunable gyrotron with operating mode TE_{011}.It had a frequency of about 35 GHz, tunable over 300 MHz.

At the begining we have tested this tube at the beam voltage 65 kV. Figure 5 shows the measured dependencies of output power and efficiency on beam current. The magnetic field in the cirquit and the cathode regions, drive frequency and input power were adjsted to maximize the output power at each data point. The maximum power of about 540 kW occured at a current 37A. At higher power level a HF breakdown problem in the second cavity took place. It was caused by the microwave heating of its inner surface.The peak efficiency was 26% and it was achieved at 18 A. The decrease in efficiency at low current is due to the impossibility of achievement of the velocity ratio required for optimal interaction of electron flow with HF field in the output cavity. The decrease in efficiency at higher current is caused by the exitation of spurious oscillations in the downtaper region before the input cavity.

The dependencies of the output power and gain on input power are illustrated in Fig. 6. Beam voltage and current were fixed , all other parameters corresponded to maximum efficiency (ME) at this point. The peak saturated gain was 22dB , the small-signal gain was 30 dB.

Figure 7 shows the dependencies of the output power on drive frequency measured at beam current 34 A. All other parameters were

fixed at the ME point. The bandwidth width at half-maximum of 0.87 percent with output power of 500 kW has been observed. In accordance with the simulation results, the bandwidth is limited by the Q-factor of the output cavity and the longitudinal velocity spread of electrons.

Further, this tube was modified by applying the improved sistem of cooling of the second cavity. It allowed to operate with the beam voltage 74 kV and current up to 45 A. Besides, the Q-factor of the second cavity was increased up to 320. Figure 8 indicates the measured output power as function of electron beam current. Maximum power was 750 kW at 42.5-A beam current, efficiency was 24% . The maximum efficiency of 32% with output power of about 300 kW has been observed. As it can be seen in Fig. 9, the measured half-power bandwdth was 0,61 percent with output power of 600 kW . The narrowing of the bandwidth may be explained by the increasing of the Q-factor of the output cavity.

3 94-GHz experiments

Two versions (pulsed and CW) of 94-GHz four cavity gyroklystron with operating TE_{011} mode have been designed and tested in IAP.

In pulsed regime the largest output power 65 kW with the efficiency of 26% was obtained at a beam voltage 55 kV and a beam current of 4.5 A. Maximum efficiency of about 34% has been achieved with output power 57 kW. Large-signal gain of 33 dB, small-signal gain of about 40 dB, and half-maximum bandwidth of 0.3% have been observed at 3.4-A current and 55 kV. The design and operating characteristics of this tube are presented in [6].

In CW regime peak output power of 2.5 kW and efficiency of 25% were observed at a beam voltage 22 kV and a beam current 0.46 A. Large-signal gain of 30 dB and half-power bandwidth of about 0.35% have been also measured.

Conclusion

In the framework of joint programme of IAP and "Tory" Company two versions of 35 GHz pulsed powerful gyroklystrons have been created and examined. In the first version the peak output power of 230 kW with efficiency 32% , gain of 40 dB and half-maximum bandwidth of about 1.5% have been obtained. In the second version of the gyroklystron the output power of 750 kW has been attained with efficiency of 24%, gain of 20 dB and bandwidth of about 0.6%. In other tube the width of half-maximum bandwidth of about 0.87% have been observed.

Two versions of 94 GHz four-cavity gyroklystron with operating TE_{011} mode have been designed and tested in IAP. In pulsed regime the largest output power of 65 kW with efficiency 26% , gain of about 35 dB and half-maximum bandwidth of 0.3% has been obtained. In CW regime peak output power of 2.5 kW, efficiency of 25% , large-signal gain of 30 dB and half-power bandwidth of about 0.35% have been measured.

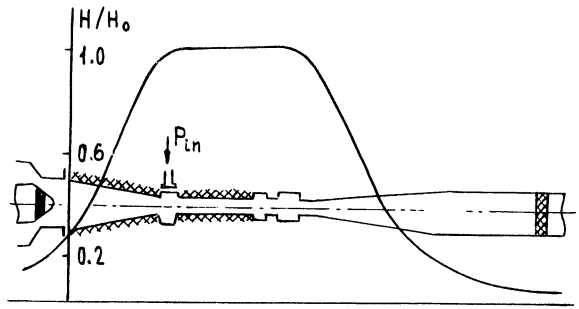

Fig 1. A schematic view of the three cavity gyroklystron with operating TE_{011} mode.

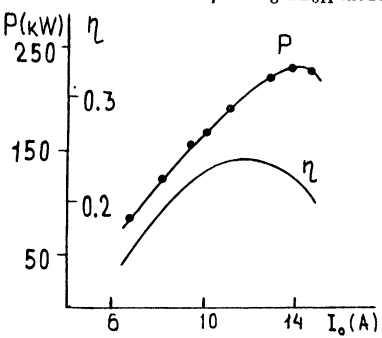

Fig 2 Output power and efficiency versus beam current for three cavity gyroklystron ($V0 = 50$ kV, $P_{in} = 60$ W)

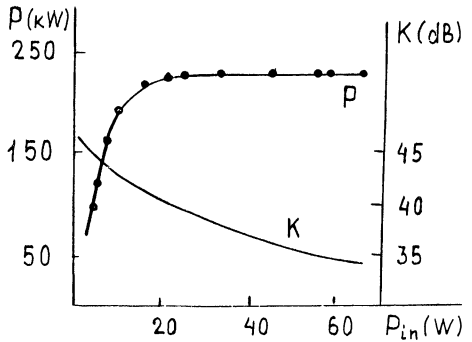

Fig. 3 Output power and gain as functions of the input power ($V_0 = 50$ kV, $I_0 = 14$ A, $P_{in} = 100$ W).

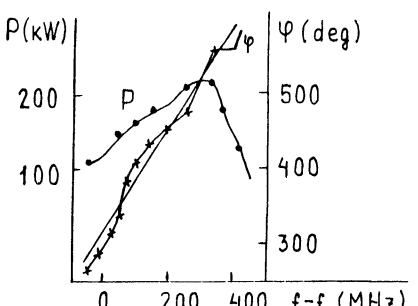

Fig 4 The dependencies of the output power and phase on frequency detuning (V_0 50 kV, I_0 -- 14 A, P_{in} = 100 W)

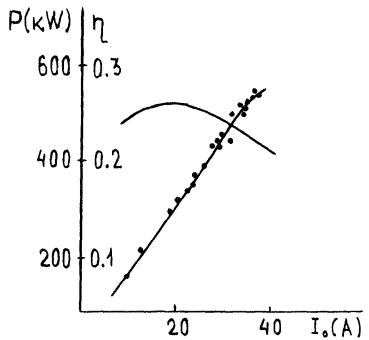

Fig 5 Output power and efficiency versus beam current for gyroklystron with operating TE_{021} mode ($V_0 = 65$ kV)

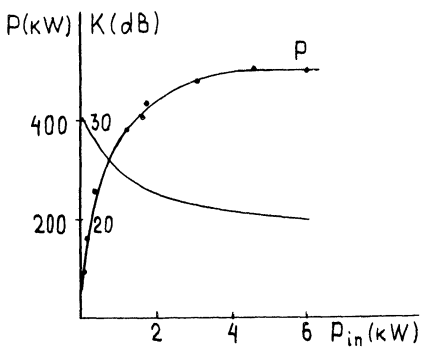

Fig. 6 Dependencies of output power and gain on input power ($V_0 = 65$ kV, $I_0 = 34$ A)

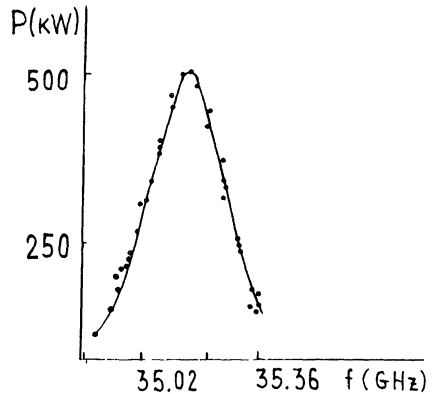

Fig 7 Output power as a function of drive frequency ($V_0 = 65$ kV, $I_0 = 34$ A, $P_{in} = 4$ kW)

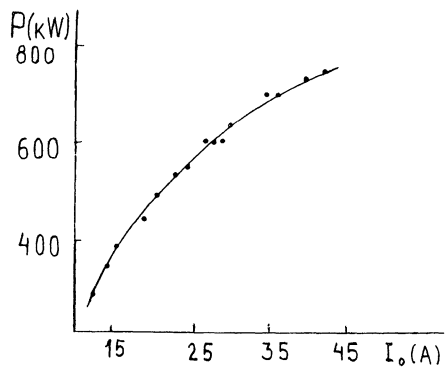

Fig 8 Output power versus beam current for modified tube with operating TE021 mode ($V_0 = 74$ kV, $P_{in} = 3.7$ kW)

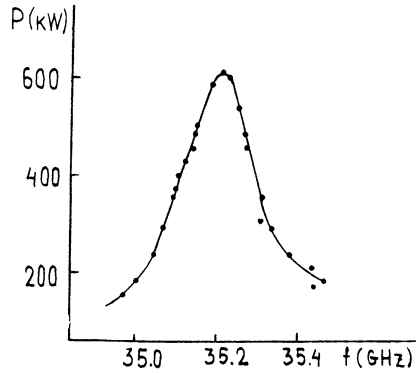

Fig 9 Dependence of output power on drive frequency for modified tube ($V_0 = 74$ kV, $I_0 = 28$ A, $P_{in} \doteq 3\,5$ kW)

References

1. A.V. Gaponov, A.L. Goldenberg, V.K. Yulpatov., Abstracts of the Vth All-Union Conference on Microwave Electronics, Saratov University, 1966, 20 (in Russian).

2. Wachtel J.M., Hirshfield J.L., Phys.Rev.Lett., 1966, Vol. 17, N 7, 348.

3. A.V. Gaponov, M.I. Petelin, V.K. Yulpatov., Radiophisics and Quantum Electronics, 1967, Vol. 10, 794.

4. A.V. Gaponov, A.L. Goldenberg, G.N. Rapoport, V.K. Yulpatov. Multi-cavity cyclotron resonance maser. Authors Certificate 273001 (USSR). Filed 16.06.67, publ. 15.05.75;
I.I. Antakov, A.V. Gaponov, V.A. Gintsburg, A.L. Goldenberg, M.I. Petelin, V.K. Yulpatov. Amplifier of electromagnetic oscillations in the centimeter, millimeter and submillimeter wavelength band: Authors Certificate 302050 (USSR). Filed 16.06.67, publ. 5.11.75.

5. I.I. Antakov, L.A. Aksenova, E.V. Zasypkin, M.A. Moiseev, L.G. Popov, E.V. Sokolov, V.K. Yulpatov., Proc. Int. Workshop "Strong Microwaves in Plasmas" Suzdal: Nizhny Novgorod, 1990, Vol. 2, 773. 6. I.I. Antakov, E.V. Sokolov, E.E. Zasypkin., Proc. II Int. Workshop "Strong Microwaves in Plasmas". Nizhny Novgorod: Russia, 1993 (in print).

STATE OF THE ART OF GYROTRON INVESTIGATION IN RUSSIA

V.A.Flyagin, A.L.Goldenberg, V.E.Zapevalov
Institute of Applied Physics of Russian Academy of Sciences,
Nizhny Novgorod, Russia

ABSTRACT

Parameters of modern family of ECRH OSMW gyrotrons are described. Some outlines of strategy of elaboration of new family of ECRH gyrotrons with 1 MW output are given.

INTRODUCTION

For ECRH systems at fusion plasma installations, the family of 0.5 MW gyrotrons with near - 1 s pulse duration at frequency range from 53 up to 160 GHz is created (see table 1). These gyrotrons satisfy the most part of modern fusion devices. For future ones, RF output power 1 MW and pulse duration 10 s or CW regime are regarded as obligatory. Problems of development of the new family of ECRH gyrotron can be classified in following 4 groups.

1. Creation of intense electron helical beam with low velocity spread and rather large share of gyration energy and transportation of the beam to resonant cavity;

2. Selective excitation of an operating mode with high efficiency in highly oversized gyrotron cavity;

3. Spatial separation of electron beam from RF radiation and high-efficiency conversion of the operating mode into wave beam which is convenient for its emission from gyrotron and further transportation to load;

4. Effective thermal drain from thermal loaded gyrotron's parts (cavity, collector, internal mirrors and output window).

Generally the accomplishment of the 1 MW long pulse gyrotrons will require larger dimensions of all their main parts and higher operating modes.

1. ELECTRON FLOW

For computation and optimization of gyrotron's electron gun, the adiabatic theory[1], trajectory analysis[2] and experimental methods[3] are used. In the latest time, the more attention is paid to theoretical and experimental determination of the velocity distribution functions of electrons in gyrotrons. Some experimental distribution function in a 140 GHz/0.5 MW tube given in Fig. 1 show explicit changes in their width and form at various beam currents. These changes can influence the beam's stability and gyrotron's efficiency.

The stability of an electron beam actually defines the maximum electron beam current. There can be various mechanisms of instabilities, particularly associated with potential depression in beams[4]. At typical parameters of

gyrotrons, thresholds of such instabilities can be overcome at currents near 50 A, which are necessary for 1 MW tubes. The deformation of the electron velocity distribution function can be a signal of some instabilities in electron beams.

2. SELECTION OF OPERATING MODE

The calculation of oscillations in a gyrotron cavity is carried out using the non-linear theory of multimode gyrotron[5]. In principle it is possible to attain 1 MW level at frequencies up to 110 GHz with modes which are proved to be stabilized by rather ordinary means of electron and electrodynamic selection[6]. Now new experiments are planned to check the stability of operating modes at 1 MW gyrotrons at frequencies up to 150 GHz.

3. SEPARATION OF ELECTRON BEAM RF RADIATION

In ECRH gyrotrons an electron beam is separated from RF radiation by means of an quasi-optical mode converter. Internal mirrors transform the radiations into a narrowly directed wave beam escaping a gyrotron through its output window transversely to the tube's axis. This provides relatively high resistance of such gyrotron against reflections in an external transmission line and protects a window against bombardment by stray electrons, ions and neutrals especially during internal breakdowns.

Measurements of the spatial structure and frequency spectrum of the output radiation allow to estimate the mode contents and to design first elements of an external transmission line. Results of measurements of the structure of the output wave beam of an industrial 110 GHz gyrotron are given in Fig.2. The analysis of it shows that with attained accuracy of measurements about 2 %, in the gyrotron the single $TE_{15,4}$ mode was excited.

4. THERMAL REGIMES

Two kinds of cooling systems are used in long pulse gyrotrons, depending on the ratio of thermal time constant τ_T to pulse duration τ. If $\tau_T / \tau < 1$ the heat capacity of material can be used, while relatively non-intense flow of coolant removes just mean thermal load; if $\tau_T / \tau \geq 1$ rather intense flow of coolant removing the maximum thermal load must be used. For metal parts τ_T can be close to 1 s, for windows τ_T is usually from 10 to 100 s.

4.1. Collector

Designing a collector, the acceptable thermal load and stability of operation to external magnetic fields are to be taken into consideration. Now in ECRH gyrotrons with over 0.5 s - pulses, scanning of an electron beam along the collector surface by a special coil with alternating magnetic field is usually used.

4.2. Cavity

Thermal load is one of main factors defining an operating mode of gyrotron's cavity. At pulses near 0.5 s duration and cooling based on the heat

capacity of cavity's walls, the maximum load reaches 1.5 kW/cm^2. At longer pulses and CW regime an intense flow of coolant is used, and the maximum thermal load in a cavity can be up to 2 ... 2.5 kW/cm^2.

4.3. Mirrors

In 1 MW gyrotrons with pulses longer than 3 ... 5 s, the RF ohmic losses can essentially heat up the mirrors. This leads to necessity of their cooling.

4.4. Window

Usually maximum transmitting power of an output window limits output power of ECRH gyrotrons. Now the main version of an output window for 1 MW CW gyrotrons at frequencies up to 150 GHz is the single-disk sapphire window cooled down to and below the L N_2 temperature.

5. CONCLUSION

Modern ECRH gyrotrons can not attain the goal of 1 MW multisecond or CW output. For this, new investigations and developments are needed. The most serious problems seem to be associated with stability of electron beams and transmitting power of output windows.

REFERENCES

1. A.L.Goldenberg and M.I.Petelin, Formation of helical electron beam in the adiabatical gun, Izvestiya Vysshikh Uchebnykh Zavedenii. Radiofizika, Vol.16, p. 141-149, 1973.

2. A. L. Goldenberg et al., Adiabatic Theory and Trajectory analysis of Gyrotron Electron Gun, Gyrotrons (Gorky, Institute of Applied Physics, Akad. Nauk SSSR), p. 86-106, 1981.

3. A. N. Kuftin et al., Numerical simulation and experimental study of magnetron-injection guns for powerful short-wave gyrotrons, Int. J. Electronics, Vol. 72, N5, 6, p. 1145-1151, 1992.

4. Sh. E. Tsimring, Limiting current of the helical electron beam, Radiotechnika et Electronika, Vol. 35, N6, p. 1284-1288, 1990.

5. G. S. Nusinovich, Mode Interaction in Gyrotrons, Int. J. Electronics, Vol. 51, p. 457, 1981.

6. A. V. Gaponov et al., Powerful Millimeter-Wave Gyrotrons. Int. J. Electronics, Vol. 51, N4, p. 227, 1981.

Table 1.

Experimental and industrial ECRH gyrotrons.

N°	frequency GHz	output MW	efficiency %	cavity wall losses kW/cm^2	pulse duration S	output mode
1	83	0,5	37	1,2	1,5	Gauss
2	82	1,0	50	2,5	10^{-4}	high
		1.5	36	-4	10^{-4}	
3	100	0.5	50	1,3	10^{-4}	high
		1,0	40	2,6	10^{-4}	
4	110	1,0	44	3,1	10^{-4}	Gauss
		0,5	35	1,5	0,5	
5	140	0,8	38	2,5	10^{-4}	high
6	140	0,5	36	1,5	0,5	
		0,9	36	2,8	0,3	
		0,6	34		2	
7	167	0,5	30	3...4	0,7	Gauss

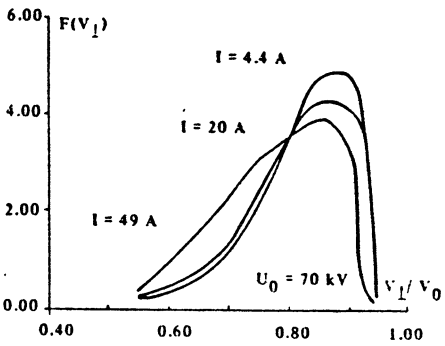

Fig. 1. Distribution function of gyrotron velocities in electron beam of 140 GHz gyrotron at various beam currents I.

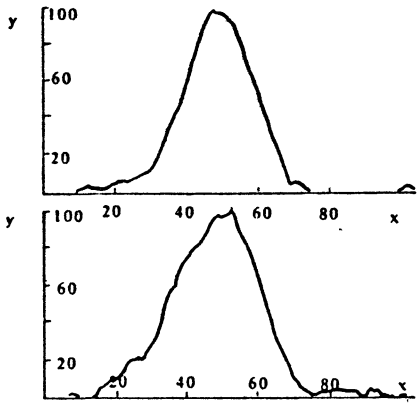

Fig. 2. Wave beam structure at output window of 140 GHz gyrotron.

x- horizontal axis. y - vertical axis.

DEVELOPMENT OF A HIGH POWER GYROTRON FOR FUSION APPLICATION IN JAERI

K.Sakamoto, A.Kasugai, M.Tsuneoka, S.Maebara,
T.Nagashima and T.Imai
Japan Atomic Energy Research Institute, Naka Fusion Research Establishment, Naka-machi, Ibaraki, Japan 311-01
T.Kariya, Y.Okazaki, N.Shirai and T.Okamoto
Electric Tube Division, Toshiba Co., Ohtawara-shi, Tochigi, Japan 329-26
K.Hayashi, Y.Mitsunaka and Y.Hirata
Research and Development Center, Toshiba Co.,Ukishima, Kawasaki-shi, Japan 210

Abstract

A high power gyrotron for a fusion application is under development. Up to now, an output power of 410kW with a pulse duration of 1.3sec, and 550kW with 2msec was obtained at 110GHz with a built-in mode converter gyrotron. Followed this, a gyrotron with collector potential depression system(CPD) is designed for an efficiency improvement. With this gyrotron, the efficiency enhancement of the factor of 1.5 is expected. In the cooling experiment of the cryogenic window, it was confirmed that the window temperature was decreased from room temperature to 13 °K within 2 hours.

1. Introduction

An electron cyclotron range of frequency (ECRF) wave has outstanding characteristics for a fusion application. In the experiment of the medium sized tokamak, the validity of an electron cyclotron heating (ECH) [1] and a current drive(ECCD) [2-4] of the plasma, a plasma initiation and the active control of the plasma, i.e., a suppression of the disruptive instability[5] and a sawtooth stabilization[6], etc., were proved. From the technological point of view, ECRF has advantages; good accessibility with the plasma, high power density capability of the launcher, no impurity generation from the launcher, small heat load and neutron damage on the launcher since the antenna could be placed far from the plasma. For the application of ECRF to the large sized tokamak, e.g. ITER, JT-60U, a high power RF source of an output power of >1MW, 100GHz band with a continuous operation is needed. In these year, a lot of works are extensively devoted to the development of the high power gyrotron in Russia[7,8], US[9-11], EC[12,13] and Japan[14,15]. In JAERI, a development of the high power gyrotron for fusion application has been carrying on with a cooperation of Toshiba Co. The present status of the gyrotron development is; the 500kW level gyrotrons of an operation mode of a whispering gallery mode ($TE_{12,2}$) with a built-in mode converter had been developed and the power of 460kW with a pulse duration of 0.1sec was attained in 1992. Followed this, a longer pulse gyrotron is developed and tested. The design value of the gyrotron is a power generation at the power level of 500kW at

110GHz with a pulse duration of 1sec. To keep the heat load on the cavity wall as low as approximately 1.5kW/cm^2, the oscillation mode is selected to be $TE_{22,2}$ whispering gallery mode(WGM) at 110GHz. On the other hand, the efficiency enhancement is also an important issue for a fusion application. For this purpose, a gyrotron with a collector potential depression system (CPD) is under fabrication.

For a long pulse high power gyrotron or a transmission line, a ceramic window for a vacuum sealing or a tritium sealing is inevitable. It is well recognized that the temperature increase of the window due to the RF power absorption is so severe for a power penetration of 1MW with CW at 100GHz band. Therefore, it is strongly demanded the development of the window available for high power long pulse power transmission. As a candidates of the window, a cryogenically cooled window using a refrigerator is proposed, which utilizing the characteristics that the loss tangent of the ceramic decrease and a heat conductivity increase as the temperature decrease.

In this paper, the experimental results of the long pulse (1sec) gyrotron of WGM of $TE_{22,2}$, and a design of the gyrotron with the CPD system are described in Secs. 2, 3, respectively. Also, the designed and the result of its cooling test is presented in Sec.4. Summary is given in Sec.5.

2. $TE_{22,2}$ long pulse gyrotron

2-1 Design of $TE_{22,2}$ long pulse gyrotron

The radius and the length of the cavity are 13mm and 12mm, respectively. The quality factor of the cavity is 495 at $TE_{22,2}$ WGM with a cold state. The radius of the electron beam is set to be 10.1mm. In Fig.1, the heat load on the cavity wall at the power oscillation of 625kW is shown with the dimension of the cavity. Here, the beam energy E_b is 80keV, beam current I_b is 22A, pitch factor $\alpha=v_{perp}/v_{para}=1.8$ and the beam thickness and the spread of α are assumed to be zero. The maximum cavity heat load is $1.4kW/cm^2$ (the electric conductivity of the copper: $3.0x10^7S/m$). The temperature on the cavity wall after the 1sec oscillation is estimated to be ~194 °C with an initial temperature of 20 °C assuming the heat transfer ratio between the copper and the cooling water as $3W/cm^2$. The maximum stress of 240MPa appears at the center of the cavity. The cycle operation of ~2000 times should be permitted, which is expected from the heat cycle test on the copper wall using the heater. However, some improvement on the material, the operation mode or the cooling method may be needed for longer pulse operation.

The oscillated power of $TE_{22,2}$ is converted to a Gaussian like beam mode using a built-in type quasi-optical mode converter (Vlasov converter), and the power is extracted horizontally through the double disk window of sapphire[14], whose surface is cooled by FC-75. The diameter and the thickness of the window is 136mm and 3.57mm. respectively. The estimated temperature increase after

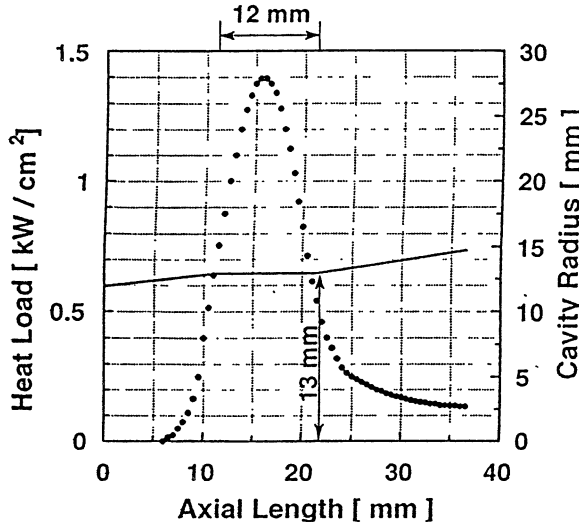

Fig.1: The dimension of the cavity and its heat load at 625kW oscillation.

1sec oscillation with 500kW output is 136 °C at the vacuum surface and 80 °C at the FC-75 cooled surface, which is smaller than that of boiling temperature of FC-75. The maximum compression stress is 158MPa at the window center and the maximum tensile stress is 52MPa at r=40mm, which are well small than those of critical values, 3000MPa and 2300MPa, respectively (Fig.2).

The collector is designed assuming the most severe case, i.e., the electron beam of 80keV,30A, 1sec is injected with a duty of 1/15 and no electron reflection exist. The inner radius of the collector is 270mm. The collector is cooled with a vapor cooling system, and the diameter of the water jacket is ~800mm.

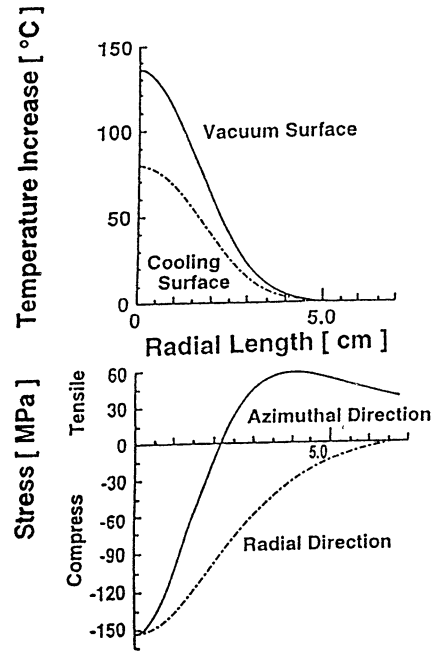

Fig.2: Radial distribution of temperature increase and stress of the surface cooled window after 1sec, 500kW penetration of RF(110GHz).

The maximum heat load into the collector wall is 2.2kW/cm^2. As this value is too large for the 1sec operation, the electron beam is swept using a sweeping coil of 1Hz. Then, a beam landing area is expanded from 40mm to 430mm, as a result, the heat load is reduced to 300W/cm^2 in average (650W/cm^2 at maximum) as shown in Fig.3. After the beam injection during 1sec, the temperature increase up to 260 °C at maximum and 117 °C at the cooling surface, which are acceptable for the 1sec operation.

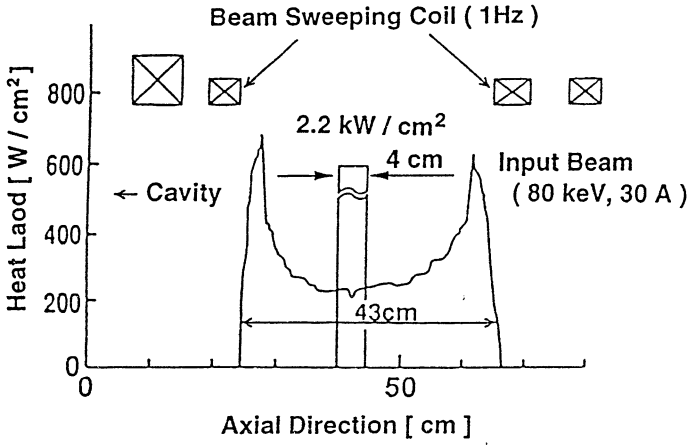

Fig.3: Heat load on the collector wall with a beam injection of 80keV,30A.

2-2 Experimental study of the oscillating parameters

The oscillation experiment was carried out using the 80kV, 35A level test stand. At first, the parameter dependence on the oscillation was obtained with a pulse duration τ=2msec. Figure 4 shows B_c dependence on the output power P_c and its frequency f. Here, V_b~77kV, I_b~33A. The value of α is estimated to be 1.4~1.5 from a simulation of MIG. The output power P_o is measured from the temperature increase in the cooling water in the dummy load. The maximum power of 550kW is obtained at B_c~4.29T. It should be noted that the power is measured at the outside of the window, so the oscillation power may be 700kW if the efficiency of mode

converter 78% is taken into account. The oscillation frequency, which is measured with the spectrum analyzer, increase with B_c. The oscillation frequency shifts to the higher side as B_c increase as expected from the nonlinear theory. The I_b dependence on the output power P_o and an efficiency η at V_b~77kV is shown in Fig.5. Here, B_c is optimized to have the maximum power for each I_b. The output power increase with I_b and the maximum power of 550kW is obtained at I_b=33A. The maximum efficiency (23%) is observed at I_b=22A. The efficiency seems low comparing the design value(~28%). This is considered to be caused mainly by the difference of pitch factor α between the design and the experiment. The design is optimized to have the maximum efficiency at α=1.8.

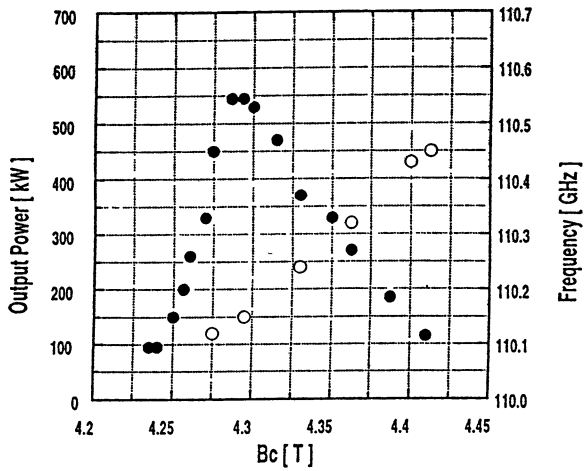

Fig.4: Cavity field B_c dependence on the output power P_o (closed circle) and its frequency f(open circle). V_b~77keV, I_b~33A.

In the experiment, however, the efficiency tend to saturate and the anode current increase (>100mA) when the anode voltage is raised to have α more than 1.5. These are supposed that α saturate at a low level than that of expected and/or the divergence of α increase.

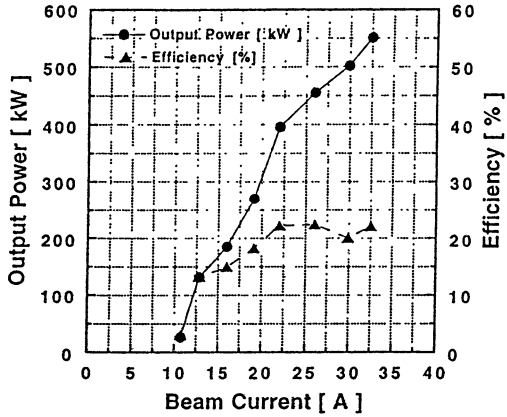

Fig.5: Beam current I_b dependence on the output power P_o and the efficiency η. V_b~77keV. The optomized cavity fields for each data are denoted in the figure.

2-3 Long pulse operation

After the parameter study, the pulse extension experiment was carried out. Then, the collector sweeping coil was used, which superimpose an additional magnetic field of ~50 G at the collector section with 1Hz. The output power couples with the corrugated waveguide of 88.9mm in diameter with a combination of the phase correlated mirror system, and introduced to the long pulse dummy load via a transmission line of 3m in length with two phase

correlated miter bends. The corrugated waveguides are made of aluminum, whose inner corrugation is mechanically cut with a pitch of 0.84mm, width of 0.42mm and a depth of 0.62mm. Arcing in the transmission line and the gyrotron window are monitored with the photo and the phono sensors. The whole system of the transmission line include the dummy load is evacuated less than 10^{-2} Pa. Approximately 90% of the output power was transmitted to the dummy load. For the pulse extension, slow but steady outgassing process (conditioning) seems inevitable. As a result, the maximum pulse duration of 1.3 sec was obtained with P_O=410 kW, in which about 40 days conditioning was required. The oscillation frequency shift downward by about 150MHz after 1sec. operation, which is considered to be caused by the thermal expansion of cavity radius by approximately 20 microns.

3. Design of CPD gyrotron

The gyrotron with single stage CPD system is under fabrication. The design of MIG and the oscillation mode ($TE_{22,2}$) are the same with non-CPD gyrotron described in section 2. The conceptual picture of the CPD gyrotron and its modified power supply system are shown in Fig.6. High voltage up to 50kV can be applied between the collector and the body section, and between the collector and the casing around the body section. The insulation material between the body section and the outer casing is resins of about 15mm in thickness and a ceramic cylinder of about 120mm in length between the body and the collector. The collector and the casing are earthed. In the normal operation, a beam accelerating

voltage V_a is equal to the voltage of the main power supply V_c then the body voltage to the ground is zero. If V_c decrease, the voltage of the body increase, as a result, the electron decelerating voltage appear between the body and the collector keeping the beam acceleration voltage V_a constant. As the total power consumption is determined by that of the main power supply, the total efficiency $\eta_{CPD}=P_{RF}/(V_cI_b)$ increase with the decrease of V_c. η_{CPD} is rewritten as

$$\eta_{CPD}=\frac{P_{RF}}{V_aI_b}\frac{V_a}{V_c}=\eta_{RF}\frac{V_a}{V_c} \quad .$$

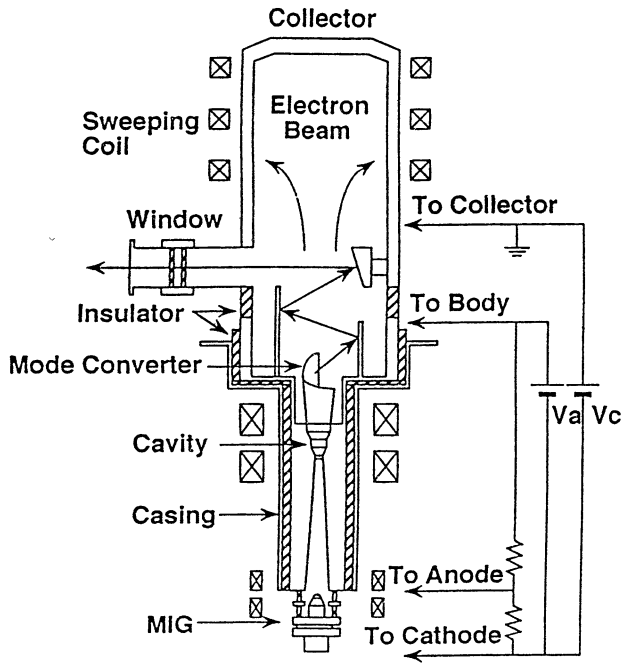

Fig.6: Conceptual view of the CPD gyrotron and the power supply system for CPD gyrotron.

The beam depression potential V_d ($=V_a-V_c$) must be smaller than the critical value of the electron returning voltage.
For instance, if the depression voltage of 25kV can be applied for the case of V_a=80kV, then the efficiency is expected to improve by a factor of 1.5;

$$\eta_{CD} \sim \eta_{RF} \frac{80kV}{55kV} \sim 1.5\eta_{RF}.$$

At the same time, the heat load on the collector wall also reduced(~65% of non CPD case).

4. Cooling test of cryogenic window

Figure 7 (a) and (b) are the side view and the front view of the window system, respectively. A sapphire disk is placed between the corrugated waveguide of 60.3mm in the inner diameter. A thickness of the disk is 1.33mm and the gap between the corrugated waveguides is 3.3mm. The corrugated waveguides are covered with a stainless bellows which separate the vacuum of both sides of the window. The disk is thermally isolated from the waveguide or outer casing and connected to the cryogenic refrigerator through the copper rod (thermal anchor) and cooled down to 13 °K. The cooling capability of the refrigerator is 7W at 20 °K. The temperature of the window disk is measured by the thermocouple. Figure 8 shows the result of cooling test of the window. The temperature of the disk decreased from room temperature to 13 °K within 2 hours. The results of the high power transmission experiment will be published elsewhere.

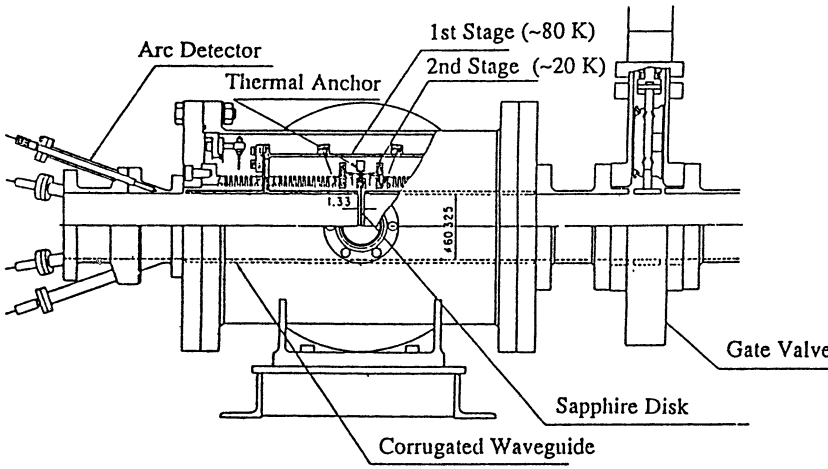

(a) side view

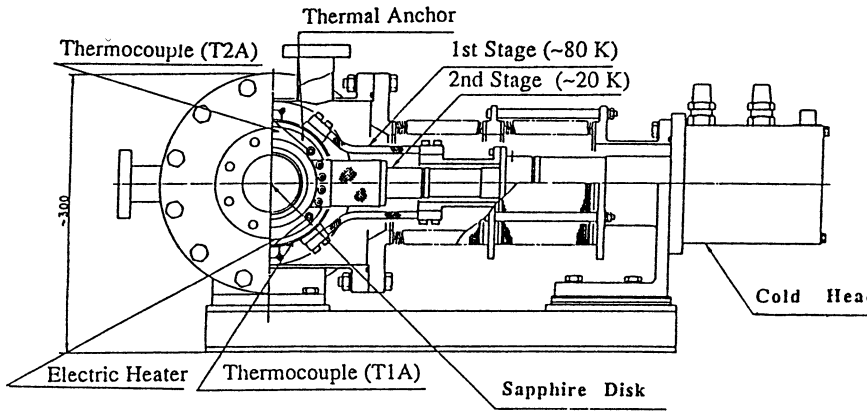

(b) front view

Fig.7: Schematic view of the cryogenic window.

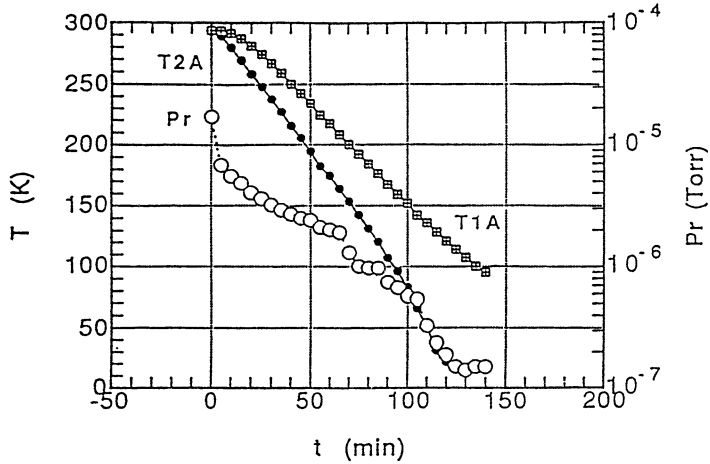

Fig.8: Result of cooling test of the cryogenic window.
Closed circles and squares indicate the temperature at the edge of window(T2A) and bellows(T1A), respectively. Open circles indicate a pressure.

5. Summary and future works

The results of the design and operation of the long pulse gyrotron for fusion application were described. On $TE_{22,2}$ WGM gyrotron with a built-in mode converter, the maximum power of 550kW (2msec), and 410kW with the pulse duration of 1.3 sec were obtained at 110GHz. Also, the gyrotron with a CPD system for an efficiency enhancement is under fabrication. The CPD system is realized by applying the beam decceleration voltage between a body and a collector (collector is earthed). The efficiency enhancement of the factor of 1.5 is expected. In the cooling experiment of the cryogenic window, it was confirmed that the window temperature was decreased from room temperature to 13 °K within 2 hours.

Acknowledgments

The authors would like to thank to Mr.H.Fujita and Mr.M.Kikuchi for supporting the operation of the gyrotron test facility and Mr.K.Yokokura for operation of the cryogenic window. They also thank to Dr.T.Ito and of Toshiba Corp. and Drs.T.Yamamoto, S.Shimamoto, S.Tamura and M.Yoshikawa of JAERI for their supports and encouragements.

References

1. V.V.Alikaev, et al., Plasma Phys. and Controlled Fusion, vol.29, 1285 (1987).
2. H.Tanaka,et. al., Phys.Rev.Lett, vol.60, 1033 (1988).
3. V.V.Alikaev et al., Nucl.Fusion, vol.32, 1811 (1992).
4. R.A.James et al., Phys.Rev. A 45, 8783 (1992).
5. K.Hoshino,et. al., Phys.Rev.Lett. vol.69,No.15, 2208 (1992) .
6. K.Hanada, et al.,Phys.Rev.Lett., vol.66, 1974 (1991).
7. A.V.Gaponov and M.I.Petelin, Proc. of Int.Workshop on strong Microwaves in Plasmas, edited by A.G.Litvak, p.677 (1991).
8. V.E.Zapevalov, A.N.Kuftin, ibid., p.726.
9. K.Felch,et al., Digest of 17th Int.Conf. on Infrared and Millimeter Waves, Edited by R.Temkin, p184 (1992).
10. M.E.Read, G.S.Nushinovich, et al., ibd., p.192.
11. K.E.Kreisher, W.C.Guss and R.J.Temkin, ibid, p.194.
12. G.Grantenbein, et al., ibid.,p.186.
13. T.L.Grimm, et al, ibid.,p.190.
14. K.Sakamoto, et al., ibic., p188.
15. T.Shimozuma, et al. J. of Electronics, vol.74,no.1,137 (1992).

THE FOM-FUSION-FEM as a tunable ECRH source

A.G.A. Verhoeven, W.A. Bongers, B.S.Q. Elzendoorn, P. Manintveld, F.C. Schüller, A. Tulupov, M.J. van der Wiel, W.H. Urbanus.

FOM-Instituut voor Plasmafysica 'Rijnhuizen',
Association EURATOM-FOM
P.O. Box 1207, 3430 BE Nieuwegein, the Netherlands

V.L. Bratman, G.G. Denisov, A.V. Savilov, M.Yu. Shmelyov.
Institute of Applied Physics, Nizhny Novgorod, Russia

H.-U. Nickel, M. Thumm.
IHE Universität Karlsruhe and ITP KfK Karlsruhe, Germany

W. Kasparek, J. Pretterebner, D. Wagner.
Institut für Plasmaforschung, Stuttgart, Germany

M. Caplan, C. Shang
Lawrence Livermore National Laboratory, Livermore, CA, USA

1 Introduction

A Free Electron Maser is being designed for ECRH applications on future fusion devices. The FEM will have an output power of 1 MW, with a central frequency adjustable within the complete frequency range of 130 GHz to 260 GHz and a fast tunability of $\pm$ 5 % around the chosen central frequency. For the first phase of the project a pulse length of 100 ms is foreseen, but with the intention to extend this to cw in a later phase.

The FEM operates with a thermionic electron gun. Fast tunability is achieved by variation of the voltage of the 2 MeV electrostatic accelerator. After interaction with the millimeter waves (mmw) in the undulator, the energy of the electron beam will be recovered by means of a decelerator and a multi-stage depressed collector. See fig. 1.

The -low emittance- electron beam of 12 A will be transported throughout the system without bends to minimize current losses to

less than 20 mA. This lost current is to be delivered by the 2 MV dc accelerating voltage power supply. Simulations indicate that the overall efficiency will be over 50 %.

Since the electron beam line is straight it is necessary to bend the mm waves away from the electron beam. A very new solution to separate the electron beam from the mm waves will be incorporated.

2 Application on future fusion devices

The specifications for the FOM-Fusion-FEM are optimized for ECR applications on future fusion devices. Emphasis is given to the application on ITER. The FEM will be tunable over ± 5 % of the central frequency, to enable to change the location of the power deposition. The adjustment of the frequency can be done on a timescale of 100 ms.

The frequencies (130-260 GHz) are chosen such that for ITER (with a toroidal magnetic field of 6 T on axis) both fundamental on-axis heating at 170 GHz and off-axis heating (140-200 GHz) can be achieved. Furthermore, the ideal frequency for EC current drive at upshifted frequencies is around 230 GHz [1]. The lower frequency of 130 GHz is enables second harmonic heating at the RTP tokamak at FOM.

A FEM combines the advantages of all other ECRH sources (like gyrotrons) with the additional advantage of fast tunability and -in principle- a higher efficiency and a higher power per unit.

Recognized advantages of ECRH above other heating methods are: • localised absorption is up to 100 %, throughout the plasma cross-section.

• pre-ionization by ECH and ECH-assisted start-up are well proven.

• the launching system is simple, far away from the plasma, and can handle high power densities. There are no problems in coupling power to the plasma through a vacuum layer, therefore impurity sources due to plasma/antenna interaction are avoided.

• the barrier window can be sited remotely behind a radiation shield.

- current drive possibility, with predictable efficiency.

Additional advantages of using a source with an adjustable frequency are:

- all flux surfaces in the plasma can be reached without changing the toroidal magnetic field, so without changing the target plasma.
- for m=2 mode stabilisation the variations in the q-profile can be followed by tuning the absorption region to the change of the q=2 radius.
- fine control over break-down location is possible in case of pre-ionization by ECH and ECH-assisted start-up.
- ECRH can control of Edge Localised Modes by changing the resonance location [2,3].
- a simple and small waveguide launcher can be used [4]. Whereas in case of a fixed-frequency source a mirror launcher at variable angles is needed which requires a substantially larger opening in the wall.
- current drive is easier to apply and can be more efficient, since the absorption region can be chosen more accurately.

3 Basic lay-out of the FOM-Fusion-FEM

In the FOM-Fusion-FEM the electron beam line comprises a thermionic electron gun, an electrostatic accelerator, an undulator and mmw system, an electrostatic decelerator and a depressed collector. The design is based on a dc accelerator and decelerator system rather than an rf system. This enables easy frequency tuning by variation of the accelerator voltage, i.e. the electron energy.

The undulator and mmw system are located in a terminal at a voltage of maximum 2 MV, inside a vessel filled with SF_6 at a pressure of 7 bar. See fig. 1. The pressure vessel measures 11 m in length and 2.6 m in diameter.

The high voltage for a FEM is much higher than for other high-power mm-wave sources, like gyrotrons and CARMs. In our case, due to the energy recovery, the main current has to be supplied at a

voltage of no more than a few hundred kV. The 2 MV power supply has to deliver only the current lost during transport. Our target is to keep the electron loss current below 20 mA, which is some 0.2 % of the total beam current of 12 A. Because of this stringent requirement, a simple, straight electron-beam line will be used.

4 Interaction

The interaction between the electron beam and the mm waves is simulated using both a 1-D, non-stationary code and a fully 3-D, stationary, amplifier code. Results with both codes indicate that -with a beam current of 12 A- an output power of over 1 MW can be generated for all required frequencies with a beam energy ranging from 1.3 MeV (for 128 GHz) via 1.75 MeV (for 201 GHz) to 2 MeV (for 253 GHz).

Simulations were performed for the actual step-tapered undulator being built for the project. The first section of the undulator has 20 periods with a strength, K_{rms}, of 0.52 (0.2 T), a period of 40 mm and a pole gap of 25 mm. Then follows a 60 mm long drift space and then a second section consisting of 14 periods with the same period and pole gap, but with K_{rms} =0.42 (0.16 T).

Results with the 3-D, non-linear, CRMFEL code show that with a drive power (i.e. the feedback power) of 0.4 MW a net power of 1.35 MW can be generated [5]. Results of the calculations for 201 and 253 GHz are shown in fig. 2. In fig. 3. the results are given for 128 GHz for 2 sets of parameters for the second undulator section. For an overview of the simulation results, see Table I.

It is clear from these results that by changing only the electron energy and the reflection coefficient (this is the fraction of mmw output power that is used as feedback) the FEM can be tuned over the entire frequency range. In the section on the mmw system it will be shown that a very simple way to adjust the reflection coefficient will be part of the FOM-Fusion-FEM.

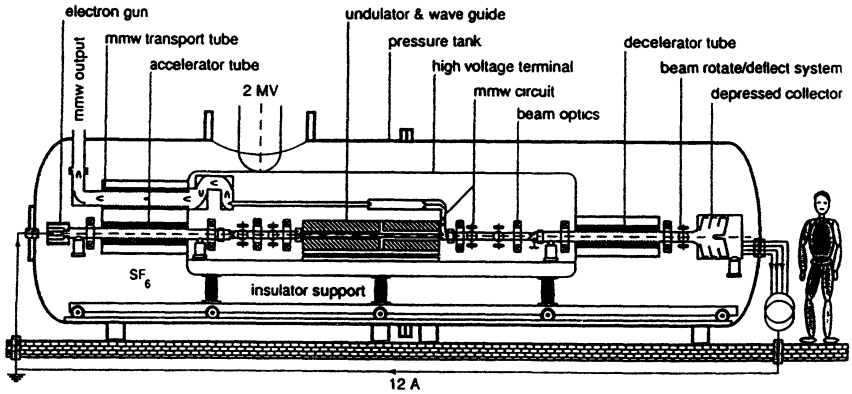

Fig. 1. General layout of the FOM-Fusion-FEM.

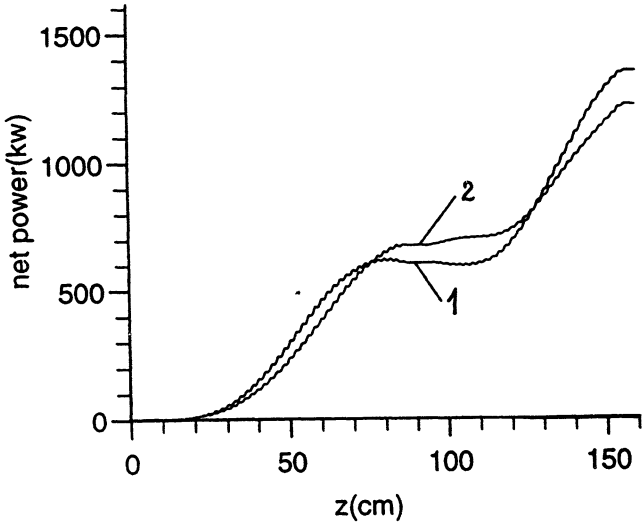

Fig. 2. Net power level vs undulator length for 1.75 MeV (1: 201 GHz) and 2.00 MeV (2: 253 GHz). Reflection coefficient (i.e. the fraction of mmw output power that is used as feedback) R = 0.29.

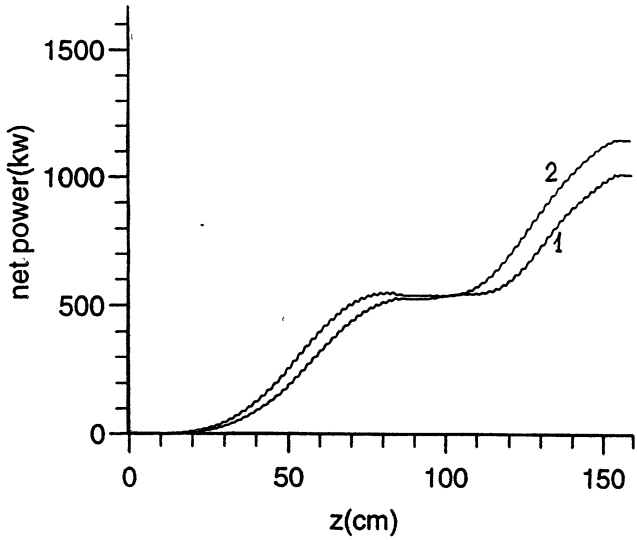

Fig. 3. Net power level vs undulator length for 1.35 MeV (128 GHz), for 2 different second undulator sections: 1: 0.16 T and R = 0.11; 2: 0.15 T and R = 0.15.

I_e [A]	E_e [MeV]	ε_n [mm mrad]	f_{mmw} [GHz]	R_{mmw} [%]	P_{net} [MW]
12	2.0	50	253	34	1.25
12	1.75	50	201	29	1.35
12	1.35	50	128	11	1.05

Table I.
Overview of the simulation results at 128, 201 and 253 GHz.

The picture for stationary behaviour appears to be rather convincing with a good agreement between the various codes that have simulated this configuration. However, initial analyses with time-dependent codes seem to indicate the possibility of non-stable output power with a wide frequency spectrum.

From earlier experiments [4] it is known that the dynamics of high-frequency oscillators (like our FEM) is defined by the parameter of excess over threshold L (analogous to the Reynolds number), where $L = \frac{\omega}{c} lC$, which is proportional to the interaction space length l and to the Pierce amplification parameter C, where $C \sim \sqrt[3]{I}$. If L is smaller than its starting value $L = 1$, autooscillations do not excite. In case $1 < L < 3$, stable, single-frequency operation can be expected (see fig. 4, upper plot). During start-up there is high-frequency noise on all longitudinal modes but one longitudinal mode suppresses all other modes and a pure spectrum results, eventually. However, in case L becomes more than 3, a complex regime is to be expected with many longitudinal modes excited and with non-stationary temporal behaviour of the output signal. See fig. 4, middle plot (L=3.2) and bottom plot (L=4.5).

In view of these problems, we have chosen the design of the FOM-Fusion-FEM such that not only the beam current I, but also the reflection coefficient can be varied easily. The earliest experiments will give a clarification of the exact temporal behaviour. In the mean time considerable attention will be given to simulations with non-stationary codes.

5 The mmw sytem

The FEM will be configured as a mmw oscillator, consisting of a waveguide amplifier section and a feedback system. Inside the undulator an oversized rectangular corrugated HE_{11} waveguide is located with a cross section of 15x20 mm^2, with the $\vec{E}$-field parallel to the broad side of the waveguide.

Behind the undulator the mm waves will be separated from the electron beam by means of a stepped waveguide [7,8], see fig. 5. Here the broad side of the waveguide is stepping up. As a result of this step, the initial HE_{11} beam is splitted into two identical off-axis HE_{11} beams at about 1.5 m from the step. At this position two mirrors will be located with a hole in between, large enough to pass the electron beam without disturbing the mmw beams, see fig. 6. At the mirrors the two mmw beams are reflected with an adjustable phase difference by changing the position of one of the mirrors, see fig. 7. This enables a 0-100 % variation of the reflection coefficient, i.e. the fraction of the power which returns through the interaction waveguide to the input side of the undulator, see fig. 8. Here a 100 % reflector is located based on the same principle. Low-power measurements on a prototype separation system were performed and were very encouraging.

Tunability is achieved by variation of the width of the waveguide a (after the step), which is given by $a = \sqrt{2\lambda\Lambda}$, where Λ is the length of the electron-beam/mmw splitter: 1.5 m. A system is being designed to move the sidewalls of the splitter in order to optimize the dimension a for all frequencies from $a = 60$ mm for 260 GHz to $a = 85$ mm for 130 GHz. This system enables variation of the frequency over the complete range of 130 to 260 GHz by changing the accelerator voltage, the splitter width and the reflection coefficient. All these parameters can be controlled remotely in the time scale of a few minutes.

The transverse mode purity has been investigated numerically [8]. Via a matrix algorithm the propagation of the mmw beam through the entire cavity has been simulated, while in the primary waveguide the interaction between the electron beam and the mmw beam have been taken into account. The simulation uses an input of with 10 transverse modes HE_{1m}, with m odd, at the input of the primary waveguide. Fig. 9. shows the result of the simulation after 1,2 and 3 roundtrips. Even with a very non-symmetric input signal, after 20 roundtrips over 99.9 % of the mmw power is in the required HE_{11} mode.

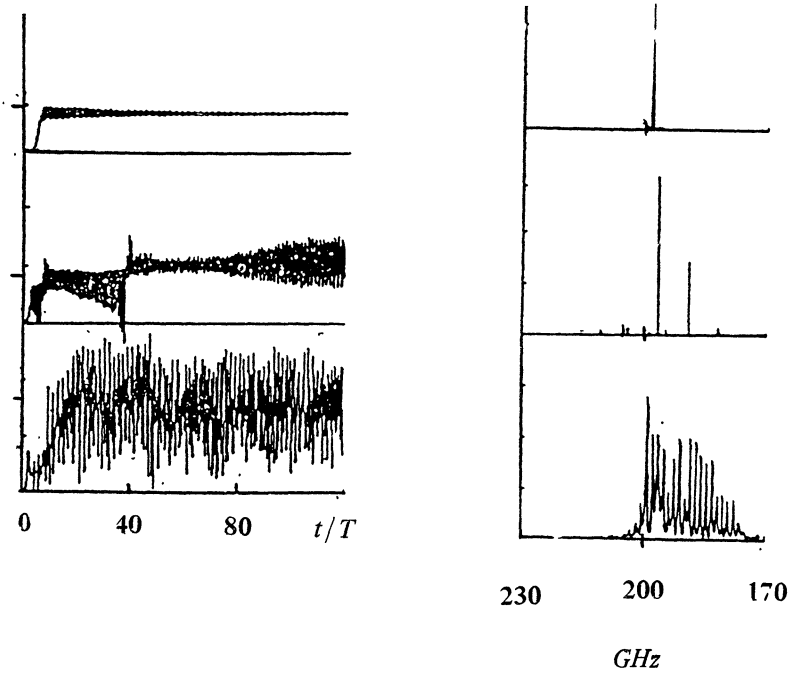

Fig. 4. Temporal behaviour and spectrum for different values of L. Upper plot: L = 2.5 ; middle plot: L = 3.2; lower plot: L = 4.5. T = roundtrip time; Arbitrary units on the vertical scale.

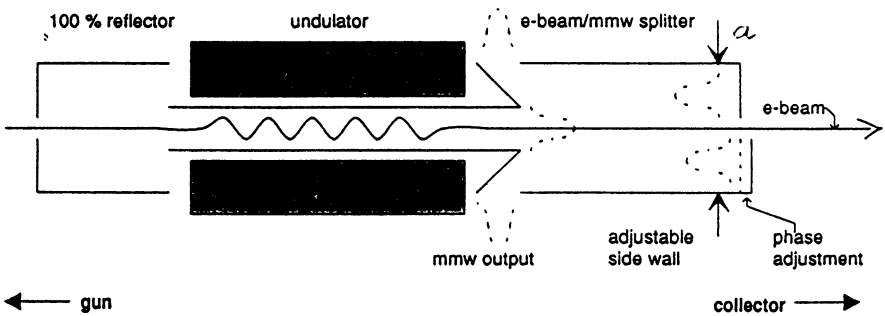

Fig. 5. The mmw system.

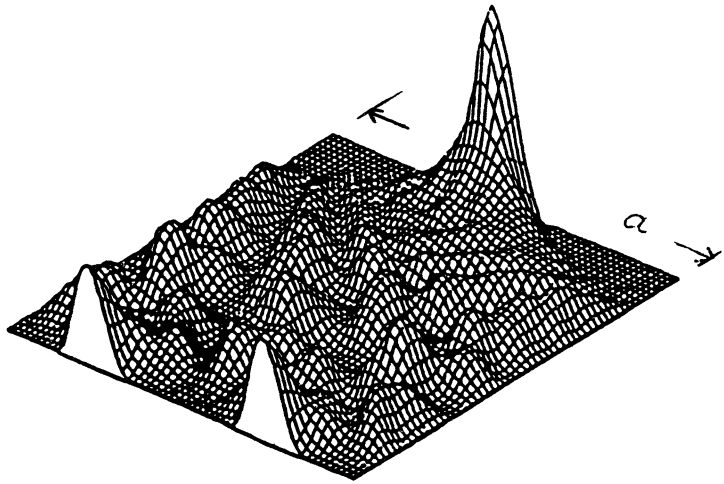

Fig. 6. Splitting of one beam into 2 beams.

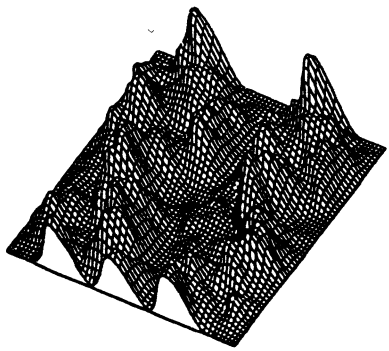

Fig. 7. Two beams are transformed into 3 beams at a phase shift of 0.63π.

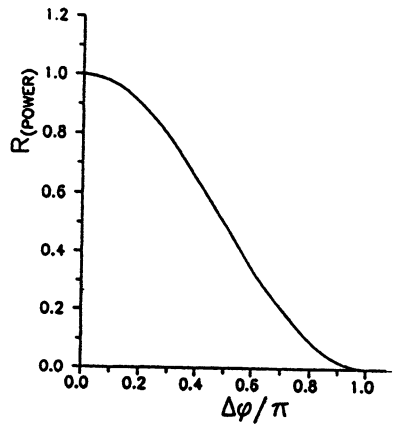

Fig. 8. Reflection coefficient vs phase shift.

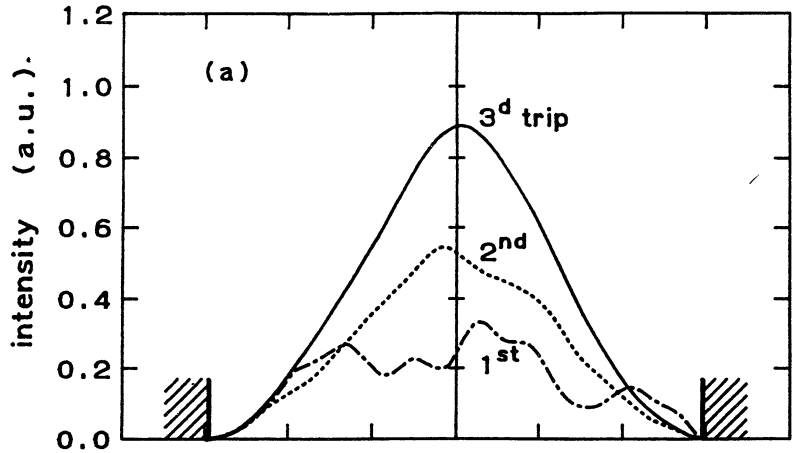

Fig. 9. Transverse field structure of the mmw beam at the end of the waveguide inside the undulator after 1,2 and 3 roundtrips.

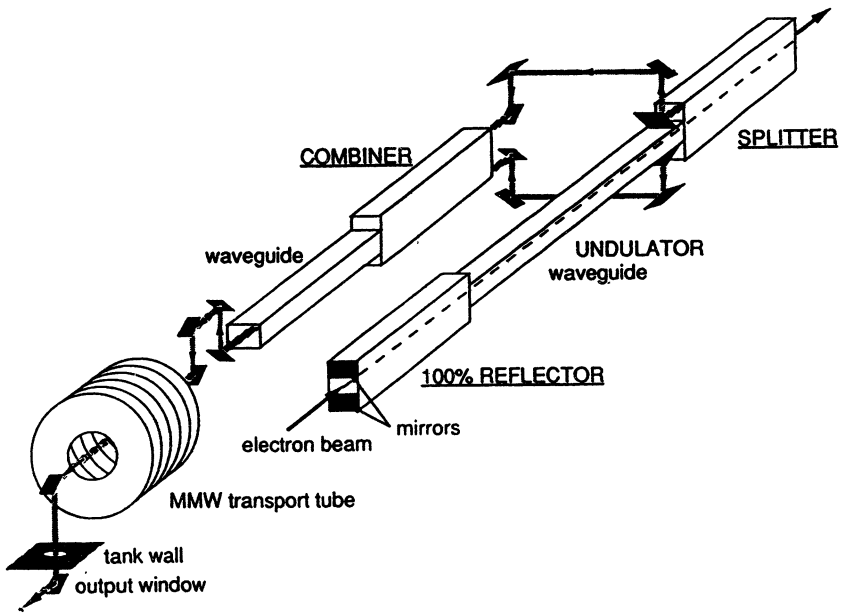

Fig. 10. Complete mmw system with splitter, 100 % reflector and combiner.

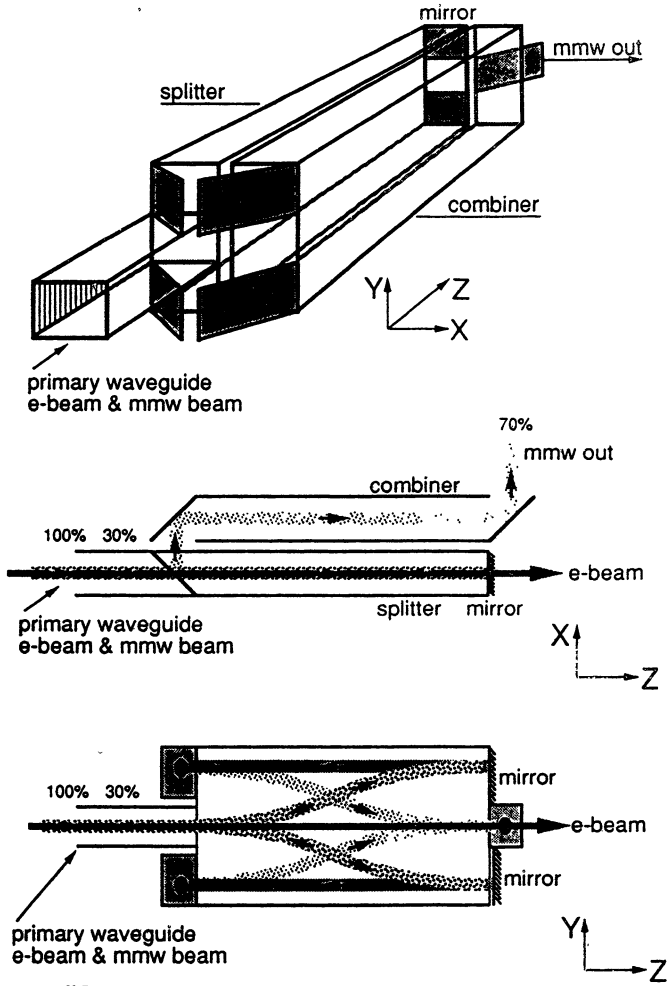

Fig. 11. "Two-storey" combiner.

At the "lower" storey the electron beam is separated from the mm waves. The electron beam leaves the system to the right. The mm waves are reflected (with adjustable phase difference) and by 2 more reflections the output beams go to the "upper" storey recombine and leave the system to the rigth. The feedback mmw beam stays at the lower storey and returns to the undulator (to the left). This complete system will be made with adjustable side walls for wide bandwith.

Transport of the mm waves from the electron beam/mmw splitter to outside the pressure vessel will be done in the following way. The two mmw output beams (see fig. 10) are combined into one beam by means of a combiner system: the same system as the splitter mentioned before, but this one working in the reverse sense. By using a quasi-optical confocal mirror system the single beam is transferred to the insulator tube. This is a tube very similar to the 2 MV accelerator tube. However, to let the mm waves pass from the 2 MV level to earth potential a wider -tapered- bore hole is used for the electric-field steering electrodes. An advantage of this method of transport is that no vacuum windows are required at a pressure of 6 bar.

To combine the two output beams a choice has to be made between the use of a separate combiner system (as in fig. 10) or a system using a combiner similar to the splitter on top of the real splitter. The two mmw beams are reflected by two 45° mirrors to the "upper store" and here combined and coupled out, see fig. 11.

6 Broadband output window

Since the frequency of the FEM has to be varied over a very wide frequency range it is necessary that the vacuum barrier is broadband as well.

To enhance the frequency band some possibilities have been worked out to enable permittivity transition on both sides of the window, either by adiabatic structures (tapers) or by resonant structures ($\lambda/4$ transformers).

Although these solutions have indeed a much wider frequency band then usual, still many windows are needed, each one covering just a small part of the entire frequency band. Therefore we have now chosen for a window at the Brewster angle. A disadvantage is the large angle between the incoming mmw beam and the normal to the window surface. This angle, the Brewster angle, is equal to $\arctan\sqrt{\epsilon_r}$ so for fused silica (SiO_2, $\epsilon_r = 3.8$) $\alpha_B = 62.9°$ and for alumina (poly-crystalline Al_2O_3, $\epsilon_r = 9.7$) $\alpha_B = 72.2°$.

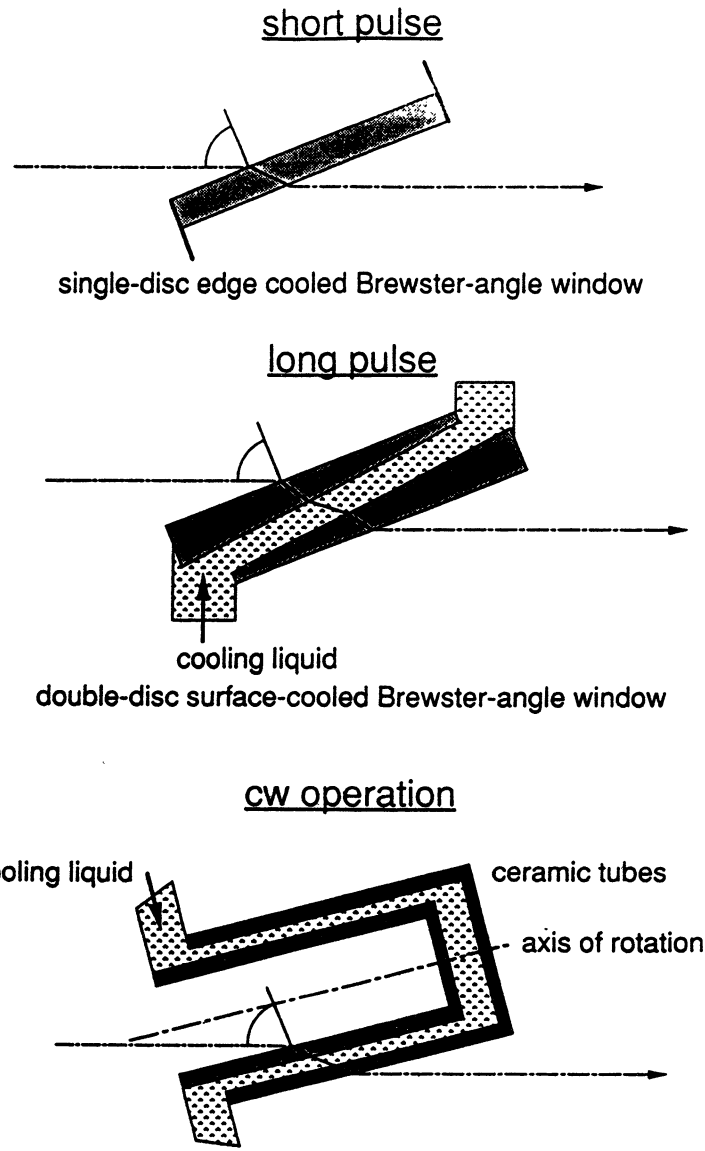

Fig. 12. Broad-band Brewster-angle windows.

For the first stage of the project a single-disc, edge-cooled Brewster angle window will be sufficient to withstand 100 ms pulses, see fig. 12. For long-pulse experiments novel ideas like a double disc Brewster window using for example FC75 as cooling liquid are being worked out. For cw operation a rotating "cup" can spread the power over a sufficient large area.

7 Conclusions

Having obtained funding last year, we are now finalizing the design. Major components such as the undulator, electron gun, accelerator, power supply and parts of the mmw system are under construction. First experiments are foreseen at the end of 1994.

For the more remote future new developments are under consideration to enlarge the pulse length from 100 ms in phase I to cw. Furthermore, first ideas for still larger unit power are being worked at. An upgrade to 3 MW seems feasible with a system very similar to the 1 MW system [9]. This could make ECRH a truly competitive method for plasma heating and current drive.

Acknowledgements

The work described here was performed as part of the research programme of the association agreement between the "Stichting voor Fundamenteel Onderzoek der Materie" (FOM) and Euratom, with financial support from the "Nederlandse Organisatie voor Wetenschappelijk Onderzoek" (NWO) and Euratom.

References

1. Report written by the members of the Coordinating Committee on Electron Cyclotron Wave Systems: F. Troyon, S. Cirant, J.A. Hoekzema, J.P. Rager, L. Rebuffi, A.C. Riviere, M. Thumm, G. Tonon, M.Q. Tran, A.G.A. Verhoeven and R. Wilhelm with the help of: M. Cox, T.C. Hender, B. Lloyd, A.W. Morris, R. O'Brien, A. Pochelon. *Evaluation of Electron Cyclotron Heating Applications to a next step device.* Lausanne, 1992.

2. R. Prater *et al., Proc. Int. Conf. on Plasma Physics and Contr. Nucl. Fusion Research, Nice, Vol 1, 527 (1988).*

3. J. Lohr *et al., GA Report A20182, May 1991, submitted to Nuclear Fusion.*

4. W. Kasparek, H. Kumrić, G.A. Müller, J. Pretterebner, P.G. Schüller, D. Wagner. *Conceptual design of an EC wave system for NET/ITER, IPF-91-6, July 1991.*

5. A.V. Tulupov, et al. *Simulations of performance of FEM oscillator for Fusion at 130-250 GHz, Proc. of the 5th European FEL workshop, January 1993, Daresbury Lab., UK, Ed. M.W. Poole.*

6. V. Bratman, et al. *this conference* and N.S. Ginzburg, A.S. Sergeev, 1991.

7. L.A. Rivlin, *Laser Focus (1981) p. 82.*

8. G.G. Denisov, et al. *this conference.*

9. M. Caplan. *Private communication*

SUPER-HIGH-POWER MICROWAVE RADARS

W.M. Manheimer,
Naval Research Laboratory, Washington, USA,

G.A. Mesyats,
Institute of Electrophysics, Russian Academy of Sciences,
Ekaterinburg, Russia,

M.I. Petelin,
Institute of Applied Physics, Russian Academy of Sciences,
Nizhny Novgorod, Russia.

For radars, any increase in the radiation power or in the radiation frequency provides further enhancement of range and resolution capacities. Prospects on this way have been analyzed in profound works by Merrill Skolnik, Boris Bunkin, Alexey Tolkachev and their colleagues [1-3]. The authors of this short survey, being not radar experts, will only try to correlate these prospects with the progress of high power microwave electronics and electrodynamics, emphasizing on microwave sources driven by sub-relativistic and relativistic electron beams. In our estimates we shall use the simplest radar equation [1]

$$R_{max}^4 = K_{tr}\, K_{eds}\, K_{rcv}, \qquad (1)$$

where

$$K_{tr} = P\tau / kT, \qquad (2)$$

P is the transmitted power, τ is the microwave pulse duration, kT=4·10^{-21} W/Hz,

$$K_{eds} = \sigma A^2 / 4\pi\lambda^2, \tag{3}$$

σ is the effective target cross section, $A=\pi R^2$ is the antenna area, $\lambda = 2\pi c / \omega$ is the wave length,

$$K_{rcv} = \{F_n (S_0 / N_0)_{\min} L_s\}^{-1}, \tag{4}$$

S_0/N_0 is the signal to noise ratio, F_n is the noise factor, L_s is the total system loss. The receiver frequency band is assumed to satisfy the optimum filtration condition $\Delta_f \tau \cong 1$.

SPACE DEBRIS MONITORING RADAR

Space stations planned to be placed at high orbits over the Earth (e.g. the well-known "Freedom" project) will meet a risk to collide with remnants of vehicles launched in previous decades. So it is necessary to detect the debris, to track them and to examine their parameters. The problem can be solved, in particular, by high power microwave radars based on the Earth surface.

The minimum size of the dangerous debris is assumed to be 1 cm. For such an object, to avoid the Raleigh case when the effective radar cross section proves to be less than the physical one, the operating wavelength should belong to the millimeter band. On the other hand, from the atmospheric absorption viewpoint, among the millimeter wavelengths the most reliable are those close to 8 mm; the corresponding carrier frequency is near to 35 GHz. A version of such a radar based on the active array concept was presented in [3].

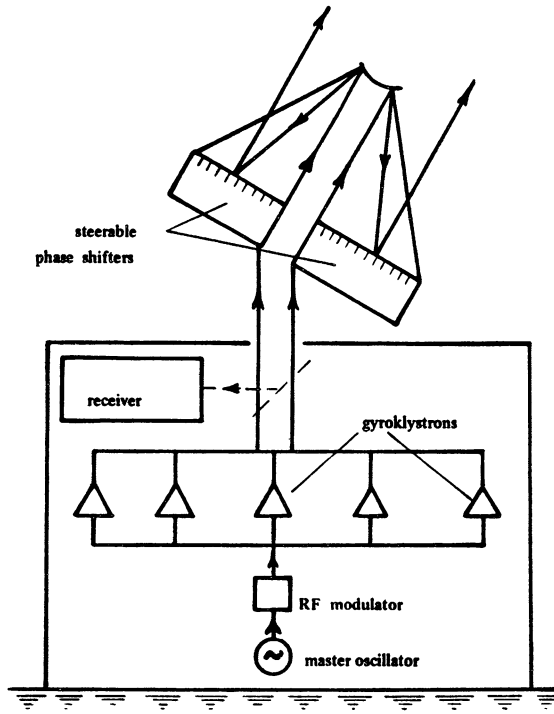

Fig. 1. Principal scheme of space debris monitoring radar

A passive array version of the 35 GHz radar can be discussed as well. Indeed, let us take

- antenna radius, R_a	10	m,
- signal-to-noise ratio, S_0/N_0	15	dB,
- noise factor, F_n	10	dB,
- total loss of the system, L_s	10	dB,
- microwave pulse length, τ	100	μs.

Under the above assumptions, according to the radar equation, the system will be able to detect objects of cross section s=1cm^2 at distances up to 1000 km (of interest for the space stations), if the transmitted power is 10 MW. To obtain such a power, one can sum powers from a number of amplifiers driven by one master oscillator

and a common RF modulator (Fig. 1). The present day gyroklystrons have pulse power about 1 MW [4] and there are no serious problems to provide 0.1 MW average power per device. So 10 gyroklystrons are sufficient for the radar.

The radar would operate in two modes:

a) Pulse Doppler mode ([1], Chapter 4). For space objects with radial (relative to the system) velocities up to 5 km/s the Doppler frequency shift $(2v_r/c)f$ is up to 1 MHz. To match the receiver of the 10 kHz frequency band to the reflected signal with such a Doppler shift, it is possible to use a combination of a filter bank and a pulse-to-pulse changing of the transmitter frequency or of the local oscillator frequency: e.g., twenty filters in the bank and ten discrete LO frequencies. If the pulse repetition rate is 1 kHz, all possible velocities at a fixed direction will be analyzed during 10^{-2} s. During this time the angle shift of the space object with azimuthal velocity of 7 km/s will be $7 \cdot 10^{-5}$ rad, that is much less than the radiation pattern width. The resolution of the system will be 15 km in range and 30 m/s in velocity.

b) Pulse compression mode ([1], Chapter 11). In this regime the emitted pulse should be frequency modulated, and the receiver should contain a pulse compression (analogue or digital) filter. The pulse compression radar has a relatively large range-velocity ambiguity; but if the target velocity radial to the radar is known, the target range can be measured in a single pulse with precision $\Delta R \sim \lambda(\omega/\Delta\omega)$, where $\Delta\omega$ is the emitted pulse frequency deviation. For $\Delta\omega/\omega \sim 10^{-2}$, which is typical for the gyroklystron, $\Delta R \sim 1$ m.

With the 20m diameter antenna, the radiation-reception pattern will have angle $5 \cdot 10^{-4}$ rad (2'). To scan the wave beam (see Fig. 1), one may combine

- a slow broad-angle change of the antenna direction by a mechanical method (with rotary joints) and
- a fast narrow-angle change of the beam direction by a distributed system of electrically controlled phase shifters.

CLUTTER REJECTION NANOSECOND-GIGAWATT RADAR

Conventional radars in a certain part of their applicability region meet some difficulties resulting from the traditional signal processing technique. To combine a long range of target detection with a high precision of measuring the distance, they use long (0.1 ms) modulated RF pulses, which after reflection from the target are compressed in the receiver. But the compressed pulse is always accompanied by side lobes, and no one practical scheme can reduce their level beyond -(30-35) dB. If side lobes of pulses reflected from different objects are mutually overlapped, the resulting signal becomes distorted (note that the receiver sums not RF intensities, but RF fields) and the resolution reduces. So, it is difficult to detect a low-reflection moving object among high-reflection local objects and under complicated weather conditions.

These difficulties would be considerably less, if the emitted RF pulse be short enough, but sufficiently energetic [1,2]. If the radiated microwave pulse is of nanosecond duration and no pulse compression in the receiver is used, the pulse from the elementary (point) reflector,

if optimally filtered, acquires only a short exponentially fading tail. This results in

- better resolution of mutually close objects with big differences of effective scattering surfaces,

- better possibility to identify the object using its reflection image (there is no correlation of signals reflected from different bright points of the extended object and, so, no strong dependence of the image on the orientation of the object),

- some other advantages pointed in [1] (page 421); see also [5] [1]).

To estimate the radar capacity, let us take

- carrier frequency, f_0	10 GHz,
- transmitted power, P	1 GW,
- pulse duration, τ	5 ns,
- frequency band, Δ_f	200 MHz,
- signal-to-noise ratio, S_0/N_0	15 dB,
- noise factor, F_n	7 dB,
- total loss of the system, L_s	7 dB;
- antenna radius, R_a	0.5 m,
- target cross section, σ	1 m^2 ,

then from (1)-(4) we obtain

$$R_{max} = 75 \text{ km.}$$

To verify the merits of the nanosecond radio location, a model of radar with the carrier frequency 10 GHz and radiated microwave pulse power 0.5 GW was made by a cooperation of Russian research institutes [2]. Microwave pulses of 5 ns duration were produced by an

---

[1]At the same Varenna school there was also a very interesting report by Donald Prosnitz, who analyzed a possibility to make a radar based on a 35 GHz free electron laser. A very detailed report on the nanosecond radar was presented at 9th Russian Symposium on High-Current Electronics, 1992 by Vadim Skosyrev and Michael Osipov. Regretfully, the both reports have not been printed.

auto-oscillator driven by an intense relativistic electron beam. The source of the electron beam was a high-current accelerator. The pulse repetition frequency was 100 Hz. In the receiver, to maximize the contrast of the moving object among non-movable and slowly changing local objects, an over-period pulse subtraction MTI technique was used.

The radar (Fig. 2) was tested at a bank of river Ob near Tomsk. In the view of the radar there were the water surface, islands, forests etc. The moving objects were a small airplane with effective scattering cross-section 1 m^2 and small motor boats. The airplane flying at altitude 50 m over the forest was reliably detected at distances within 50 km (direct visibility). The distance portray of the plane represented a sequence of separate bright points varying slowly with the change of the plane orientation. The boats were clearly seen among waves and islands. The range resolution was within 1m. The dead zone was 10 m .

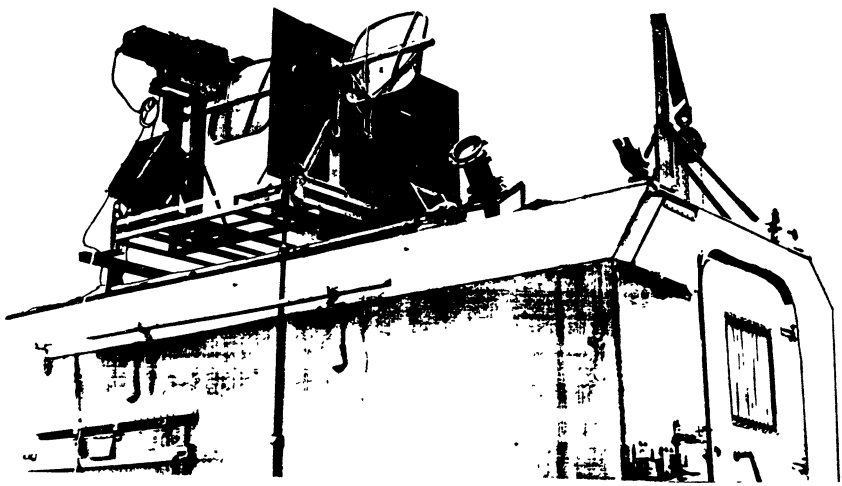

Fig. 2 Nanosecond radar

Among possible applications of the nanosecond radar there is control of aircraft movement and sea vessels navigation under heavy conditions.

ACTIVE MONITORING OF ATMOSPHERE

In the frame of the atmosphere study problem, main peculiarities of microwaves are related with the following effects:

- the atmospheric inhomogeneities result in much higher reflectivity for microwaves, than for longer ones, and , on the other hand,
- the microwaves penetrate into clouds, smoke and dust more easily than the light.

Of course, it is expedient to combine microwave methods with other, in particular optical, ones.

The millimeter waves are especially attractive to investigate the turbulence of the near-ground atmosphere , because in this frequency band the back scattering of the waves is expected to be especially pronounced; these waves are also effective to detect the presence and investigate parameters of aerosols [6,7]. On the other hand, because absolute coefficients of the back scattering are not very large, it is necessary to use transmitters of high power and receivers of high sensitivity.

An experiment of the sort [8] was performed with a kind of radar system composed of a transmitter based on a 84 GHz 30 kW quasi-CW gyrotron and a receiver of 10^{-12} W sensitivity in 1 GHz band with 10^{-3} s averaging time. In a visually clean atmosphere the back scattering at 50-200m altitudes was registered. The magnitude of

the received signal corresponds either to a rather intense near-ground turbulence (the standard coefficient $C_n^2 = 10^{-12}$ $cm^{-2/3}$) with minimum scale within 3-4 mm or to a presence of dust particles (about 1 particle of 100 μm diameter per 1 cubic decimeter). To solve the ambiguity a double frequency experiment is planned. For such experiments frequency tunable gyrotrons are especially attractive [7].

The main goals of these experiments are the study of fundamental atmospheric phenomena and the ecological monitoring.

CONCLUSION

The general prospects of the high power microwave radars are clear for a very long time; so the estimates presented in this report seem quite obvious and even trivial. Let us note, however, that reliable high power sources of the shortest microwaves and relevant (quasi-optical) electrodynamic components have been really developed only in the recent decade. Hopefully, it will stimulate a rapid progress of radars.

ACKNOWLEDGEMENTS

The authors are grateful to Prof. A. Tolkachev, Dr. B. Levitan, Prof. M. Osipov, Prof. V. Skosyrev, Dr. M. Tokman, Prof. M. Kristiansen, Dr. B. Wardrop, Dr. F. Adams and Dr. A. Dean for constructive discussions.

The Russian co-authors thank the Russian Fund of Fundamental Research for a partial support of investigations related to millimeter wave radars.

REFERENCES

1. M.I. Skolnik, Introduction to Radar Systems, McGraw-Hill, N-Y, London, 1980.
2. B.V. Bunkin et al., ZhTF Letters, Vol.18, No.9, pp. 61-65, 1992.
3. V.P. Botavin et al., Int. 92 Conf. on Signals & Systems, Geneva, Jun 92, Summaries, pp. 51-52.
4. I.I. Antakov et al., Proc. of "Suzdal-2" Conf., Moscow-Nizhny Novgorod, 1993.
5. C. B. Wharton, Proc. of Int. School "High Power Microwave Generation and Applications", Varenna, Italy, 1991, pp. 227-243.
6. R. Lhermitte, IEEE Trans. Geoscience and Remote Sensing, 26, 207, 1988.
7. W.M. Manheimer, NRL memorandum report 6830, 1991.
8. Y.V. Bykov et al., 17th Russian Conf. on Propagation of Radio Waves, Ulyanovsk, Sept 1993, Abstracts, sections 2a and 2b, p.44.

Development of Submillimeter Wave Gyrotrons

T. Idehara
Department of Applied Physics, Faculty of Engineering,
Fukui University, Fukui 910, Japan

Development of medium power, step tunable gyrotrons which cover millimeter to submillimeter wave range is described. Single mode operations at the second and the third harmonics enable our gyrotron to be used as millimeter and submillimeter wave sources. At the second harmonic, 636 GHz (0.472 mm in wavelength) is achieved under fairly high power of several kW. Long pulse operation up to 0.6 sec is also achieved. An amplitude modulation of gyrotron output in the submillimeter wave range is described. A fairly high frequency (up to several hundred kHz), 100 percent modulation of the output has been attained under only a few percent modulation of anode voltage. Applications of the gyrotrons to plasma scattering measurements are also described and some preliminary experimental results are shown.

1 Introduction

The development of gyrotrons has proceeded in two directions. One is the development of high power gyrotrons as sources in the millimeter wave range for electron cyclotron heating of nuclear fusion plasmas. An output power of 0.8 MW for single tube has been achieved at 140 GHz.[1] The other is the development of medium power gyrotrons for plasma diagnostics and for far-infrared spectroscopy.[2)-4)] The gyrotrons described in this literature are ones of the latter.

Operation at the harmonics of the electron cyclotron frequency allow higher frequencies to be obtained at lower magnetic fields. A number of near-millimeter wave gyrotrons have been developed by using the second harmonic of the cyclotron frequency.[5)-9)] Recently, several kilowatt in a 1 μsec pulse have been obtained at 503 GHz [10)] and low-cw power, tunable gyrotrons have attained 330 GHz at the fundamental and 590 GHz at the second harmonic.[11)-13)] A related device, a gyropeniotron, operating at the third harmonic has delivered 8 kW in a 200 μsec pulse at 70 GHz.[14)]

At Fukui University, an earlier gyrotron has operated at both the second harmonic (220 GHz) and the third harmonic (160 GHz).[15)] New gyrotrons operating at the second harmonic has been designed and costructed.[16)-21)]

The gyrotron design was optimized for operation at the second harmonic of the electron cyclotron frequency in the TE_{261} cavity mode, whose resonant frequency is 384 GHz. Experimental results show that second harmonic operation can occur without mode competition as long as the beam current I_b is low (I_b <0.8A), but as the current is increased, the fundamental TE_{231} cavity mode increases and eventually suppresses the second harmonic (I_b >1A). The competition between the two modes is studied in detail. The starting current for second harmonic operation is also studied experimentally and compared with calculated results. Other resonances have also been examined. With the present superconductiong magnet, the maximum frequency achieved is 402 GHz (second harmonic operation in the TE_{551} cavity mode) at several kilowatts.

Another gyrotron we have developed is a demountable one. It has achieved higher frequency operations up to 636 GHz at the second harmonic resonance under the high magnetic field up to 12 T. 100 percent, amplitude modulation of its output power in the high frequency range up to several hundred kHz has been achieved under only a few percent modulation of anode voltage.

Uses of such a gyrotron as a power source of scattering measurement of plasma give us following advantages. 1) The gyrotron is frequency-tunable, so we can adjust the frequency at the best for the

measurement. 2) The output power is fairly high even for the operations at the second and the third cyclotron harmonic resonances. So, we can detect the scattered signal from plasma waves with small density fluctuations, because of a high signal to noise ratio of the measurement system using the gyrotron as a power source.

2 Design of the submillimeter wave gyrotrons

The design is constrained by the high voltage beam power supply (maximum voltage is 40 kV and maximum current is 6 A) and the superconducting magnets(maximum magnetic fields are 8 T and 12 T).

The diameter and the length of a cavity in the gyrotron using 8 T magnet are 4.85mm and 14.5mm, respectively. We call this gyrotron 'GYROTRON A'. For the TE_{261} cavity mode, the resonant frequency is 384 GHz and the total Q value is 12,300. The large total Q value ensures that the threshold value of the beam current for gyrotron operation is small. The optimum magnetic field for the mode at the second harmonic is 7.31 T. Fig.1 shows the calculated beam current I_b necessary to sustain an output power $P = 1$ kW for many cavity modes, as functions of the magnetic field intensity B_0, where the injection radius r_0 of electron beam is assumed to be 1.25 mm. $N(= f/f_c)$ is the harmonic number. For higher harmonic operation, higher beam currents I_b are necessary to sustain the same output power (1 kW). Note that for some modes, for example, the TE_{811}, a high beam current ($\sim$ 3A) is needed, because there is only one radial maximum in the high frequency field and that is located near the cavity wall. Consequently, in these cases, the interaction between the field and beam electrons injected at $r_0 = 1.25$ mm is weak.

Another gyrotron using 12 T magnet ('GYROTRON B') is also designed by computer simulation. The diameter and the length of the cavity are 3.9 and 10 mm, respectively. The gyrotron operates in the higher frequency range. At the second harmonic, 636 GHz can be achieved by the TE_{081} cavity mode and 595 GHz by the TE_{181} mode.

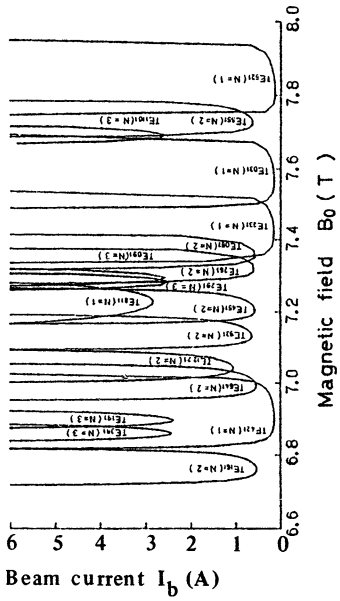

Fig. 1: The beam current I_b to sustain output power $P = 1$ kW versus magnetic field B_0.

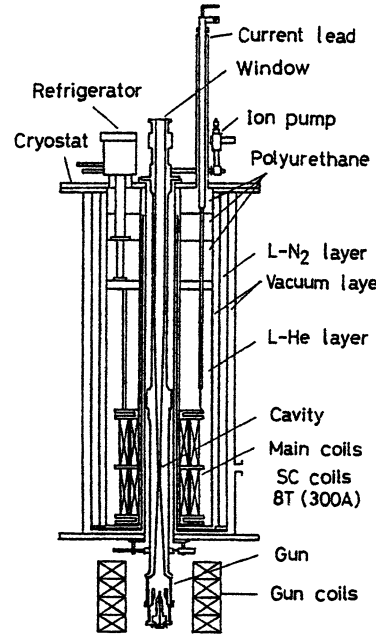

Fig. 2: The submillimeter wavelength gyrotron (GYROTRON A).

3 Experimental arrangement

The gyrotrons used in this work consist of a gyrotron tube, a superconducting magnet and four copper coils, as shown in Fig.2. The superconducting magnets supply the main magnetic field up to 8 T and 12 T over the cavity region of the tube and the copper coils supply an independently variable magnetic field over the electron gun region. This arrangement allows the ratio between the magnetic fields in the two regions to be changed, which enables the injection point of the electron beam in the cavity to be optimized for different modes.

A pulsed high voltage up to 40 kV is supplied to the magnetron injection gun from the beam power supply. The pulse width is varied from 100 μsec to 1 msec and repetition rate from 1 to 5 Hz.

The output power is transferred by circular waveguides, inner diameter of 28 mm, and several 90° corner bends, and, for measurement purposes, fed to the Fabry-Perot and Michelson interferometers. The output of the Fabry-Perot interferometer is monitored by a pyroelectric detector, sampled and integrated by a boxcar integrator, and recorded on an XY recorder as a function of the distance between meshes. This measurement gives the wavelength of gyrotron output.

The output of the Michelson interferometer is fed to a signal analyzer and Fourier transformed to give a frequency spectrum of the gyrotron output. This measurement is important, because it allows the power in the fundamental ($N = 1$) and the different harmonics ($N = 2, 3, 4$) to be monitored and the amount of mode competition to be assessed.

The pyroelectric detector was calibrated to yield output power by comparing it with calorimetric measurements using a water load at several frequencies. The radiation pattern of output was measured by sweeping the detector above the output window of gyrotron or by observing the pattern on a liquid crystal sheet placed above the window of the gyrotron.

4 Experimental results of GYROTRON A

4.1 Operation at the fundamental, the second and the third harmonics

Fig.3 shows a typical result obtained by the Fabry-Perot interferometer. The magnetic field in the cavity region is set at 7.34 T, which lies near the optimum value for second harmonic operation of TE_{261} mode (see Fig.1). At the low beam current of I_b =0.5 A (lower trace), a single mode with a half wavelength of 0.392 mm is observed. This wavelength corresponds to a frequency of 383 GHz, which is almost equal to the calculated resonant frequency of 384 GHz for the

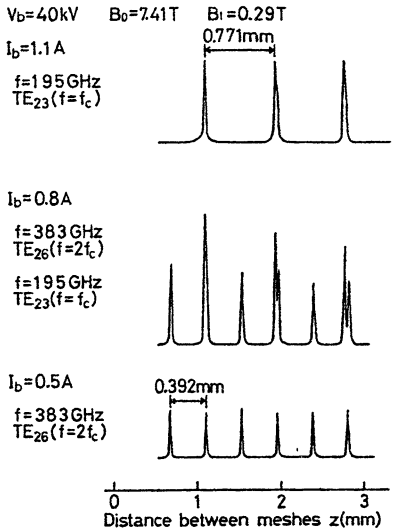

Fig. 3: Typical experimental results using the Fabry-Perot interferometer, for both the TE_{261} mode at the second harmonic and the TE_{231} mode at the fundamental at various I_b. B_0=7.14 T.

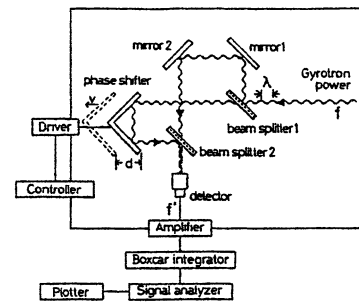

Fig. 4: Drawing of frequency spectrum measurement system using Michlson interferometer.

TE_{261} cavity mode. The magnetic field corresponds to a cyclotron frequency of 192 GHz, which is about half the value of the observed frequency. So, this trace indeed shows an excitation of a single mode at the second harmonic.

When the beam current is increased to 0.8 A (middle trace), a new signal whose wavelength is nearly equal to twice that seen at 0.5 A appears superimposed on it. The frequency of the new mode is about 195 GHz, which is the resonant frequency of the TE_{231} mode. So, this trace shows the simultaneous occurrence of both fundamental and second harmonic. As the beam current is increased, a kind of competition between the two types of operations develops. At the still higher beam current of 1.1 A (upper trace), only the fundamen-

tal occurs and the second harmonic is completely suppressed. The suppression may result from the degradation of the quality of electron beam, for example, the velocity spread and the decrease in the value of the velocity ratio $\alpha = v_\perp / v_{||}$, which can occur along the length of the cavity, when the strong fundamental resonance is excited.

Under the other condition, single mode operation at the third harmonic has been observed. The frequency is 354 GHz which corresponds to the resonance frequency of TE_{161} cavity mode and the output power is about 20 W.[18)]

4.2 Measurement of frequency spectrum

The Michelson interferometer combined with fast Fourier Transform (FFT) techniques is used to observe the frequency spectrum of submillimeter wave output of gyrotron.[21)] Fig. 4 shows a drawing of measurement system. Gyrotron output power is fed to beam splitter 1. Beam splitters 1 and 2 are metal meshes (60 lines/in.). Mirrors 1 and 2 are metal plates. The phase shifter is composed of two metal plate mirrors. The response of the pyroelectric detector has been checked and is linear in the power range used here. When a phase shifter is driven at a constant speed v, the detected interference signal alternates with frequency

$$f' = \frac{v}{\lambda/2} = \frac{2v}{c} f \qquad (1)$$

where λ and f are wavelength and frequency of the gyrotron output. The signal from the pyroelectric detector is amplified and Fourier analized by a signal analyzer. Because the gyrotron is pulsed, a boxcar integrator is installed before the signal analyzer to sample the output. The observed frequency (f') spectrum can be easily converted to a real gyrotron frequency (f) spectrum by using Eq. (1).

Fig.5 shows a typical result of the measurement. Fig.5 (b) shows a frequency spectrum of the gyrotron output obtained by Fourier transforming the detected signal shown in Fig.5 (a). It is seen that the gyrotron is operating at the fundamental of the electron cyclotron

frequency at 196.8 GHz, as well as at the second harmonic,at 388.8 GHz and at the third harmonic, at 580.8 GHz. The sensitivity $\mu(f)$ has a frequency dependency determined by that of the reflection coefficient $R(f)$ of beam splitters through the equation $\mu = R(1-R)$. At 282 GHz, R is equal to 0.5 and μ is a maximum. Considering this frequency dependence of μ, we can compare the power of one peak in the frequency spectrum with that of the other peak.

Fig.6 shows all frequencies observed in such frequency spectra as functions of B_0. It is seen that many modes at the fundamental ($N = 1$) and the harmonics ($N = 2, 3, 4$) are excited.

4.3 Competition between fundamental and second harmonic

The output powers P of the fundamental and the second harmonic can be estimated from the heights of the peaks in Fig.3, which are shown as functions of beam current I_b in Fig. 7, with the magnetic field B_0 as a parameter. The magnetic field was varied over the range 7.36-7.45 T. For each value of B_0, as long as the beam current is low, only the second harmonic is observed. When B_0 increases,the starting current for the second harmonic I_{b2} decreases and the rate of increase of power P with beam current I_b becomes steeper. This result suggests that, to obtain the lowest possible starting current for the second harmonic, the magnetic field should have a value higher than 7.45 T. For each B_0, the fundamental appears at the beam current I_{b1} which is higher than I_{b2} in the field range 7.36-7.45 T. So, in the current region $I_{b2} < I_b < I_{b1}$, we can get a single mode (TE_{261}) at the second harmonic. When I_b is increased further ($I_b > I_{b1}$), competition between both the second harmonic and the fundamental occurs. The second harmonicis eventually suppressed by the fundamental. When the output power of the fundamental exceeds some high value (6 kW to 9 kW), the second harmonic disappears.

A culculation of the power in the second harmonic and the fundamental versus the beam current is shown in Fig. 8. This calculation was carried out by integrating the slow equations of motion for the general case where both the second harmonic and the fundamental

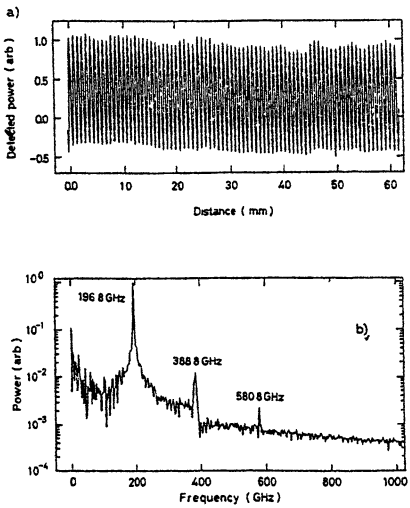

Fig. 5: Frequency analysis of the output of GYROTRON A. (a) Interfering signal observed by Michelson interferometer. (b) Frequency spectrum obtained by FFT.

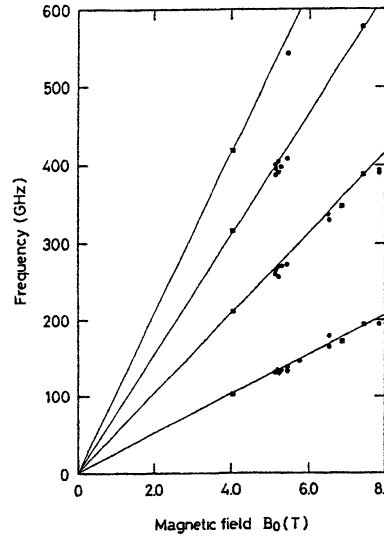

Fig.6: Observed frequencies plotted against the external magnetic field B_0 (GYROTRON A).

were present. The appearance of the second harmonic and the fundamental and the eventual suppression of the second harmonic, as the beam current increases, closely matches what is seen experimentally. We can, following Chu et al,[22] attribute the mode suppression to a change in the electron velocities, as the fundamental mode grows, from having a distribution that is favorable to the second harmonic to having one that is not. Differences between our experimental results and our calculations are due to not including the initial spread in the components of the electron velocity and not including the detail how the potentials of the gun electrodes build up in each pulse. The experimental values of the magnetic fields are slightly higher than the calculated ones. This difference can be accounted for by the fact that the accuracy of our gaussmeter is no better than 3 percent.

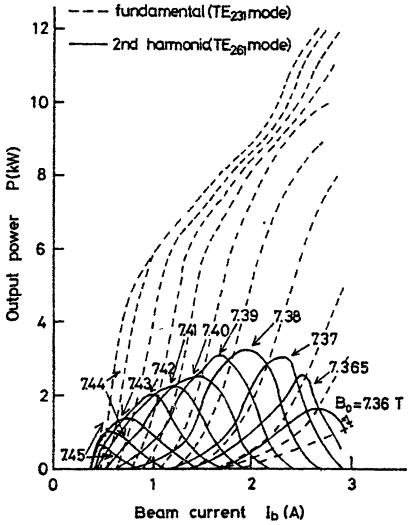

Fig. 7: Output power P for the TE_{261} mode at the second harmonic (solid lines) and for the TE_{231} mode at the fundamental (broken lines) as functions of beam current I_b, with B_0 as the parameter.

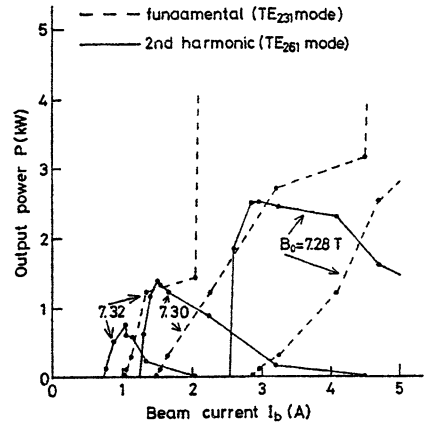

Fig. 8: Calculated output power P for the TE_{261} mode at the second harmonic (solid lines) and for the TE_{231} mode at the fundamental (broken lines) as functions I_b for various fields B_0.

Equipower contours for second harmonic and fundamental operations in the parameter space $I_b - B_0$ are shown in Fig. 9. The hatched region corresponds to where a single mode at the second harmonic occurs. It is clearly seen from Figs.7-9 that the setting of I_b and B_0 to obtain a single mode at the second harmonic is critical.

The comparison between experimental and calculated results for the TE_{261} mode at the second harmonic is shown in Table 1. The lower experimental value of efficiency is probably a consequence of mode competition with the TE_{231} mode at the fundamental. The agreement is good.

Fig. 10 shows similar results for the second harmonic TE_{641} and the fundamental TE_{421} modes. In this figure, equipower contours for

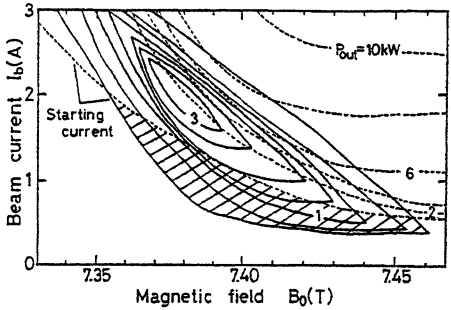

Fig. 9: Equipower lines for the TE_{261} mode at the second harmonic (solid lines) and for the TE_{231} mode at the fundamental (broken lines) in the parameter space $I_b - B_0$.

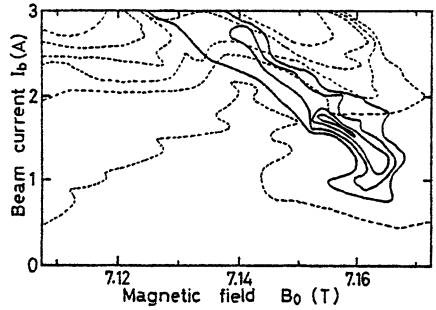

Fig. 10: Equipower lines for the TE_{641} mode at the second harminc (solid lines) and for the TE_{421} mode at the fundamental (broken lines) in $I_b - B_0$.

Table 1: Comparison between the experiment and simulation for the second harmonic TE_{261} mode.

	Experimental	Theoretical
Beam voltage V_k	40kV	40kV
Beam current I_b	1.05 A	0.6 A
Magnetic Field B_0 (in a cavity region)	7.43 T	7.31 T
Magnetic Field B_1 (in a gun region)	0.30 T	0.29 T
Oscillation frequency f	383 GHz	384 GHz
Output power P	1.3 kW	1.0 kW
Efficiency η	3.0 %	4.1 %

both modes are plotted in the parameter space $I_b - B_0$. However, in this case, single mode operation of the TE_{641} mode cannot occur even at low currents. This is because the frequency of the second harmonic

is very much closer to twice the frequency of the fundamental and, as a result, the optimum conditions for both occur at almost the same magnetic field intensity B_0. Where the TE_{641} mode is strongest, the TE_{421} mode is partially suppressed and a "valley" appears in equipower contours for the TE_{421} mode. When the TE_{421} mode is strongest, the TE_{641} mode is suppressed completely.

4.4 The starting beam current for a single mode at the second harmonic

Single mode operation at the second harmonic is important for high frequency gyrotron operation at low magnetic fields. As described above, we can, for certain modes, get a single mode at the second harmonic, with a correctly set magnetic field and a suitably low beam current. Fig.11(a) shows the measured output powers P as functions of beam current I_b for the TE_{261} mode operation at the second harmonic. The acceleration voltage is kept constant, and the magnetic field is adjusted to the optimum value. The starting current I_{bs} is very close to 150 mA. The result is compared with the theoretical result below.

The starting current for the TE_{mln} mode at Nth harmonic resonance is given analytically, as follows:

$$I_{bs} = \frac{-\pi^3 \varepsilon_0 m_0}{4e} \frac{\gamma \omega v_{\parallel}}{Q_{total}} \frac{n^2 R^2}{L} \frac{(\xi_{ml}^2 - m^2) J_m^2(\xi_{ml})}{\xi_{ml}^2} \times \left[\frac{1}{v_{\parallel}} \left(-\frac{\beta_{\perp}^2 \omega}{2kv_{\parallel}} \frac{dG}{dX} P + GQ \right) \right]^{-1}, \quad (2)$$

where Q_{total} is given by $1/Q_{total} = 1/Q_{diff} + 1/Q_{Ohmic}$.

The diffraction Q, Q_{diff}, can be calculated from the shape of cavity and the Ohmic Q, Q_{Ohmic}, is taken to be $R/2\delta$, where R is radius of cavity, δ is skin depth of low-conducting surface layers. Other notations are defined as follows:

$$G = \frac{(-1)^n \cos \pi X - 1}{2(X^2 - 1)^2}, \quad (3)$$

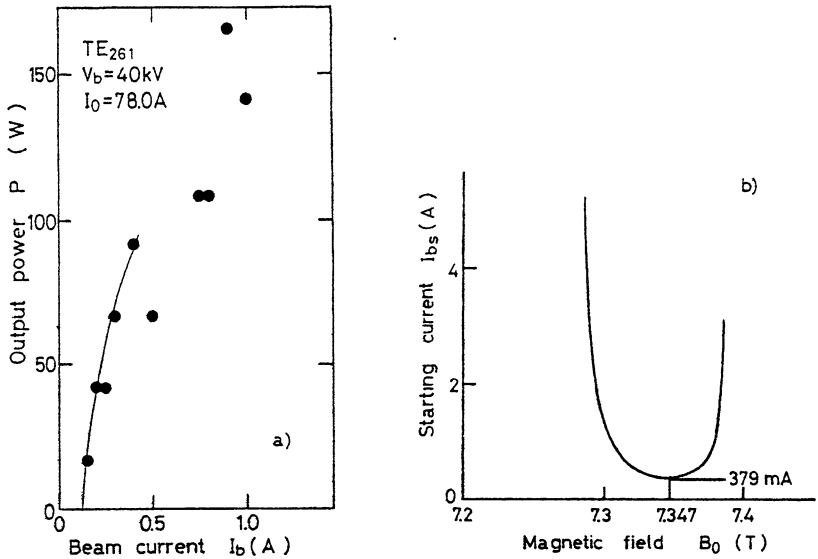

Fig.11: (a) Observed power P plotted as a function of beam current I_b, for the TE_{261} mode at the second harmonic. (b) The calculated starting current I_{bs} for the TE_{261} mode at the second harmonic as a function of B_0. V_k = 40 kV, α= 1.5, and r_0= 1.25 mm.

where

$$X = -\frac{\omega - N\omega_c}{kv_{||}}, \tag{4}$$

$$P = \frac{\left[J^2_{N+m}(\xi_{ml}r_0/R) + J^2_{N-m}(\xi_{ml}r_0/R)\right](N\beta_\perp)^{2N-2}}{2^{2N}[(N-1)!]^2}, \tag{5}$$

where $\beta_\perp = v_\perp/c$, J_s is a Bessel function, ξ_{sl} is the lth zero of its derivative, r_0 is injection point of electron in cavity, and $Q = NP$.

In Fig.11(b), the starting current I_{bs} is calculated as a function of the magnetic field B_0 for the TE_{261} mode at the second harmonic, under the conditions assumed for the previous simulation (Fig.1), that is, V_k=40 kV, α=1.5, and r_0=1.25 mm. The minimum starting current is about 379 mA, which is only a little higher than the

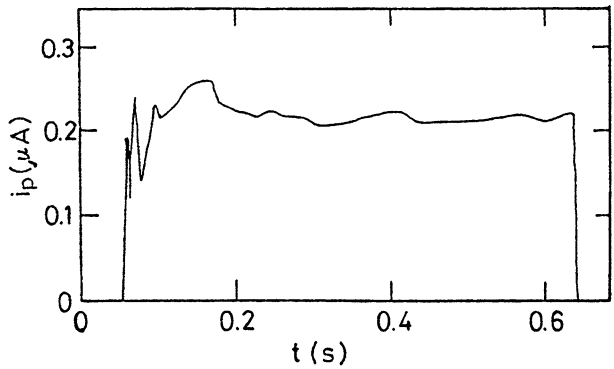

Fig.12: Long pulse operation for the TE_{161} mode at 354 GHz.

experimental result. The difference may mainly come from ignoring the spread in $v_{||}$ in the cavity and an uncertainty in the total Q because of the reflection of a part of power from the window and other components back into the cavity.

4.5 Long pulse operation at the second harmonic

To apply our gyrotrons as power sources for submillimeter wave scattering measurement, we tried long pulse operation at the second harmonic just above the starting current ($I_b > I_{b2}$). Fig.12 shows the output power measured by using a pyroelectric detector. 600 msec pulse operation is achieved. The output power is about 110 W, which is high enough for power source for the scattering measurement.

4.6 Frequency step tunability

As shown in Fig.1, our gyrotron can be used as a medium power source covering a wide frequency range. As the magnetic field intensity is raised, one after another is excited and the frequency changes in step. When operations at both the fundamental and the second harmonic resonances occur at the same time, we can select either one by using a high-pass or a low-pass filter.

Table 2: Observed frequencies, operating modes, and output powers at fundamental and second harmonic resonances.

Magnetic field B_0(T)	Frequency f(GHz)	Mode	Harmonic number N	Power P(kW)
2.86	76	TE_{011}	1	5.46
3.75	104	TE_{411}	1	
3.81	200	TE_{031}	2	
4.09	107	TE_{121}	1	
4.67	247	TE_{431}	2	
4.77	125	TE_{511}	1	
4.86	252	TE_{721}	2	
4.88	259	TE_{241}	2	
4.93	131	TE_{221}	1	
4.93	263	TE_{041}	2	
5.25	138	TE_{021}	1	10.08
5.52	150	TE_{611}	1	
5.54	299	TE_{631}	2	
6.23	155	TE_{321}	1	
6.56	336	TE_{541}	2	
6.68	165	TE_{131}	1	
6.84	172	TE_{711}	1	
6.84	354	TE_{161}	2	0.92
7.16	183	TE_{421}	1	
7.16	363	TE_{641}	2	
7.25	372	TE_{931}	2	
7.28	192	TE_{811}	1	
7.32	377	TE_{451}	2	
7.41	383	TE_{261}	2	1.4
7.45	195	TE_{231}	1	9.8
7.61	388	TE_{061}	2	
7.62	200	TE_{031}	1	
7.83	402	TE_{551}	2	
7.92	208	TE_{521}	1	

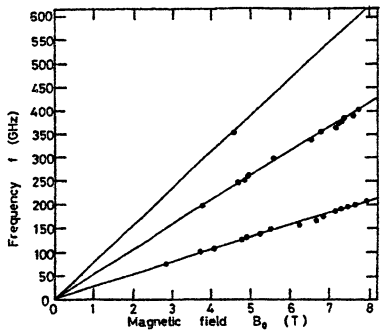

Fig. 13: Observed frequencies versus magnetic field B_0 (GYROTRON A).

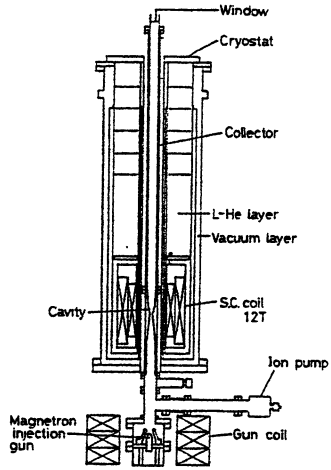

Fig.14: Drawing of the whole device of GYROTRON B using 12 T magnet.

The gyrotron covers wide frequency range from 100-400 GHz. Table 2 lists all resonances we have observed, together with their frequencies f, output power P, harmonic number N, and corresponding magnetic field B_0. Fig.13 shows the frequencies observed as functions of the field intensity B_0. Observed points lie near the fundamental (N=1), the second (N=2) and the third (N=3) harmonic resonance lines. Operation frequency varies from 76 GHz to 402 GHz.

5 Experimental results of GYROTRON B

Fig.14 shows a schematic drawing of the whole device of GYROTRON B. The magnet produces a high magnetic field up to 12 T. The superconducting magnet consists of two coils, an inner coil made of Nb_3Sn wire, and an outer coil of NbTi wire. The gyrotron is demountable and essentially a vacuum chamber set in the room

temperature bore of the cryostat. The diameter of the bore is 70 mm and the inner diameter of the vacuum chamber is 36 mm. Inside the chamber there are three parts: a guiding tube for the electron beam, a cylindrical resonant cavity, and a collector for the electron beam which also acts as the output waveguide. The diameter and the length of the cavity are 3.9 and 10 mm, respectively. Conventional magnet coils around the electron gun allow the field intensity in the region of gun to be varied independently of that in the region of the cavity.

5.1 Frequency tunability up to 636 GHz

Fig.15 shows a number of typical frequency measurement using the Fabry-Perot interferometer. When the field intensity is changed, many instances of single mode operation are observed. Fig.15 (a) corresponds to operation at the fundamental and Fig.15 (b) to operation at the second harmonic. The measured frequencies are indicated on the figure.

In only one case, when the field intensity is just below 12 T, is there operation at both the fundamental and the second harmonic. The TE_{721} cavity mode (fundamental) and the TE_{081} cavity mode (second harmonic) are excited at the same time. The frequency corresponding to this second harmonic is 636 GHz, which is the maximum frequency attained by GYROTRON B and, we believe, may be a record for a gyrotron. For other single mode operations, measured frequencies are noted near the corresponding interferometer patterns in Figs.15 (a) and (b).

In Fig.16, all of the frequencies f observed until now are plotted as functions of the magnetic field intensity B_0. The gyrotron is a step tunable, millimeter to submillimeter wave source covering a wide frequency range. Powers of several hundred watts are obtained at both the fundamental and the second harmonic.

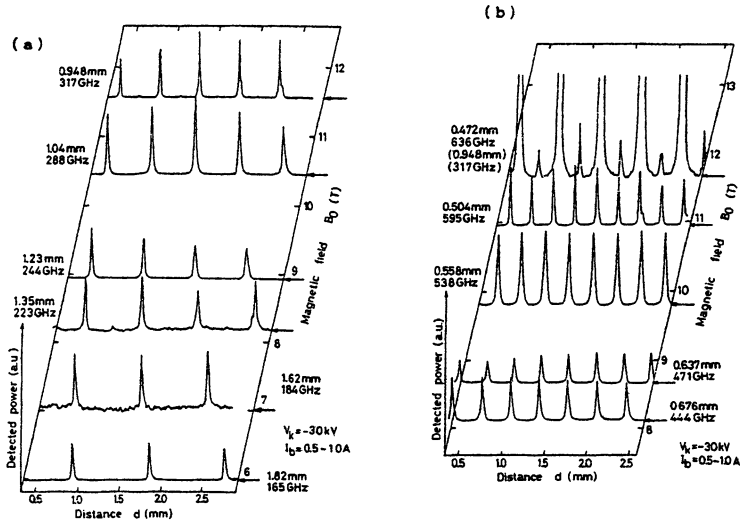

Fig.15: Outputs of a Fabry-Perot interferometer for operation at (a) the fundamental and (b) the second harmonic. V_k = 30 kV and I_b= 0.5 ~ 1.0 A.

5.2 Amplitude modulation of submillimeter wave gyrotron output

An amplitude modulation of gyrotron outputs is important for its effective applications to various objectives, for example, plasma wave excitation by a ponderomotive force, observation of a flow of millimeter wave energy in plasma coupled to its surface by ECR antenna, phase sensitive detection of scattered signal from plasma, studies of relaxation phenomena in plasma and other materials and so on. While such an importance is recognized well, the experimental efforts have not done except a few works.[23)]

GYROTRON B has a familiar triode type electron gun (so-called, a magnetron injection gun). Anode voltage V_a can be modulated to modulate a velocity distribution function of electron beam. The modulation of gyrotron output results from the moduration of an energy transfer function from electrons to electromagnetic field due

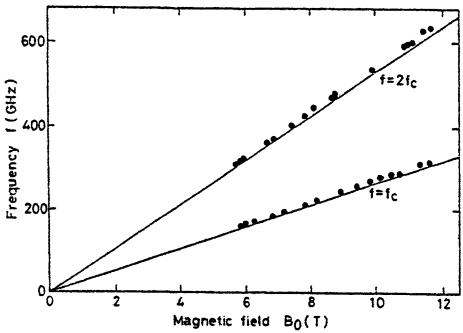

Fig. 16: Obderved frequencies versus magnetic field B_0 (GYROTRON B).

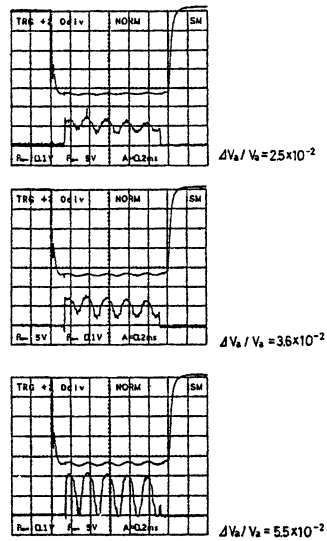

Fig. 17: Modulated outputs of GYROTRON B and the modulated voltages applied to anode V_a. f_m=5 kHz, f=444 GHz, N=2, V_k = 30 kV, V_a = 21.4 kV and I_k=400 mA.

to a velocity modulation of electron beam.

In a modulation frequency (f_m) range from 0.5 to 5 kHz, we use a high-voltage pulse supply having special operation modes to modulate an anode voltage, whose modulation ratio is varied up to 25 percent and modulation modes are sinusoidal and square waves. While, in a higher modulation frequency range up to 1MHz, the output of a high power rf oscillator is fed to an anode overlapping on a dc high voltage pulse. A modulation mode is only a sinusoidal wave. Typical values of operation parameters are shown in Table 3.

Fig.17 shows a typical result of a modulation of submillimeter wave gyrotron output with moduration rate ($\Delta V_a/V_{a0}$) of anode voltage as a parameter. The gyrotron operates under the second harmonic of cyclotron resonance. The cavity mode is TE_{161}, its fre-

Table 3: Typical experimental conditions for study of amplitude modulation of submillimeter wave gyrotron output.

Frequency of output	f	444 GHz
Harmonic number	$N = \omega/\Omega$	2
Cavith mode		TE_{161}
Output power	P_{out}	300 W
Cathode voltage	V_k	30 kV
Anode voltage	V_a	20 kV
Modulation frequency of V_a	f_m	< 1 MHz
Modulation rate of V_a	$\Delta V_a/V_a$	< 0.25 ($f_m < 5$ kHz)
		$< 2 \times 10^{-3}$ ($f_m < 1$ MHz)
Modulation mode		sinusoidal or square wave

quency and output power are 444 GHz and about 300 watt. The upper traces show high voltage pulse output applied to an anode whose modulation mode is a sinusoidal wave and the lower traces outputs of gyrotron. Modulation rate ($\Delta P_{out}/P^0_{out}$) of gyrotron output increased with that of anode voltage ($\Delta V_a/V_{a0}$). P^0_{out} is the output power, when an anode voltage is not modulated. 100 percent modulation ($\Delta P_{out}/P^0_{out}$=1.0) is attained under the modulation rate of anode voltage of only several percent ($V_a/V_{a0} \sim 0.073$).

Fig.18 shows a modulation rate of gyrotron output $\Delta P_{out}/P^0_{out}$ as functions of that of anode voltage V_a/V_{a0} for both sinusoidal and square wave modulations. $\Delta P_{out}/P^0_{out}$ is linearly related to $\Delta V_a/V_{a0}$ as $\Delta P_{out}/P^0_{out} = (17.3 \pm 3.6)\Delta V_a/V_{a0}$.

Fig.19 (a) shows a typical result of high frequency modulation of gyrotron output. Modulation frequency f_m and ratio $\Delta P_{out}/P^0_{out}$ are 38.5 kHz and 23 percent, respectively. Fig.19 (b) shows a frequency spectrum of modulated output of gyrotron. Modulation frequency observed in the spectrum is 38.5 kHz and the second harmonic component ($2f_m$=77.0 kHz) is -17 dB lower than the fundamental one (f_m=38.5 kHz). Amplitude modulations of gyrotron output under higher frequency up to 1 MHz has been tried. 400 kHz modulation is attained at a low modulation ratio of anode voltage $\Delta V_a/V_{a0} =$

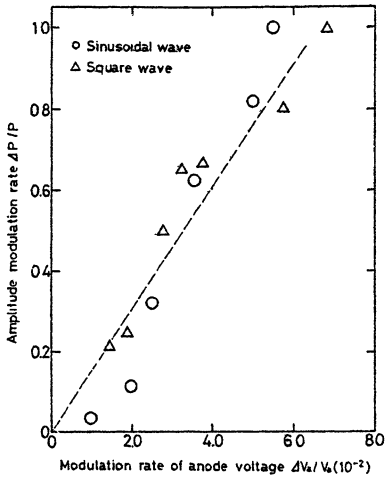

Fig. 18: Amplitude modulation rate $\Delta P_{out}/P^0_{out}$ versus modulation rate of anode voltage $\Delta V_a/V_a$. Modulation modes are sinusoidal(○) and square(△) waves. A broken line shows a calculation result estimated by Eq. (16).

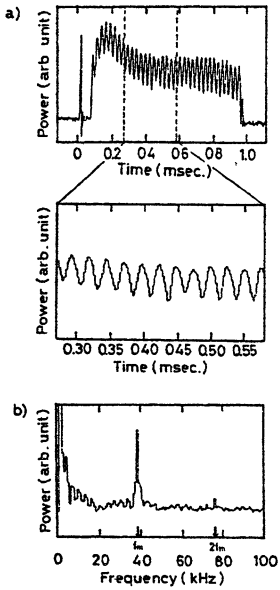

Fig. 19: (a) High frequency, amplitude modulation of gyrotron output. f_m=38.5 kHz, $\Delta V_a/V_a = 9.0 \times 10^{-3}$, N=2, f = 444 GHz, V_k =30 kV and I_b=430 mA. (b) Frequency spectrum of amplitude modulated gyrotron output.

1.12×10^{-3}. Modulation efficiency is $(\Delta P_{out}/P^0_{out})/(\Delta V_a/V_{a0}) \sim$ 49.9, at f_m=400 kHz.

5.3 Consideration about amplitude modulation results

To analyze the experimental results, we can use an expression for energy transfer $\tilde{P}_{ss}$ from electrons to electromagnetic wave in a TE_{mln} mode cavity, which is given by G.F.Brand[11], as follows,

$$\tilde{P}_{ss} = \frac{2e^2|E_0|^2\nu}{k^2 P_{||}} \left\{ \tilde{G} \left[\frac{\beta_\perp^2 \omega}{2kv_{||}} \frac{1}{2\tilde{G}} \frac{d\tilde{G}}{dX} P - Q \right] + \tilde{H} \left[\frac{\beta_\perp^2 \omega}{2kv_{||}} \frac{1}{2\tilde{H}} \frac{d\tilde{H}}{dX} P - Q \right] \right\}, \quad (6)$$

for a cold electron beam having a small gyroradius, and

$$\tilde{G} = -\frac{(-1)^n e^{jn\pi X} - 1}{2(X^2-1)^2}, \quad (7)$$

$$\tilde{H} = \frac{jn\pi X}{4(X^2-1)}, \quad (8)$$

E_0 is an amplitude of electromagnetic wave in cavity, ν electron charge density involved in a unit length in z direction, k wave number of the wave, $p_{||}$ and $v_{||}$ components of momentum and velocity of electron.

Output power P_{out} from a cavity is calculated as follows,

$$P_{out} = Re\left(\tilde{P}_{ss}\right) - A, \quad (9)$$

where $A = \omega\varepsilon/Q_{ohm}$, ε is electromagnetic wave energy stored in a cavity and Q_{ohm} ohmic Q factor of a cavity.

The real part of the energy transfer function $Re(\tilde{P}_{ss})$ for the second harmonic operation ($N = 2$) of TE_{161} cavity mode has a maximum value near $X = -1$, as follows

$$Re\left(\tilde{P}_{ss}\right) = \frac{\pi^2 e^2 |E_0|^2 \nu}{16k^2 p_{||}} P \left[\frac{\beta_\perp^2 \omega}{2kv_{||}} - 4 \right], \quad (10)$$

and P is proportional to $\beta_\perp^2$.

When an anode voltage V_a is modulated as

$$V_a = V_{a0} + \Delta V_a sin\omega_m t, \quad (11)$$

quantities $\beta_\perp$, $v_{||}$, $p_{||}$ and ν are modulated as follows,

$$\beta_\perp = \beta_{\perp 0}\left(1 + \frac{\Delta V_a}{V_{a0}} sin\omega_m t\right), \tag{12}$$

$$v_{||},\ p_{||} = v_{||0},\ p_{||0}\left(1 - \alpha^2 \frac{\Delta V_a}{V_{a0}} sin\omega_m t\right), \tag{13}$$

$$\nu = \nu_0\left(1 + \alpha^2 \frac{\Delta V_a}{V_{a0}} sin\omega_m t\right), \tag{14}$$

where higher order terms of small modulation ratio $\Delta V_a/V_{a0}$ are neglected.

Instituting Eqs. (10) $\sim$ (14) to Eq. (9), and using experimental data for Q_{ohm}, $\beta_\perp$, $v_{||}$, $p_{||}$, ω, r_0 and ν, we estimate P_{out} as

$$P_{out} = P^0_{out}\left[1 + \frac{1}{1 + A/Re(\tilde{P^0}_{ss})}\left(2\alpha^2 + 2 + \frac{2\pi(\alpha^2+2)}{2\pi - 1}\right)\frac{\Delta V_a}{V_{a0}}\right], \tag{15}$$

$\tilde{P^0}_{ss}$ is the energy transfer from electrons to rf field, when an anode voltage is not modulated. Amplitude moduration rate is given as follows,

$$\frac{\Delta P_{out}}{P^0_{out}} = \frac{1}{1 - A/Re(\tilde{P^0}_{ss})}\left(2\alpha^2 + 2 + \frac{2\pi(\alpha^2+2)}{2\pi - 1}\right)\frac{{\Delta V_a}^2}{V_{a0}}, \tag{16}$$

From this equation, the efficiency of amplitude modulation $(\Delta P_{out}/P^0_{out})/(\Delta V_a/V_{a0})$ is determined and plotted by a broken line in Fig.18. The line gives a qualitative explanation to the experimental data. That is, the mechanism for the amplitude modulation of gyrotron output is considered as follows. The moduration of electron beam velocity results from that of anode voltage. As the energy transfer from electrons to rf field is depend sensitively on the electron beam velocity in the cavity, the moduration of electron beam velocity causes that of gyrotron output.

An amplitude modulation of submillimeter wave gyrotron output has been achieved in the fairly high frequency range up to 400 kHz. 100 percent modulation is attained under only a small modulation

rate of anode voltage $\Delta V_a/V_{a0}\sim$ several percent in the low frequency moduration case ($f_m < 5$ kHz). A qualitative explanation is given by a simple model using a energy transfer function from electrons to high frequency electromagnetic wave.

6 Scattering measurement system using the gyrotron as a power source

Fig.20 shows a scattering measurement system of 350 GHz band using the GYROTRON A as a power source.[24] The TE_{161} mode, second harmonic operation at 354 GHz is used and the output power of several hundred watt is transmitted by a circular waveguide system. Two dimensionally focusing, quasi-optical antenna is used as a launcher. So, a spatial resolution of the measurement is good. Now, the system is being applied to measure the spontaneously excited drift

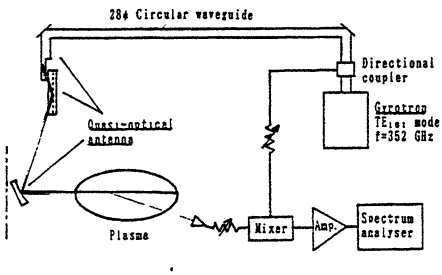

Fig.20: Scattering measurement system using a GYROTRON A as a submillimeter wave source.

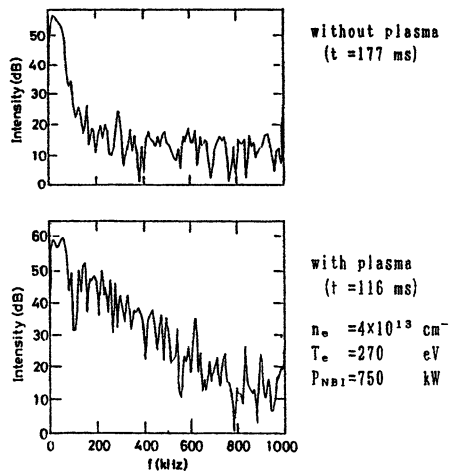

Fig. 21: Scattering signal from CHS. (Compact Helical System).

wave in CHS (Conpact Helical System) of the National Institute for Fusion Science. Fig.21 shows a preliminary results. Low frequency (<1MHz), scattering signal from CHS plasma heated by a neutral beam injection is observed.

7 Conclusion

We have designed, constructed, and tested high frequency gyrotrons (GYROTRON A and GYROTRON B) for submillimeter wavelengths. Both gyrotrons are step tunable and can operate at the fundamental and the second harmonic of the electron cyclotron frequency over a broad frequency range.

Experimental results of GYROTRON A are as follows,

1. The gyrotron covers a frequency range from 100 to 400 GHz. For almost all operations, the output power is several kW.

2. The third harmonic operation at 354 GHz (TE_{161} mode) is achieved, whose power is 20 watt.

3. Mode competition between the fundamental and the second harmonic is examined. Even at the optimized value of B_0 for the second harmonic, the operation is suppressed by the powerful operation of the fundamental, when I_b is increased. While, at low I_b, the single mode operation at the second harmonic occurs.

4. Long pulse operation is necessary for the source of scattering measurement. Using the gyrotron, 600 msec operation has been achieved.

Experimental results of GYROTRON B are as follows,

1. As 12 T magnet is used in the gyrotron, a wider frequency range up to 636 GHz is covered by both the fundamental and the second harmonic operations.

2. 100 percent amplitude modulation of the gyrotron output is attained under only a few percent modulation of anode voltage. The highest modulation frequency examined is 400 kHz.

A submillimeter wave scattering measurement system using GYROTRON A as a power source is constructed and installed to CHS device (Compact Helical System). Preliminary experimental results for spontaneously excited low frequency drift wave has been obtained. In future, we will apply the measurement system to study propagation of incident waves in plasma, in the cases of the electron cyclotron wave heating and the lower hybrid wave heating.

References

[1] For example, K.Felch, C.Hess, H.Huey, E.Jongeward, H.Jory, and R.Pendleton, in *13th Int. Conf. on Infrared and Millimeter Waves*, Hawaii, USA, edited by R.J.Temkin (International Society for Optical Engineering, Bellingham, WA, 1988), pp.175-176.

[2] Y.Terumichi, S.Kubo, A.Ando, Y.Yanagimoto, K.Ogura, H.Tanaka, J.Takahashi, I.Tonai, M.Nakamura, T.Maekawa, S.Tanaka and T.Idehara, in *9th Int. Conf. on infrared and Millimeter Waves*, Takarazuka, Japan, edited by K.Mizuno (Japan Society of Applied Physics, Tokyo, 1984) pp.411-412.

[3] P.Woskoboinikow, D.R.Cohn, M.Gerrer, W.J.Mulligan, R.S.Post, R.J.Temkin, and J.Trulsen, Rev. Sci. Instrum. **56**, 914 (1985).

[4] M.D.Bowden, P.W.Fekete, M.J.Ballico, G.F.Brand, I.S.Falconer, B.W.James, K.J.Moore, and T.Idehara, in *13th Int. Conf. on Infrared and Millimeter Waves*, Hawaii, USA, edited by R.J.Temkin (International Society for Optical Engineering, Bellingham, WA, 1988), pp.150-151.

[5] N.I.Zaytsev, T.P.Pankratova, N.I.Petelin, and V.A.Flyagin, Radio Eng. Electron. Phys. (USSR) **19**, 103 (1974).

[6] J.D.Silverstein, Int. J. Infrared and Millimeter Waves **6**, 339 (1985).

[7] J.L.Byerly, B.D.Danly, K.E.Kreischer, R.J.Temkin, W.J.Milligan, and P.Woskoboinikow, Int. J. Electron. **57**, 1033 (1984).

[8] J.P.Shivly, K.Felch, H.Tory, and J.Neilson, in *12th Int. Conf. on Infrared and Millimeter Waves*, Florida, USA, edited by R.J.Temkin (IEEE, New York, 1987), pp.240-241.

[9] T.Idehara, T.Tatsukawa, H.Tanabe, S.Matsumoto, K.Kunieda, K.Hemmi, and T.Kanemaki, Phys. Fluids B **3**, 1766 (1991).

[10] S.E.Spira, K.E.Kreischer, and R.J.Temkin, in *13th Int. Conf. on Infrared and Millimeter Waves*, Hawaii, USA, edited by R.J.Temkin (International Society for Optical Engineering, Bellingham, WA, 1988), pp.150-151.

[11] G.F.Brand, in *Infrared and Millimeter Waves*, edited by K.J.Button (Academic, New York, 1985), Vol.14, pp.371-408.

[12] G.F.Brand, P.W.Fekete, K.Hong, K.J.Moore and T.Idehara, Int. J. Electronics **68**, 1099 (1990).

[13] K.D.Hong, G.F.Brand, P.W.Fekete, and T.Idehara, Int. J. Infrared and Millimeter Waves **13**, 215 (1992).

[14] S.Ono, H.Ansai, N.Sato, K.Yokoo, K.Hemmi, T.Idehara, T.Tatsukawa, I.Okazaki, and T.Okamoto, in *11th Int. Conf. on Infrared and Millimeter Waves*, Pisa, Italy, edited by G.Moruzzi (ETS Editrice, Pisa, 1986), pp.37-39.

[15] T.Idehara, T.Tatsukawa, S.Matsumoto, K.Kunieda, K.Hemmi, and T.Kanemaki, Phys. Lett. A **132**, 344 (1988).

[16] T.Idehara, T.Tatsukawa, I.Ogawa, H.Tanabe, T.Mori, S.Wada, and T.Kanemaki, Appl. Phys. Lett. **56**, 1743 (1990).

[17] T.Idehara, T.Tatsukawa, I.Ogawa, H.Tanabe, T.Mori, S.Wada, G.F.Brand, and M.H.Brennan, Appl. Phys. Lett. **57**, 1594 (1991).

[18] T.Idehara, T.Tatsukawa, I.Ogawa, S.Wada, K.Yoshizue, F.Inoue, and G.F.Brand, Phys. Fluids B **4**, 769 (1992).

[19] T.Idehara, T.Tatsukawa, I.Ogawa, H.Tanabe, T.Mori, S.Wada, G.F.Brand, and M.H.Brennan, Phys. Fluids B **4**, 267 (1992).

[20] T.Idehara, T.Tatsukawa, I.Ogawa, Y.Shimizu, S.Makino, and T.Kanemaki, Phys. Fluids B **5**, 1377 (1993).

[21] T.Idehara, T.Tatsukawa, I.Ogawa, Y.Yamagishi, and T.Kanemaki, Appl. Phys. Lett. **62**, 832 (1993).

[22] K.R.Chu, L.R.Barnett, W.K.Lau, L.H.Chang, A.T.Lin, and C.C.Lin, Phys. Fluids B **3**, 2403 (1991).

[23] E.Borie, G.Dammertz, O.Dumbrajs, G.Gantenbein, T.Geist, M.Kuntze, A.Mobius, H.U.Nickel, B.Piosczyk, and M.Thumm, in *16th Int. Conf. on Infrared and Millimeter Waves*, Lausanne, Switzerland, edited by M.R.Siegrist (Centre de Recherches en Physique des Plasmas, Lausanne, 1991), pp. 260-263.

[24] T.Idehara, T.Tatsukawa, I.Ogawa, and G.F.Brand, in *5th Aust. Symp. on Millimeter and Submillimeter Waves*, (sponcered by IEEE South Australian Section, Adelaide, 1992), pp.100-103.

DEVELOPMENT OF HIGH-POWER 140 GHZ GYROTRONS FOR FUSION PLASMA APPLICATIONS

M. Thumm*, E. Borie, G. Dammertz, G. Gantenbein, M. Kuntze, A. Möbius, H.-U. Nickel*, B. Piosczyk, A. Wien*

Kernforschungszentrum Karlsruhe, Institut für Technische Physik
P.O. Box 3640, D-76021 Karlsruhe, Germany
* also Univ. Karlsruhe, Inst. f. Höchstfrequenztechnik u. Elektronik
Kaiserstr. 12, D-76131 Karlsruhe, Germany

The state of development work at KfK for 140 GHz high-power gyrotron oscillators is described. In particular the design and experimental results of a 0.5 MW gyrotron tube with axial rf output operating in the $TE_{10,4}$ mode are presented. In short pulse operation ($\leq$ 5 ms) an output power of 690 kW has been obtained with an electronic efficiency of 31% and a mode purity of about 99%. The experiments have shown that it is possible to use for step frequency tuning the azimuthal neighbours of the $TE_{10,4}$ mode, $TE_{9,4}$ at 132.6 GHz (420 kW) and $TE_{11,4}$ at 147.3 GHz (300 kW) as working modes by decreasing and increasing the magnetic field respectively. In view of a planned long pulse operation the $TE_{10,4}$ tube is presently being modified by incorporating an advanced quasi-optical mode converter that provides a separation between the electron beam and the linearly polarized Gaussian beam output. The design of this tube and the next development steps towards 1 MW output power with a $TE_{22,6}$ mode cavity are discussed.

1 Introduction

A main goal of the gyrotron development program at KfK is the design, construction, and test of high-power gyrotron oscillators for

electron cyclotron wave applications in thermonuclear fusion experiments. For the next generation of fusion research devices such as ITER, millimeter wave generators operating at long pulses up to cw with an rf output power in excess of 1 MW per unit at frequencies around 140 GHz are needed. In order to fulfil these requirements development work is still necessary.

As a first step a 140 GHz tube using a $TE_{0,3}$ mode resonator, capable of delivering an output power of 120 kW with a mode purity of larger than 98% was developed and tested [1]. With pulse durations up to 0.4 s this tube has been successfully used for the worldwide first 140 GHz plasma heating and plasma diagnostic experiments performed at the Wendelstein 7-AS stellarator of the Max-Planck-Institut für Plasmaphysik in Garching [2].

To reach higher power (> 500 kW) at increased pulse length a cavity mode of higher order must be chosen to reduce the Ohmic losses at the resonator surface. As a next step KfK has designed, built, and tested a 140 GHz gyrotron that operates in the $TE_{10,4}$ mode. With this tube an output power up to 690 kW with a mode purity of about 99% at pulse lengths up to 5 ms has been achieved. The design of the gyrotron and the related measurements, including frequency step-tuning experiments are described in chapter 2. Both tubes, the $TE_{10,4}$ as well as the previous $TE_{0,3}$ version, are of conventional design with the rf power coupled out via an axial window. The next version of the tube will use a built-in quasi-optical mode converter to transform the rotating $TE_{10,4}$ resonator mode into a Gaussian free-space wave which will be coupled out by a lateral window. The use of the built-in mode converter has several principal advantages for high-power operation as will be discussed in chapter 3. To operate the gyrotron with the built-in converter a superconducting magnet with a rather large bore hole ($\phi = 275$ mm) will be used. It may then be possible to extend the pulse length up to about 0.2 s at 500 kW limited by the design of the window and the collector.

In order to achieve an rf output power of at least 1 MW at long pulses up to cw modes of higher order than the $TE_{10,4}$ are required. The $TE_{22,p}$ modes with $p = 5$ or 6 have been found to be suitable for output powers up to 1 MW with tolerable maximum surface loss density (< 3 kW/cm^2) in the resonator. At the considered frequencies

the presently available rf windows with cooling at room temperature limit the maximum power to about 0.5 MW for pulses of 2 s length [3]. The design of a 1 MW gyrotron operating in the $TE_{22,6}$ mode and employing a diode-type electron gun and an improved, compact quasi-optical mode transducer is presented in chapter 4. For transmission of rf powers of at least 1 MW at pulses up to cw, windows operated at cryogenic temperatures are under development [4].

2 $TE_{10,4}$ gyrotron with axial output coupling

2.1 Design

One of the critical factors in the design of a high-power gyrotron is the minimization of the Ohmic losses in the resonator walls. This is the main reason for using a highly overmoded cavity, although the resulting higher density of eigenmodes enhances competition by unwanted neighbouring modes. Higher efficiencies and more stable operation can be achieved if the working mode is chosen to be as isolated as possible from competing modes. One reason for choosing the $TE_{10,4}$ mode, in addition to the necessity of using an already existing superconducting magnet with a small bore hole, was its rather good isolation from possible nearby competitors. The space charge of the electron beam leads to a potential depression proportional to $\ln(R_b/R_w)$ where R_b is the beam radius and R_w is the wall radius in the cavity. A consequence of the voltage depression is a limiting current, which is the maximum current that can be transported through a beam duct for a given accelerating voltage [5]. A decrease in the ratio R_b/R_w reduces the limiting current and increases the tendency to beam instabilities. The design current should be considerably less than the limiting current. For the foreseen values of voltage and current, the value of $R_b/R_w = 0.45$ for the $TE_{10,4}$ mode is just at the expected lower limit. Some of the main gyrotron design parameters are summarized in Table 1. As the 100 mm bore hole of the existing magnet did not permit the installation of a tube with radial output coupling, first experiments were performed with an axially arranged

tube. Since the given magnetic field configuration of the magnet leads to beam deposition on the walls of the uptaper section (high power density due to small diameter), the maximum pulse length is limited to a few milliseconds.

beam volt. U_{beam}	80 kV	cav. radius R_w	8.11 mm
mod. volt. U_{mod}	25 kV	cav. length	11 / 16 mm
beam current I_{beam}	$\leq$ 25 A	quality factor Q	590 / 1150
emitter curr. dens.	$\leq$ 6 A/cm^2	velocity ratio at cav. α	1.5-1.7 / 1.1
mag. field at cath.	0.187 T	mag. field at cav. B_{cav}	5.5-5.6 T
cathode radius	19.8 mm	beam radius at cav. R_b	3.65 mm
cathode angle	26.6°	beam thickness at cav.	0.5 mm

Table 1: Design parameters of the 500 kW, 140 GHz $TE_{10,4}$ mode gyrotron employing a triode-type magnetron injection gun with an impregnated tungsten emitter coated with Osmium.

Two different resonators have been designed and tested (cf. Table 1). For the first one (length $\approx$ 11 mm), the realistic maximum Ohmic losses at 500 kW output power are approx. 3 kW/cm^2. The choice of geometry was a compromise between the beam current allowing operation at 500 kW (high quality factor Q), and low maximum wall losses (which require low Q). As discussed below, the second, higher Q resonator (length = 12 mm + 4 mm due to rounded transitions) was used to compensate for unexpectedly poor beam quality with an average velocity ratio of about 1.1. Long pulse operation with such a resonator would not be possible due to the high wall losses.
Several rf output windows with different reflectivity curves were used (Figure 1): a double disk sapphire window with tunable spacing between the disks (DDW), a single disk sapphire window (SDW1), and a fused silica single disk window (SDW2). The electrical thickness of each window disk is 5 half wavelengths in the dielectric at 140 GHz. The relative permittivity at room temperature is 9.4 for sapphire (E-vector perpendicular to c-axis) and 3.8 for fused silica.
The measurements have been performed either with the sapphire windows and the 11 mm resonator or with the fused silica window and the 16 mm cavity.

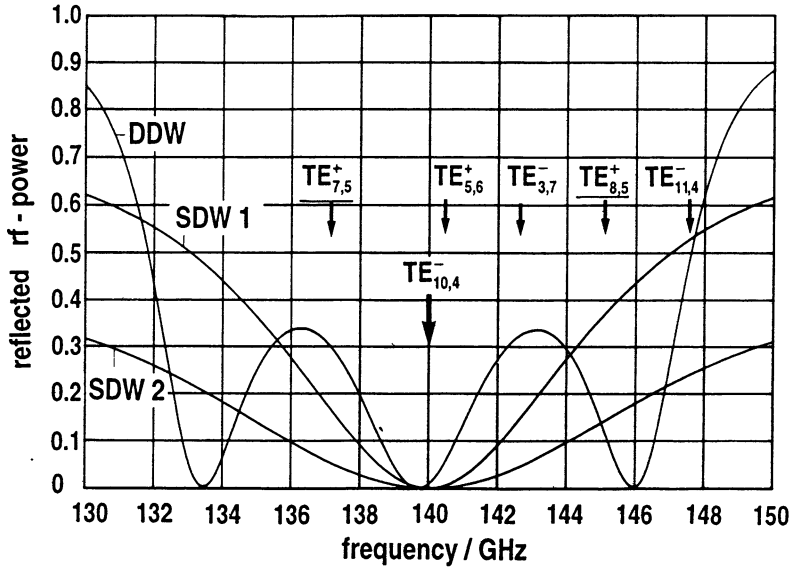

Fig. 1: Power reflection coefficient versus frequency of the three different output windows used. The spacing of the air-filled gap in the DDW is 4.41 mm. The arrows indicate the location of the competing modes observed. With the SDW2 only the underlined modes have been observed.

2.2 Experimental results

The operating mode can be identified by measuring the frequency of the output signal. A contiguous filterbank receiver with a spectral resolution of 100 MHz [6] is used for this purpose. In addition, instantaneous frequency measurement during a single pulse is performed with a set-up described in [7]. Purity of waveguide modes is measured with a wave number spectrometer [8] and power measurements are made using an octanol-filled static calorimeter [9]. During the experiments with the 11 mm resonator and the sapphire windows (DDW, SDW1 in Figure 1) at $B_{cav} \approx 5.6$ T several modes in the vicinity of the $TE_{10,4}$ namely the $TE_{7,5}$ at 137.32 GHz, $TE_{5,6}$ at 140.46 GHz, $TE_{3,7}$ at 142.48 GHz, $TE_{8,5}$ at 145.08 GHz and even

the azimuthal neighbour on the high frequency side, the $TE_{11,4}$ at 147.53 GHz, appeared as competing modes. The measured frequencies of the working mode and the various competing modes agreed very well with the calculated values. It has been shown that the starting currents of the competing modes depend strongly on the spacing of the two disks of the double disk window. As an example, Figure 2 shows the calculated power reflection of the $TE_{7,5}$ mode and the measured starting current of the same mode as a function of disk spacing. Figure 3 shows the calculated starting current of the $TE_{10,4}$ and $TE_{7,5}$ modes as a function of beam voltage U_b. In addition the starting current of the $TE_{7,5}$ mode, calculated assuming a power reflection coefficient of 35% ($\Delta\varphi = 270°$) is shown. In this example, the reflections of the parasitic mode lead to a reduction of the starting current, thus increasing the danger of oscillations in the wrong mode during startup. Similar results have been obtained for the $TE_{8,5}$ and $TE_{11,4}$ modes, and also for the single disk sapphire window [10].

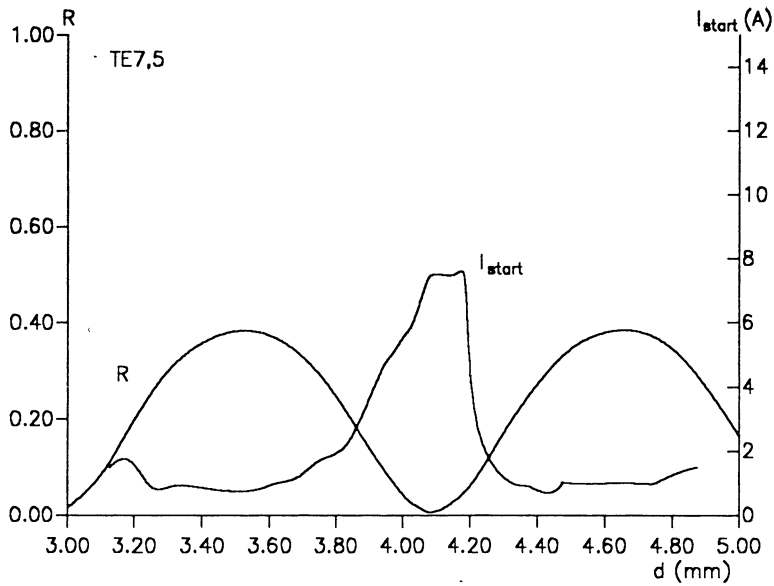

Fig. 2: Calculated power reflection coefficient of the $TE_{7,5}$ mode as a function of window spacing and the corresponding starting current (experimental).

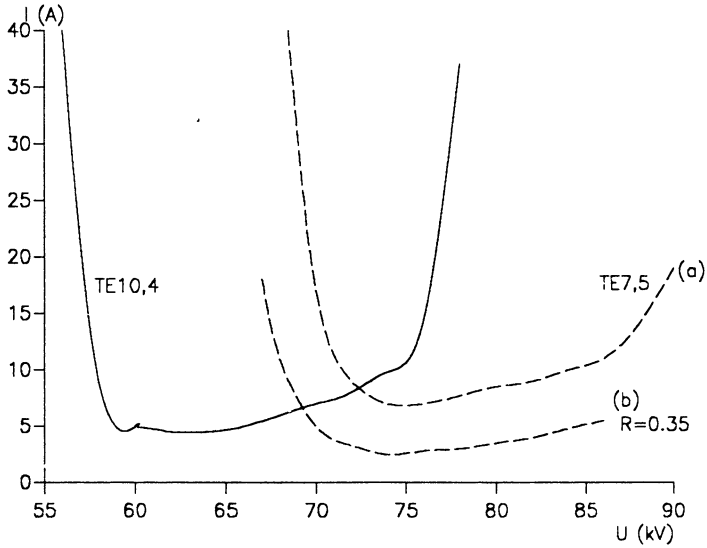

Fig. 3: Calculated starting current of the $TE_{10,4}$ mode and $TE_{7,5}$ mode, including the effect of reflections (curve b).

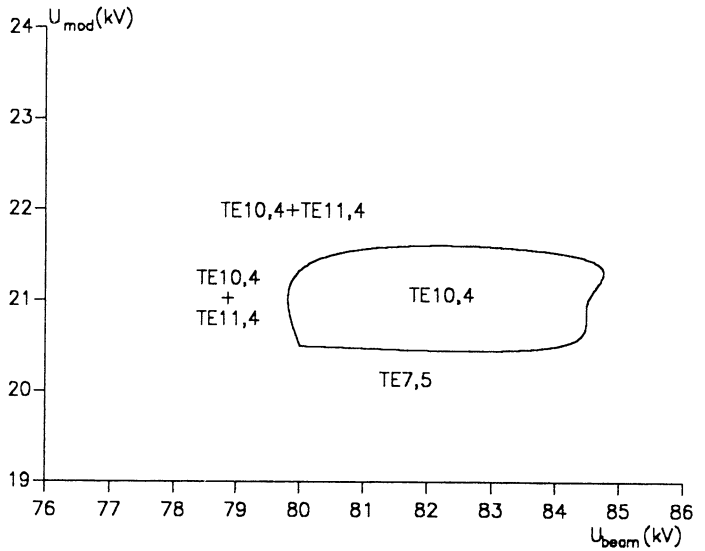

Fig. 4: Oscillating area of the $TE_{10,4}$ mode (single disk sapphire window).

Figure 4 displays the measured mode map for this case. The oscillating area of the $TE_{10,4}$ mode is limited by $TE_{7,5}$- and $TE_{11,4}$-mode oscillations. It was not possible to operate the electron gun with the design values of the mod anode voltage U_{mod} owing to an unacceptable increase of the leakage current to the modulation anode and due to instabilities of the electron beam. Both effects were probably caused by reflected electrons resulting from the velocity spread of the beam electrons. Thus the achievable velocity ratio was limited to about 1.1, instead of the design value of 1.5-1.7, leading to a substantially reduced efficiency. In spite of this low velocity ratio, it was possible to generate about 450 kW of rf power in the desired mode, and over 500 kW with a small contribution from the $TE_{11,4}$ mode. To overcome the problems with the low velocity ratio the second resonator was designed to give higher efficiency. The length of the cylindrical mid-part was increased to 12 mm and the transitions from the mid-part to the tapered input and output sections have been made with smooth curvatures. This cavity has a higher theoretical efficiency at reduced α-values and is less sensitive to velocity spread of the electrons. The curved transitions between the cylindrical and conical parts of the resonator result in reduced conversion to spurious modes [11].

In this second gyrotron version, in addition to the change of the cavity, the output window was replaced by a fused silica window in order to alleviate problems due to window reflections. The new window had a low reflectivity over a relatively broad frequency range (SDW2 in Figure 1) and it was tilted by about 0.5° with respect to the waveguide axis. With this new tube very encouraging results were obtained. The mode competition problem was reduced since only the modes underlined in Figure 1 ($TE_{7,5}$, $TE_{8,5}$) appeared as competitors. The reduction of the window reflections for $TE_{11,4}$ (from 53% to 23%) results in a considerably larger oscillating area of the $TE_{10,4}$ mode (see Figure 5). At high beam voltage the operation of the $TE_{10,4}$ mode is limited by competition with the $TE_{7,5}$ mode at low U_b and high U_{mod} the $TE_{8,5}$ mode is prefered. To achieve an efficient interaction the tube has been operated at a beam voltage as high as possible to ensure stable $TE_{10,4}$ oscillations.

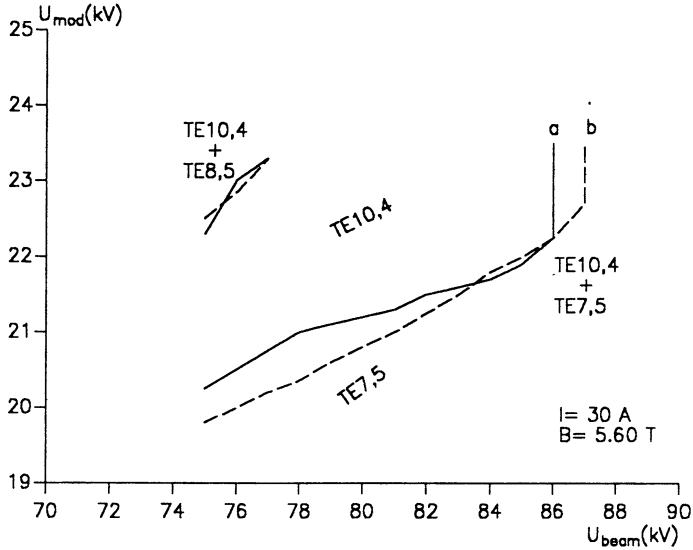

Fig. 5: Oscillating area of the $TE_{10,4}$ mode with the single disk fused silica window having a relatively wide passband.

The high-power working region was only accessible via a diode-type startup scenario (see Figure 6) in which U_b and U_{mod} are raised simultaneously. Figure 7 shows the output power and the total efficiency as a function of beam current. The magnetic field was kept constant at about 5.6 T, while the beam voltage and mod anode voltage were adjusted for maximum power. Care was taken that single mode oscillation occured. A maximum output power of 690 kW has been measured at 87 kV with a beam current of 30 A, corresponding to a total efficiency of 26%. When the internal losses in the resonator, uptaper, collector, window, and waveguide towards the calorimeter as well as the voltage depression, are taken into account, the electronic efficiency is estimated to be about 31%. The maximum total efficiency (29%) was measured for a beam current of 23 A and output power of 560 kW. The corresponding electronic efficiency is about 33%. The dashed lines in Figure 7 correspond to numerical simulations with an average velocity ratio of 0.95 and 1.05 and a velocity spread of $\Delta\beta_\perp/\beta_\perp \approx 30\%$ (FWHM) [10].

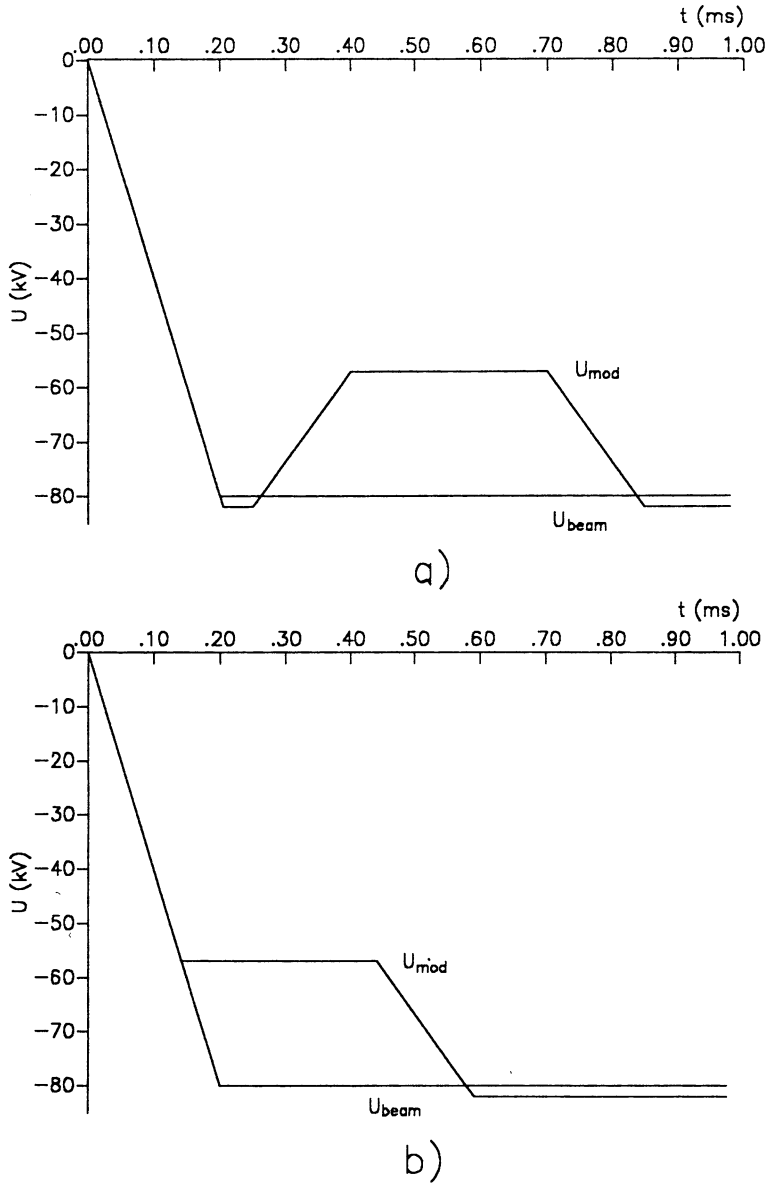

Fig. 6: Voltage startup scenario: (a) triode-type, (b) diode-type.

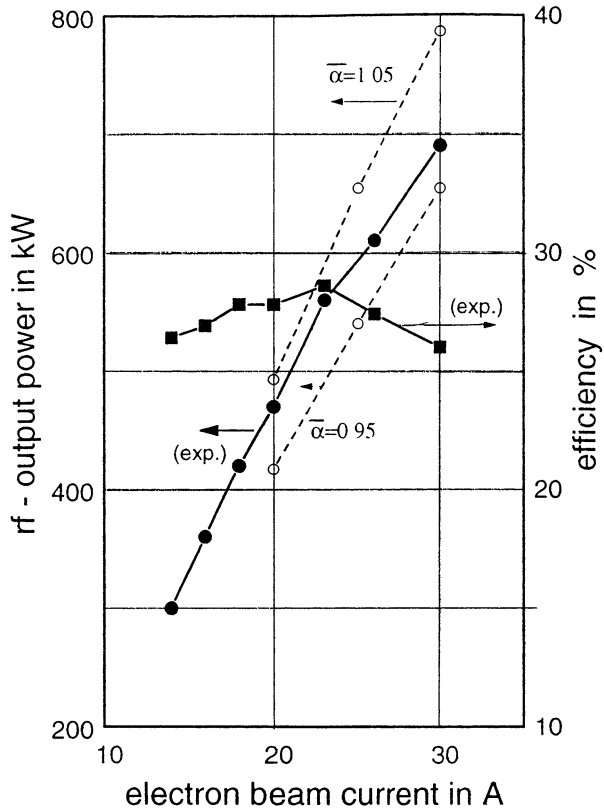

Fig. 7: Output power and total efficiency versus beam current for the $TE_{10,4}$ mode with 16 mm cavity.

2.3 Stepwise frequency tuning

In gyrotrons the frequency can be varied in the percent range by changing the operating mode [12, 13]. Table 2 gives the frequencies and output powers which were achieved during step-wise frequency tuning by excitation of the azimuthal neighbours $TE_{9,4}$ and $TE_{11,4}$. The tuning required a variation of the cavity magnetic field B_{cav} and an optimization of the beam voltage ($75 \leq U_{beam}/\text{kV} \leq 87$). P_{25} and P_{30} denote the rf output power at a beam current of 25 A and 30 A

respectively. In the $TE_{9,4}$ mode a power of 420 kW was achieved at 25 A compared with 600 kW in the $TE_{10,4}$ mode. A strong competition with the $TE_{8,4}$ mode at 124.96 GHz and the $TE_{11,3}$ mode at 126.24 GHz was observed. It is assumed that this effect is supported by a high amount of reflections at the frequencies of these modes (up to 35%) since the window is tuned to 140 GHz. Taking realistic beam properties and window reflections into account, the measured peak output power of the $TE_{9,4}$ mode is in reasonable agreement with numerical calculations.

Mode	B_{cav}/T	f/GHz	P_{25}/kW	P_{30}/kW
$TE_{9,4}$	5.2	132.6	420	-
$TE_{10,4}$	5.6	140.0	600	690
$TE_{11,4}$	5.9	147.3	230	300

Table 2: Frequencies and output powers achieved during step-tuned operation.

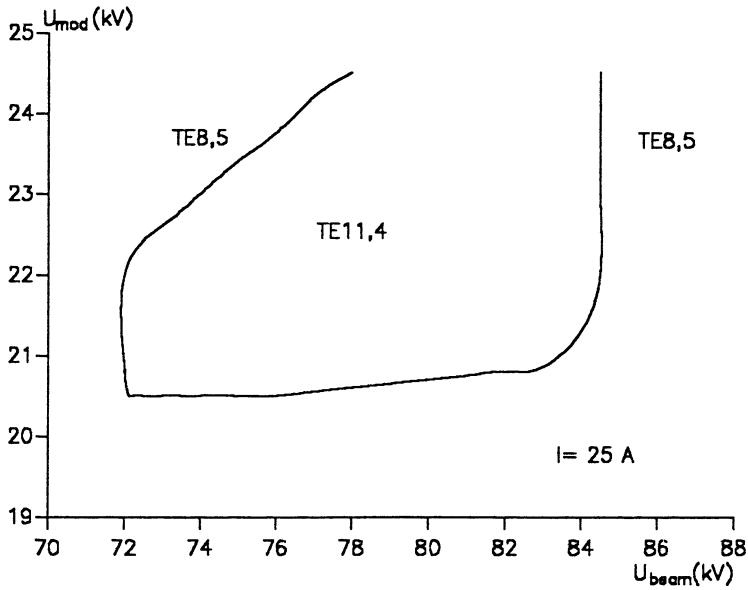

Fig. 8: Oscillating area of the $TE_{11,4}$ mode.

Figure 8 shows the oscillating area of the $TE_{11,4}$ mode in the U_{mod}-U_b plane. Several frequencies spaced by approximately 60 MHz have been observed for this mode, corresponding to different longitudinal modes of the long-line cavity formed by the gyrotron resonator and the partially reflecting window. The maximum output power in this case was 300 kW. In order to reduce the reflected power in a step tunable gyrotron various types of broadband windows are currently under investigation [14].

3 $TE_{10,4}$ gyrotron with radial output coupling and advanced quasi-optical mode converter

Radial output coupling of the rf power of a gyrotron into a Gaussian ($TEM_{0,0}$) mode has three significant advantages for high-power operation. First, the linearly polarized $TEM_{0,0}$ mode is directly usable for low-loss transmission as well as for effective interaction with the fusion plasma and no further mode converters are needed. Second, the converter separates the electron beam from the rf wave path, so that the electron collector is no longer part of the output waveguide as in the case of an axially arranged tube. Hence, the collector can be designed especially for handling the high electron beam power. In addition, energy recovery with a depressed collector becomes possible. Third, the influence of rf power reflected from the output window and the load is expected to be significantly reduced, especially for modes rotating in the opposite direction from the design mode.

The arrangement of the $TE_{10,4}$ mode gyrotron with a quasi-optical mode converter is shown in Figure 9. The rotating $TE_{10,4}$ cavity mode is converted to a linearly polarized Gaussian beam by an advanced mode conversion system designed according to [15, 16]. It consists of a helically cut quasi-optical aperture antenna with a deformed feed waveguide and three beam-forming mirrors (see Figure 10). The rotating mode is converted by the feed waveguide section into a mode mixture that assures an almost sidelobe-free radiation pattern when launched through the antenna aperture.

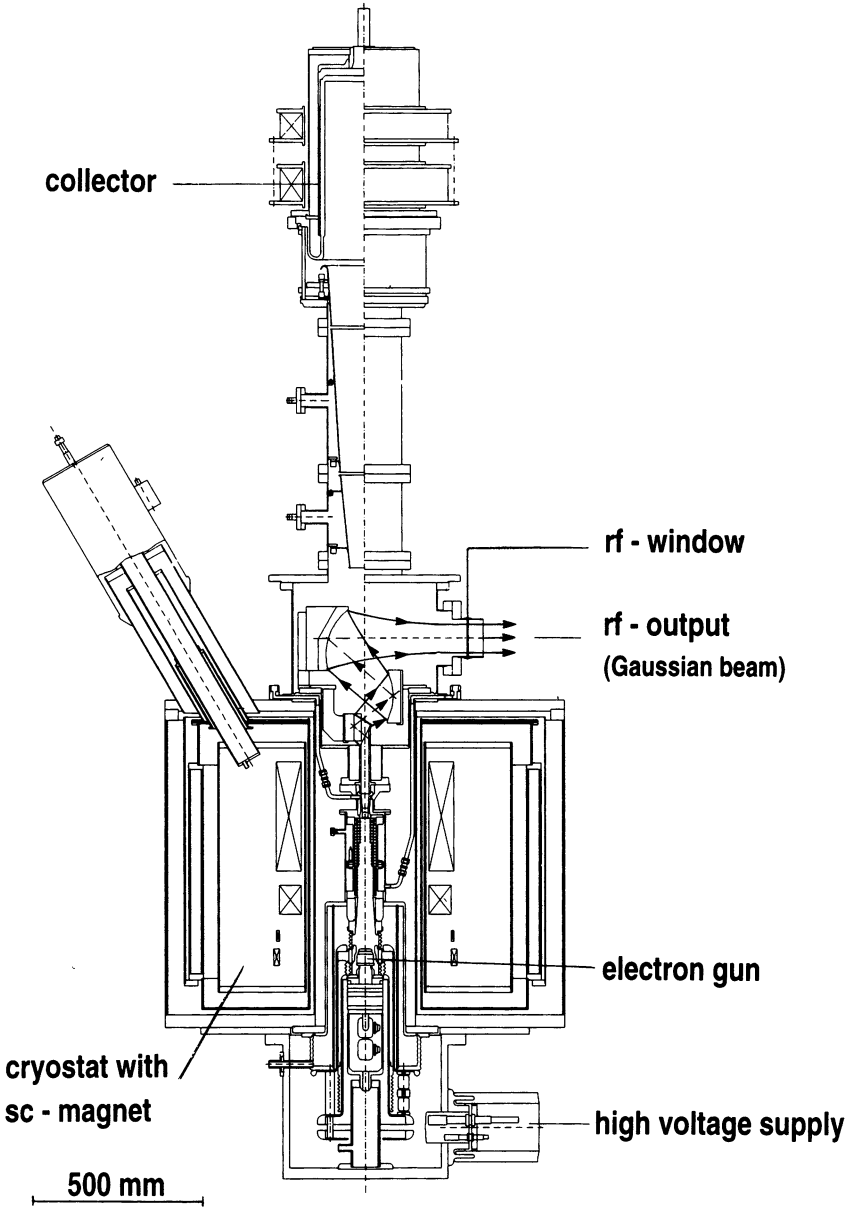

Fig. 9: Schematic layout of a $TE_{10,4}$ mode gyrotron with quasi-optical mode converter. Note that the launcher cut is helical. Indicated dimensions are in mm.

After being refocused by a quasi-parabolic mirror, that corrects the phase in the transverse plane, an astigmatic Gaussian beam is obtained. Two further mirrors remove the astigmatism and direct the rf beam through the output window. The beam waist has a radius of 22 mm ($1/e^2$ drop of power density) and is located about 12 cm outside the window. The single disk window is made of pyrolytic boron nitride which has a permittivity of about 4.7. The transmission capacity of the edge cooled disk is estimated to be around 500 kW for up to 0.3 s. The electron gun and the beam tunnel are used unchanged from the axially arranged tube. The collector and sc magnet have been fabricated and tested. After assembly and bake-out of the tube, first tests are expected in September 1993.

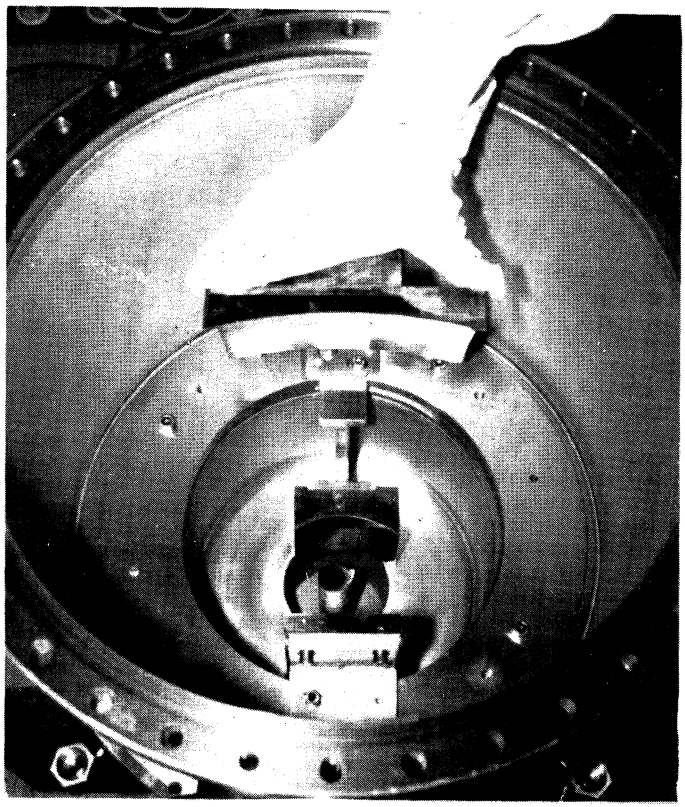

Fig. 10: Photograph of the gyrotron tank with the advanced quasi-optical mode converter.

4 1 MW $TE_{22,6}$ gyrotron with radial output coupling and compact quasi-optical mode converter

In order to generate an output power of 1 MW or even more at long pulses up to cw, modes of higher order than $TE_{10,4}$ have to be used. The $TE_{22,p}$ modes with $p = 5$ or 6 have been shown to be suitable for output powers up to 1 MW with tolerable maximum Ohmic surface losses (< 3 kW/cm^2) in the cavity [3]. Mode competition calculations taking into account $TE_{22,6}$ and $TE_{19,7}$ [10, 17] show a wide region in which the $TE_{22,6}$ mode should operate stably (Figure 11). The computations clearly indicate that a simultaneous increase of beam energy and α during the startup phase is required in order to reach the stable high-power working point of the design mode, a feature that was also observed experimentally with the $TE_{10,4}$ mode tube (Figures 5 and 6) as well as in earlier experiments at 150 GHz with the $TE_{0,3}$ mode [18]. The use of a diode-type electron gun automatically leads to a startup scenario of this type. The construction of a 1 MW $TE_{22,6}$ mode tube (pulse length 100 ms) has been started at KfK. Some of the main design parameters are summarized in Table 3.

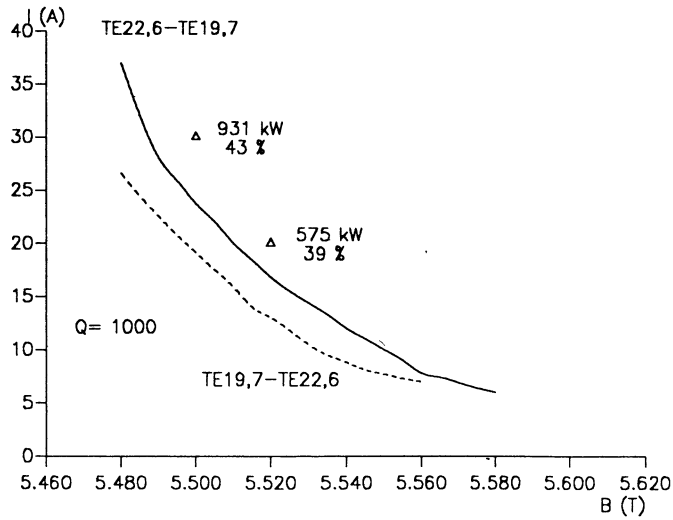

Fig. 11: Region of stable $TE_{22,6}$ mode oscillations. The indicated points correspond to self-consistent computations.

beam volt. U_{beam}	80 kV	cav. radius R_w	15.57 mm
		cav. length	15 mm
beam current I_{beam}	$\leq$ 40 A	quality factor Q	$\approx$ 1000
emitter curr. dens.	$\leq$ 3.6 A/cm^2	velocity ratio at cav. α	1.4
mag. field at cath.	0.187 T	mag. field at cav. B_{cav}	5.5 T
cathode radius	45.2 mm	beam radius at cav. R_b	7.93 mm
cathode angle	21.5°	beam thickness at cav.	0.5 mm

Table 3: Design parameters of the 1 MW, 140 GHz $TE_{22,6}$ mode gyrotron employing a diode type gun with LaB_6 emitter.

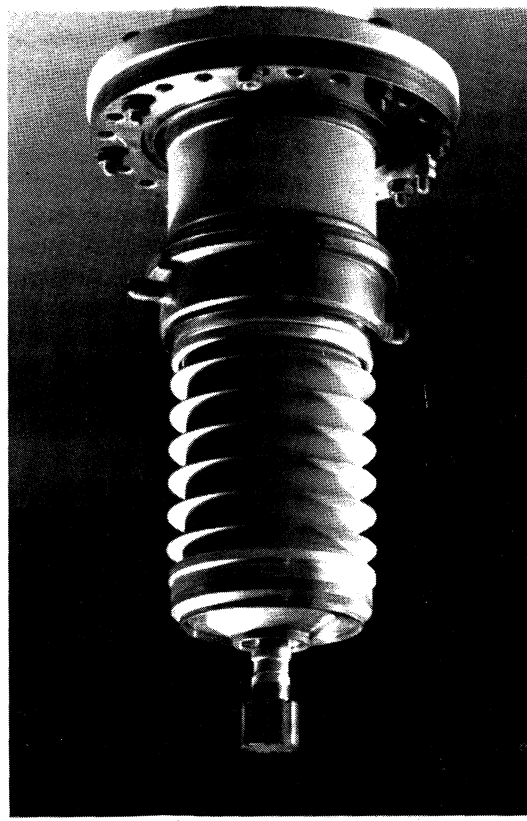

Fig. 12: Photograph of the 3.2 MW diode-type magnetron injection gun for the 140 GHz $TE_{22,6}$ gyrotron oscillator.

The diode-type magnetron injection gun (MIG) for this gyrotron was designed in collaboration with IAP Nizhny Novgorod and has been manufactured and successfully tested there (α, $\Delta\beta_\perp/\beta_\perp$ and rf generation). A photograph of the MIG is shown in Figure 12.

An improved quasi-optical launcher for a high order mode like $TE_{22,6}$ utilizing a periodically perturbed, mode-converting feed waveguide is either so long that it will be difficult to integrate it into the vacuum system of the tube or it needs to be operated very close to cutoff where reflections may cause problems. Thus here the type of feed waveguide deformations proposed in [19] will be used. The general idea is an improvement of the two-subreflector approach, where an initial caustic formed by rays is transformed via an intermediate caustic into the desired final caustic. Figure 13a shows the cross section of the deformed waveguide in the present converter design with the circular initial caustic U, the resulting intermediate caustic V, and the circular final caustic W, where the ray density has a Gaussian distribution. In a three dimensional consideration four in-waveguide mirrors provide axial and azimuthal bunching of the rays. The rays at the aperture are launched from the final caustic W which forms a circularly bent parallelogram with a Gaussian ray density distribution in both directions. The phase front correction by the quasi-parabolic mirror leads to a weak ray density alteration. This can be compensated by a slight predistortion of the ray density on the final caustic W. In general the total length of the converter section (N in-waveguide mirrors) and the launcher for a $TE_{m,n}$ mode (eigenvalue $x'_{m,n}$, wave numbers $k_\parallel$ and $k_\perp$) is given by the expression

$$L_{tot} = 2\left(\pi + N\arccos\left(\frac{m}{x'_{m,n}}\right)\right)\frac{k_\parallel}{k_\perp}R_w\,\frac{\sqrt{1-\dfrac{m^2}{x'^2_{m,n}}}}{\arccos\left(\dfrac{m}{x'_{m,n}}\right)}.$$

The waveguide perturbations synthesized by means of geometrical optics have to be analysed using diffraction theory. In our model the

calculation is separated in axial and azimuthal directions and the Huygens integrals are solved on surfaces depending on two dimensions. In this approach it is assumed that the field is radiated from a single caustic and it is calculated on the waveguide surfaces by means of Hankel functions. To obtain the radiation field of the launcher the reflected field from the last waveguide mirror surface is computed (Figure 13b).

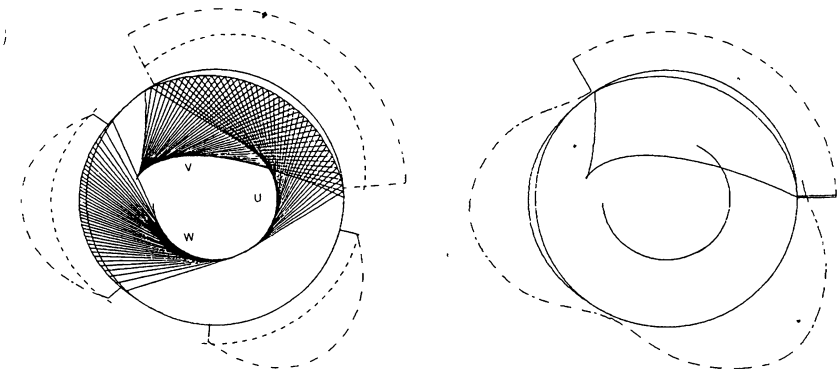

(a) geometrical optics (b) diffraction optics

Fig. 13: Cross section of the mode converter feed waveguide with two in-waveguide mirrors (azimuthal bunching), caustics, amplitude distributions (-----), and phase distributions (---): (a) geometrical optics, (b) diffraction optics.

5 Acknowledgment

We gratefully acknowledge the assistance of the KfK gyrotron team technical staff: W. Baumgärtner, H. Budig,, U. Feißt, P. Grundel A. Hornung, R. Lehm, N. Münch, G. Redemann, J. Szczesny, anc R. Vincon. This work was performed under the auspices of the 'Projekt Kernfusion' at the KfK and was partly supported by the European Communities within the European Fusion Program.

6 References

1. E. Borie et al., *Int. J. Electronics*, **72** (1992), 687-720.
2. V. Erckmann et al., Int School of Plasma Physics, Vol. ISPP-10, Varenna, Italy, 1991, pp. 511-518.
3. G.G. Denisov et al., Proc. 16th Int. Conf. on Infrared and Millimeter Waves, 1991, Lausanne, Switzerland, SPIE **1576**, 632-635 and private communication.
4. P. Norajitra et al., KfK-Report 4930, Karlsruhe, Germany.
5. A.K. Ganguly, K.R. Chu, *Int. J. Infrared and Millimeter Waves*, **5** (1984), 103-121.
6. T. Geist et al., Proc. 16th Int. Conf. on Infrared and Millimeter Waves, 1991, Lausanne, Switzerland, SPIE **1576**, 274-275.
7. G. Gantenbein et al., Proc. 14th Int. Conf. on Infrared and Millimeter Waves, 1989, Würzburg, Germany, SPIE **1240**, 221-222.
8. W. Kasparek, G.A. Müller, *Int. J. Electronics*, **64** (1988), 5-20.
9. H. Stickel, *Int. J. Electronics*, **64** (1988), 63-76.
10. G. Gantenbein, Dr.-Ing. Thesis, University of Karlsruhe, 1993.
11. O. Dumbrajs et al., *Int. J. Infrared and Millimeter Waves*, **13** (1992), 825-840.
12. K.E. Kreischer, R.J. Temkin, *Phys.Rev. Lett.*, **59** (1987), 547-550.
13. V.I. Kurbatov et al., Proc. Int. Workshop on Strong Microwaves in Plasmas (Suzdal, 1990), Nizhny Novgorod, Russia, 1991, Vol. 2, 765-772.
14. H.-U. Nickel et al., Proc. 17th Int. Conf. on Infrared and Millimeter Waves, 1992, Pasadena, USA, SPIE **1929**, 462-463.
15. G.G. Denisov et al., *Int. J. Electronics*, **72** (1992), 1079-1091.
16. J. Pretterebner et al., Proc. 17th Int. Conf. on Infrared and Millimeter Waves, 1992, Pasadena, USA, SPIE **1929**, 40-41.
17. G. Gantenbein et al., Proc. 16th Int. Conf. on Infrared and Millimeter Waves, 1991, Lausanne, Switzerland, SPIE **1576**, 264-265.
18. B. Jödicke, Dr.-Ing. Thesis, University of Karlsruhe, 1989 (KfK-Report 4603).
19. A. Möbius, J. Pretterebner, Proc. 16th Int. Conf. on Infrared and Millimeter Waves, 1991, Lausanne, Switzerland, SPIE **1576**, 531-532.

Cyclotron Autoresonance Masers: achievements and prospects of advance to the submillimeter wavelength range

V.L.Bratman, G.G.Denisov and S.V.Samsonov

Institute of Applied Physics, Russian Academy of Sciences, 46 Ulyanov Street, 603600 Nizhny Novgorod, Russia.

Abstract

The cyclotron autoresonance maser (CARM) is considered as a possible source of high-power millimeter and submillimeter coherent radiation. At present the most acute problems of CARM creation are formation of a curvilinear relativistic electron beam with a small spread of velocities and parasitic modes discrimination. Results of preliminary CARM experiments are presented as well as achievements of two recent experimental investigations where improved electron beam pumping systems (kickers) and high selective microwave systems were used. In short pulse operation a power 25-50 MW was obtained at millimeter wavelength range with an efficiency up to 10%. Proposals of modifying electron-optical and microwave systems of CARM on the way of advance to submillimeter wavelength range are discussed and two conceptual projects of submillimeter CARM's are considered.

1. Principles of CARM operation

The cyclotron autoresonance maser (CARM) [1-3] represents simultaneously an efficient modification of two types of the short-wave relativistic HF devices: cyclotron resonance maser (CRM) and free-electron maser (FEM). Electrons in the interaction space of CARM (Fig.1b) move along helical trajectories in a homogeneous magnetic field like in another (higher-developed) CRM modification - gyrotron (Fig.1a). By virtue of the well-developed strong homogeneous magnetic fields technology the cyclotron frequency of the electron oscillations ω_H can be very high. Besides, electrons in CARM interact at the conditions of the cyclotron resonance with an electromagnetic wave propagating unlike in the gyrotron not across but nearly along particles translation motion. So, at relativistic translation velocities of electrons V_{II} the wave frequency greatly exceeds the cyclotron frequency due to the Doppler effect:

$$\omega \approx \frac{\omega_H}{1-\beta_{II}/\beta_{ph}} \qquad (1)$$

In formula (1) $\beta_{II} = V_{II}/c$ and $\beta_{ph} = V_{ph}/c$ are the normalized translation velocity of particles and phase velocity of the wave, respectively. It is well-known that the same effect provides high-frequency properties of another FEM modification - ubitron, where electrons move in a space-periodic magnetostatic field (Fig.1c). However, creation of a strong short-period magnetic field is essentially more difficult than of the homogeneous one. As a result, at the millimeter and submillimeter wavelength range the CARM requires particle energies significantly lower

than those for the ubitron, and magnetic fields smaller than those for the gyrotron. According to this, in a number of cases CARM seems to be an optimal solution [4-9].

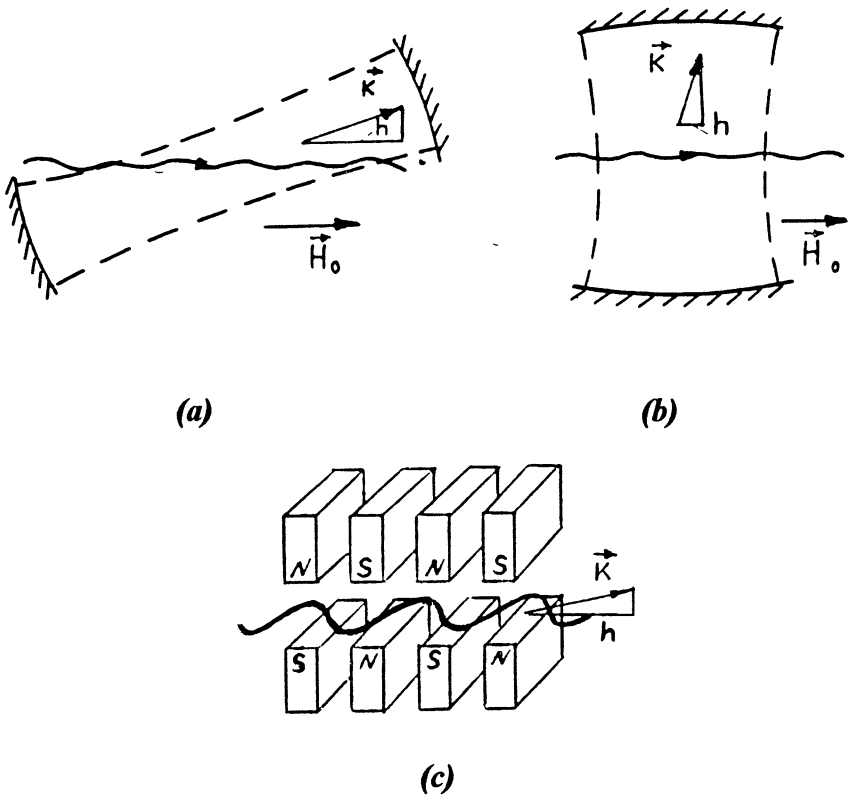

Figure 1. Simplest schemes of: (*a*) CARM, (*b*) gyrotron, and (*c*) ubitron

2. Electron-optical and electrodynamic problems in the elaboration of the effective CARM

Besides the Doppler frequency up-conversion, another consequence of the quasi-longitudinal propagation of the wave in CARM (when the wave phase velocity is close to the velocity of light) is partial autoresonance [10,11] compensation of the variation of cyclotron frequency $\Delta\omega_H$ by the Doppler shift $\Delta(hV_{II})$. By virtue of this compensation the electrons resonantly interact with the wave even at considerable variations of their energies and CARM efficiency at large enough rotational velocities of particles $\beta_\perp \sim \gamma^{-1}$ ($\gamma = \mathcal{E}/mc^2$ is relativistic factor of electrons) can be some tens per cent. It is due to the same reason that CARM is characterized by small sensitivity to particle energy spread. But like other FEL's and FEM's, CARM is very sensitive to the spread in the pitch angles of particles. Indeed, the spread is acceptable only when the phase shifts of various electrons $\Theta = (\omega - hV_{II} - \omega_H) L/V_{II}$ during their interaction with the wave differ from one another by less than 2π. This imposes the following restriction

$$\frac{\delta\beta_\perp}{\beta_\perp} \le \frac{1}{4bN} \quad , \tag{2}$$

where N is the number of gyrorotations, $b = \dfrac{\beta_\perp^{\,2}}{2\beta_{II}\beta_{ph}(1-\beta_{II}/\beta_{ph})}$ is a parameter characterizing electron recoil during radiation. Numerical calculations confirm estimation (2).

Thus, in order to attain high electron efficiency in CARM, the electron-optical system must produce an electron beam with a sufficiently great rotational velocity of particles at the small spread. The beam may be tubular, plane or thin-solid depending on the type of the microwave system and operating mode.

Another problem that is essential in realization of an efficient CARM is suppression of excitation of the parasitic modes. The gyrotron and backward waves are usually most difficult to suppress. In principle, this problem can be solved by using as an operating mode a lower mode of a regular waveguide in the regime of tangential dispersion characteristics of the wave and of the beam, or in a regime close to it. In a number of cases it appears more natural to employ higher modes, although this requires, generally speaking, development of effective methods for suppressing low-frequency generation, for example, a use of an open waveguide as a highly selective microwave system .

3. Experimental investigations of CARMs at millimeter wavelengths

Early experiments [12] demonstrated the short-wave properties of CARM. For relatively low energies of 350-600 keV and magnetic fields of 10-20 kOe, the chosen modes: $H_{1,1}$, $H_{2,1}$ and $H_{4,1}$ of cylindrical resonators with Bragg mirrors were excited selectively at the wavelengths ranging from 4.5 mm to 2.4 mm with the output power on the order of 10 MW.

A high amplification coefficient in the absence of parasitic generation was obtained in the joint experiment of the Institute of Applied

Physics of the Russian Academy of Sciences (IAP) and the Institute of High-Current Electronics on the first CARM-TWT [13,14]. The experiment was performed on the high-current direct-action "Sinus-6" accelerator employing an electron beam with energy 500 keV, current 0.5 kA and pulse duration 25 ns. The $H_{1,1}$ -mode of a circular waveguide in the regime of tangential dispersion characteristics of the wave and beam was used as an operating mode. The amplified external signal with the wavelength 8.2 mm was injected into the operating waveguide by means of a directional coupler. The amplification amounted to 30 dB with the maximum output power 10 MW and efficiency 4 %. Similar results were obtained in the investigation of the CARM-TWT in MIT [15].

New experimental investigations of CARM-generators are now carried out on the "Sinus-6" accelerator at IAP and on the LIA-unit at the Joint Institute of Nuclear Research (JINR). These investigations are aimed at producing efficiencies that will be much higher than those in the early experiments. For this purpose improved kickers are used to provide greater rotational velocities $\beta_\perp \approx \gamma^{-1}$ with smaller spread and the spread influence is decreased by shortening the length of the interaction space down to N~5-7.

In the joint experiment of the IAP and JINR that was carried out at the LIA-unit in Dubna a thin solid electron beam with energy 1-1.2 MeV and current 300-500 A produced in a co-axial diode with magnetic insulation was used [17]. The beam acquired the rotational velocity $\beta_\perp \leq 0.3$ in the kicker in the form of two rectilinear currents of opposite directions which were located perpendicular to the beam on its both sides at the distance of a half of the Larmor step $1/2\, L_H$ from one another

(Fig.2). The lower $H_{1,1}$ -mode of a cylindrical Bragg resonator 10 mm in diameter was used as the operating mode.

Two generation regimes were realized in the experiment. In the first regime (point 1 in Fig.2b), the electron energy was 1.2 MeV and the magnetic field 10 kOe. Correspondingly, the dispersion characteristics of the beam and the wave intersected in two points. With sufficiently great reflection coefficients and short length of the interaction space the operating mode with the wavelength 4.4 mm was excited. However, besides that mode a rather powerful radiation at close frequencies was also observed throughout all the band of cyclotron resonance Δf ~20% and did not disappear even without Bragg mirrors. The radiation power at the operating wavelength was 50 MW with efficiency 8 %.

In the second regime (point 2 in Fig.2b), the electron energy was 1.0 MeV and the magnetic field, 7 kOe. The dispersion characteristics of the electron beam and of the wave did not intersect (the characteristic of the beam was slightly lower than the tangential point). In that case the power of parasitic radiation was much lower and the radiation efficiency at the 6-mm wave corresponding to high-Q oscillation of Bragg resonator was higher: the radiation power amounted to 30 MW with efficiency 10%.

Experiments performed at the "Sinus-6" accelerator employed a thin tubular electron beam having the energy of 400 keV and current 600 A that was produced in a co-axial diode with magnetic insulation [16]. Special attention at the new stage of this experiment was paid to investigation of the quality of the electron beam, formed in the field emission injector as well as to improvement of the microwave system. Initially rectilinear tubular electron beam having thickness 0.3-0.5 mm

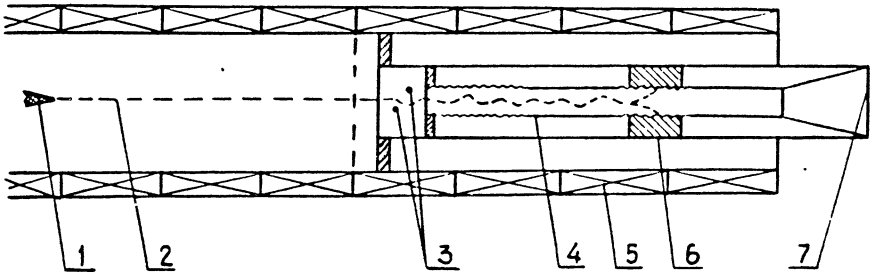

(a)

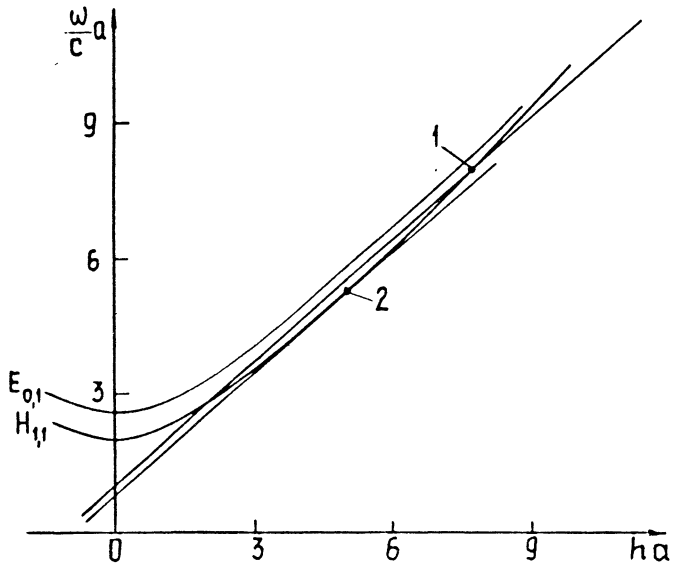

(b)

Figure 2. (*a*) Scheme of CARM with Bragg resonator: 1-cathode; 2-electron beam; 3-kicker in the form of two rectilinear currents; 4-Bragg resonator; 5-sectioned solenoid; 6-copper ring (magnetic screen) for magnetic field attenuation that provides electron collection; 7-vacuum window; (*b*) Brillouin diagram.

acquired rotational velocity $\beta_{\perp} \leq 0.6$ in the kicker in the form of one or two coils that were co-axial to the beam.

A two-coil kicker had the coils with opposite directions of current that were placed inside and outside the beam at the distance $\approx 1/2\, L_H$ (in the longitudinal direction) from one another (Fig.3). This kicker formed a transverse component of the magnetic field pumping electrons that was sufficiently homogeneous through the radius at the electron passing space. So, a position spread of particles (due to a finite thickness of the beam) would lead to an insignificant spread in the particles' rotational velocities at the kicker output. The calculations show that for a rectilinear 0.5 mm thick beam of electrons, moving initially strictly along the axis, the rotational velocity spread of the electrons at the output does not exceed 1-3 % in the wide band (≈ 50 %) of the magnetic guide field.

A one-coil kicker had only the outside coil, and, according to the calculation, imparts to electrons of the 0.5 mm thick rectilinear beam the operating rotational velocity with 17 % spread.

However, the advantage of the two-coil kicker disappears if electrons initially have no spread in the radii of guiding centers but the thickness of the beam is caused by existence of initial rotational velocities of particles leaving the edge of the field emission cathode under some angles to the guiding magnetic field. In this case, if phases of the gyrorotation of the particles are uniformly mixed over (0, 2π) and a maximum value of the initial rotational velocities equals to $\beta_{\perp in}$ at the input then the values of electron rotational velocities will lie between $\beta_{\perp kick} - \beta_{\perp in}$ and $\beta_{\perp kick} + \beta_{\perp in}$ after a kicker.

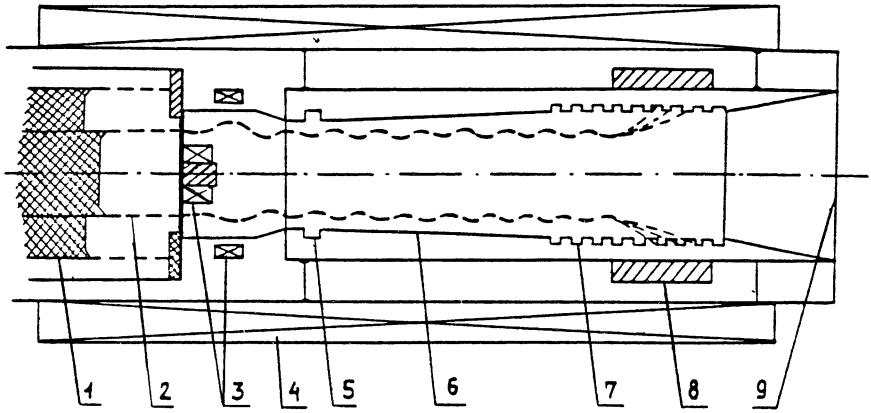

Figure 3. Scheme of the 36 GHz CARM: 1-double cathode; 2-electron beam; 3-two-coil kicker; 4-solenoid; 5-short reflector; 6-operating section; 7-Bragg reflector, 8-copper ring (magnetic screen); 9-vacuum window.

The value of the rotational velocity spread in the electron beam after the two-coil kicker was measured in the experiment. Moving a thin graphite disk along the longitudinal axis **Z** (Fig.4) we measured the current passed over the disk at fixed values of the magnetic field, the electron energy and the kicker coils current. For a perfect thin electron beam without any spread in the rotational (and, correspondingly, in the translation) velocities of particles (Fig.4a) the dependence of the passed current on the distance Z_D looks like a step-periodical function with the period equal to the Larmor step (Fig.4b). The particles' trajectories begin to mix in the presence of the translation velocity spread and at the difference between gyrophases π the beam become homogeneous along **Z**-axis of about the Larmor diameter thickness (Fig.4c). The trajectory

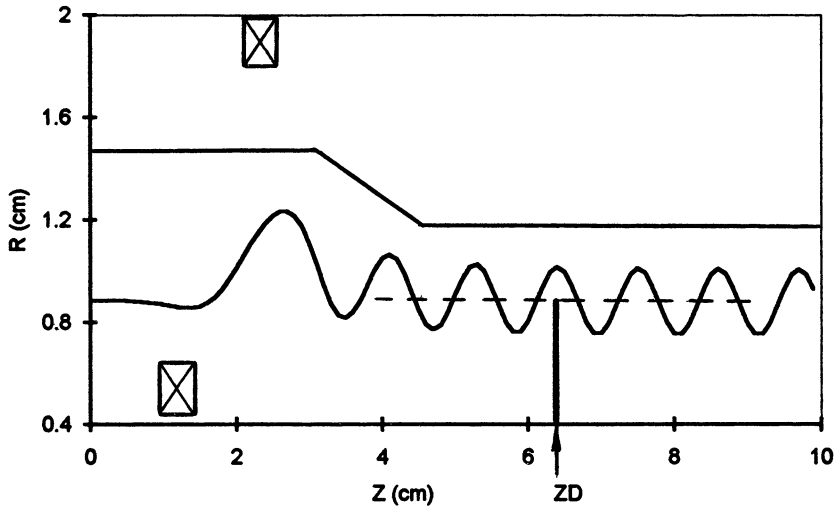

(a)

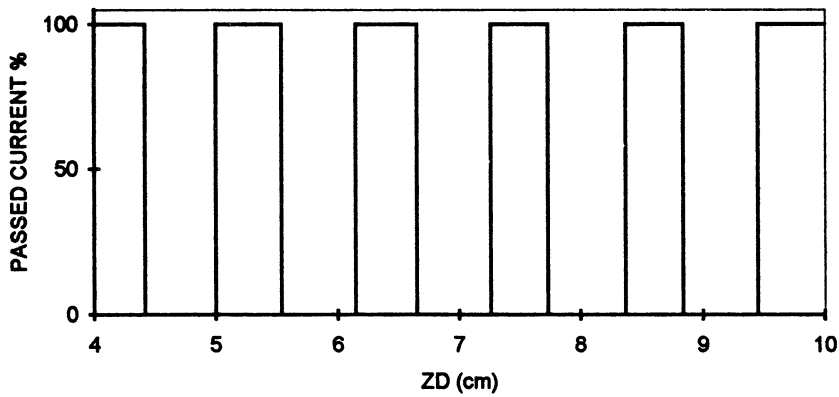

(b)

Figure 4. (*a*) An electron beam without any spread in the two-coil kicker; (*b*) Current passed over the disk for the perfect beam vs distance to the disk.

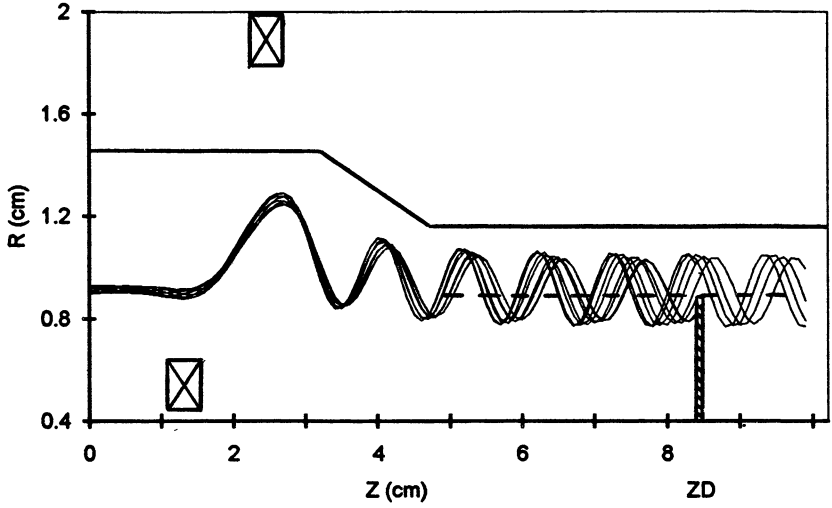

(c)

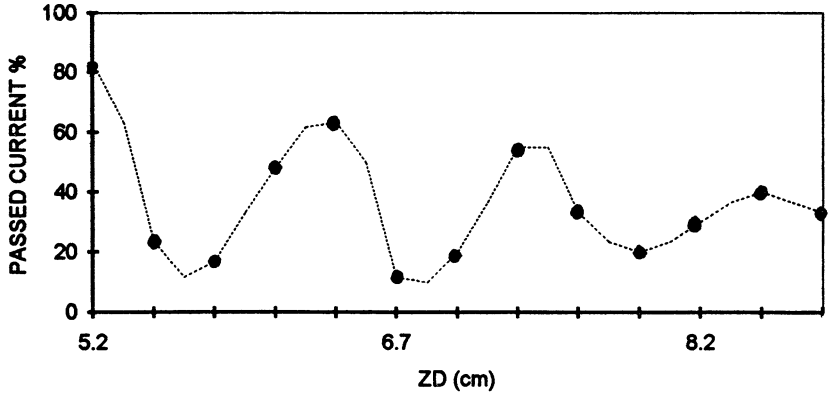

(d)

Figure 4. (*c*) Calculated electron trajectories in the two-coil kicker $\beta_{\perp in} = 0.05$; (*d*) Current passed over the graphite disk vs distance to the disk (experimental results).

analysis shows that the experimental results (Fig.4d) correspond to the value of the rotational velocity spread in the beam of about 20 %. In the case of the two-coil kicker this spread value can be explained by the presence of parasitic initial oscillations in the beam of magnitude up to $\beta_{\perp in}$ =0.05. Experiments on realization of the CARM-oscillator employing this electron beam showed insignificant difference in the level of the obtained efficiency at using of the one-coil and two-coil kickers, which also proved the truth of stipulating large particle velocity spread by the presence of the essential initial oscillations in the electron beam provided by the field emission injector.

A sufficiently high mode of a cylindrical waveguide $H_{5,1}$ was used as an operating mode of the CARM-oscillator. In this case, as seen in the Brillouin diagram (Fig.5), the parasitic excitation of lower modes at the quasi-critical frequencies (especially $H_{3,1}$ mode according to the preliminary calculations) presents a serious danger. That is why special measures to prevent the gyrotron low-frequency generation were taken.

A 2° tapered section of a conical waveguide was used as an operating part of the CARM cavity (see Fig.3), and allowed to increase considerably start current of the parasitic oscillation in compare with the case of the use of a regular cylindrical waveguide. Start current of the operating mode increases in a much smaller degree and, according to the calculations, due to favorable distribution of the operating wave phase velocity, the electron efficiency grows 1.8 times and reaches 30 % at the consideration of the electron beam without velocity spread of particles.The "hot" experiments confirmed the danger of the gyrotron generation and the possibility of its suppression using the conical section.

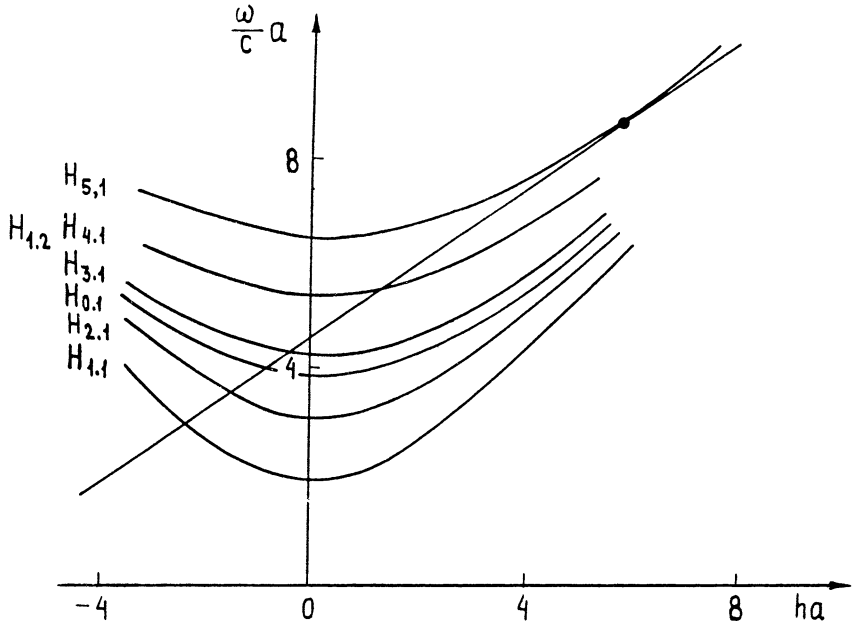

Figure 5. Brillouin diagram of the 36 GHz CARM

A new thing in this experiment was employment of a very short reflector for the operating mode (see Fig.3) [18]. The operation principle of such a reflector is based on the resonance reflection from a subsidiary cavity of the operating wave connected with an eigenmode of this cavity (in this case $E_{5,1}$ mode). The use of this short reflector at the cathode side of the CARM cavity allowed to essentially shorten the oscillating electron beam length, what simplified the gyrotron excitation suppression. The cathode-side reflector provides a reflection of the $H_{5,1}$ mode in frequency band of about 2 % with maximum reflection coefficient close to 100 % at 36 GHz frequency.

On the collector side of the cavity, where the electron beam was collecting on the walls, a comparatively long traditional Bragg reflector with the 5 % frequency band and 85 % reflection coefficient was used.

The frequency f = 36 GHz and the quality $Q \approx 1000$ of the two-reflector CARM cavity were measured in the "cold" microwave experiments and were in a good agreement with the calculations.

As a result of the "hot" experiments the generation of the $H_{5,1}$ mode at the operating frequency 36 GHz (the wavelength $\lambda \approx 8.3$ mm) with maximum output radiation power of 25 MW (corresponding efficiency above 10 %) was obtained. HF energy in a radiation pulse (Fig.6) was measured by a calorimeter and the pulse shape and duration which was 10-15 ns were controlled using a crystal microwave detector.When the particle rotational velocities was larger than $\beta_\perp = 0.45$ the gyrotron low-frequency generation with the power 2-3 times higher than in the operating mode and the radiation pulse duration 20-25 ns approximately equal to that of the current pulse was observed. Besides, at the operating regime insignificant admixture of higher frequency radiation with the wavelengths up to 4-5 mm (Fig.6b) was observed. The parameters of this radiation depended weakly on the microwave system. Because of a rather large electron rotational velocity the higher cyclotron harmonics radiation could occur like in some other CARM experiments [19].

4. Possibilities of advance into submillimeter wavelength range

The use of the axial-symmetrical Bragg cavities (in the form of circular waveguide section) in the CARM-oscillators driven by thin solid

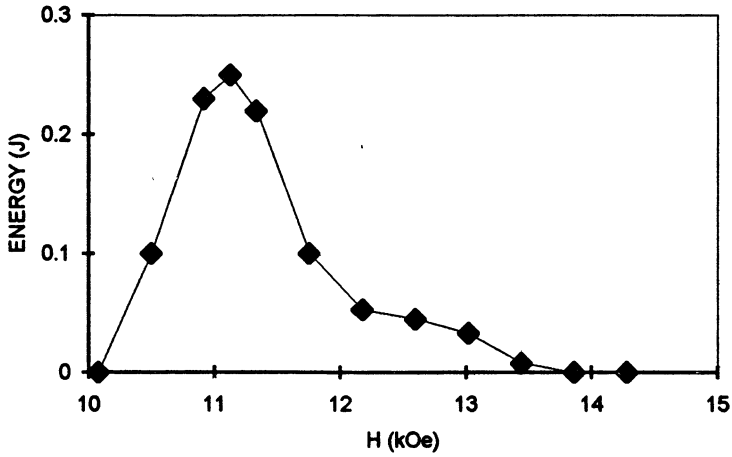

(a)

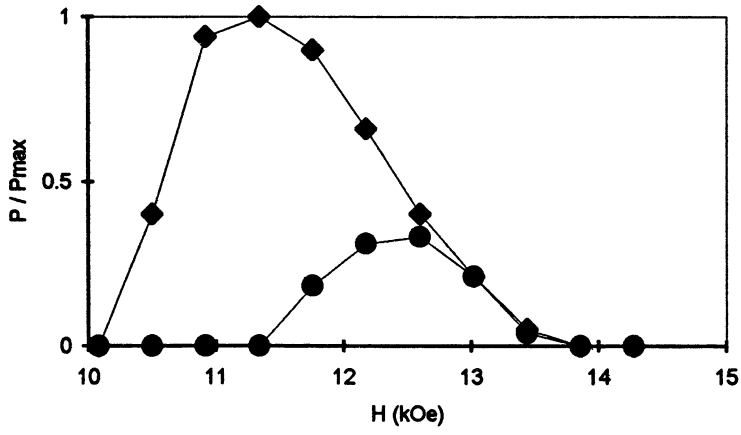

(b)

Figure 6. Experimental results of the 36 GHz CARM investigation:
(*a*) energy in a radiation pulse vs guiding magnetic field;
(*b*) Peak radiation power measured by a crystal detector vs the magnetic field: ♦ radiation at the operating wavelength; • radiation at wavelengths less than 8 mm.

or tubular electron beams allowed to obtain HF radiation with high level of the power within all range of millimeter waves. The shortest wavelength of 1.2 mm was obtained in the experiment [7], where the output radiation power amounted to 50 MW at the efficiency 3 %. This result, as well as our recent achievements, encourage us to develop all the submillimeter wavelength range.

At the advance into the submillimeter range a microwave system of CARM inevitably should become more overmoded and the problem of parasitic generation more acute. Under such circumstances, apparently, it is more expedient to give up the axial symmetry and to move on to more selective - open from sides - microwave systems, namely, to cavities where quasi-plane waveguides (Fig.7a) and quasi-plane reflectors of various types (including Bragg ones) (Fig.7b) are used. As operating modes of these cavities having small losses *H*-modes with the electric field parallel to the plane of symmetry (Fig.7a) should be used. For modes composed of rays propagating across Z-axis, as well as for along-propagating waves in the frame moving with their group velocity this quasi-plane waveguide looks like an open two-dimensional cavity. If the Fresnel parameter for any mode of the waveguide is small

$$N_F = \frac{b^2 \nu}{8\pi a^2} \leq 1 \qquad (3)$$

then this mode will have high diffraction losses and small Q-factor. In formula (3) a and b are waveguide cross-section dimensions (see Fig.7a), and $\nu \approx \pi n$ is the transverse wavenumber of the n-th mode. One can use this circumstance for discrimination of the low-frequency gyrotron modes in CARM operating at a high-order mode.

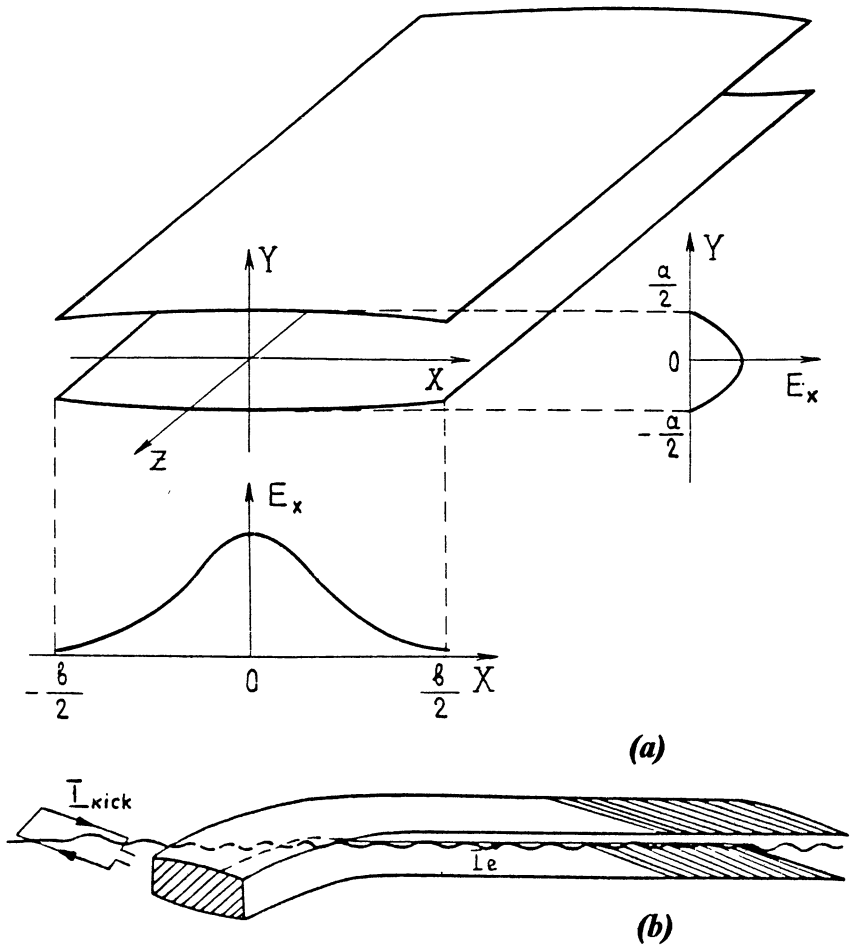

Figure 7. (*a*) open quasi-plane waveguide and its first *H*-mode; (*b*) Scheme of a submillimeter CARM.

Such an open microwave system gives flexibility in choosing a scheme of CARM. For example, there is a simple possibility to bend this open waveguide in the plane of symmetry with a comparatively small radius without operating wave losses, which allows to effectively solve the problem of splitting electron and microwave beams (Fig.7b).

As an example we consider a submillimeter CARM project based on employing existent high-current accelerators with electron energy 1.5 MeV, current about 100 A and moderate value of the magnetic field 40 kOe. At sufficiently high Doppler frequency up-conversion the wavelength λ=0.8 mm should be reached using a microwave system similar to one described above and a solid electron beam about 1 mm thick. We intend to impart the necessary rotational velocity $\beta_{\perp} = 0.25$ to electrons of initially rectilinear beam in a kicker formed by two wires like in experiment [17]. For the effective CARM operation the value of initial oscillations in the beam should not exceed $\beta_{\perp in} \approx 0.01$. As an operating mode, the third mode of the open quasi-plane waveguide (see Fig.7a) with the height a 10 times larger than the wavelength is intended to be used. The waveguide width b and their surfaces curvature radius are chosen so that the operating wave propagates with small losses but the first mode (in this case this very mode is dangerous as the parasitic gyrotron one) at frequency close to the cutoff is unstable, because its Fresnel parameter is three times smaller than those of the operating mode. By virtue of the possibility of splitting electron and microwave beams the feedback in the CARM-oscillator should be simple to realize. A 100% reflection blind metal mirror on the cathode side, a 80% Bragg reflector on the collector side (Fig.7b) and an operating waveguide section of about 150λ length should provide necessary Q-factor of the cavity and the optimal for CARM operation length at the current 100 A. A sufficiently small coupling coefficient in the Bragg reflector, i.e., small corrugation of its surface provides a narrow frequency band of the reflection, which allows to select a single longitudinal mode of the cavity and obtain a single-

frequency efficient operation. According to the calculations, the efficiency of the CARM-oscillator and the output radiation power amount 20% and 30 MW, correspondingly, without the particle velocity spread, and 10% and 15 MW at the spread $\Delta\beta_\perp / \beta_\perp$=0.1.

Using an accelerator with higher electron energy up to 2 MeV and enhanced magnetic field of 120 kOe it should be possible to create a powerful submillimeter CARM at 1.5 THz frequency (wavelength of 0.2 mm) for α-particles diagnostics of fusion plasma that has been announced to be necessary for ITER. In this CARM project, we consider a comparatively low current (10-12 A) and a very thin (0.2-0.3 mm in diameter) electron beam produced by strong compression in the tapered magnetic field. A microwave system similar to one described above providing small losses for an operating mode can be chosen. Because of a relatively low electron current the first *H*-mode of the open waveguide concentrating near the beam should be used as the operating mode. It is due to the same reason that the operation section length normalized to the wavelength and the Bragg mirror reflection coefficient should be increased up to 450λ and 90%, correspondingly, and the waveguide height decreased to 6λ in compare with the previous project. At solving electron-optical problems and producing the electron beam with rotational velocity of particles up to $\beta_\perp = 0.2$ with the spread less than 5-7 % the 1.5 THz CARM of megawatt level radiation power could be realized.

Acknowledgement

This work was supported by Russian Foundation of the Fundamental Research, Project No. 93-02-842.

REFERENCES

1. Petelin,M.I, 1974, On the theory of ultrarelativistic cyclotron self-resonance masers. Izv. Vyssh. ucheb. Zaved. Radiofiz., 17, 902-908; also in Radiophys. Quantum Electron., 17, 686-690.
2. Bratman,V.L., Ginzburg,N.S., Nusinovich,G.S., Petelin,M.I., and Yulpatov,V.K., 1979, Cyclotron and synchrotron masers. Relativistic HF Electronics, Vol. 1, edited by A.V. Gaponov-Grekhov (Gorky, U.S.S.R.: Institute of Applied Physics), pp 157-216.
3. Bratman,V.L., Ginzburg,N.S., Nusinovich,G.S., Petelin,M.I., and Strelkov,P.S., 1981, Relativistic gyrotrons and cyclotron autoresonance masers. Int. J. Electron. 51, 541-567.
4. Wang Q.S., Lin A.T., Luhmann N.S.,Jr. et.al.- in: 13th Int. Conf. on IR and MM Waves ,Conf. Digest, SPIE, 1039, Th44 (1988).
5. Fliflet,A.W., McCowan,R.B., Sullivan,C.A., Kirkpatrick,D.A., Gold,C.H., and Manheimer,W.M., 1989, Development of high power CARM oscillators. Nucl. Instr. and Meth., A 285, 233-238.
6. Mc Cowan,R.B., Fliflet,A.W., Gold,S.H., Black,W.M., Kinkead,A.K., Granatstein,V.L., and Sucy,M.S., 1989, The design of a 100 GHz CARM oscillator, I.E.E.E. Trans. on Electron Devices, 36, 1968-1975.
7. Caplan,M., and Kulke,B., 1989, Design of an induction linac driven CARM oscillator at 250 GHz. In: M. von Artenberg, ed. Conf. Digest, 14 Int. Conf. Infrared and Millimeter Waves, 420-421, S.P.I.E.
8. Bratman,V.L., Denisov,G.G., Ofitserov,M.M., Petelin,M.I., 1990, Cyclotron autoresonance masers for electron-cyclotron plasma heating in controlled fusion installations. 5th All-Union Conf. on Engin. Probl. of Fusion Reactors, Leningrad, U.S.S.R. Digest of Reports, p. 34.
9. Goodman,D.L., Birx,D.L., Danly,B.G., 1991, Induction linac driven relativistic klystron and cyclotron autoresonance maser experiments. Proc. 1991 S.P.I.E. Conference on Intence Microwave and Particle Beams, Los Angeles, January, 1991.

10. Kolomenskij,A.A., and Lebedev,A.N., 1962, Autoresonance motion of particle in a plane electromagnetic wave. Dokl. Acad. Nauk S.S.S.R., 145, 1259-1261.
11. Davydovskij,V.Ya., 1962, On the possibility of accelerating charged particles by electromagnetic waves in a constant magnetic field. Pis'ma Zh. Eksp. Teor. Fiz., 43, 886-888.
12. Bratman,V.L., Denisov,G.G., Ginzburg,N.S., and Petelin,M.I., 1983, FEL's with Bragg reflection resonators. Cyclotron autoresonance masers versus ubitrons. I.E.E.E. J. quantum Electron., 19, 282-296.
13. Bratman,V.L., Gubanov,V.P., Denisov,G.G., Korovin,S.D., Movshevich,B.Z., Polevin,S.D., Rostov,V.V., Smorgonsky,A.V., 1986, Coherent radiation of modulated high-current beam of relativistic electrons. 6th All-Union Symposium on High-Current Electronics, Novosibirsk, U.S.S.R., Symp. Digest , part 3, pp.6-8.
14. Bratman,V.L., Denisov,G.G., Korovin,S.D., Movshevich,B.Z., Polevin,S.D., Rostov,V.V., Smorgonsky,A.V., 1990, Experimental study of a CARM-amplifier. Relativistic HF electronics, Vol.6, edited by A.V.Gaponov-Grekhov (Gorky, U.S.S.R.: Institute of Applied Physics, pp.206-216).
15. Bekefi,G., DiRienzo,A., Leibovitch,C., and Danly,B.G., 1989, A 35 GHz Cyclotron Autoresonance Maser (CARM) Amplifier. Appl. Phys. Lett., 54, 1302-1304.
16. Bratman,V.L. and Denisov,G.G., 1992, Cyclotron Autoresonance Masers - Recent Experiments and Prospects. Int. J. Electronics, 72, 969-981.
17. Bratman,V.L., Denisov,G.G., Ofitserov,M.M., Samsonov,S.V. and Arkhipov,O.V., Kazacha,V.I., Krasnykh,A.K., Perelstein,E.A., Zamrij,A.V., 1992, Cyclotron Autoresonance Maser with High Doppler Frequency Up-Conversion. Int. J. Inf. and MM Waves, 13, 1857-1873.
18. Bratman,V.L., Denisov,G.G. and Samsonov,S.V., 1992, Cyclotron Autoresonance Masers - Recent Experiments and Prospects. Proc. 9th Int. Conf. on High-Power Particle Beams, Washington, 1992, 1520-1525.
19. Danly,B.G. Private Communication.

TUNABLE SOURCES OF MICROWAVE RADIATION

G. Nusinovich, B. Levush, T. Antonsen, Jr.,
A. Bromborsky*, and V. Granatstein
Laboratory for Plasma Research
University of Maryland
College Park, MD 20742 USA

1 Introduction

For many applications of high-power microwaves the frequency tunability of microwave sources is very desirable. Among these are such applications as plasma heating and current drive as well as suppression of plasma instabilities.

In principle, the development of frequency tunable microwave sources has a very long history. However, in the last decades, when microwave sources driven by relativistic electron beams and gyrodevices were developed, this issue in new devices was not studied systematically enough.

The purpose of this paper is to consider in a more or less general manner the frequency tunability of high-power sources of microwaves and to illustrate this consideration with a number of examples showing the tunability in relativistic backward-wave oscillators, free electron lasers and gyrotrons.

*U.S. Army Research Laboratory, Adelphi, MD

2 How the operating frequency can be tuned

In general, all means that can be used for frequency tuning can be split into two classes: electronic means that affect the electron beam and mechanical means that affect the microwave circuit. A traditional method of electronic tuning which is widely used in backward-wave oscillators is variation of the operating voltage. In microwave sources based on coherent Bremsstrahlung radiation of electrons oscillating in external magnetic fields (gyrodevices, free electron lasers) not only voltage but also magnetic field variation can be used for frequency tuning. The methods of mechanical tuning include those shown in Fig. 1 as sliding walls of resonator structures, variable distance between two mirrors of open resonators, 'accordion'-like and 'periscope'-like slow wave structures, tuning probes, etc.

For a slow time scale frequency tuning (in milliseconds and slower) all methods can be used. For fast tuning in frequency agile microwave sources, obviously, only the tuning by deviation of the voltage is available.

To illustrate the methods discussed above it is reasonable to look at the dispersion diagrams shown in Fig. 2. In Fig. 2a the fast-wave interaction is shown, which is typical for such fast-wave devices as free electron lasers and cyclotron resonance masers (including gyrodevices). Here the dispersion curve of a smooth waveguide is described by the equation

$$\omega^2 = c^2 \left(k_\perp^2 + k_z^2\right) \tag{1}$$

and the beam line corresponds to the condition of the resonance between electron oscillations in external static fields and Doppler-shifted frequency of the electromagnetic (EM) wave

$$\omega - k_z v_z = s\Omega. \tag{2}$$

In Eqs. (1), (2) ω, $k_\perp$ and k_z are, respectively, frequency, transverse and axial wavenumbers of the EM wave, v_z, Ω and s are electron axial velocity, oscillation frequency and resonant harmonic number. As follows from Fig. 2a there are possible resonant interactions with forward ($k_z > 0$) and opposite ($k_z < 0$) waves. The partial case is

the operation near cut-off ($k_z \ll \omega/c$), which is realized in gyrotrons and involves interaction with both waves.

In Fig. 2b the slow-wave interaction is shown, which is typical for such slow-wave Cherenkov devices as traveling-wave tubes (TWTs) and backward-wave oscillators (BWOs). Here the dispersion curve of a periodic slow-wave structure, which is usually a circular waveguide with rippled metallic walls, depends on the period, d, and the height, δ, of ripples. In such a structure the EM field can be represented according to the Floquet theorem as the superposition of spatial harmonics, $\vec{E} = \sum_\ell \vec{E}_\ell e^{i\ell(2\pi/d)z}$, and correspondingly, the condition of Cherenkov synchronism between electrons and the wave can be written as

$$\omega = \left(k_{z0} + \ell\frac{2\pi}{d}\right) v_z, \tag{3}$$

where k_{z0} is the axial wavenumber of the zero harmonic. In backward wave oscillators this condition is valid for the first spatial harmonic. In Fig. 2b there are shown the cases of electron interaction with the traveling wave at the zero harmonic and with the backward wave at the first harmonic (for the last wave the group velocity, $v_{gr} = d\omega/dk_z$, is negative).

From these simple pictures one can make two quick conclusions:

1. The most attractive operation for frequency tuning is that of TWTs in the middle of their passband when in a large frequency band the condition of the beam line grazing to the dispersion curve, $v_{gr} = v_z$, is fulfilled. Also attractive is operation of fast-wave devices with traveling waves near grazing points. For fast waves the grazing condition can be written as $v_{ph}v_z = c^2$, where the phase velocity, $v_{ph} = \omega/k_z$, relates to v_{gr} as $v_{ph}v_{gr} = c^2$.

2. The less attractive for frequency tuning is operation at ends of the passband (near cut-off, at $\pi-$ and $2\pi-$ points, where $k_z = \pi/d$ and $2\pi/d$, respectively).

The grazing condition can be realized only in traveling-wave amplifiers which are more complicated devices than oscillators. Second, this operation can be very sensitive to electron velocity spread. On

the other hand, the operation near cut-off can be realized in more simple oscillators. When such oscillators (like gyrotrons) have an extended interaction space, the frequency spectrum of available modes is very dense. Therefore, by changing the operating voltage or magnetic field one can hop from one mode to another, i.e. realize a frequency step-tunable oscillator. From this point of view, operation of oscillators based on excitation of backward and opposite waves can also be quite robust and effective. We distinguish here the two cases because for backward waves $v_{ph} > 0$ and $v_{gr} < 0$, so $\vec{v}_{ph} \uparrow\downarrow \vec{v}_{gr}$, while for opposite waves $v_{ph} < 0$ and $v_{gr} < 0$, so $\vec{v}_{ph} \uparrow\uparrow \vec{v}_{gr}$.

3 General formalism

To analyze the frequency tunability of the microwave sources one can use a simple and quite general formalism which is based on consideration of Eqs. (1)–(3). Note that although Eq. (1) was written for fast waves it is also valid for the zero spatial harmonic of the slow wave if we consider operation which is far from π-point.

Let us combine the resonance conditions given by Eqs. (1), (2) into one by presenting it in the form

$$\omega - k_{z\ell} v_z = s\Omega, \tag{4}$$

where $k_{z\ell} = k_{z0} + \ell(2\pi/d)$ and for fast-wave devices $\ell = 0$, $s \neq 0$ while for slow-wave Cherenkov devices $\ell \neq 0$ and $s = 0$. Then from Eq. (1) one can find relation between changes in frequency and axial wavenumber:

$$\frac{\Delta k_{z0}}{k_{z0}} = \frac{1}{h^2} \frac{\Delta\omega}{\omega}, \tag{5}$$

where $h = k_{z0}c/\omega$ is normalized axial wavenumber. Using Eq. (5) one can find from Eq. (4) the effect of variation in all parameters on the frequency tuning:

$$\frac{\Delta\omega}{\omega}\left(1 - \frac{\beta_{z0}}{h}\right) = \frac{\omega - s\Omega}{\omega} \cdot \frac{\Delta v_z}{v_{z0}} - \ell\frac{2\pi}{d}\frac{v_{z0}}{\omega}\frac{\Delta d}{d} + \frac{s\Omega}{\omega} \cdot \frac{\Delta\Omega}{\Omega}. \tag{6}$$

Here, $\beta_{z0} = v_{z0}/c$ is the initial axial electron velocity normalized to the speed of light. The grazing condition $v_{ph} \cdot v_z = c^2$ corresponds here

to $h = \beta_{z0}$. So, this is the case when the coefficient of $\Delta\omega/\omega$ is equal to zero. This means that for operation near grazing condition one has to take into account second order terms proportional to $(\Delta\omega/\omega)^2$ that give the frequency tuning

$$\left(\frac{\Delta\omega}{\omega}\right) \sim \left(\frac{\Delta v_z}{v_z}\right)^{1/2}, \left(\frac{\Delta d}{d}\right)^{1/2}, \left(\frac{\Delta\Omega}{\Omega}\right)^{1/2},$$

which is much larger than in the general case described by Eq. (6).

Equation (6) describes the effect of possible variations in electron axial velocity, period of a slow-wave structure and electron oscillation frequency on the operating frequency of any microwave source. Now let us consider this effect in a number of high-power microwave tubes.

3.1 Backward wave oscillators

In linear electron beams the voltage variation, ΔV, causes the variation in electron axial velocities, Δv_z, which are related as

$$\frac{\Delta v_z}{v_{z0}} = \frac{1}{\gamma_0(\gamma_0+1)}\frac{\Delta V}{V}. \tag{7}$$

From here it follows that effects of electronic and mechanical tuning in relativistic BWOs cause the frequency shifts according to the following formula:

$$\frac{\Delta\omega}{\omega}\left(1+\frac{\beta_{z0}}{\sqrt{1-\kappa^2}}\right) = \frac{1}{\gamma_0(\gamma_0+1)}\frac{\Delta V}{V} - \frac{\lambda}{d}\beta_{z0}\frac{\Delta d}{d}. \tag{8}$$

Here $\kappa = k_{\perp c}/\omega$ is normalized transverse wavenumber and $\gamma_0 = 1 + eV/mc^2$ is the initial relativistic factor of electrons. From Eq. (8) it follows that as the voltage grows, the electronic tuning described by the first term in the RHS of Eq. (8) becomes less efficient since the electron velocity remains close to the speed of light even at large variations in voltage.

Consider, for example, a relativistic BWO with the operating voltage in the range of 500 kV ($\gamma_0 \simeq 2$) and the ratio of the wavelength to the slow-wave structure period, $\lambda/d = 1.5$ that corresponds to

the operation in the middle between $\pi-$ and $2\pi-$ points. For these parameters Eq. (8) gives us

$$\frac{\Delta\omega}{\omega} \simeq 0.05\frac{\Delta V}{V} - 0.39\frac{\Delta d}{d}, \tag{9}$$

that shows that mechanical tunability caused by variation in the structure period is more efficient than the electronic one.

3.2 Gyrodevices with traveling (forward and opposite) waves

In contrast to linear beam devices (like TWTs and BWOs) in gyrodevices beams are used in which electrons move in the external homogeneous magnetic field along spiral trajectories. In the general case shown in Fig. 3 the magnetron-type electron guns used in gyrodevices are double anode. The voltage applied between the cathode and the first anode is called the modulation voltage, V_m, and the voltage applied between the cathode and the second anode (resonator) is called the beam voltage, V_b. Correspondingly, using the elementary adiabatic theory of electron beams formed in such electron guns [1] one can find the effect of variation in V_m and V_b on the axial velocity of electrons:

$$\frac{\Delta v_z}{v_z} = \frac{1+\alpha^2}{\gamma_0(\gamma_0+1)} \cdot \frac{\Delta V_b}{V_b} - \alpha^2\frac{\Delta V_m}{V_m}. \tag{10}$$

Here $\alpha = v_\perp/v_z$ is ratio of orbital to axial components of electron velocity. For single-anode electron guns it is enough to assume in Eq. (10), $\Delta V_m/V_m = \Delta V_b/V_b$.

Substituting Eq. (10) into the general Eq. (6) with $\ell = 0$ one can easily derive a corresponding formula for gyro-traveling-wave devices. We will present here only its simplified version for constant magnetic fields which describes the frequency agility of these devices, i.e. the effect of frequency tunability caused by voltage deviation:

$$\frac{\Delta\omega}{\omega}\frac{h-\beta_{z0}}{h^2\beta_{z0}} = \left[\frac{1+\alpha^2}{\gamma_0(\gamma_0+1)} - \frac{1-h\beta_{z0}}{h\beta_{z0}}\frac{\gamma_0-1}{\gamma_0}\right]\frac{\Delta V_b}{V_b} - \alpha^2\frac{\Delta V_m}{V_m}. \tag{11}$$

Here the second term in square brackets accounts for the voltage dependence of electron cyclotron frequency. Recall that in the case of operation with opposite waves h is negative.

Let us illustrate this equation by considering a relativistic electron beam ($\gamma_0 \simeq 2$, $\alpha = 1$) interacting with traveling waves with normalized axial wavenumber $|h| = 0.4$. In the case of a forward-wave gyro-TWT Eq. (11) gives us

$$\left(\frac{\Delta\omega}{\omega}\right)_f = 0.7\frac{\Delta V_b}{V_b} + 0.465\frac{\Delta V_m}{V_m} \tag{12}$$

and in the case of an opposite-wave gyro-TWT

$$\left(\frac{\Delta\omega}{\omega}\right)_{op} = -0.28\frac{\Delta V_b}{V_b} + 0.1\frac{\Delta V_m}{V_m}. \tag{13}$$

Comparing Eqs. (12), (13) with Eq. (9) one can conclude that the strong dependence of the relativistic electron cyclotron frequency on the voltage leads to larger voltage tunability of relativistic gyro-traveling-wave devices than that of linear beam backward-wave tubes.

In quasioptical gyrotrons where two-mirror open resonators are used it is also possible to tune the frequency mechanically be changing the distance between mirrors, L (see Fig. 1). The modes of such resonators are formed by electromagnetic waves propagating between mirrors. Correspondingly, the mechanical tunability may be estimated by a simple formula:

$$\frac{\Delta\omega}{\omega} \simeq -\frac{\Delta L}{L}.$$

Of course, for gyrotron operation this mechanical tuning must be supplemented with magnetic field variation.

4 Free Electron Lasers (FELs)

In FELs electrons oscillate in a periodic external magnetic field with the frequency $\Omega = 2\pi v_z/d_w$ where d_w is a wiggler period (wiggler is a set of magnets or solenoids producing a periodic magnetic field).

When the pitch-ratio of electron velocity components, α, is small enough ($\alpha^2 \ll 1$) the tunability of traveling-wave FELs with variable wiggler period can be described by the following equation:

$$\frac{\Delta\omega}{\omega}\left(1-\frac{\beta_{z0}}{h}\right)=\frac{1}{\gamma_0(\gamma_0+1)}\cdot\frac{\Delta V_b}{V_b}-(1-h\beta_{z0})\frac{\Delta d_w}{d_w}. \qquad (14)$$

For instance, when the operating voltage is the same as in previous examples ($\gamma_0 \simeq 2$) and FEL operates with the frequency up-conversion $\omega/\Omega = 2$ that corresponds to excitation of the forward traveling wave with $h \simeq 0.58$, Eq. (14) gives us

$$\frac{\Delta\omega}{\omega}\simeq -0.376\frac{\Delta V_b}{V_b}+1.13\frac{\Delta d_w}{d_w}. \qquad (15)$$

So, again, one can conclude that for these parameters mechanical tuning is, in principle, more efficient than the electronic one.

5 Effect of frequency tuning on the efficiency

For operation of practically all sources of microwaves the important parameter is a detuning of synchronism between electrons and EM waves. Given above Eqs. (2)-(4) describe the exact synchronism, however, efficient operation of electron beams with EM fields in such devices as TWTs and BWOs, gyrodevices and FELs usually takes place at a certain mismatch of synchronism, which corresponds to formation of electron bunches in the decelerating phase of the EM field. Since the frequency tuning may change this mismatch it can lead to degradation in the efficiency of operation.

To study this effect it is necessary, in principle, to analyze a set of equations which describe the operation of a microwave tube and are different for every specific device. However, there is, at least, one specific regime of operation when all devices discussed above can be described by the universal set of equations. This regime is often called 'operation with the dominant inertial bunching' [2] that means the operation when small changes in electron energy caused by interaction with the EM field lead to significant phase bunching of electrons.

Introducing this phase according to Eq. (4) as $\theta = (\omega - k_{z\ell}v_z - s\Omega)t$, one can present the corresponding set of equations for traveling wave devices in the form:

$$\begin{cases} \frac{d^2\theta}{d\zeta^2} & = & \mathrm{Re}(Fe^{i\theta}) \\ \frac{dF}{d\zeta} + i\Delta F & = & \pm\frac{1}{\pi}\int_0^{2\pi} e^{-i\theta}d\theta_0. \end{cases} \tag{16}$$

Here dimensionless axial coordinate ζ, mismatch Δ and field amplitude F are normalized to the beam current parameter. Interaction with the forward wave is described by the equation for wave excitation (14b) with sign + in its RHS and the corresponding boundary condition is $F(\zeta = 0) = F_0$. Interaction with the backward/opposite wave is described by this equation with sign − in its RHS and the boundary condition $F(\zeta = \zeta_{out}) = 0$. For electrons in both cases the boundary condition is homogeneous distribution in phases at the entrance: $\theta(\zeta = 0) = \theta_0$ where $0 \le \theta_0 < 2\pi$.

Integrating Eq. (16) one can determine the normalized efficiency

$$\hat{\eta} = \frac{1}{2\pi}\int_0^{2\pi} \frac{d\theta}{d\zeta}\,|_{\zeta=\zeta_{out}} d\theta_0 \tag{17}$$

which is related to the electron efficiency, η, as

$$\eta = C\gamma_0(\gamma_0 + 1)\hat{\eta} \tag{18}$$

where C is the Pierce parameter (C^3 is linearly proportional to the beam current and the coupling impedance of electrons to the EM field). The expressions for the Pierce parameters can be found: for linear beam Cherenkov devices - in [3], for gyrodevices - in [4], for FELs - in [5].

When the normalized efficiency is optimized with respect to the mismatch Δ in the operating point, the variation in parameters around this point, as follows from Eq. (18), affects on the electron efficiency as

$$\frac{\Delta\eta}{\eta} = \frac{2\gamma_0 + 1)(\gamma_0 - 1)}{\gamma_0(\gamma_0 + 1)} \cdot \frac{\Delta V_b}{V_b} + \frac{\Delta C}{C}. \tag{19}$$

Here the last term in RHS should be analyzed for a specific microwave tube.

6 Examples of frequency tunable designs

6.1 Relativistic BWOs with mechanical tuning

Let us consider two kinds of tunable slow-wave structures for relativistic BWOs. The first one is an accordion-like structure shown in Fig. 1. It can be manufactured as bellows. Since the total length of the structure is constant, the variation in its period causes variation in the height of ripples. For the rippled-wall radius

$$R = R_0 \left\{ 1 + \delta \cdot \cos\left(\frac{2\pi}{d} z\right) \right\} \tag{20}$$

this corresponds to the condition

$$d \left[1 - \left(\pi \delta \frac{R_0}{d} \right)^2 \right] = \text{const.} \tag{21}$$

The second structure is a periscope-like structure also shown in Fig. 1. It may consist from N sliding elements. Each of them contains one period of the structure with the fixed height. In such a structure the variation in its period, d does not affect on its ripples height.

These two kinds of slow-wave structures were studied using the code described in [6] for a 1.5 GHz frequency range relativistic BWO driven by 500 kV, 100 A electron beam. Results are presented in Fig. 4, where the operating frequency is given as the function of the period of slow-wave structure for three cases: one is accordion-like structure with variable height, δ, two others are periscope-like structures with two particular values of the height δ. From Fig. 4 it follows that the most efficient version is the periscope-like structure with $\delta = 0.273$. The coupling of this structure to electron beam depends on its period very slightly. In such a structure the 40% change in the period leads to the 13% frequency tuning.

6.2 Sheet electron beam tapered FEL with the electronic tuning[7]

This design has been studied in the frame of the program of the development of 94 GHz FEL with a sheet beam configuration at the

Laboratory for Plasma Research, University of Maryland. The 10-13 A, 500 keV electron beam with the cross-section 0.1 × 2 cm^2 is placed into rectangular waveguide 0.32 × 4 cm^2 operating at the TE_{01}-mode. The wiggler parameters are: total length 200 cm, the length of the first, untapered section 74.5 cm with the period d_w= 0.96 cm, the wiggler field is about 5 kG.

The results of the study of frequency tunability are presented in Fig. 5 where circles show results of voltage optimization at each frequency when the beam current is fixed (10 A) while diamonds show results of both voltage and current optimization for the maximum efficiency, at each frequency. Figure 5 a shows the optimal voltage as the function of frequency. Figure 5b and c show, respectively, the corresponding dependence of the efficiency and output power (for 1 kW input power). Here the optimal current is 12-13 A. The results presented demonstrate 20% tunability with more or less the same efficiency and output power.

6.3 Frequency step-tunable gyrotron [8]

As it was mentioned above, in gyrotrons with over-moded resonators operating near cut-off it is possible to provide the frequency step-tuning by varying the voltage or external magnetic field, and correspondingly, hoping from one mode to another. Since for millimeter-wave gyrotrons superconducting solenoids with a large inductance are used, the typical time of frequency tuning by magnetic field variation is very large. Even when an additional coil with a low inductance is used for this purpose, the typical time scale of magnetic field variation in a few percents is hundreds of milliseconds or more. Such a version of frequency step-tunable gyrotrons has been considered in [9].

Below we will consider the tunability of gyrotrons by changing operating voltages that can be realized much faster. Results presented in Fig. 6 show the map of oscillations for a 140 GHz, MW-level gyrotron operating in the $TE_{50,3}$-mode and its neighbors ($TE_{51,3}$- and $TE_{49,3}$-modes). The frequency separation between these modes is about 2% that corresponds to significant changes in the region of

microwave power deposition to plasma in large-scale tokamaks like ITER.

It is supposed that the beam voltage can be varied from 50 to 100 kV and the modulation voltage (see Fig. 3) up to 30 kV. The beam current is about 50 A, and the pitch-ratio, α, at V_b = 80 kV is 1.5. Other details of this design are given in [8].

Results presented in Fig. 6 show that each of these modes (0 mode is $TE_{50,3}$, +1 mode is $TE_{51,3}$, −1 mode is $TE_{49,3}$, etc.) has the region of stable operation where the orbital efficiency can exceed 60% (orbital efficiency shows efficiency of extraction of the energy of electron gyration). These regions are shown by hatched curves Fig. 6. Superimposing these three curves one can find voltages corresponding to efficient operation at each of these three modes. Note, that there will be an overlapping of hatched curves that means an existence of hysteresis phenomena. This means that in the region of overlapping, when voltage rises the higher mode operates with a larger efficiency and when the voltage falls the lower mode operates with a smaller efficiency.

7 Conclusion

Basic possibilities to realize the frequency tuning in high-power sources of microwaves have been considered above in a quite simple and general manner. This consideration was illustrated with a number of examples showing different versions of frequency-tunable microwave devices.

This work was supported by US DOE and US Army Research Laboratory.

References

1. Gol'denberg A.L., Petelin M.I., Radiophys. and Quantum Electron., 1973, **16**, 106.

2. Bratman V.L., Ginzburg N.S., Kovalev N.F., Nusinovich G.S., Petelin M.I. in High-Frequency Relativistic Electronics, Ed. A.V. Gaponov-Grekhov. Gorky, USSR: IAP, 1979, 249.

3. Ginzburg, N.S., Kuznetsov S.P., Fedoseeva T.N., Radiophys. and Quantum Electron., 1978, **21**, 728; Levush B., Antonsen T.M. Jr., Bromborsky A., Lou W-R, and Carmel Y., IEEE-PS, 1992, **20**, 263.

4. Gaponov A.V., Petelin M.I., Yulpatov V.K., Radiophys. and Quantum Electron., 1967, **10**, 794; Bratman V.L., Ginzburg N.S., Nusinovich G.S., Petelin M.I., and Strelkov P.S., Int. J. Electronics, 1981, **51**, 541; Fliflet A. Int. J. Electron., 1986, **61**, 1049.

5. Kroll N.M. in Novel Sources of Coherent Radiation, Ed. S.F. Jackobs, M. Sargent III, M.O. Scully. Addison Wesley Publishing Co., 1978, **5**, 115.

6. Bromborsky A. and Ruth B., IEEE-MTT, 1984, **32**, 600.

7. Levush B., Freund H., and Antonsen T.M. Jr., 15th Int. FEL Conference, August 23-27, 1993, Hague, Netherlands, Conf. Digest, 104.

8. Dumbrajs O. and Nusinovich G.S., IEEE-PS, 1992, **20**, 452.

9. Denisov G.G. et al., Frequency-tunable gyrotrons, ITER-IL-HD-6-0-21.

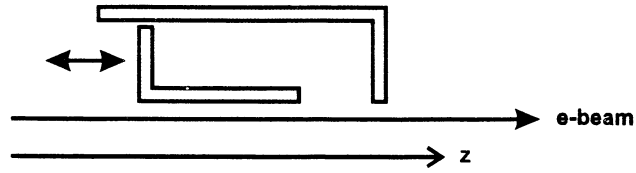

a) resonator with a sliding wall

b) open resonator with movable mirrors

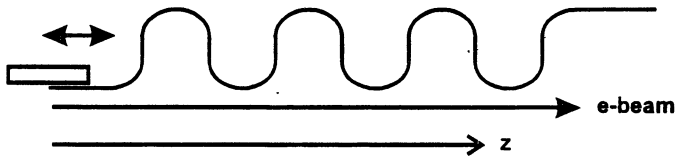

c) 'accordion' - like slow-wave structure

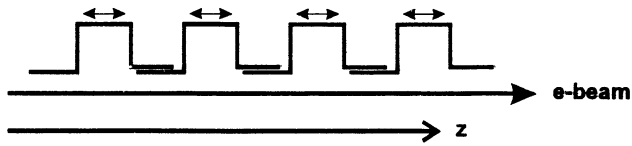

d) 'telescope' - like slow-wave structure

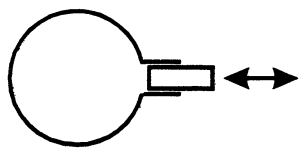

e) resonator with a movable probe

Fig. 1. Methods of mechanical tuning of the frequency.

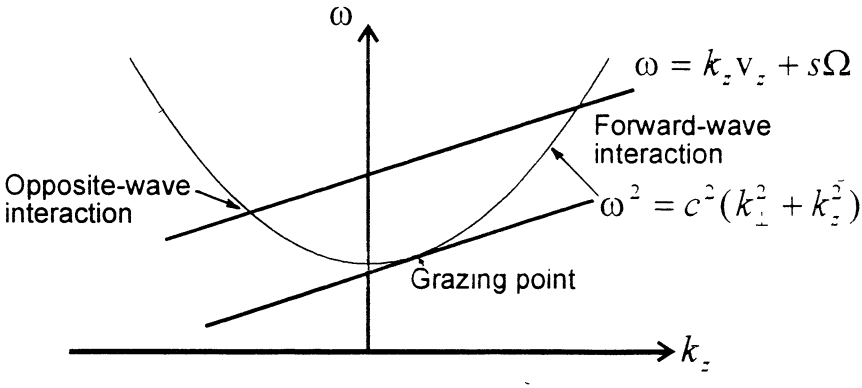

a) Fast-wave interaction

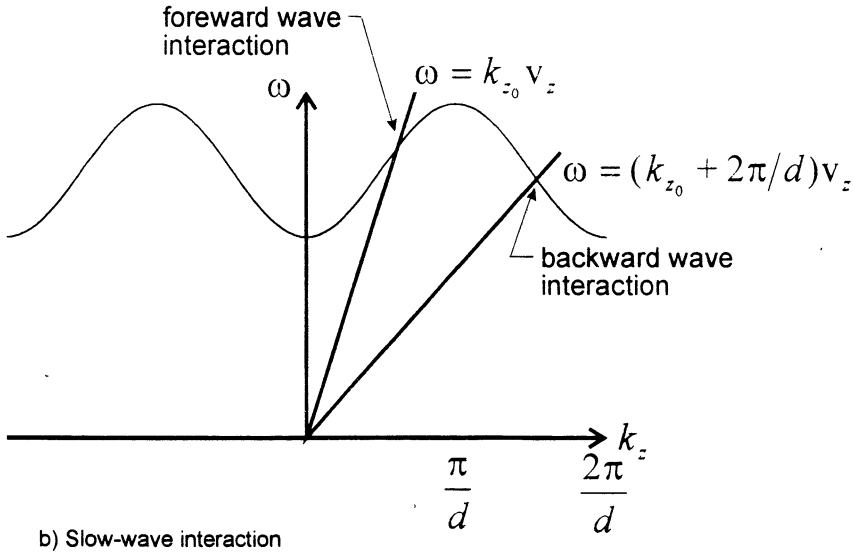

b) Slow-wave interaction

Fig. 2. Dispersion diagrams.

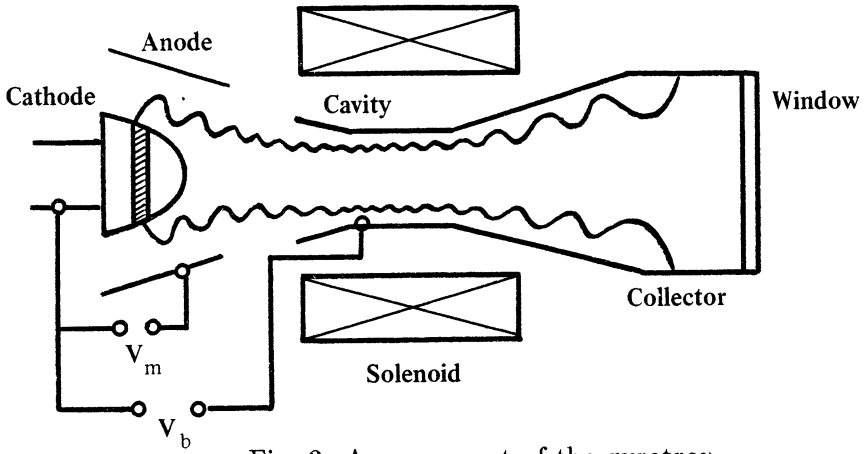

Fig. 3. Arrangement of the gyrotron.

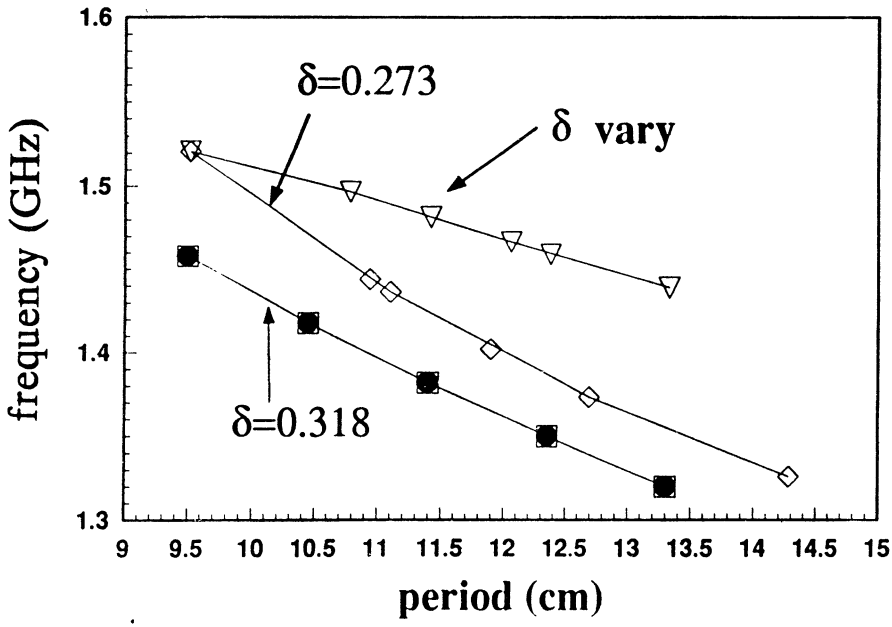

Fig. 4. The operating frequency of relativistic BWOs with mechanical tuning as a function of the slow-wave structure period.

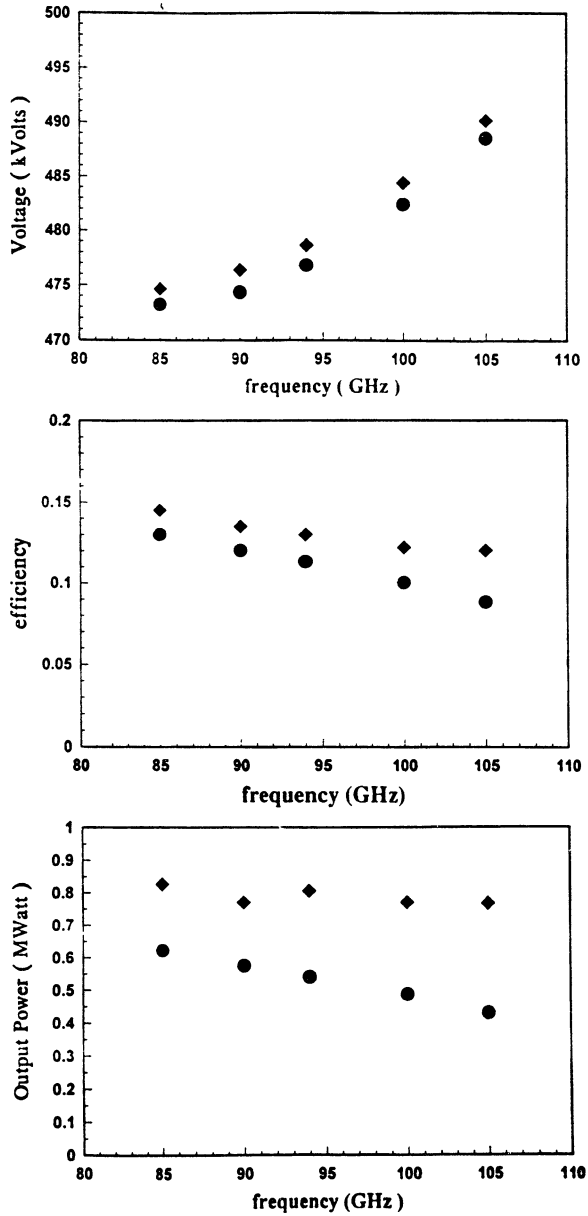

Fig. 5. Electronically tunable FEL: (a) optimal voltage, (b) efficiency, and (c) output power as functions of frequency.

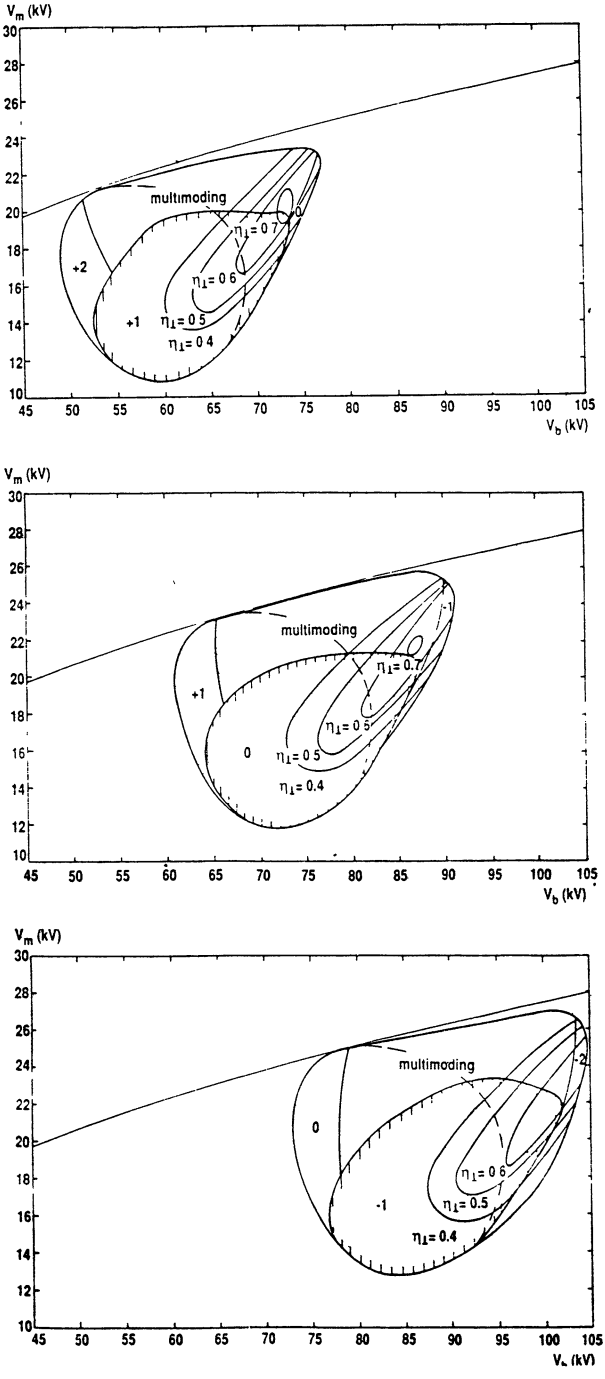

Fig. 6. Oscillation map for a frequency step-tunable gyrotron [8].

HARMONIC CONVERTER AS A HIGH-POWER SOURCE FOR PLASMA HEATING AND CONTROL

J. L. Hirshfield
Omega-P, Inc., 2008 Yale Station, New Haven CT 06520 USA; and
Physics Department, Yale University, New Haven CT 06511 USA

Abstract

The theory for production of power at a harmonic of the rotation frequency of a spatiotemporally modulated gyrating electon beam is reviewed. Simulations showing the evolution of beam parameters in a 2.856 GHz cyclotron autoresonance accelerator used to create the required beam for a harmonic converter are given, including estimates of the effects of dc space charge. Parameters derived from nonlinear multimode simulations are given for a megawatt-level 140 GHz, 13th harmonic device suitable for plasma heating.

I. Introduction

It has been evident for several years that high-power mm-wave gyrotrons have proven difficult to bring into practice. This is due to (a) the presence of serious mode competition in large-diameter overmoded resonators that are needed to accomodate high voltage beams and bring thermal wall loading down to acceptable levels, (b) diminution of potential efficiency due to irreducible axial velocity spread on high current beams, and (c) arduous spent beam collector designs needed to dissipate the huge unused beam energy. Yet mm-waves have proven useful in fusion energy research for plasma pre-ionization, bulk heating, profile control, and instability quenching. As tokamak parameters demand higher mm-wave powers at shorter wavelengths, the problems with gyrotrons will only magnify. This paper outlines an alternative to the gyrotron that may circumvent some or all of these issues, and thereby help to allow mm-waves sources to continue to play a significant role in fusion energy research.

This paper is organized as follows. Section II reviews linear and nonlinear theory and numerical simulations for the generation of radiation at the n-th harmonic of the rotation frequency for a spatiotemporally modulated gyrating beam. The beam is taken as having been prepared using a cyclotron autoresonance accelerator driven at high power with a source such as a cm-wavelength gyrotron or klystron. Examples of a nonlinear multimode simulation are given that show efficient 13th harmonic generation at 140 GHz with insignificant competition from neighboring modes. A device based on this analysis could be used for tokamak heating and control. Section III shows results of simulation studies of the phase-space evolution for a finite-emittance beam as it undergoes cyclotron autoresonance acceleration. The accelerator parameters have been chosen to yield a beam with energy, current, velocity ratio and axial velocity spread that the theory demands for a 5th - 11th harmonic converter now under construction at Yale University. For this beam, an estimate is given of the effects of space charge on spatial coherence

for the rotating helical equilibrium. Section IV contains some concluding comments.

II. Review of Theory

A theoretical exposition of the generation of coherent radiation at harmonics of the rotation frequency of a spatiotemporally modulated gyrating electron beam has been given [1-4]. This theory takes as given a beam with parameters from a cyclotron autoresonance accelerator. (See Section III.) Such a beam contains particles moving on helical orbits rotating at the pump frequency p at which the accelerator is driven, with a pitch-number $\xi = (p - \Omega)/v_z$, where Ω is the relativistic gyration frequency $eB/m\gamma$ for the electrons, and v_z is their axial velocity. These orbits cause the beam to behave as a wave having an effective axial phase velocity $v_z/(1 - \Omega/p)$, a quantity that can be larger or smaller than the speed of light. The orbits can thus be phase-matched to traveling fast guided waves. Maximization of harmonic coupling [1] leads to the additional condition $\Omega/p = 1 - \beta_z^2$, where $\beta_z = v_z/c$. This is equivalent to requiring that the axial beam velocity equals the wave group velocity. Matching to both phase and group velocity is equivalent to operating at the so-called "grazing" point in the ω-k_z plane, where most conventional gyro devices also operate.

Linear analysis for the generation of coherent radiation at frequency $\omega = mp$, where m is the harmonic index, shows that traveling-wave power can grow with z in a first-order process proportional to $I_0^2\alpha^2K_m^2(z/R)^2/\beta_z$, where I_0 is the dc beam current, α is the velocity ratio, K_m is the harmonic coupling coefficient, and R is a transverse dimension of the waveguide. In a rectangular waveguide [2], several waveguide modes can be driven at a given harmonic simultaneously. But with a cylindrical waveguide with an axisymmetric beam, it has been shown [4] at the m-th harmonic that only TE_{mn} modes will grow. This powerful selection rule helps to mitigate against mode competition at each value of m. Still, it must be shown that conditions can be found where competition between modes with different m-values is not serious.

Several important effects are omitted from the above idealized description. One is the presence of a spread in β_z on an actual beam. Another is the slippage from grazing that will occur as the beam gives up energy to a wave, and γ and v_z change. Linear theory can give an estimate of the effect on wave growth of a spread in axial velocity, showing that the growth falls to half that for a cold beam if $\Delta\beta_z/\beta_z$ exceeds $7.6N^{-1}$, where N is the number of interaction guide wavelengths. However it is clear that a nonlinear theory is needed to properly account for the full dynamics of this process, and to be able to include a tapered guide magnetic field $B(z)$ to offset the aforementioned phase slippage. Such a nonlinear theory has been developed and applied to harmonic conversion [3,4]. Numerical simulations based on this theory have explored the relevant parameters and shown that virtually all the perpendicular energy on a cold beam can in principal be drawn off into a TE_{m1} mode at frequency mp when matching is preserved along the interaction. An example of the predictions of these simulations is shown in Figs. 1 and 2 for a megawatt-level 140 GHz source

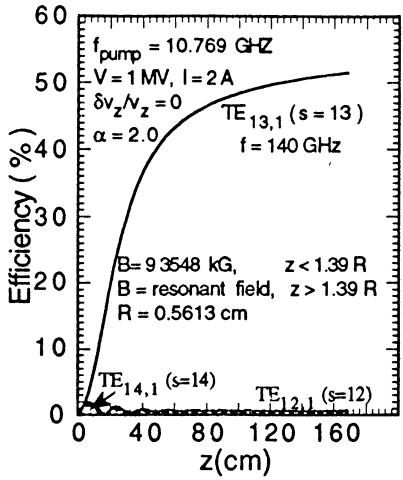

Fig. 1. Results from multimode simulation for conversion efficiencies at the 12th, 13th and 14th harmonics. Parameters are given in the Figure.

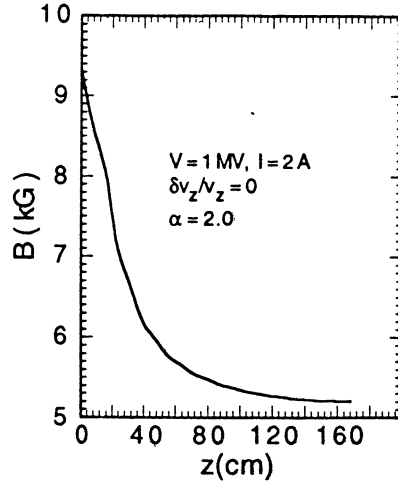

Fig. 2. Resonant magnetic field profile for the 13th harmonic example shown in Fig. 1. (Simulations for the 12th and 14th harmonic cases were run for this profile as well.)

operating with m = 13. A cold 1 MV, 2 Amp beam with α = 2.0 is chosen with a pump frequency of 10.77 GHz. It is presumed that for this an efficient 2.5 MW X-band klystron or gyrotron could be built on the basis of existing knowledge. Fig. 1 shows results from a multimode simulation [3,4] for efficiency *versus* axial coordinate z for the 12th, 13th, and 14th harmonics in the $TE_{12,1}$, $TE_{13,1}$ and $TE_{14,1}$ modes, respectively. The 12th and 14th harmonics pose the greatest threat to operation at the 13th in this case. Coupling to the 12th and 14th is so weak as to hardly be discernable on the scale of Fig. 1. The magnetic field profile is taken to be resonant, i.e. it is determined in the course of the simulation to be that field which preserves a constant phase between the wave and the gyrating electrons. The particular field profile found for the example shown here is shown in Fig. 2. The field tapers down to 5.2 kG from an initial value of 9.35 kG. (This shows quite dramatically the effect on magnetic field of operation at a high gyro-harmonic: in contrast to the cryogenic-level magnetic fields usually required for mm-wave devices, one needs here a field that is obtainable from conventional coils or from permanent magnets.)

Preservation of phase matching with the $TE_{13,1}$ mode insures that phase matching is not observed for potential competitors, such as the $TE_{12,1}$ and $TE_{14,1}$ modes. Indeed, these are shown in Fig. 1 to extract almost no power from the beam. The 13th harmonic efficiency is seen in Fig. 1 to reach about 52%, corresponding to an output power of more than 1 MW. But the efficiency grows quite slowly with interaction length after transverse energy on the beam is depleted

leading to a diminution in the harmonic coupling factor K_m. Extraction of the remaining beam energy could be achieved using a single-stage depressed collector, since the spent beam electrons are nearly monoenergetic and in phase. Alternately, the beam could conceivably be spun-up again with a non-adiabatic magnetic field cusp, and allowed to interact harmonically in a second stage output section.

The theory for gyro-harmonic generation in a cylindrical waveguide [4] has also led to the following general results:

(a) A beam with a uniform spread of guiding centers will have a rate of growth of harmonic power in the TE_{mn} mode that is no less than 90% that of a beam having no guiding-center spread if the ratio of the outer guiding-center radius R_b to the waveguide radius R is less than $0.894/s_{mn}'$, where s_{mn}' is the n-th zero of $J_m'(s)$. For a 13th harmonic converter in the $TE_{13,1}$ mode, this requires R_b/R to be less than 0.060.

(b) Power transfer from a cold axisymmetric beam to TM modes is zero when the beam axial velocity and the wave group velocity are equal. For a beam with a small spread in axial velocity, nonlinear simulations have shown negligible power transfer into TM modes as well.

(c) For a linear magnetic field taper, i.e. a taper that is not exactly resonant along the interaction length, the maximum achievable efficiency is lower than for the case of a resonant taper. However, the conversion efficiency is more resiliant to axial velocity spread for a linear taper than for a resonant taper. For 5th harmonic conversion, the efficiency was found to not fall below 50% unless the axial velocity spread exceeded 14%, while for the resonant taper, efficiency fell below 40% for spreads greater than 1%.

III. Beam Formation

On the basis of the theory and numerical simulations, experiments have been designed for 5th - 11th harmonic conversion using a 20 MW, 2.856 GHz driver. The optimum beam energy range for these experiments is in the range 300-600 keV, with α in the range 1 - 2. A 100 keV axially-directed beam from a convergent-flow Pierce gun with perveance 1.2×10^{-6} is to be injected into a cyclotron autoresonant accelerator [5]. Here, a $TE_{1\,1}$ mode traveling wave remains in phase with the beam during acceleration by the use of a carefully tailored magnetic field up-taper. Prior studies have shown that, in this way, beams can be produced up to a limiting energy that depends on the wave's phase velocity [6]. This limit arises since the rf magnetic field of a fast wave is incapable of overcoming the radial component of the tapered guide magnetic field, the net result of which is axial deceleration of the beam. Acceleration can progress to higher energy as the wave's phase velocity is reduced towards c, but higher order waveguide modes pass above cutoff as this occurs, thereby complicating the interaction. Prior studies did not examine growth in axial velocity spread as the limiting energy is approached, and as the mean axial velocity decreases. Results are presented here that show these important details. The accelerator waveguide radius was chosen to be 4.8 cm, a value that allows the TM_{01} mode to propagate, as well as the TE_{11}. This reduces the TE_{11} mode phase velocity and increases the limiting energy

somewhat from its value when the TM_{01} mode is cutoff. It also leads to a greater acceleration length, with a concomitant lower (and more conveniently arranged) magnetic field gradient. Coupling to the TM_{01} mode should not be significant, due to its azimuthal orthogonality with the TE_{11} mode.

For the example to be shown in Figs. 3-7, an injected monoenergetic 30 Amp, 100 keV beam with an initial axial velocity spread of 0.5% is assumed. These parameters are close to what is expected from the Litton L5892 gun being employed in the experiments. The guide magnetic field is specified along the interaction length so as to preserve phase matching for electrons with the mean axial velocity and energy. The energy gain thus varies, depending upon deviations from the mean. Fig. 3 shows the growth in mean energy, in terms of the Lorentz factor γ, as a function of axial coordinate z (in cm). Growth from 100 keV to 613 keV is shown, over a length of 53 cm. In Fig. 4, the profile of axial magnetic field is shown, rising from 708 to 1580 G along the acceleration length. Fig.

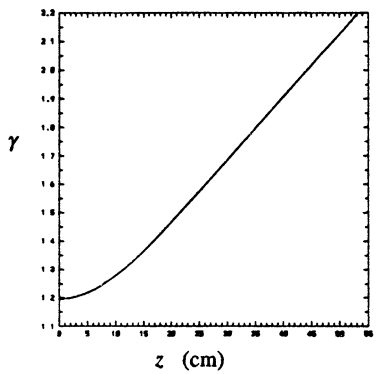

Fig. 3. Relativistic energy factor γ as a function of acceleration length z. See text for parameters.

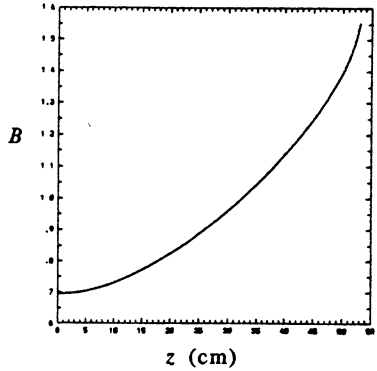

Fig. 4. Magnetic field B as a function of axial distance z along accelerator. Units of B are kG/1.096.

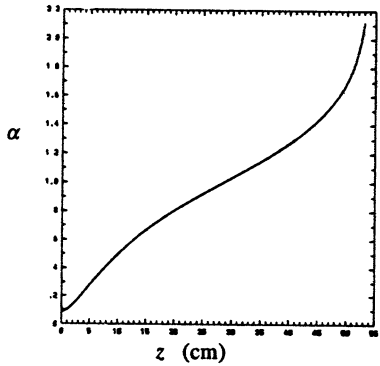

Fig. 5. Velocity ratio α as a function of axial distance z along accelerator.

5 shows the mean value of velocity ratio α as a function of z. The rapid rise in α towards the end of the acceleration is due mainly to a diminution in axial velocity, as is shown in Fig. 6. Finally, the growth of axial velocity spread is shown in Fig. 7, rising from an initial value of 0.45% to (1.0, 1.5, 2.0)% at distances of (37.0, 42.7, 46.5) cm, and at mean energies of (434, 496, 537) keV. At a beam current of 30 Amps, the accelerator efficiency would be (50, 59, 66)%. If a beam energy below 434 keV is desired, this can be

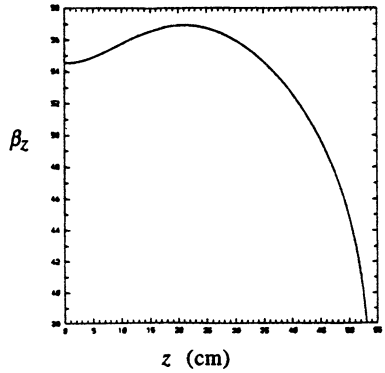

Fig. 6. Normalized axial velocity β_z as a function of distance z along the accelerator.

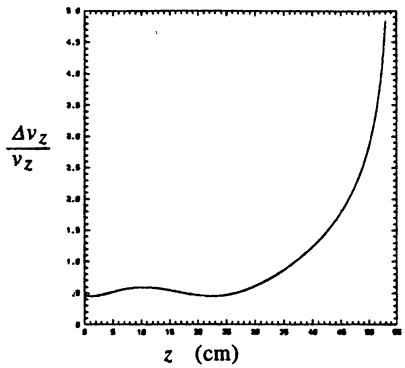

Fig. 7. Normalized rms axial velocity spread (in %) as a function of distance z along the accelerator.

achieved with an accelerator shorter than 37 cm, or with lower rf drive power. These results indicate that beams with the desired energy, current, velocity ratio α, and velocity spread can be created with cyclotron autoresonance acceleration under conditions as described here.

The results shown in Figs. 3-7 do not include the effects of either dc space charge fields or self magnetic fields. The space charge electric field will tend to disperse the particles along the field lines, and thereby to smear out any well-defined spatial feature. This tendency is opposed by the self magnetic field, which will tend to cancel fully the influence of the electric field as the electron speeds approach c. The quantitative effect of these fields on the beam equilibrium can be estimated by finding an approximate axial force on an electron at the beam edge. In a cylindrical coordinate system centered on the helical beam, the locally radial electric field E_r and azimuthal magnetic field B_θ are given by

$$E_r = I/2\pi\varepsilon_o r_b v_z; \quad B_\theta = -\mu_o I v_z/2\pi r_b,$$

where I is the current in Amps and r_b is the beam minor radius. The axial force on an edge electron is

$$F_z = eI\sin\phi(1 - \beta_z^2)/2\pi\varepsilon_o c\beta_z r_b,$$

where $\beta_z = v_z/c$, and ϕ is the pitch angle, which at grazing is given by $\tan\phi = \beta_z pR/c$, with R the mean helix radius. The axial acceleration can be written approximately as

$$d^2z/dt^2 = (2c^2\sin\phi/r_b\gamma_z^2)(I/I_A),$$

with $I_A = 4\pi\varepsilon_o mc^3/e = 17.05$ kAmps. This equation can be used to find the incremental distance Δz from the mean that the edge electron moves within an interaction length L. The result is

$$\Delta z = (I/I_A)L^2\sin\phi/[r_b(\gamma_z^2 - 1)].$$

This distance will exceed one-fourth the helix pitch $\lambda_o\beta_z$ when the beam current exceeds I_c, where

$$I_c = I_A\beta_z\gamma_z^2\lambda_o r_b/4L^2\sin\phi,$$

with $\lambda_0 = 2\pi c/p$, the pump free-space wavelength. For the parameters shown in Fig. 3 one finds I_c to equal 30 Amps at L = 32 cm, and to equal 15 Amps at L = 45 cm. These figures indicate that self fields can effect the equilibrium distribution of a spatiotemporally modulated beam if the current and/or interaction length are too large.

IV. Conclusions

The theory of harmonic conversion to produce high power mm-wave power from a spatiotemporally modulated gyrating electron beam has been reviewed. The results of both analysis and numerical simulation indicate that efficient high harmonic operation could be possible without undue competition from adjacent modes and other harmonics. An example of a megawatt-level 140 GHz source at the 13th harmonic was given, showing a conversion efficiency above 50% using a tapered magnetic field no greater than 9.4 kG. Power flow to the 12th and 14th harmonics was predicted to not exceed 2% of the beam power when a resonant magnetic field taper was employed.

The formation of an electron beam with parameters appropriate for harmonic conversion has been discussed. Cyclotron autoresonance acceleration using an up-tapered resonance guide magnetic field was shown to allow a 100 keV 1.2 μperv beam to be accelerated up over 500 keV without experiencing undue growth in axial velocity spread. The effects of self fields of the beam were examined using an approximate model for the force on an edge electron. Parameters typical of cyclotron autoresonance accelerators for harmonic conversion were considered. For a 30 Amp beam, it was shown that an edge electron will be displaced axially relative to a central electron by an amount equal to one-quarter of the beam's helical pitch after a drift distance of approximately 32 cm. This indicates that lower currents should be employed to maintain good beam quality.

For the 2 Amp, 1 MV beam used in the 140 GHz, 13th harmonic example, self field effects are less pronounced. This suggests that it may be possible to demonstrate harmonic conversion efficiencies comparable to those shown in Fig.1 that were computed by neglecting the self fields. If so, it could make possible a new class of mm-wave sources as possible alternatives to the gyrotron for fusion plasma heating and control.

Acknowledgements

Important contributions to the material presented in this paper were made by A. K. Ganguly, B. Hafizi, and P. Sprangle. This work was supported by the Office of Naval Research and by the Department of Energy.

References

[1] J. L. Hirshfield, Phys. Rev. A **44**, 6845 (1991).

[2] J. L. Hirshfield, Phys. Rev. A **46**, 5161 (1992).

[3] A.K. Ganguly and J.L. Hirshfield, Phys. Rev. Lett. **70**, 291 (1993).

[4] A.K. Ganguly and J.L. Hirshfield, Phys. Rev. E **47**, 4364 (1993).

[5] B. Hafizi, P. Sprangle, and J. L. Hirshfield, Proc. 1993 Particle Accelerator Conf. (to be published).

[6] C. Chen, Phys. Rev. A **46**, 6654 (1992).

One Megawatt Gyrotron Development for LHD

M.Sato, K.Ohkubo, S.Kubo, T.Takita, T.Kuroda
National Institute for Fusion Science
322-6 Oroshi Toki-shi Gifu-ken 509-52, Japan

Introduction / Whispering Gallery Tube

Large Helical Device (LHD) is being built in targeting to begin the experiment by 1998. It requires 10 megawatts 84 GHz ECRH system for initiating and heating plasma with 10 kev and 10^{20} m^{-3} electron temperature and density respectively. NIFS is developing one megawatt cw gyrotrons for LHD in two steps with Varian. The first step was a cavity mode output tube with a radial gap which extracts the spent electron beam from the waveguide to large area of 610 mm diameter collector.The tube demonstrates the operation in long pulse at 500 kw and 900 kw at short pulses as shown in fig-1.

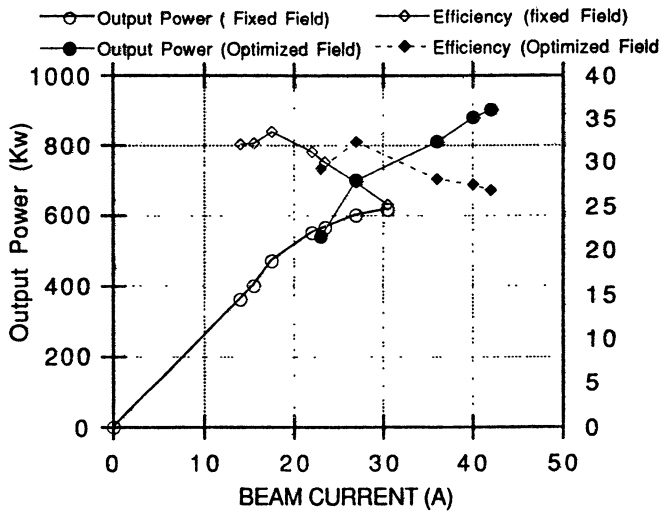

fig-1

The dynamic ranges in the rf power against operating parameters such as the beam and anode voltage, beam current and magnetic field strength, are applicably wide for daily practical use for LHD experiments. The specific heat load on the collector is less than 0.5 kw at 22 amps with 500kw output. It is low enough even to handle 40 amps beam at the cw conditions. The results show the success of designs of the electron gun, beam shaver, cavity and collector.

Build in Mode Converter Tube

Using the spare components of first tube, the second tube is under assembling. It has quasi-optical built in mode converter and mirrors. It has 4" diameter FC-75

cooled double disk window which will be able to operate pure cw at 500 kw.
The two kind of improved efficiency mode converters were considered. One is a 2 " diameter two dimensional quasi-optical converter with a Visor. The other is the so called dimple adiabatic 3 dimensional converter. The cavity region is 380 mm under the top plate of superconducting magnet. The numbers of mirrors must be placed for 3D converter. 2 D converter needs only two mirrors except for visor. Accounting all the diffraction losses, the efficiency of both converters are in same order.
Considering the merits of simple structure and short development period, 2D system is employed for the modified tube. The focus mirror generates a hybrid mode of HE11 + HE21 to the window at the expecting efficiency of 90 %. The cross-sections of converter and the cold test radiation pattern at focus mirror are shown in fig.2 (a) and (b).

fig-2 (a) Converter / Mirror Layout

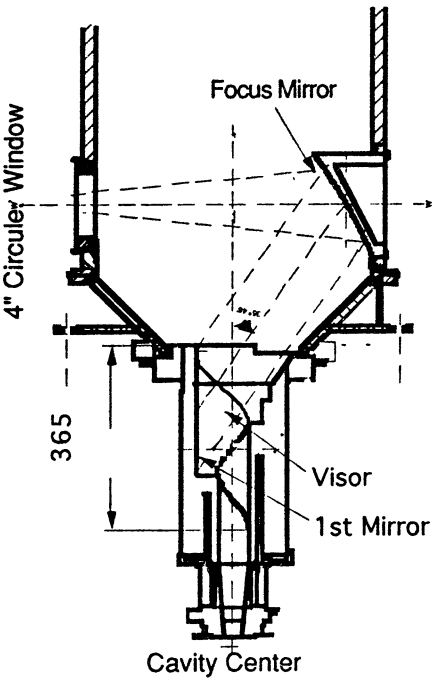

fig-2 (b) Radiation Pattern on Mirror

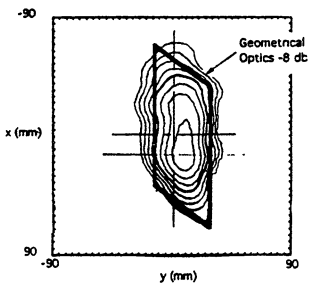

Window Development
The window is last hurdle to reach to goal of 1000 kw cw operation.
Many ideas of 1000 kw cw window have been studying in many laboratories [1] [2] .
NIFS is studying the new window materials which have higher heat conductivity and lower or equivalent dielectric loss than that of sapphire. It can realizes the edge

water cooled single disk window. Diamond is the best material, but it is very hard to make a single crysral in large size. The diamond or CBN base hybrid composite is the most realistic candidate.
The multi-crystalline diamond diaphragm can be produced by the new improved CVD method up to 0.5 mm thickness in keeping the quality in reasonable manufacturing hours. The preliminary test shows that the heat conductivity reaches to 1000 w / m k.
We can make a window disk by laminating the diaphragms by ceramic bonding. The diamond changes to graphite at about 600 deg.C in atmospheric pressure. The kind of BSiO glass is examined as bonding, since the sintering temperature of it can be reduced to lower than 600 deg.C and adjust the coefficient of thermal expansion to diamond. The problem of BSiO is its high dielectric loss. The key is how we can make thin bonding layers. Using sapphire, the technique for bonding in 5 mm thickness is under studying.

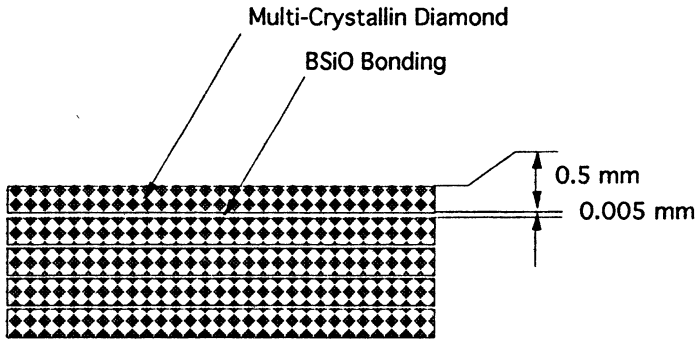

fig-3 Schematic Viev of Diamond Disk

The maximum microwave power through the window disk is estimated, assuming to consists of five layers of each 0.5 mm thickness diamond and 0.01 mm BSiO layers inserting in a waveguide of 100 mm diameter cooled by water from outsid. Total 5 kw rf absorption increases the central temperature up to 270 deg.C. Improving the edge cooling condition, it can handle more power.

Another material is CBN-Al_2O_3 multi-crystallin composit. The CBN is stable up to 1300 deg.C. Applying 28 GHz gyrotron, it is reported that Al_2O_3 can sinter at below 1250 deg.C. [3] The weight fraction 50,90 and 95%of CBN with Al_2O_3 is trying to sinter in the 28 GHz 10 kw microwave oven. If we succeed in the sintering, we can expect material with 100-200 w / m k and with low dielectric loss as sapphire. It can be applied to surface-cool double disks window handling 1000 kw cw microwave.

[1] C.Moeller: Distributed Windows,Proc. 2nd Biennial Workshop on ECRH Transmission Line Systems, San Diego, 1992

[2] T. Yamamoto, et al; Development of Cryogenic Window for High Power Millimeter Wave, ,Proc. 2nd Biennial Workshop on ECRH Transmission Line Systems, San Diego, 1992
[3] M. Janny, et al ; Diffusion Controlled Processes in Microwave fired Oxide Ceramics, MRS symposium Proc. Vol189, 1990, p215

USE OF FREQUENCY-TUNABLE MICROWAVE SOURCES FOR PLASMA DIAGNOSTICS

O. Dumbrajs, J.A.Heikkinen, and K.Sarparanta
Nuclear Engineering Laboratory,
Helsinki University of Technology, SF-02150 Espoo, Finland

In the fusion machines, microwaves in the frequency range 30 GHz to 1 THz are used for electron heating, plasma start-up assist, control of plasma disruptions and MHD modes, and diagnostics of the plasma parameters. To have a well localized absorption in plasma heating and possibilities for varying the scattering geometry in diagnostics, special requirements for frequency spectrum of microwave sources have to be satisfied. The present work discusses the needs of frequency-tunable sources for plasma diagnostics based on collective scattering with particular emphasis on the use of gyrotrons.

1 Frequency tuning in scattering diagnostics

A. Resolving wave vectors. Because of recent technical developments the collective Thomson scattering technique [1] appears now to be feasible for measuring radial and velocity space features of energetic ion distribution features, and many aspects of plasma turbulence. From the energy and momentum conservation laws

$$\omega_s = \omega_0 + \omega, \quad \vec{k}_s = \vec{k}_0 + \vec{k}, \tag{1}$$

one finds $k \approx 2k_0 \sin(\theta/2)$ for the fluctuation wave vector k from which the electromagnetic radiation of wave vector $\vec{k}_s$ scatters through an

angle θ from an incident wave with the frequency ω_0 and wave vector $\vec{k}_0$. This approximation for the fluctuation wave vector is valid for $\omega_0,\ \omega_s \gg \omega$. For given orientations of the emitting and receiving antennas, the scattering region, the angle θ, and the scattering wave vector $\vec{k}$ become fixed. In order to resolve the wave vector spectrum of fluctuations in the same spatial region, the measurement has to be either repeated with different antenna positions or by using several antennas. In an alternative, the incident wave frequency could be tuned to change the magnitude of the wave vector $\vec{k}$. The frequency tuning by small steps would be valuable for e.g. to evaluate the group velocity of the low frequency modes, while tuning in a wider range would be needed to resolve dispersion relations.

Because the dispersion of resonant modes can be affected by energetic ions, it has been proposed [2] to get information on ion distribution with good signal to noise ratio by measuring the resonant enhancement of scattered power. Here, we consider as an example the resonant lower hybrid waves damped by alpha particles. In the parameter regime where $\omega/k_z v_e \gg 1$ and $\omega/kv_i \gg 1$, the electron and ion contributions to the spectral function $S(\vec{k},\omega)$ are exponentially small, and the alpha particle contribution can be dominant. We then have for the spectral function [1]

$$S(\vec{k},\omega) = |\chi_e|^2 \frac{2\pi n_\alpha q_\alpha^2}{|\vec{k}| n_e} \frac{F(u)|_{\omega/k}}{|\epsilon_I(\vec{k},\omega)|^2}, \tag{2}$$

where χ_e is the electron susceptibility, n_α and n_e are the alpha particle and electron densities, respectively, q_α is the charge of alpha particles, $F(u)$ is their distribution function, $u = \omega/k$, and $\epsilon_I = -i\pi \frac{\omega_{p\alpha}^2}{k^2} \frac{dF}{du}|_{\omega/k}$ is the imaginary part of the dielectric function of the lower hybrid waves. Here, $\omega_{p\alpha}$ denotes the plasma frequency due to the alpha particles. From the approximate dispersion relation $\epsilon_r(\vec{k},\omega) = (k_\perp^2/k^2)(1 + \omega_{pe}^2/\Omega_e^2 - \omega_{pi}^2/\omega^2) + (k_z^2/k^2)(1 - \omega_{pe}^2/\omega^2) = 0$ of the lower hybrid waves, we can easily see that ω does not change when k is changed by tuning ω_0 for a fixed scattering angle. Note that $k_z/k_\perp$ remains constant for fixed scattering geometry. This means that u can be varied by tuning. Hence, it is possible to integrate

Eq. (2) for the distribution $F(u)$ using the measured $S(u)$. In an analogous method [3], measurements at different k_z with fixed ω_0 and k with an array of detectors placed on a circle would also resolve $S(u)$. In the scheme based on frequency tuning only one detector is needed. However, ω_0 has to be varied in a rather wide regime in order to cover a significant part of the velocity disribution.

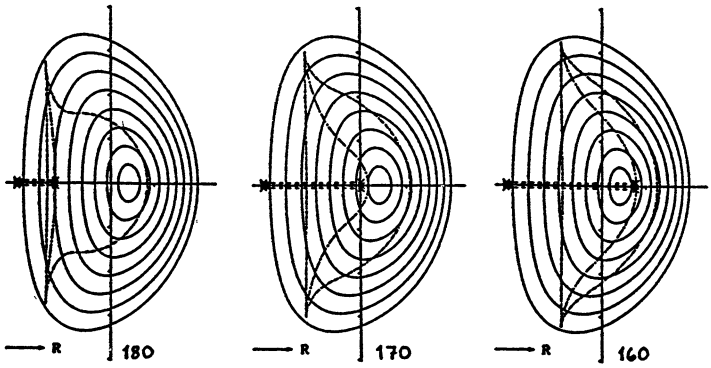

Fig. 1 The positions (chain-dashed) of the cyclotron resonance ($\omega_0 = \Omega_e$), upper hybrid resonance and cut-off (from left to right in the figure) of the incident wave with frequencies 180, 170 and 160 GHz on the poloidal cross section of a ITER-sized tokamak with a major radius 6 m, minor radius 2 m and magnetic field 5 T at the plasma center. The ray trajectories of the wave are shown by a dashed line for the perpendicular incidence from the inside in the cold plasma limit.

B. Scanning the scattering region. In another proposal [4], the incident wave reaches one of the resonances in the plasma. Here, the wave amplitude and wave vector are enhanced, and the scattering is dominated from that region. Frequency tunability offers an obvious way to scan this scattering volume over the radial space in plasmas. Fig. 1 shows the position of the upper hybrid resonance in a tokamak poloidal cross section for a variety of frequencies.

As shown in Fig. 2, the wave vector of the incident wave is strongly enhanced in the very vicinity of the upper hybrid resonance. This together with the varying separation of resonance layers

for different frequencies offers interesting possibilities for frequency tunable power sources to scan different plasma regions with a good signal to noise ratio. For instance, with step tunable gyrotrons with $\Delta\omega_0 = \pm 2.5 - 10$ %, a rather large region can be scanned within the same measurement. Because of accessibility problems in high temperature plasmas ($T_e \geq 2$ keV), this method is relevant only in small plasmas or on the periphery of large plasmas.

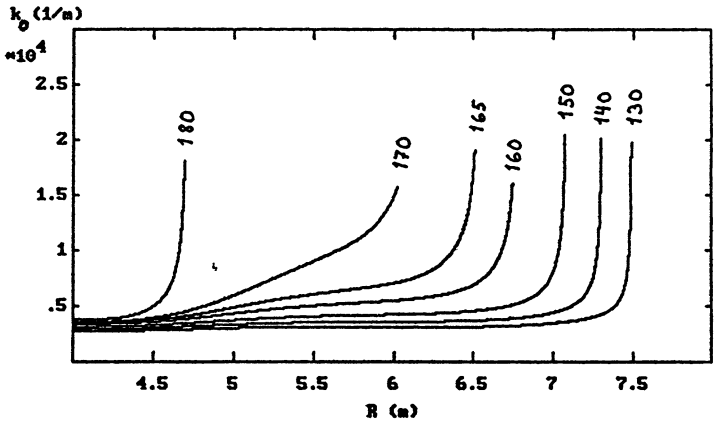

Fig. 2 The wave vector of the incident wave as a function of position for the ray trajectories shown in Fig. 1 with various frequencies.

2 Gyrotrons for plasma diagnostics

It appears that a gyrotron is the most valuable microwave source for plasma diagnostics [5–7]. Indeed, gyrotrons have important combined capabilities of high-power, long-pulse length, and narrow linewidth operation. The high power makes it possible to suppress the background noise, the long pulse length to study temporal dependence of fluctuations, the narrow linewidth to study frequency dependence of fluctuations, and the good mode purity to localize the scattering volume and to minimize stray radiation. It is possible to modulate the injected power to discriminate between the scattered radiation and the background cyclotron emission. These capabilities are unique for a single source in the millimeter wavelength range.

A typical gyrotron for diagnostics based on the collective scattering has a frequency of 140 GHz, the power of about 500 kW, and pulse length of about 1 sec. The linewidth of the gyrotron is of the order of 10 MHz which is narrower than of any other unlocked high-frequency microwave tube. The mode purity is better than 95%. The overall noise level, i.e., including both white noise and spurious modes, at 50 MHz from the central line is less than -110 dB below the central-line power. The frequency stability is of the order of 100 MHz and is mainly affected by the magnetic field which is very stable in superconducting magnets. Electron beam voltage and current variations influence the gyrotron frequency only indirectly.

As is clear from what has been said in Sec. 1, for plasma diagnostics based on resonant modes or scattering at plasma resonances a frequency-step-tunable gyrotron would be of great value. The simplest method of changing a frequency of a gyrotron consists in varying the external magnetic field. This technique is well understood and tested experimentally [8]. For example, it would be possible to step-tune a gyrotron by changing the magnetic field and jumping from one operating mode to another: 119 GHz ($TE_{12,2}$), 126 GHz ($TE_{13,2}$), 133 GHz ($TE_{14,2}$), 140 GHz ($TE_{15,2}$), 147 GHz ($TE_{16,2}$), etc. Unfortunately, owing to high inertia of the magnetic field, this way of changing frequency is slow (seconds) and cannot be used in cases when rapidly varying plasma parameters have to be studied, or a rapid frequency modulation of the injected power is desired.

It has been shown recently [9] that it is possible to tune the frequency of a gyrotron very fast (in microseconds) by changing both the modulation and beam voltages. The theoretical results demonstrate that it is possible to provide a single-mode operation in whispering gallery modes separated in frequency by 2.3 GHz in a 140 GHz gyrotron, for example, 137.7 GHz ($TE_{49,3}$), 140 GHz ($TE_{50,3}$), and 142.3 GHz ($TE_{51,3}$). Here, some important issues as, for example, stable operation of the electron gun of a gyrotron at different voltages may need further consideration.

3 Conclusions

- Frequency tuning of the power source in Thomson scattering diagnostics may open possibilities to resolve the dispersion characteristics of turbulence within the same measurement at a given spatial location. In the scattering off resonant modes, the scattered power can give information on velocity distribution of energetic ions with a good signal to noise ratio, provided the source frequency could be tuned in sufficiently wide regime.

- For the scattering at plasma resonances on tokamaks, useful scanning of the scattering region can be achieved with moderately tuned source frequency (± 2.5 % ..± 10 %).

- The relatively complicated and limited frequency tunability of gyrotrons, in comparison with tunability of, for example, free electron lasers, is counterbalanced by their robustness and relatively small size. One can expect that just gyrotrons will be the first microwave sources used in plasma diagnostic experiments requiring frequency tuning.

References

1. Costley, A.E., Hoekzema, J.A., Hughes, T.P., Stott, P.E., and Watkins, M.L., JET Report R(88)08, 1988.
2. Baranov, Yu.F. and Piliya, A.D., Pis'ma Zh. Techn. Fiz., 1991, **17**, 21.
3. Wong, K.L., Phys. Fluids, 1991, **B3**, 1501.
4. Piliya, A.D., Zh. Tekn. Fiz., 1966, **36**, 2195.
5. Woskoboinikov, P., Cohn, D.R., and Temkin, R.J., Int. J. Infrared and Millimeter Waves, 1983, **4**, 205.
6. Woskoboinikow, P., Rev. Sci. Instrum., 1986, **57**, 2113.
7. Erckmann, V., Suvorov, E.V., Holzhauer, E., and Kasparek, W., 5th Joint Russian–German Meeting on ECRH and Gyrotrons, June 28 – July 2, 1993.
8. Brand, G.F., Infrared and Millimetwer Waves, 1985, **14**, 371.
9. Dumbrajs, O. and Nusinovich, G.S., IEEE Transactions on Plasma Science, 1992, **20**, 452.

RESONATOR DESIGN FOR INDUSTRIAL GYROTRONS

O. Dumbrajs
Nuclear Engineering Laboratory,
Helsinki University of Technology, SF-02150 Espoo, Finland
M. Thumm
Kernforschungszentrum Karlsruhe, ITP,
Postfach 3640, D-76021 Karlsruhe,
and Institut für Höchstfrequenztechnik und Elektronik,
Universität Karlsruhe, Germany

Mode selection, mode competition, and resonator design for industrial gyrotrons are considered. It is shown that the $TE_{0,2}$ mode at second harmonic and the $TE_{0,3}$ mode at third harmonic are good candidates for the operating mode in an industrial gyrotron. Starting currents for these modes and modes oscillating at lower harmonics are calculated. It is emphasized that in industrial gyrotrons owing to a relatively large length of the cavity it is possible to increase significantly the electron efficiency by introducing inhomogeneity in the profile of the guiding magnetic field in a caviy. The important issue of the negative influence of the electron velocity spread on the efficiency is studied quantitatively both for the tapered and untapered magnetic field. This is of interest also for gyrotrons used for fusion plasma heating and diagnostics.

1 Mode selection

Typical parameters of a gyrotron for industrial applications are: frequency F_0=30 GHz, accelerating voltage V=20 kV, output power

P_{out}=20 kW in CW operation, and beam current I=2 A.

The design of a resonator begins with the choice of the operating mode and the number of the cyclotron interaction harmonic. Since the output power is low, the expected wall losses are also low, and there is no need to use highly oversized cavities. This means that industrial gyrotrons can operate in the low-order modes: $TE_{0,1}$, $TE_{3,1}$, $TE_{4,1}$, $TE_{1,2}$, $TE_{5,1}$, $TE_{2,2}$, $TE_{0,2}$, etc. To operate a gyrotron at a frequency 30 GHz at the fundamental resonance, one needs a magnetic field of the order of 1 T. Since the magnetic system of a gyrotron constitutes one of the major cost factors, the question arises, whether it is possible to operate an industrial gyrotron at higher harmonics, and, thus, reduced strength of the required magnetic field and dimensions of the corresponding magnetic system.

From the general gyrotron theory it is known [1,2] that in principle it is possible to operate a gyrotron at higher harmonics with rather high efficiencies: 0.7 for the first and second harmonic, and 0.55, 0.45, and 0.35 for the third, fourth, and fifth harmonic, respectively. Therefore, it is reasonable to assume that the second and, possibly, third harmonic are suitable for industrial gyrotrons.

It is well known that generally mode competition is a serious problem in gyrotrons used for fusion plasma heating or diagnostics. In gyrotrons working at second or third harmonic mode competition between lower and higher harmonic modes can occur, as well as competition between higher harmonic modes themselves. However, since spacing between the low-order modes mentioned above is large (with exception of the modes $TE_{4,1}$ and $TE_{2,1}$), mode competition in industrial gyrotrons is not an important matter, as in gyrotrons used in fusion plasma physics applications. Here it is instructive to recall some general methods used to facilitate operation at higher harmonics and suppress lower harmonics:

- choose a higher harmonic where the value $\frac{1}{2}\nu(n=2)$ or $\frac{1}{3}\nu(n=3)$ is in the center of as large a gap as possible between consecutive values of lower harmonic mode indices $\nu(n=1,2)$;
- use guns with a smaller cathode radius and a higher value of $\beta_\perp$, since $I^{start}(n=2) \sim I^{start}(n=1)/(4\beta_\perp^2)$;

- place the beam in a position where the coupling to lower harmonic is weak;
- design a cavity where the ratio of the quality factors $Q(n = 2)/Q(n = 1)$ is as large as possible.

2 Magnetic field tapering

It is known [3] that in principle it is possible to obtain almost a 100% perpendicular efficiency by using a complicated profiling of the magnetic field in a resonator. In high-frequency, high-power gyrotrons used in fusion plasma physics the length of the cavity is only about 10-15 mm. Technically it is not possible to produce over such a short distance a magnetic field of intricate shapes. Just for this reason the idea of improving efficiency of a gyrotron by means of a varying magnetic field in a resonator was tested experimentally only in the simplest case of fields increasing by about 5% over the resonator length.

Industrial gyrotrons offer a unique possibility to realize this idea in practice. Indeed, here the length of the cavity is about 100 mm, or more. Over such a distance it should be technically possible to create desired field profiles.

3 Examples

We first consider the $TE_{0,2}$ mode at second harmonic as the working mode in the resonator shown in Fig. 1. The corresponding mode map is shown in Fig. 2.

Next we consider the $TE_{0,3}$ mode at third harmonic as the operating mode. Since efficient operation at third harmonic at relatively low power requires either a long cavity, or/and a cavity with high value of Q, we first consider a cavity with iris and length 7λ as shown in Fig. 3. The corresponding mode map is shown in Fig. 4.

It is important to note that one and the same efficiency enhancement can be obtained with two distinctly different shapes of the mag-

netic field in the input and output sections of the resonator but a similar shape in the central section, where most of the energy exchange between the beam and the high-frequency field takes place (compare the solid and dash-dot curves in Fig.3). This means that in a practical design of a magnetic system it is not necessary to create the complicated shape of the field in the input and output sections of the cavity, what matters is the sine-like profile in the central part of the cavity. The cavity shown in Fig. 3 has a very high quality factor. This, as already mentioned, is beneficial for the perpendicular efficiency, but leads to very high overall losses which cannot be accepted.

There are two possibilities of reduction of Q, while keeping or even increasing the length of the cavity needed for high efficiency operation. One can operate a gyrotron in a mode with the axial index equal to two, or taper the middle part of the cavity. We have examined these posibilities and found that here also inhomogeneity of the magnetic field leads to a considerable increase of efficiency: 25%→32% in the first case, and 19%→25% in the second case ($\Theta_2 = 0.1°$).

It is evident from Figs. 2 and 4 that the working mode $TE_{0,2}$ at second harmonic is well isolated from its closest potential competitors – the $TE_{2,2}$ and $TE_{6,1}$ modes at second harmonic, and the $TE_{0,1}$ mode at fundamental –, and the working mode $TE_{0,3}$ at third harmonic is well isolated from its closest potential competitors: the $TE_{2,1}$ mode at fundamental, and the $TE_{5,2}$ mode at third harmonic. This means that by accurate adjustment of the magnetic field it should be possible to operate a gyrotron in these working modes without any danger of excitation of parasitic modes.

4 Velocity spread

It is known [4] that electron velocity spread can reduce considerably efficiency of a gyrotron. Now the question arises whether this negative effect of velocity spread is enhanced in the case of inhomogeneity of the magnetic field in the cavity, i.e., whether the ad-

vantage of tapering is invalidated by the velocity spread? We investigated this problem by simulating the velocity spread by means of a simple triangular model for the velocity distribution consisting of six fractions of electrons and assuming that $\delta v_\perp = 45\%$. As expected, the velocity spread of electrons degrades the efficiency of a gyrotron: $\eta_{tot}=42\% \rightarrow \eta_{tot}=34\%$ for the cavity shown in Fig. 1, and $\eta_{tot}=21\% \rightarrow \eta_{tot}=17\%$ for the cavity shown in Fig. 3. The corresponding numbers in the case of optimized distribution of the magnetic field are: $\eta_{tot}=53\% \rightarrow \eta_{tot}=45\%$ and $\eta_{tot}=24\% \rightarrow \eta_{tot}=19\%$, respectively. The beneficial effect of tapering the magnetic field in a cavity survives under the destructive effect of the velocity spread.

5 Conclusions

- On the basis of the starting currents calculated in the linear theory we have shown that the $TE_{0,2}$ mode at second harmonic and the $TE_{0,3}$ mode at third harmonic are good candidates for the working mode in an industrial gyrotron.
- Tapering of the magnetic field in a cavity can increase considerably the efficiency of a gyrotron.
- Relative degradation of efficiency by the velocity spread of electrons in an inhomogeneous magnetic field is of the same order as in a constant magnetic field.

References

1. Nusinovich G.S. and Erm R.E., Elektron. Tekh., Ser. 1, Elektron. SVCh., 1972, **8**, 55.
2. Danly B.G. and Temkin R.J., Phys. Fluids, 1993, **29**, 561.
3. Kuraev A.A., Stepukhovich V.A., and Zhurakhovskij V.A., Pis'ma v ZhETF, 1970, **11**, 429.
4. Ergakov V.S., Moiseev M.A., and Erm R.E., Elektron. Tekh., Ser. 1, Elektron. SVCh., 1980, **3**, 20.

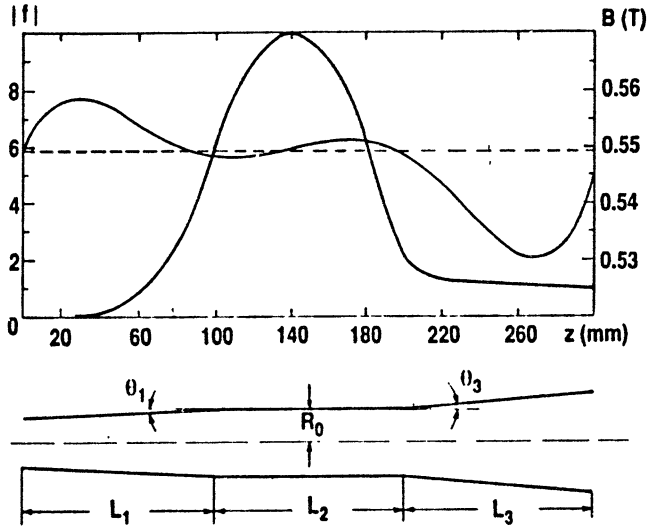

FIG. 1. $TE_{0,2}$ mode at second harmonic. Geometry of the cavity: L_1=100 mm, L_2=100 mm, L_3=100 mm, $\Theta_1 = 0.1°$, $\Theta_2 = 0°$, $\Theta_3 = 3°$, and R_0=11.14 mm. The boldface curve is the absolute value of the longitudinal high-frequency field in the cavity, where F=30.07 GHz and Q=6113. The dashed straight line is the guiding constant magnetic field B=0.549 T. Here $\eta_\perp$ =60%. The solid curve is the guiding inhomogeneous magnetic field, where $\eta_\perp$ =76%.

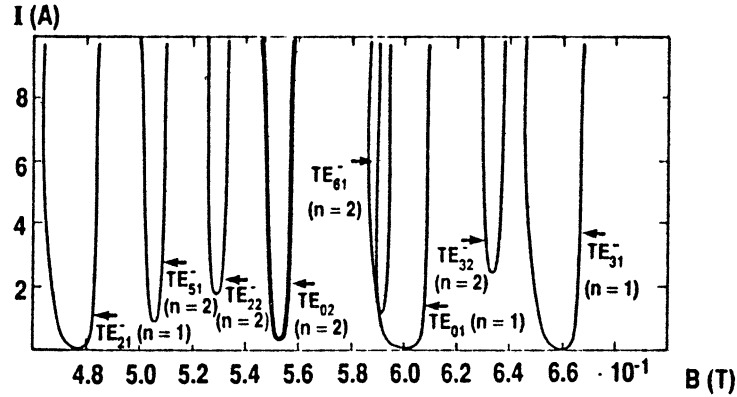

FIG. 2. Mode map corresponding to the cavity shown in Fig. 1. (R_{el}=4.86 mm).

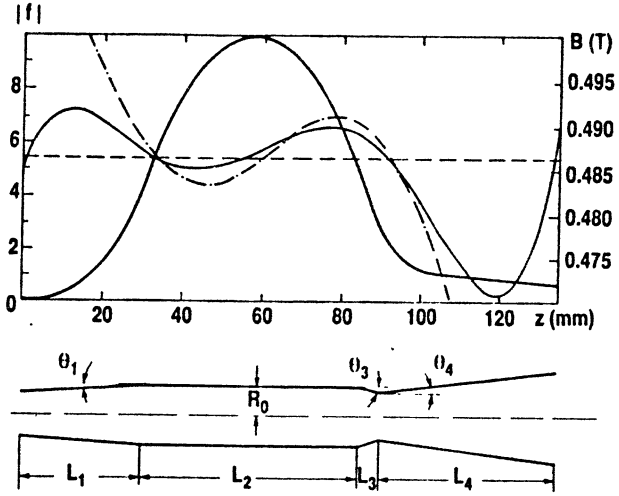

FIG. 3. $TE_{0,3}$ mode at third harmonic. Geometry of the cavity: L_1=30 mm, L_2=55 mm, L_3=10 mm, L_4=40 mm, $\Theta_1 = 1°$, $\Theta_2 = 0°$, $\Theta_3 = -1°$, $\Theta_4 = 3°$, and R_0=12.75 mm. The boldface curve is the absolute value of the longitudinal high-frequency field in the cavity, where F=38.12 GHz and Q=12590. The dashed straight line is the guiding constant magnetic field B=0.4865 T. Here $\eta_\perp$ =30%. The solid curve is the guiding inhomogeneous magnetic field, where $\eta_\perp$=35%. The dash-dot curve is another inhomogeneous magnetic field for which also $\eta_\perp$=35%.

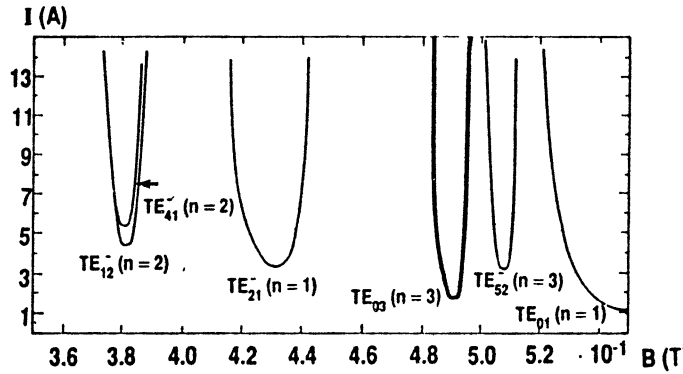

FIG. 4. Mode map corresponding to the cavity shown in Fig. 3. (R_{el}=5.27 mm).

DESIGN AND PERFORMANCE OF 94-GHz HIGH POWER MULTICAVITY GYROKLYSTRON AMPLIFIER

I.I.Antakov,E.V.Sokolov and E.V.Zasypkin
Institute of Applied Physics, Russian Academy of Science,
Nizhny Novgorod, Russia

Four - cavity gyroklystron has been built and tested in pulse operation. At the TE_{011} cavity mode output power of 65 kW with efficiency 26% has been observed. Maximum efficiency 34% has been achieved with the output power 57 kW. The peak saturated gain was about 33 dB , the small-signal gain achieved 40 dB . Half-maximum bandwidth was about 0.3% .

1 Design

A triode magnetron-injection-type gun was utilized to produce a hollow annular electron beam with a current of 3-5 A and a beam voltage V0 of 55 kV. The Tsimring code [1] was used to optimize an electrode shapes. The simulation predicted a transverse velocity spread of 15% with velocity ratio $\alpha = v_\perp/v_\parallel = 1.73$ when the anode voltage V_a is equal to 0.3 V_0. The diameter of the emitter was 8 mm , its width was 4 mm. The beam diameter in the interaction region was about 1.8 mm.

The nominal magnetic field in the interaction region was 3.7 T and the value of magnetic compression was 25. The cathode coil was used to control the beam's velocity ratio.

A schematic view of the RF circuit together with the longitudinal distribution of the constant magnetic field is shown in Fig. 1. The RF

circuit consists of four circular cavities operating in the TE_{011} mode at the fundamental cyclotron frequency.These cavities were separated by drift lengths ($L^{dr}_{1,2,3} \simeq 2\lambda$, where λ is the operating wavelength), which were cut off at the operating frequency for TE_{21} mode and other high-order modes. The optimal parameters of the cavities designed with the help of the nonlinear theory of gyroklystron [2] were following: input cavity—$Q_1 = 150$, $L_1 = 1.3\lambda$, intermediate cavities—$Q_2 \simeq Q_3 \simeq 250$, $L_2 = L_3 = 1.5\lambda$, output cavity—$Q_4 = 300$, $L_4 \simeq 2\lambda$. The drive signal was introduced to the first cavity through a single - mode rectangular waveguide connected with the cavity by a system of four longitudinal slits .The input RF power was supplied by a 100 μs, 100 W orotron which was mechanically tunable from 92.5 to 94.5 GHz. The gyroklystron usually operated at a pulse repetition frequency of 5 Hz and a pulse duration of 100 ms.

2 Experimental results

Figure 2 plots measured dependencies of output power and efficiency on beam current. Beam and anode voltages, input power level were fixed, and all other parameters—drive frequency, magnetic fields in the interaction region and cathode region—were adjusted to maximize the output power at each data point. The largest output power 65 kW with the efficiency of 26% was obtained at a beam current of 4.5 A. Maximum efficiency of about 34% has been achieved with the output power 57 kW.

Fig.3 shows the dependencies of output power and gain on input power.The peak saturated gain was about 33 dB, small-signal gain achieved 40 dB.

The dependence of the output power on drive frequency at fixed beam and anode voltages, current, input power and optimal other parameters is illustrated in Fig. 4. The optimal frequency $f_0 = 93.16$ GHz was close to the "cold" eighen-frequency of the output cavity. Half - maximum bandwidth determined, primarily, by the Q-factor of the fourth cavity was about 0.3%.

Thus, a 94–GHz pulsed gyroklystron capable of producing 65 kW

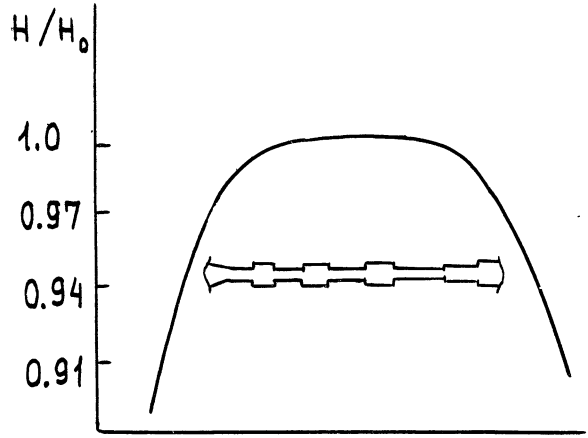

Fig. 1. Schematic view of the RF circuit and longitudinal distribtuion of the magnetic field

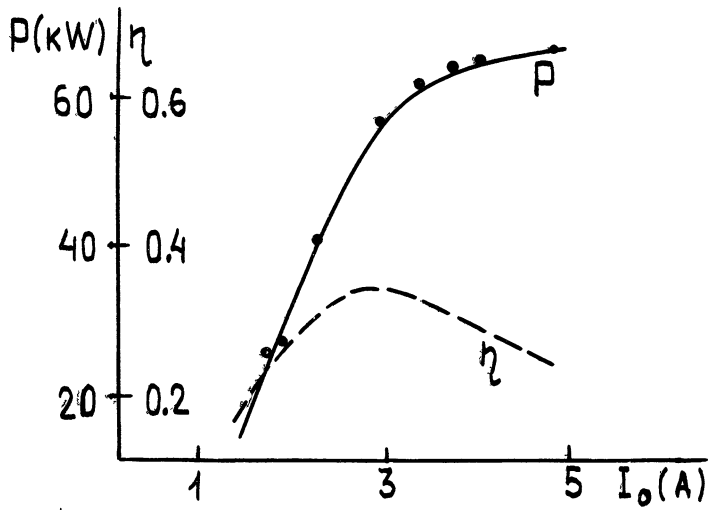

Fig. 2. Output power and efficiency versus beam current ($V_0 = 55$ kV, $V_a = 0.3V_0$, $f = f_0$) .

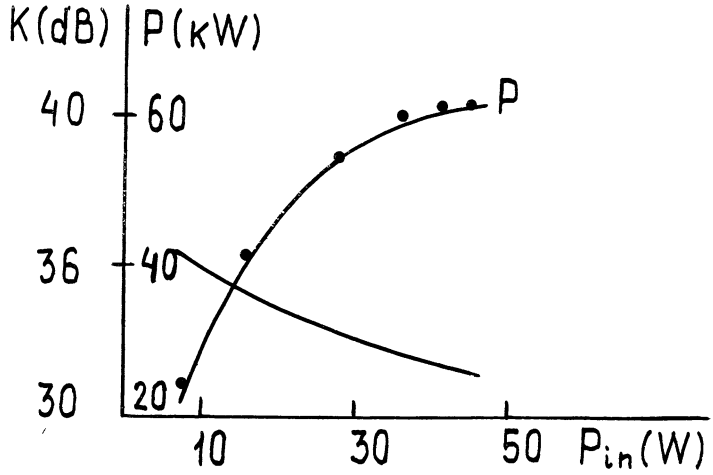

Fig. 3. Output power and gain versus input power ($V_0 = 55$ kV, $I_0 = 3.4$ A)

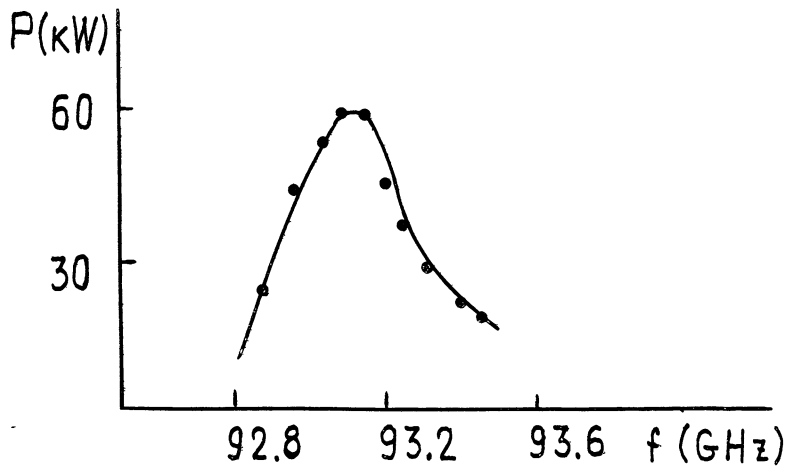

Fig. 4. Output power as function of drive frequency ($V_0 = 55$ kV $I_0 = 3.4$ A, $P_{in} = 40$ W)

with the efficiency of 26 half-maximum bandwidth of about 0.3% is now available.

References

1. V.K.Lygin, V.N.Manuilov, B.V.Rayski, Sh.E.Tsimring. Int.Journal of Infrared and Millimeter Waves.,1993, Vol.14, N 4.
2. A.V.Gaponov, A.L.Goldenberg, V.K.Yulpatov, Abstracts of the V th All-Union Conference on Microwave Electronics,Saratov University,1966 ,20 (in Russian).

Experimental Beam Parameters of Different Gyrotron Electron Guns

B. Piosczyk

Kernforschungszentrum Karlsruhe, ITP, Postfach 3640, D-76021 Karlsruhe

ABSTRACT

Measurements of the velocity distribution of gyrotron electron beams have been continued using the retarding field method. Improvements of the experimental equipment allow a larger range of scaling factors. Two different magnetron injection guns built for 140 GHz TE_{03}-gyrotrons have been examined. One of the guns is designed to have a laminar and the other a non-laminar electron flow. The results - relative "transverse" energy, average velocity ratio and velocity spread - are presented and compared with numerical calculations.

1. INTRODUCTION

The measurement of the real properties of the electron beam is as well desired for checking the limits of validity of the available numerical codes as also for a better understanding of the behaviour of a gyrotron tube and for being able to perform a reliable gyrotron design. Highly efficient operation of a gyrotron requires an electron beam with a large relative "transverse" energy $t_\perp = E_\perp/E_0$. The "transverse" and the "longitudinal" energy, $E_\perp$ and $E_\parallel$, mean that part of the total beam energy $E_0 = eU_b = E_\perp + E_\parallel$ which is related to the transverse and longitudinal momentum, respectively. U_b stays for the beam voltage. A large $t_\perp$ requires a high average velocity ratio $\alpha = \beta_\perp/\beta_\parallel$ with $\beta_\perp$ and $\beta_\parallel$ as the transverse and longitudinal velocity in units of c the velocity of light, respectively. The quantities $t_\perp$ and α are related as:

$$t_\perp = \frac{1-\sqrt{1-\beta_\perp^2}}{1-\sqrt{1-\beta_0^2}} \approx \frac{\alpha^2}{1+\alpha^2}$$

β_0 means the total velocity in units of the c. The right side of the equation is only valid for the non relativistic case.

A low velocity spread $\delta\beta_\perp$ is indispensable to achieve a high value of α without reflected electrons. In practice up to now only the method of retarding fields [1] has proved to be useful for measuring the velocity distribution of helical electron beams as used in gyrotrons. There are two main disadvantages

of this method: (1) A special experimental set-up is required. (2) As a consequence of the high power density of the electron beam, the measurements have to be performed at scaled down parameters. Therefore some uncertainty remains concerning the validity of extrapolating the measured values towards the operating parameters.

2. EXPERIMENTAL ARRANGEMENT AND PERFORMANCE

The experimental arrangement shown in Fig.1 is in principle as discribed in [2]. Some modifications have been made to allow measurements at a scaling factor k_S as low as about 5. This corresponds to operation at higher voltages and higher power densities compared to the measurements in [2]. The scaling factor k_S gives the value by which the voltages applied at the gun are reduced. In addition, to have unchanged electron trajectories the beam current I_b and the magnetic field B(z) have to be scaled down by $(k_S)^{1.5}$ and $(k_S)^{0.5}$, respectively.

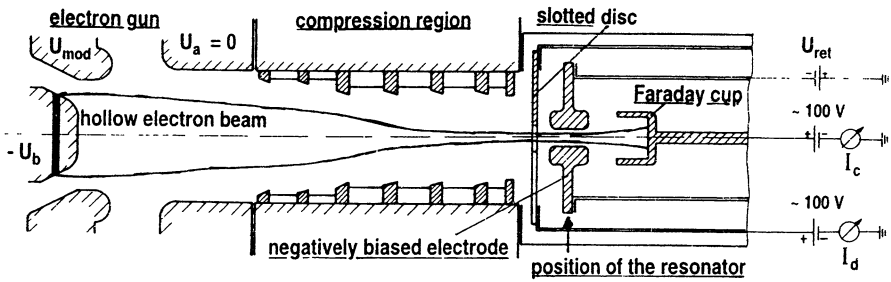

Fig.1: The experimental set-up for measurement of the velocity distribution of an electron beam with the method of retarding field.

The measurement is performed such that the main part of the electron beam is stopped in front of the velocity analyzing region at a slotted disc with a 2 mm wide slit. The part of the beam passing the slit enters the retarding field of a negatively biased electrode. The previously used cylindrically shaped electrode, as is still indicated in Fig.1, has been replaced by a highly transparent grid made out of tungsten wire. Because the motion within the retarding region is adiabatic, the retarding field acts only on the longitudinal momentum leaving the transverse momentum unaffected. Therefore, only electrons with a "longitudinal" energy $E_{\parallel} > eU_{ret}$ are able to overcome the potential barrier and contribute to the current $I_C(U_{ret})$ measured in a Faraday cup.

The measurement procedure is as discribed in [2]. For a set of gun operating parameters as the beam voltage U_b, the modulation voltage U_{mod} and the beam current I_b, the current I_C to the Faraday cup is measured stepwise in

dependence of the applied retarding potential U_{ret}. Usually, the pulse length was about 100 μsec, extended occasionally up to 2 msec, however. Out of the measured distribution of $I_c(U_{ret})$ the experimental values of the relative transverse energy $t_\perp$, the average velocity ratio α and the velocity spread $\delta\beta_\perp$ are evaluated. To be sure, that the chosen gun operating parameters are within acceptable limits, care has been taken that the current distributions $I_c(U_{ret})$ have a slope $dI_c/dU_{ret} \approx 0$ for $U_{ret} = 0$ as an indication that no electrons are already reflected at zero retarding field.

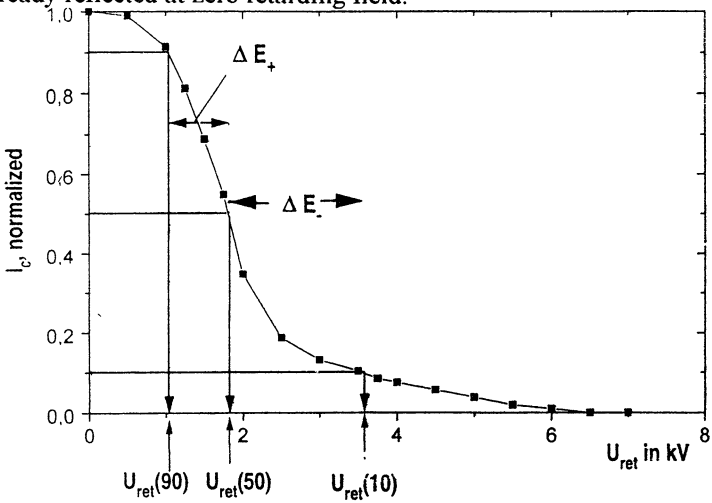

Fig.2: $I_c(U_{ret})$ as measured for the laminar gun with $k_s = 10$.

A typical distribution $I_c(U_{ret})$ measured for the laminar gun is shown in Fig.2. In that figure some quantities as needed for the evaluation of the experimental data are defined. The average "longitudinal" energy has been defined as $E_\parallel = eU_{ret}(50)$ with $U_{ret}(50)$ being the value of the retarding field at which the current I_c is reduced to 50% of the value at $U_{ret} = 0$. Since in general $I_c(U_{ret})$ is not symmetric, it was decided to take the half value $U_{ret}(50)$ instead of the average value calculated according to: $0.5*[U_{ret}(90)+U_{ret}(10)]$ as done in [2]. The average "transverse" energy is then given by: $E_\perp = e[U_b-U_{ret}(50)]$ with U_b as the accelarating beam voltage. With that, $t_\perp$ and α are achieved out of: $t_\perp = E_\perp/E_o$ and $\alpha = \sqrt{(E_\perp/E_\parallel)}$. The relative transverse velocity spread is defined as:

$$\delta\beta_{\perp+} \approx 0.5(\Delta E_+/E_\perp) \qquad \delta\beta_{\perp-} \approx 0.5(\Delta E_-/E_\perp) \qquad \delta\beta_\perp = 0.5[\,\delta\beta_{\perp+} + \delta\beta_{\perp-}]$$

ΔE_+ and ΔE_- mean the energy spread at the side with higher and lower transverse energy than the average value $E_\perp$, respectively. In case of a

symmetric distribution both values are equal. However, with a non symmetric distribution, $\delta\beta_{\perp+}$ limits the maximum achievable "transverse" energy and velocity ratio without reflected electrons. Therefore, in the case of an unsymmetric distribution $\delta\beta_{\perp+}$ and in the case of a symmetric distribution $\delta\beta_{\perp}$ is shown in the graphs.

3. RESULTS

Two guns of the MIG-type designed for a 140 GHz, TE_{03}-gyrotron have been examined. One of the guns has a laminar and the other one a non-laminar electron flow [3]. Both guns are designed for an electron current of 8 A at 70 kV. The approximate value of the space charge limited current I_{CL} calculated analytically is about 35 A and 44 A for the gun with the laminar and non-laminar electron flow, respectively. The measurements have been done within a wide range of gun operating parameters. The measured distributions $I_c(U_{ret})$ are found to be quite symmetric in the case of the gun with the non-laminar flow. However, $I_c(U_{ret})$ of the laminar flow gun has a tail with about 10% of the total beam with high "longitudinal" energies as can be seen in Fig.2.

As a result a typical experimental dependance of $t_\perp$ and of $\delta\beta_\perp$ is shown in Fig.3 and Fig.4 as a function of the beam current. The experimental value of $t_\perp$ is about 10 to 15% higher than the value calculated with the EGUN code [4]. The experimental error of determining $t_\perp$ as well as the error of the gun voltages used as input for the numerical calculations summarizes to a total error of about 10%. Within that error margin the numerically calculated values are just in agreement with the experimental results.

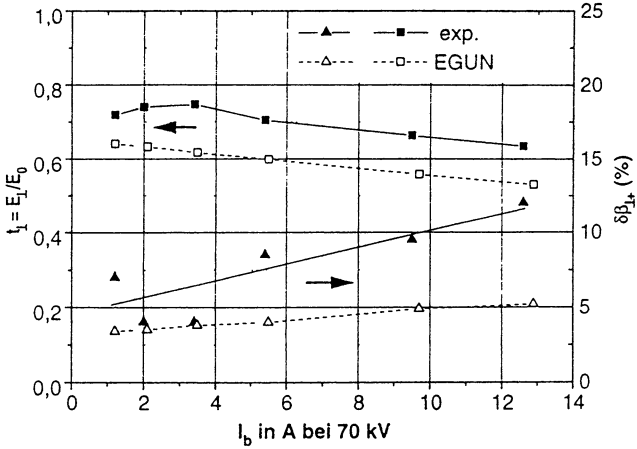

Fig.3: $t_\perp$ and $\delta\beta_\perp$ in dependence of the beam current for the laminar gun U_b=7.1 kV, U_{mod} = 2.62 kV, k_s = 10

At low beam currents the experimental values of $\delta\beta_\perp$ are quite close to the calculated ones (Fig.3 and 4). The estimated experimental error is about ±15%. The spread $\delta\beta_\perp$ increases with the beam current. At about the design current of 8 A the velocity spread is around 10%. In order to prove the validity of extrapolation of the measurements in the scaled down region, tests have been performed at scaling factors of 5, 10 and 20 for different gun parameters. The experimental result of $\delta\beta_\perp$ on the beam current are given in Fig.5. For the laminar gun $\delta\beta_{\perp+}$ and for the non-laminar gun $\delta\beta_\perp$ is shown. The spread $\delta\beta_\perp$ calculated with EGUN was found to be between about 4 and 10% depending on the operating parameters. It partly contributes to the observed spread in Fig.5. Out of the results it follows that the measured $\delta\beta_\perp$ is within an estimated accuracy of about ±15% independent of the scaling factor. This is a strong indication that the beam parameters measured at scaled down parameters can be extrapolated up to the gyrotron operating region. At high currents the slope of the increase of the velocity spread with beam current becomes steeper. This happens at significantly lower current for the non-laminar gun than for the laminar one, namely at $I_b \approx 10$ A and 25 A, respectively. This corresponds to a relative value of I_b/I_{CL} of about 0.2 for the non-laminar and about 0.7 for the laminar flow. This indicates that the non-laminar flow is more sensitive to space charge forces than the laminar flow in agreement with numerical calculations.

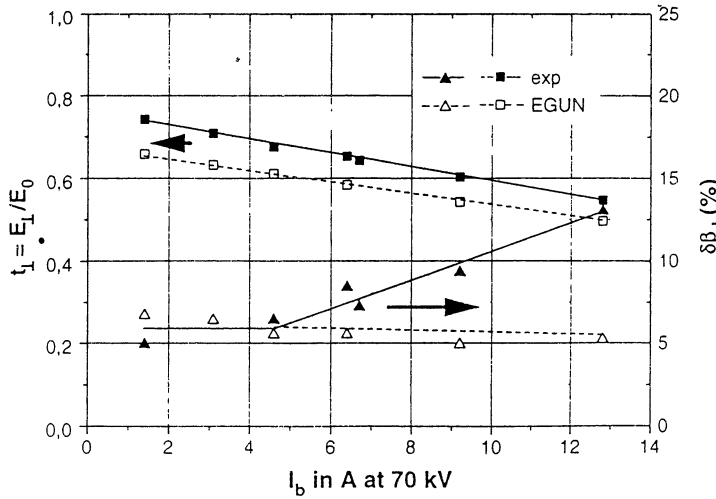

Fig.4: $t_\perp$ and $\delta\beta_\perp$ in dependence of the beam current for the non-laminar gun U_b=15.1 kV, U_{mod} = 5.78 kV, k_s = 5

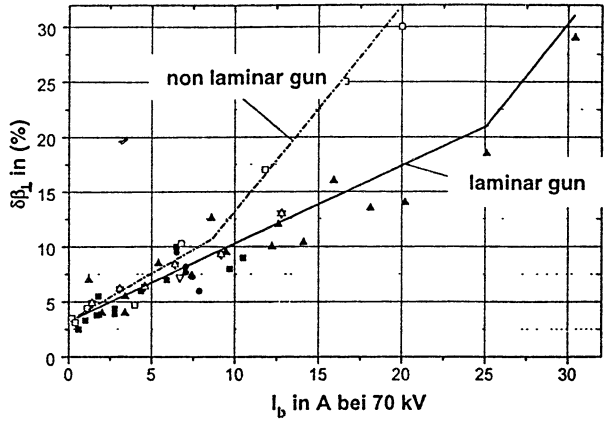

Fig.5: $\delta\beta_\perp$ vs. I_b for both guns measured with k_s=5, 10, and 20.

4. CONCLUSION

Measurements of the beam parameters with the retarding field method at different scaling factors seem to prove the validity of extrapolation up to the gyrotron operating parameters. The electron gun with non laminar flow has a symmetric distribution $I_c(U_{ret})$ in contrast to the gun with laminar flow which show a distinct asymmetry in $I_c(U_{ret})$. The reason for the asymmetry - mechanical tolerances, type of electron flow or something else - is not clear, yet. The experimental value of $t_\perp$ and α are slightly higher than the numerically calculated but still within the estimated error. Up to about the design value of the electron current both guns have a similar velocity spread. Above about 10 A the non-laminar gun shows a significantly stronger increase of $\delta\beta_\perp$ with current than the laminar gun. This confirms the results of numerical calculations.

The author gratefully acknowledges the technical support and stimulating discussions of H. Budig and Dr.G.Dammertz.

[1] E.G. Avdoshin, L.V. Nikolaev, I.N. Platonov, Sh.E. Tsimring, Radiofizika, 16(4), 605-612 (1973)
A.N. Kuftin, V.K. Lygin, Sh.E. Tsimring, V.E. Zapevalov, Int.J.Electronics, 72(5and6), 1145-1151,(1992)

[2] B.Piosczyk, 17th Int.Conf.Infrared and Millimeter Waves, Pasadena,1992; SPIE Vol.1929,p.494-495

[3] B. Piosczyk in C. Edgcombe (ed.), "Gyrotron Oscillators - their Principles and Practice", Taylor&Francis Ltd., London,1993

[4] W.B. Herrmannsfeld, Technical Report SLAC-226, UC-28, Stanford, USA (1979).

CONCEPT OF FREE ELECTRON LASERS WITH TWO-DIMENSION DISTRIBUTED FEEDBACK DRIVEN BY RIBBON ELECTRON BEAM

N.S.Ginzburg, N.Yu.Peskov, A.S.Sergeev

Institute of Applied Physics Russian Academy of Sciences, 46 Ulyanov street, 603600 Nizhny Novgorod, Russia

A.V.Arzhannikov, S.L.Sinitsky

Institute of Nuclear Physics Russian Academy of Sciences, 11 Lavrent'ev street, 630090 Novosibirsk, Russia

ABSTRACT

To realize spatial coherent radiation of sheet relativistic electron beams with transverse dimension essentially exceeding the wavelength we propose the use of a two-dimension distributed feedback. This feedback can be provided in the Bragg resonator formed by two double-periodic corrugating metal plates, when additional transverse electromagnetic energy fluxes, that synchronize the radiation of individual parts of the electron beam, take place. It is found eigenmodes of 2-D Bragg resonator and proved its high selectivity. Numerical simulation of excitation of 2-D Bragg resonator by sheet relativistic electron beam and oscillations build up demonstrates the possibility to provide spatial coherent radiation up to beam width $10^2 - 10^3$ wavelength. Concept of super-power FEL (P~20GW) millimeter wave range is discussed.

INTRODUCTION

Up to now, free electron lasers and masers with Bragg resonators formed by sections of waveguides with weak corrugation of side walls have been widely developed [1-5]. However, in the experiments the diameters of the waveguides did not exceed several wavelengths (for example, in [3-5] the radiation with wavelength $\lambda = 2 - 4\,\text{mm}$ was obtained in the resonator with diameter $D/\lambda = 2 - 3$). At the same time, in the paper [10] formation of relativistic a sheet electron beam, whose characteristic transverse size was up to $10^2\,\text{cm}$, was described. The power was tens of gigawatts, pulse duration about microsecond and energy storage $10^2 - 10^3\,\text{kJ}$. Using such beams for generation of short-wave radiation seems to be rather promising. However, when one designs generators with such beams, there arises the problem of providing of spatial coherence of radiation of individual parts of the beam, the distance between which exceeds the size of zone of diffraction divergence of the wave.

For solving this problem we proposed in the papers [7,8] to use a double-periodic Bragg resonator realizing 2-D distributed feedback, when additional transverse fluxes of electromagnetic energy, that synchronize radiation of individual parts of the electron beam, appear.

Section 1 of this paper is devoted to description of eigenmodes of the 2-D Bragg resonator. In section 2 we investigate the excitation of a such resonator by a sheet relativistic electron beam and study the build up oscillations. In section 3 the project of super-power FEL operating in the millimeter wavelength band driven by sheet REB that is formed by the accelerator U-2 (INP, Novosibirsk) is described.

1. EIGENMODES OF 2-D BRAGG RESONATOR

The transverse energy fluxes can be produced in a resonator formed by two metal plates with width l_x, length l_z and distance between them a_0 (Fig.1a), which are corrugated as

$$a = a_1\left(\cos\left(\bar{h}x - \bar{h}z\right) + \cos\left(\bar{h}x + \bar{h}z\right)\right), \qquad (1)$$

where $\bar{h} = \bar{h}\sqrt{2}/2$, $\bar{h} = 2\pi/d$, d is corrugation period, a_1 is corrugation depth. Assuming $\bar{h}a_1 << 1$ we will seek the field in the resonator in the form of four coupled waves (Fig.1b): $\mathcal{A}_\pm$ propagating in the $\pm z$ and $\mathcal{B}_\pm$ propagating in the $\pm x$ directions:

$$\vec{E} = \mathrm{Re}\Big[\vec{E}_p(y)\big(\mathcal{A}_+(x,z)e^{-ihz} + \mathcal{A}_-(x,z)e^{ihz} + \mathcal{B}_+(x,z)e^{-ihx} + \mathcal{B}_-(x,z)e^{ihx}\big)e^{i\omega t}\Big], \qquad (2)$$

where $\mathcal{A}_\pm(x,z)$, $\mathcal{B}_\pm(x,z)$ are slow functions, $h = \sqrt{\omega^2/c^2 - k_{\perp p}^2}$, $k_{\perp p} = \pi p/a_0$, $\vec{E}_p(y)$ is functions describing spatial structure along y-direction, p is the index of modes in this direction. Substituting (2) into the Helmholtz equation with periodic condition on the corrugated surface of plates (1) after averaging we obtain the following equation set for amplitudes $A_\pm = \mathcal{A}_\pm e^{\pm i\delta z}$, $B_\pm = \mathcal{B}_\pm e^{\pm i\delta x}$ (comp. [2,6]):

$$\begin{aligned} &\frac{\partial}{\partial z}A_\pm \mp i\delta A_\pm \pm i\alpha(B_+ + B_-) = 0, \\ &\frac{\partial}{\partial x}B_\pm \mp i\delta B_\pm \pm i\alpha(A_+ + A_-) = 0, \end{aligned} \qquad (3)$$

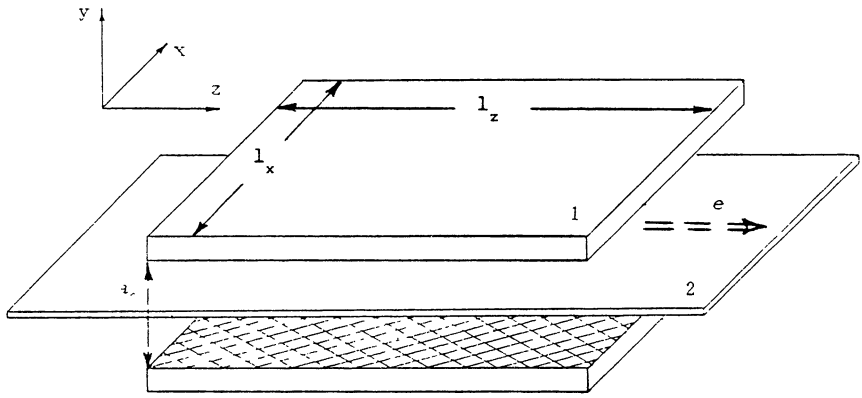

Fig.1a The general scheme of FEL-generator with two-dimension Bragg resonator (1) driven by ribbon electron beam (2) (the drift velocity of electrons directed along z coordinate)

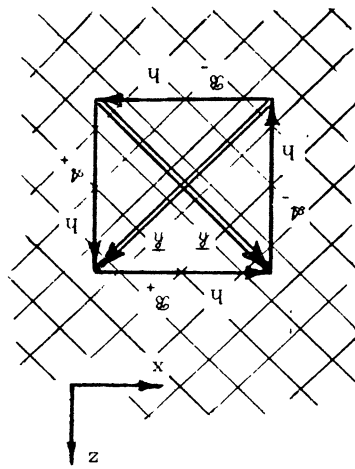

Fig.1b The diagram illustrated the scattering of the partial wave on the 2-D Bragg grating

($\vec{h}$ are the wave vectors of partial waves $A_{\pm}$, $B_{\pm}$; $\vec{\vec{h}}$ are the grating vectors)

where $\delta = \bar{h} - h$ is frequency mismatch from the Bragg resonance and α is coupling coefficient* :

$$\alpha = \omega a_1 / 4 c a_0 \qquad \text{for TEM wave,}$$
$$\alpha = h a_1 / 2 a_0 \qquad \text{for TM wave.} \tag{4}$$

Let us find Q-factors and spatial structures of the resonator modes. Assuming the fluxes of electromagnetic energy from the outside to be absent and the partial waves do not reflect at the end of cavity, we will represent the boundary conditions for Eqs.(3) in the transverse and longitudinal directions in the following form:

$$A_{\pm}(x, \mp l_z/2) = 0 \,, \quad B_{\pm}(\mp l_x/2, z) = 0 \,, \tag{5}$$

Passing over to integral presentation of Eqs.(3) with boundary conditions (5), we will find that values $f_1 = A_+(x,z) + A_-(x,z)$ and $f_2 = B_+(x,z) + B_-(x,z)$ meet the same equation:

$$f_{1,2}(x,z) = \alpha^2 \int_{-l_z/2}^{+l_z/2} \int_{-l_x/2}^{+l_x/2} f_{1,2}(x',z') e^{i\delta\left(|x-x'|+|z-z'|\right)} dz' dx' \,. \tag{6}$$

It follows from here that

$$\gamma_z \left(A_+(x,z) + A_-(x,z)\right) = \gamma_x \left(B_+(x,z) + B_-(x,z)\right) \,, \tag{7}$$

---

* The TM and TEM waves for which $\vec{E}_p \parallel \vec{y}_0$ can be used in such FEL version as ubitrons with guiding magnetic field and cyclotron autoresonans masers (CARM). For ubitrons without guiding magnetic field interaction is possible only with TE wave ($\vec{E}_p \parallel \vec{x}_0$), which have a very small coupling coefficient in this corrugation. In this case 2-D feedback may be provided by mutual scattering TE ($A_{\pm}$) and TM ($B_{\pm}$) waves.

where $\gamma_{x,z}$ are complex parameters and let us assume $\gamma_x\gamma_z = 1$. Relation (7) makes it possible to find solution of Eqs.(3) by the variable separation methods. As result taking into account boundary condition we obtain for the field amplitudes the following relations:

$$A_{\pm} = \sqrt{\delta^2 - \lambda_z^2}\,\sin\left(\lambda_z(z \pm l_z/2)\right)\left[\delta\sin\left(\lambda_x(x + l_x/2)\right) + i\lambda\cos\left(\lambda_x(x + l_x/2)\right)\right],$$

$$B_{\pm} = \sqrt{\delta^2 - \lambda_x^2}\,\sin\left(\lambda_x(x \pm l_x/2)\right)\left[\delta\sin\left(\lambda_z(z + l_z/2)\right) + i\lambda\cos\left(\lambda_z(z + l_z/2)\right)\right],$$

where $\lambda_{x,z} = \sqrt{\delta^2 - 2\alpha\delta\gamma_{x,z}}$. (8)

Eigennumbers δ and $\gamma_{x,z}$ meet the characteristic equations

$$\exp(2i\lambda_z l_z) = \frac{\alpha\gamma_z - \delta - \lambda_z}{\alpha\gamma_z - \delta + \lambda_z}, \quad \exp(2i\lambda_x l_x) = \frac{\alpha\gamma_x - \delta - \lambda_x}{\alpha\gamma_x - \delta + \lambda_x}. \tag{9}$$

Analysis of Eqs.(9) shows that the cavity has the spectrum of high-Q-factor modes ($Q \approx \bar{h}/2\,\mathrm{Im}|\delta| >> 1$) under the conditions of strong coupling of the waves $\alpha l_{x,z} >> 1$. Eigenfrequencies of the modes are situated to the left and to the right from the precise Bragg resonance $\delta \approx 0$, as well as near $\delta \approx \pm 2\alpha$ (Fig.2). Solutions for these modes are given by the relations

$$\lambda_z = \frac{\pi n}{l_z} + i\frac{\pi m}{\alpha l_z l_x}, \qquad \lambda_x = \frac{\pi m}{l_x} + i\frac{\pi n}{\alpha l_z l_x}, \tag{10a}$$

$$\delta = -\frac{\pi^2 mn}{2\alpha l_z l_x} - i\frac{\pi^2}{2\alpha^2 l_z l_x}\left(\frac{n^2}{l_z} + \frac{m^2}{l_x}\right) \tag{10b}$$

when $\delta \approx 0$ and

$$\lambda_z = \frac{\pi n}{l_z} - is\frac{\pi n}{\alpha l_z^2}, \qquad \lambda_x = \frac{\pi m}{l_x} - is\frac{\pi m}{\alpha l_x^2}, \tag{11a}$$

$$\delta = \left[2\alpha + \frac{\pi^2}{4\alpha}\left(\frac{n^2}{l_z^2} + \frac{m^2}{l_x^2}\right)\right] s - i\frac{\pi^2}{2\alpha^2}\left(\frac{n^2}{l_z^3} + \frac{m^2}{l_x^3}\right) \qquad (11b)$$

when $\delta \approx \pm 2\alpha$. In relations (10),(11) $n = 0, \pm 1, \pm 2\ldots$ is longitudinal, and $m = 0, \pm 1, \pm 2\ldots$ is transverse indexes of the modes, $s = \pm 1 = \mathrm{sign}(mn)$. According to (10),(11) , high selectivity over both the longitudinal (n) and transverse (m) indexes takes place and is provided by diffraction output of radiation not only in the longitudinal $\pm z$ directions (similar 1-D Bragg resonators), but also additionally in the transverse $\pm x$ directions. The Q-factor will be maximal for the lowest

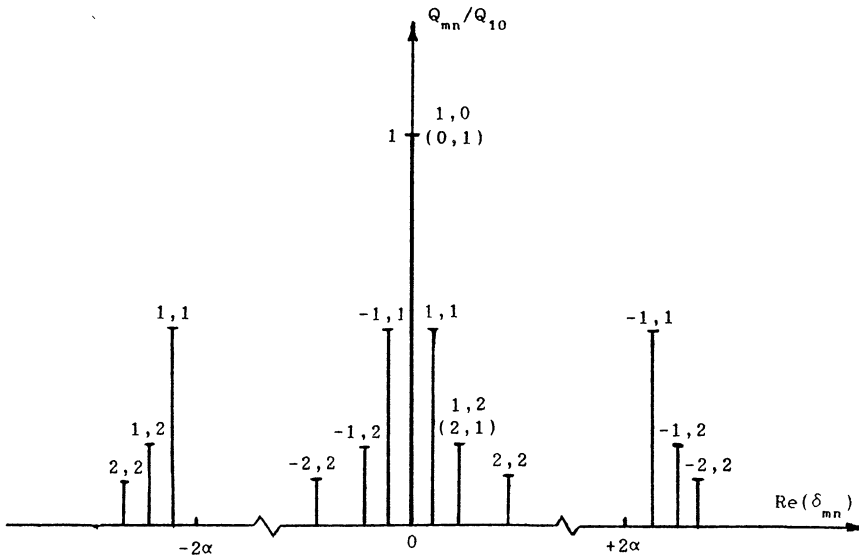

Fig.2 The spectrum of eigenfrequencies of the resonator modes and their Q-factor ($l_x = l_z$).

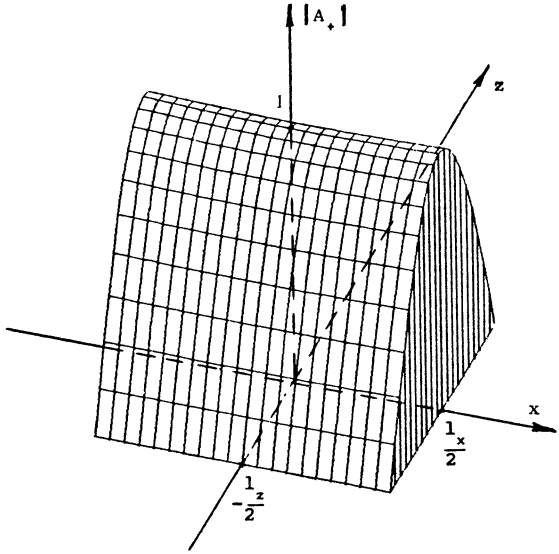

a) A_+ wave

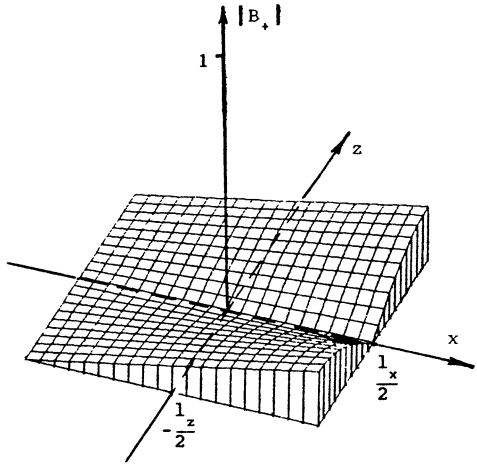

b) B_+ wave

Fig.3 The spatial structure of the most high-Q mode n = 1 m = 0

$(\alpha l_x = \alpha l_z = 5)$

modes with the indexes $n=0$ $m=1$ and $n=1$ $m=0$ (Fig.2). These modes have the same eigenfrequency ($\mathrm{Re}(\delta)=0$), and when $l_x = l_z$ they have the same Q-factor too. Figure 3 gives the spatial structure of the A_+ and B_+ wave for the mode $n=1$ $m=0$ (the structure of A_- wave is identical to the structure of A_+ wave, and B_- is a bilaterally symmetrical to B_+). For this mode the field amplitude A_+ (we suppose that the A_+ wave is synchronous to the electron beam moving in the $+z$ direction, and the rest partial waves do not interact with the beam) does not depend on transverse coordinate x. Note that, the maximal amplitude $A_\pm$ wave exceeds the maximal amplitude $B_\pm$ essentially ($A_\pm^{max}/B_\pm^{max} = \alpha l_z$). For the mode $n=0$ $m=1$ the spatial structure $A_\pm$ and $B_\pm$ waves is identical to the structure $B_\pm$ and $A_\pm$ waves accordingly, if we mutually exchange the z and x coordinate (in this case $A_\pm^{max}/B_\pm^{max} = 1/\alpha l_x$). Therefore, this mode has fairly low amplitude of synchronous wave A_+ and do not effectively excites by electron beam.

2. BUILD UP OSCILLATIONS IN FEL WITH 2-D BRAGG RESONATOR

Let us investigate excitation of a 2-D Bragg resonator by a sheet relativistic electron beam. Suppose that electrons oscillate either in the undulator field (ubitron, Fig.4a) or in the uniform axial magnetic field (cyclotron autoresonance maser - CARM, Fig.4b). As before we assume that only the A_+ wave is synchronous to the electron beam moving in the $+z$ direction and the other partial waves do not interact with the beam. The resonance condition can be written in the form

$\omega - hv_{||} = \Omega$,

where $v_{II} = \beta_{II} c$ is electron axial velocity, Ω is electron oscillation frequency (for ubitrons $\Omega = 2\pi v_{II}/d_u$ is bounce-frequency, d_u is undulator period; for CARM $\Omega = eH_0/mc\gamma$ is gyrofrequency, γ is the relativistic mass-factor).

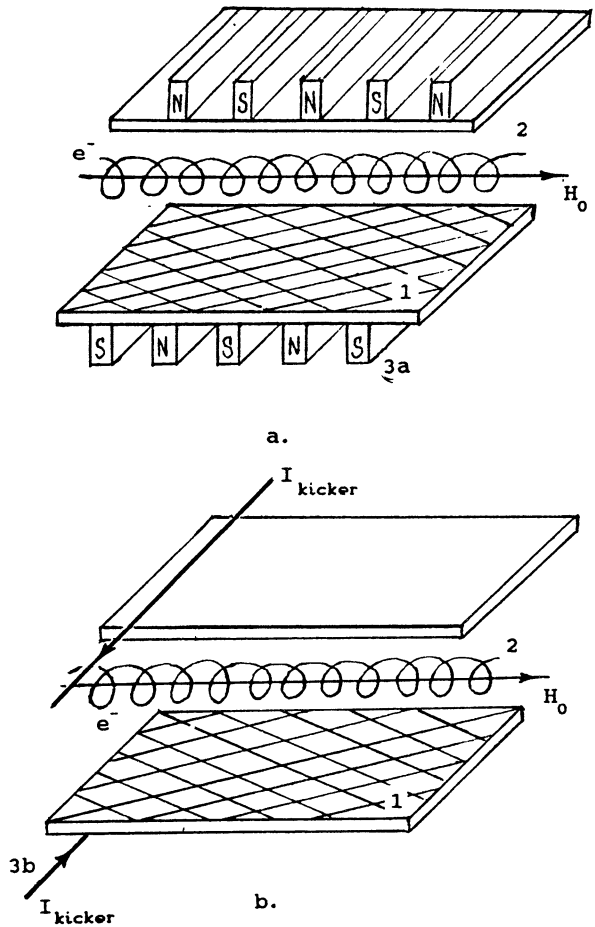

Fig.4 The scheme of ubitron (a) and CARM (b) with 2-D Bragg resonator:
(1 - 2-D Bragg resonator, 2 - electron beam, 3a - undulator,
3b - pump section (kicker), H_0 - guide field)

For investigation of transition processes we suppose that amplitudes of partial waves are slow functions of time: $A_{\pm}(x,z,t)$, $B_{\pm}(x,z,t)$ and as carrier frequency in (2) we choose the Bragg frequency ω_0 . Under such conditions interaction of the electron beam with partial waves of 2-D Bragg resonator and oscillations build up can be described by the following system of equations

$$\left(\frac{\partial}{\partial z}+\beta_{gr}^{-1}\frac{\partial}{\partial \tau}\right)\hat{A}_{+}+i\hat{\alpha}\left(\hat{B}_{+}+\hat{B}_{-}\right)=\frac{1}{\pi}\int_{0}^{2\pi}e^{-i\theta}d\theta_0 \ ,$$

$$\left(-\frac{\partial}{\partial z}+\beta_{gr}^{-1}\frac{\partial}{\partial \tau}\right)\hat{A}_{-}+i\hat{\alpha}\left(\hat{B}_{+}+\hat{B}_{-}\right)=0 \ , \qquad (12)$$

$$\left(\pm\frac{\partial}{\partial z}+\beta_{gr}^{-1}\frac{\partial}{\partial \tau}\right)\hat{B}_{\pm}+i\hat{\alpha}\left(\hat{A}_{+}+\hat{A}_{-}\right)=0 \ ,$$

$$\left(\frac{\partial}{\partial z}+\beta_{II}^{-1}\frac{\partial}{\partial \tau}\right)^2\theta=\mathrm{Re}\left(\hat{A}_{+}e^{i\theta}\right) \ .$$

Boundary conditions for Eqs. (12) take the form

$$\hat{A}_{\pm}(X,\mp L_z/2)=0 \ , \qquad \hat{B}_{\pm}(\mp L_x/2,Z)=0 \ , \qquad (13)$$

$$\theta|_{Z=-L_z/2}=\theta_0\in[0,2\pi) \ , \qquad \left(\frac{\partial}{\partial z}+\beta_{II}^{-1}\frac{\partial}{\partial \tau}\right)\theta\Big|_{Z=-L_z/2}=-\Delta \ .$$

Here we have used the following dimensionless parameters and variables: $Z=\bar{h}zC$, $X=\bar{h}xC$, $\tau=\omega_0 tC$, $\hat{\alpha}=\alpha/\bar{h}C$, $v_{gr}=\beta_{gr}c$ is group wave velocity, $\hat{A}_{\pm},\hat{B}_{\pm}=\dfrac{e\kappa\mu}{mc\omega\gamma C^2}\mathcal{A}_{\pm},\mathcal{B}_{\pm}$, $C=\left(\dfrac{eI_0\lambda^2\kappa^2\mu}{8\pi\gamma_0 mc^3a_0}\right)^{1/3}$ is gain

parameter (Pierce parameter), $\theta = \omega_0 t - hz - \int \Omega dt$ is electron phase relative to synchronous wave, $\Delta = \left(\bar{h} v_{\parallel} + \Omega - \omega_0\right)/\omega_0 C$ - initial mismatch of synchronism, κ is parameter describing coupling between wave and electrons (this parameter is proportional to the oscillatory particles velocity), μ is bunching parameter (for ubitron $\mu = \gamma^{-2}$ and for CARM $\mu = 1 - c^2/v_{ph}^2$, where v_{ph} is phase velocity of synchronous wave), I_0 is electron current, $L_{x,z} = \bar{h} l_{x,z} C$.

Electron efficiency is given by relations

$$\eta = \frac{C}{\mu\left(1-\gamma_0^{-1}\right)}\hat{\eta}\,, \qquad \hat{\eta} = \frac{1}{2\pi L_x}\int_{-L_x/2}^{+L_x/2}\int_0^{2\pi}\left(\frac{\partial\theta}{\partial z}+\Delta\right)\Bigg|_{Z=L_z/2} d\theta_0\, dX\,.$$

Dependencies of efficiency on time at the region of parameters, where the build up of the stationary regime of generation takes place, are presented in the Fig.5. Note that in numerical simulation we assumed $v_{\parallel} = v_{gr}$. At the stationary regime spatial structures of partial waves $\hat{A}_{\pm}$ and $\hat{B}_{\pm}$ are close to the structures of corresponding waves for the most high-Q mode $n = 1$ $m = 0$ of "cold" resonator (compare Fig.3 and Fig.6). The frequency of this mode as well as the oscillations frequency coincides with the Bragg frequency. The self excitation condition for this mode may be presented in the form $p = \hat{\alpha}^2 L_x L_z^4 \geq 250$, $\Delta L_z \approx \pi$ *. It is important

* Under more great excess over the threshold (governed by parameter p) it is observed excitation of another modes (in perticular, mode $m = n = 1$), as well as automodulation regimes of generation. In this case the spatial structures of waves periodically changed in time.

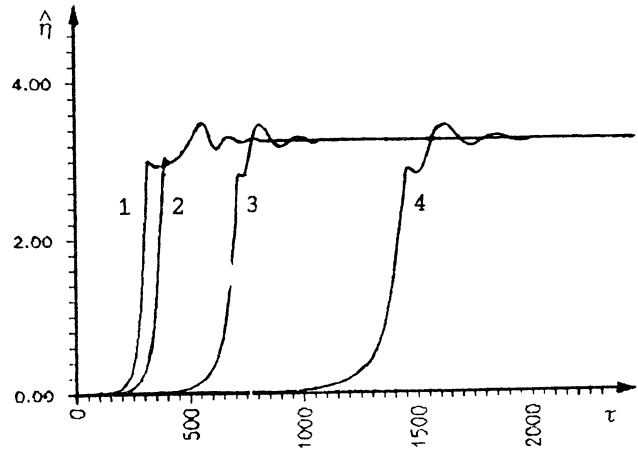

Fig.5 Build up stationary regime of oscillations. Dependencies of normalized efficiency on time: $L_z = 4$, $\Delta = -1,82$, $\hat{\alpha}^2 L_x = 1,25$:
1. $L_x = 0,8$, $\hat{\alpha} = 1,25$; 2. $L_x = 3,2$, $\hat{\alpha} = 0,625$;
3 $L_x = 12,8$, $\hat{\alpha} = 0,315$; 4 $L_x = 28,8$, $\hat{\alpha} = 0,208$.

to note that transverse distribution of amplitude of synchronous wave $\hat{A}_{\pm}$ does not depend on transverse coordinate X that provides equal energy extraction for all parts of the electron beam.

The principal problem for the considered scheme of FEL is the question about maximal transverse width of system under which the regime of space synchronization of radiation of different parts of the electron beam can be realized. From Eqs.(12) it is easy to see that at stationary conditions $(\partial/\partial\tau = 0)$ `, when the fundamental mode $n = 1$ $m = 0$ excites, the dependencies of waves $\hat{B}_{\pm}$ on the transverse coordinate may be presented as

$$\hat{B}_+ = \hat{\alpha} X \left(\hat{A}_+ + \hat{A}_-\right) , \qquad \hat{B}_- = \hat{\alpha}\left(L_x - X\right)\left(\hat{A}_+ + \hat{A}_-\right) \qquad (14)$$

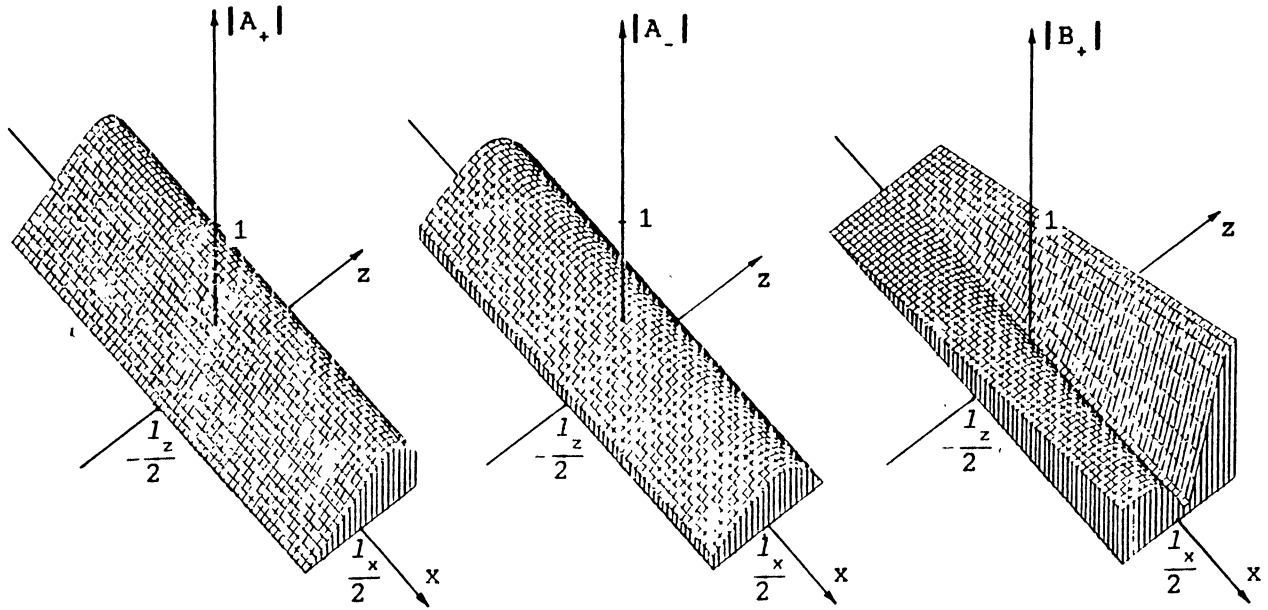

Fig.6 Spatial distribution of partial waves amplitude $\hat{A}_{\pm}$, $\hat{B}_{\pm}$ in the stationary regime of oscillations:

$L_z = 4$, $\Delta = -1{,}82$, $L_x = 12{,}8$, $\hat{\alpha} = 0{,}315$.

This allows to reduce Eqs.(12) to the form

$$\frac{d}{dz}\hat{A}_+ + i\hat{\alpha}^2 L_x\left(\hat{A}_+ + \hat{A}_-\right) = \frac{1}{\pi}\int_0^{2\pi} e^{-i\theta}d\theta_0 \ ,$$

$$\frac{d}{dz}\hat{A}_- - i\hat{\alpha}^2 L_x\left(\hat{A}_+ + \hat{A}_-\right) = 0 \ , \qquad (15)$$

$$\frac{d^2}{dz^2}\theta = \mathrm{Re}\left(\hat{A}_+ e^{i\theta}\right) \ .$$

Therefore, if the system length L_z is constant, distribution of waves along longitudinal coordinate as well as efficiency does not change when condition $\hat{\alpha}^2 L_x = const$ is satisfied. Such a scaling gives us possibility to increase the width of the interaction space simultaneously decreasing coupling parameter (for example, decreasing corrugation depth). Computer simulation of nonstationary equations (12) confirms this conclusion. If $L_z \le 5$, the synchronization regime is stable at least up to $L_x \le 30$, but the transition time increases with increasing system's width (see Fig.5).

3. CONCEPT OF SUPER POWER-MILLIMETER WAVE FEL

Using theoretical consideration carried out in Sect.1 and 2 let us estimate possibilities of realization of FEL with wavelength $\lambda = 4\,\mathrm{mm}$ driven by REB with transverse size 140cm, electron current 1kA/cm particles energy 1MeV and pulse duration 10^{-6}s. Such beams are formed by the U-2 accelerator (Novosibirsk, INP RAS) [10]. Let the undulator 4cm, transverse oscillatory electrons velocity $\beta_\sim \approx \kappa \approx 0,3$;

and parameter $\mu \approx \gamma_0^{-2} \approx 0,1$. In this case, when the distance between cavity plates $a_0 = 5\text{cm}$, gain parameter is $C \approx 0,0065$. Curve 3 in Fig.5 ($\hat{\alpha} = 0,315$, $L_z = 4$, $L_x = 12,8$) corresponds to the corrugation depth $a_1 = 0,4\text{mm}$, the cavity length 36cm and the cavity width 140cm. Transit time is about 150ns. Under efficiency 15% the radiation power amounts to 20GW. So the 2-D distributed feedback provides obtaining spatial coherent radiation under oversize coefficient $l_x/\lambda \approx 350$.

Note in conclusion that for the 2-D Bragg resonator the single-directed output of radiation (both longitudinal and transverse one) may be provided by using additional Bragg reflectors. Figure 7 presents an example of the resonator emitting only in the +z direction.

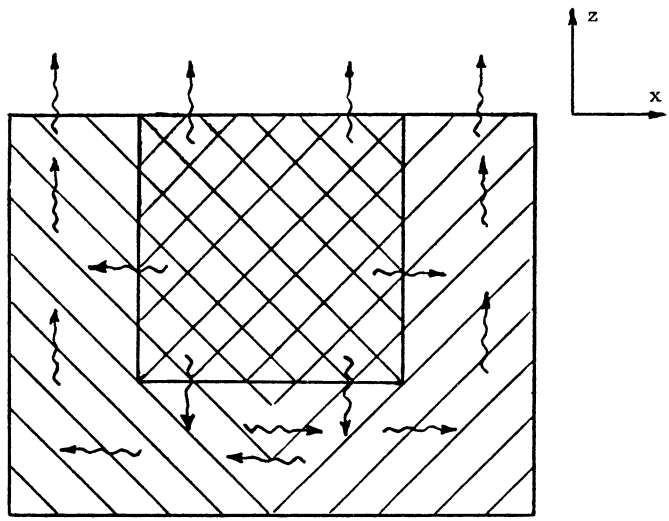

Fig.7 The scheme of resonator provided single-directed output of radiation.

REFERENCES

1. Kovalyov N.F., Petelin M.I., Reznikov M.G. "Resonator" Author's Certificate N:720591 with priority of Nov.14, 1978, Bull. Discoveries, Inventions, no.9, 1980.
2. Bratman V.L., Ginzburg N.S., Denisov G.G. // Pis'ma Zh. Tech. Fiz., 1981, vol.7, no.21, p.1320.
3. Bratman V.L., Ginzburg N.S., Denisov G.G., Petelin M.I. // IEEE J. of Quant. Electr., 1983, v.QE-19, N:3, p.282.
4. Botvinnik I.E., Bratman V.L., Volkov A.B. e.a. // Pis'ma Zh. Eksp. Teor. Fiz., 1982, vol.8, no.22, p.1386.
5. Fliflet A.W., Mc.Cowan R.B., Sullivan C.A. e.a. // Nuclear Instr. and Method in Phys. Research, 1989, v.A285, no.1-2, p.233.
6. Kovalyov N.F., Orlova I.M., Petelin M.I. // Izv. VYZ. Radiofiz., 1968, vol.11, p.783.
7. Ginzburg N.S., Peskov N.Yu., Sergeev A.S. // Pis'ma v Zh. Tech. Fiz., 1992, vol.18, no.9.
8. Ginzburg N.S., Peskov N.Yu., Sergeev A.S. // Optics Commun., 1993, v.96, p.254-258.
9. Arzhannikov A.V., Ginzburg N.S. Peskov N.Yu. e.a. // 14-th Int. FEL Conference, Kobe, Japan, 1992, p.549.
10. Arzhannikov A.V., Nikolaev V.S., Sinitsky S.L. e.a. // Preprint 92-3, Inst. of Nuclear Physics RAS, Novosibirsk, 1992.

MAGNICON A NEW POWERFUL RF-GENERATOR

M. M. Karliner E. V. Kozyrev I. G. Makarov
O. A. Nezhevenko G. N. Ostreiko B. Z. Persov
G. V. Serdobintsev V. P. Yakovlev

Budker Institute of Nuclear Physics
630090 Novosibirsk, Russia

Introduction

A magnicon[1,2] belongs to a new type of high power RF devices where the beam modulation is achieved by the circular deflection. Being an outgrowth of the gyrocon[3] a magnicon enable one to heighten an upper limit of the operation frequency and power range having high efficiency intrinsic to this class of devices.

Historically the devices of this type have been developed by the Novosibirsk Institute of Nuclear Physics for solution the problems of power sources for the electron - positron colliders. A Gyrocon [3] proposed by G.I.Budker was the first of those devices. A few gyrocons have been developed [2], that demonstrated a possibility of its successful use in the RF system in the accelerator-storage ring facilities. At the same time, it was revealed that into the range of high frequencies (a centimeter range of wavelength) is related to a substantial reduce in power and efficiency. These limitation are mainly associated with the overheating and breakdown in cavities as well as with the difficulty of the passing a high power electron beam through circular slits in the end walls of the output cavity.

A magnicon is the most advanced innovation using the gyrocon principle of beam modulation by circular deflection but it is modified

in such a way that enables one to decrease the limitation mentioned above.

1 Operation Principle of the Magnicon

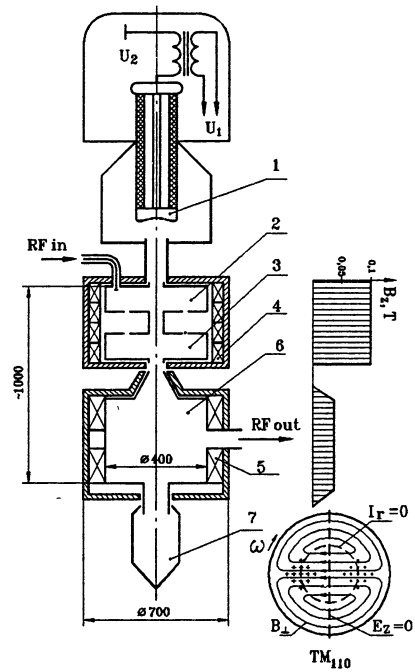

Fig.1 Layout of magnicon

The magnicon design is schematically given in Fig.1. A continuous electron beam from the gun 1 is guided into a circular deflection systems, which consists of the drive cavity 2 and one 3 or a few gain cavities in a longitudinal magnetic field ($\Omega/\omega \cong -2$, Ω-cyclotron frequency, ω-frequency of input signal)[1] produced by solenoid 4. In this cavities the beam is deflected at an angle α_0 by an RF magnetic field rotating with a deflection frequency (ω). The field distribution in the cavities is shown in Fig.1. The beam is extracted from the magnetic field near the device axis through a hole in the flux shield.

In the drift space, electrons deviate from the device axis and get into a stationary magnetic field (B_z) of the solenoid 5. While entering the magnetic field the longitudinal velocity of the electrons is transformed into a rotational transverse one, and the degree of the transformation is characterized by the pitch angle α. Further on, travelling along a helical trajectory and steadily changing their entering point in the output cavity 6, the electrons excite a wave in the cavity travelling along the azimuth (TM_{110} mode, Fig.1) and trans-

[1]Sign(-) corresponds to the same direction both of the cyclotron rotation of electrons and of the wave rotation in the deflection and output cavities

fer their energy to this wave. If the magnetic accompanying field is equal $B_z \cong 0.5(\gamma_0+1)\omega m_0/e$, where γ_0 is the initial value of electron energy the interaction can remain to be effective during many periods of RF oscillations. Therefore an output cavity length can be of a few wavelength, that leads to substantial decrease in the RF field, in ohmic losses and in a specific heat release. Besides, the large beam tunells (their diameter is approximately equal to two Larmour ones) in tandem with the "magnetic accompaniment" practically removes the problem of the current interception. The presence of magnetic guidance in the deflecting device enables one (compared to gyrocon) to increase an longitudinal size of cavity and, thereby to decrease the limitation related to the breakdown and overheating, and also, it enables one to increase substantially the gain by the use of a few passive cavities as in this case.

After interaction in the output cavity the beam gets into a collector 7. The RF power is fed from the magnicon through two waveguides 9 placed at 90° along the output cavity azimuth.

2 First Magnicon

A schematic diagram of the first magnicon is given in Fig.1 . A diode gun with a LaB_6 emitter is used as an electron source. After the gun the beam is guided into a circular deflection system. The first cavity is excited by an generator and deflects the beam at a small angle. The second cavity (passive) is excited by a predeflected beam and provides the particle deflection at the required angle ($\alpha_0 = 30^o$). The distance between the cavities $l = \beta_z\lambda/4$ is chosen to provide the maximum gain. After its flight in the drift space the beam gets into an output cavity (the magnetic field distribution is shown in Fig.1) and then into a collector section .

The main parameters of the magnicon experimentally obtained are listed in Table 1.

Table 1

Frequency, MHz	915	Output power, MW	2.6
Beam voltage, kV	300	Efficiency, %	73
Beam current, A	12	Electron efficiency, %	85
Beam power, MW	3.6	Pulse width, μs	30
Repetition rate, pps	1	Gain, dB	30

Experimental studies [1,2] have shown that a magnicon has the following features:

1. Smooth the drive characteristics.
2. The magnicon power decrease at variation of the output cavity loading is not large and makes approximately 10 % at a two-fold change in the output cavity shunt impedance. As it is theoretically predicted with the unloading of cavity the total current reaches collector, i.e. the reflection of electrons does not occur.
3. Good phase stability (exceeding the phase stability of klystron of comparable power).

Besides the experiments described above (when the magnicon was operated with absorbing loads) the device has been successfully tested with the accelerating structure of the racetrack microtron [2].

3 X - Band Frequency Doubler Magnicon

As a prototype for the microwave power source of future linear collider there has been developed at INP an advanced magnicon scheme (Fig.2) providing perveance a by an order of magnitude higher then to that of the classical one [2,4]. The device is a frequency doubler, which lacks the drift space between the deflection system and the output cavity with the deflection angle required for attaining the high efficiency being made directly in the deflection system. Magnicon is designed for an output power of 50 MW, an operating frequency of 7 GHz and a pulse duration of 2 μs.

The beam source is the diode gun 1 with an oxide cathode of 120 mm diameter. The voltage pulse from a step - up transformer is applied to the gun. The main feature of the gun is a high degree of a beam area compression [5].

The beam from electron gun passes the resonance system, which consists of a circular deflecting system and an output cavity. Beam deflecting in the drive cavity 2 and in two passive cavities 3,4 is provided by transverse magnetic field of the TM_{110} wave travelling in azimuthal direction (see Fig.1). The cavities are placed into biasing magnetic field that is excited by coils 5.

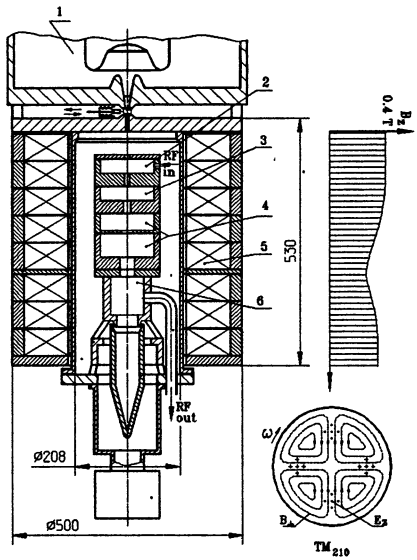

Fig.2 Layout of frequency doubler magnicon.

Drive cavity 2 excited by generator provides a small angle of the beam deflection. Further increase in the deflection angle up to $50-60^o$ is provided in passive cavities excited by a predeflected beam.

A cylindrical output cavity 6 with the TM_{210} wave (Fig.2) travelling in azimuthal direction is used to convert the beam energy to RF. The eigen frequency of the output cavity is twice greater than the deflection one [6]. This cavity is placed into biasing magnetic field too, the field value is determined by the conditions which are necessary to achieve an effective long term interaction of the electron beam with RF-field [1,2]. The RF power extraction is provided by two similar slots in the side cavity wall, which are shifted at 135^o in azimuthal direction to support the wave travelling in azimuthal direction.

At the first stage of the experiment the electron gun was tested. While testing the following data were obtained: beam power 100MW at voltage 430 kV and microperveance 0.82, pulse width $2\mu s$ and the repetition rate up to 3 pps [5,6].

The beam diameter, measured with the help of special movable

graphite diaphragms is less than 3 mm (i.e. area compression ration exceeds 1500:1 and energy density is 4 kJ/cm^2). The main problems arising in the process of investigation were caused by the last passive cavity. A few different version of this cavity had been examined (with three and two coupled cavities) before succeeded to do away with selfexcitation of both, klystron-like and operating mode TM_{110} [6].

For the time being, the very initial test of the magnicon have been carried out. The parameters obtained are listed in Table 2.

Table 2.

Frequency,GHz	7	Drive frequency,GHz	3.5
Power,MW	20	Gain,dB	47
Pulse width μs	1.3	Beam voltage,kV	400
Efficiency,%	25	Beam current,A	200
Repetition rate,pps	2		

References

1. M.M.Karliner et al., "The Magnicon - an Advanced Version of the Gyrocon", Nuclear Instr. and Method in Phys. Res., v.A269, # 3, p.459-473, 1988.

2. O.A.Nezhevenko, "The Magnicon: a New RF Power Source for Accelerators", Proceedings IEEE Particle Accelerator Conference (San Francisco, 1991), v.5, p. 2933 – 2942.

3. G.I.Budker et al., "The Gyrocon - an Efficient Relativistic High-Power VHF Generator", Particle Accelerators, 1979, v.10, p.41-59.

4. V.E.Akimov et al., "High-Power X-Band Pulse Magnicon", Proceedings EPAC 90 (Nice, 1990), v.1, p. 1000 – 1002, World Scientific, 1992.

5. Y.V.Baryshev et al., "Electron Optic System for Forming 100 MW Beam with High Current Density and Microsecond Pulse Duration for X-Band Magnicon", Proceedings of the XIII International Conference on High-Power Particle Beams, v.1, p.598-603, World Scientific, 1991.

6. O.Nezhevenko et al.,"First Test of the X-Band Pulsed Magnicon", Proceedings PAC 93, (Washington,D.C., May, 1993), to be published.

Relativistic BWO as a part of sectioned oscillators and amplifiers

E.B.Abubakirov, N.F.Kovalev

Institute of Applied Physics,
Russian Academy of Sciences
Nizhny Novgorod, Russia, 603600

The relativistic BWO is well known as a powerful, reliable and simple source of pulse microwave radiation. The main quality of BWO is its adaptivity (due to internal feed back) to the fluctuations of electron beam parameters, that is of a great importance for high-current beams formed by explosion-emission (field-emission) cathodes. Just the BWO was the first successfully realized in 1973 [1,2] relativistic microwave device. Recently pulse Cherenkov type BWOs provide output power up to 2 GW in cm wavelength band and about few hundred of MW in long mm band.

To increase the output power and to shorten operating wavelength of BWO it is necessary to use electrodynamic systems with large (in comparison with wavelength) cross sections. Such space developed systems allow to transport high currents and powerful microwaves without high frequency break-down. It should be noted that these systems are principally multimode and BWO itself has low selective properties, so the main problem for powerful and high-frequency BWO is mode selection. This problem is very difficult for BWO because of its mentioned adaptivity and internal feedback, so it seems perspective to use RBWO not as an individual microwave

source but as a part (or section) of more complicated sectioned devices.

These devices [3,4] consist of a set of sections, and their selective qualities are determined as a combination of selective qualities of each section. The idea of sectioning can be illustrated with a classical TWT with a local absorber. The absorber divides TWT into two sections, removes electrodynamic coupling between them and, by this, help to avoid parasitic excitation of tube. Similar to this sectioning of operating space allows to provide excitation of definite mode (or combination of modes) in oscillators and to rich high amplification in amplifiers.

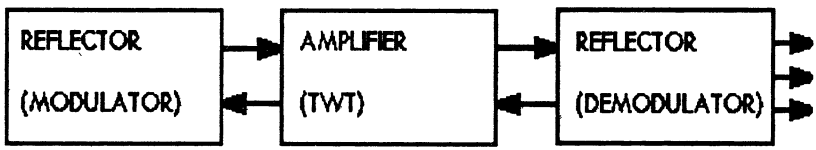

Fig. 1. Scheme of sectioned oscillator.

The Fig. 1 presents the general view of sectioned generator based on TWT. Oscillating regime in this generator is realized by means of feedback provided by reflectors. It is important to note that reflectors can provide the coupling either between electromagnetic waves or between electromagnetic and electron beam waves. In the last case the reflector operates as modulator (or demodulator) of electron beam, and BWO can be used in that position.

The operation of BWO in sectioned generator may be described by the following system of equations

$$\frac{du}{d\zeta} = \mathrm{Re}\left\{ f e^{i\theta} \right\}; \quad \frac{d\theta}{d\zeta} = -(\Delta + 2u); \quad \frac{df}{d\zeta} = \int_0^{2\pi} e^{-i\theta} d\theta_0;$$

where u, θ - are normalized energy and phase position of electrons, f - variable, proportional to the amplitude of high-frequency field, Δ - mismatch of synchronism. Boundary conditions for the system (1) depend on position of BWO: for the modulation section they corresponds to nonmodulated stationary electron beam $u(0) = 0; \theta(0) = \theta_0 \in [0, 2\pi)$ and input wave with initial amplitude f_0 which is entered to the anode edge of section $f(\zeta_e) = f_0$; for the demodulation section initial energy and phase position of electrons $u(0) = F_u(\theta_0); \theta(0) = F_\theta(\theta_0); \theta_0 \in [0, 2\pi)$ are determined by operation of previous section, $f(\zeta_e) = 0$.

Let us consider BWO in the first position as a modulator of electron beam. In this case we have just a BWO amplifier, but to obtain more selectivity it is expedient to use regime of regenerative amplification, that takes place when operating current of BWO-section is close to the excitation value. In this situation high amplification in narrow frequency band is realized. It is important to note that this bandwidth is the less the greater the amplification. So the noise factor, that is proportional to multiplication of amplification and bandwidth is constant and it is possible to provide very high amplification coefficients with low noise levels. The last moment is very useful for relativistic amplifiers with high-current and, consequently, noisy electron beams. This possibility has been demonstrated in [5], where experiments with relativistic sectioned amplifier based on combination of BWO and TWT were described.

Let us analyze properties of BWO section in another position - at the place of output reflector or demodulator. A possibility of operation of BWO in this position is rather clear: a modulated electron beam at the output of TWT section can excite in a proper condition a

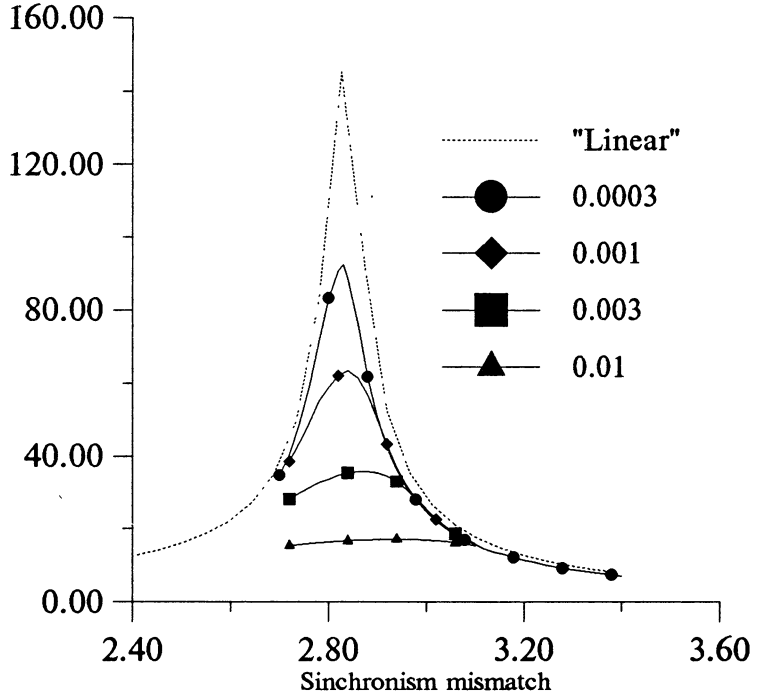

Fig. 2 Transmission coefficient for BWO-reflector for different input signal amplitudes

backward electromagnetic wave. Of course, at this situation all properties of BWO, such as regenerative amplification, can be obtained (Fig.2).

As a matter of fact, for an output section a nonlinear regime is more important and informative. The results of such study, presented in Fig. 2, show very high sensitivity of amplification or conversion

coefficient of BWO-reflector with respect to amplitude of input signal. Besides that, this sensitivity is the more the closer excitation threshold and, respectively, the greater "linear" amplification coefficient (Fig.3). So the BWO-reflector can be regarded as a kind of cleared or saturated mirror.

Let us assume some applications of this effect of nonlinear reflection provided by BWO section. First of all nonlinear operating BWO in feedback channel can realize traditionally rigid (hard) regimes in oscillators. Additionally generator with nonlinear feedback will have relatively small initial period of generation that is proportional to the difference between linear transmission coefficients of main and feedback channels.

In conclusion it should be said that strong nonlinear effects exist in every case of coherent sum of eigenwaves. Nonlinear phase shift of the waves destroys such coherent states in electron devices as regenerative amplification in BWO, Compfner deep condition in TWT, suppression of output signal in Bragg reflectors, loaded with electron beam and some others. It seems to us that application of these effects for creation of powerful electron devices is very perspective. For example, they can be used in oscillators with self-modulated quality, threshold amplifiers and so on.

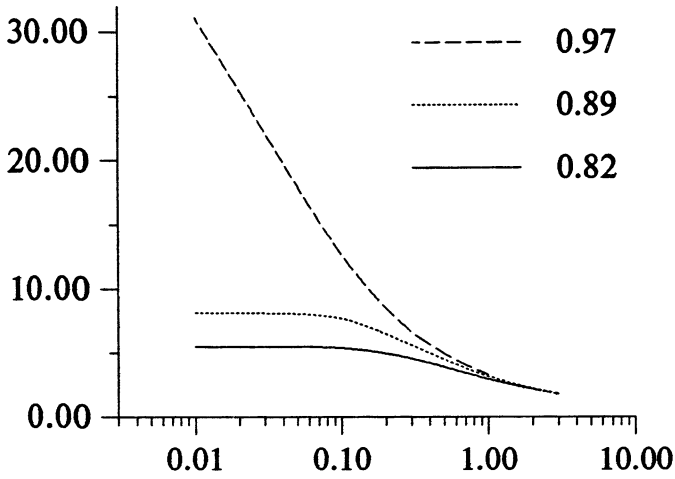

Fig. 3.

Amplification of BWO-reflector

vs. amplitude of the input signal

for various ratios of operating and starting currents.

REFERENCES

1.Kovalev N.F. et al. Pisma ZhETF (Rus), 1973, v.18, No. 4, pp. 232-235.

2.Carmel Y. et al. Phys. Rev. Lett., 1974, v.33, No.21, pp.1278-1282.

3.Abubakirov E.B. et al. Proc. of 8-th Int. Conf. on High-Power Particle Beams. World Scientific, 1991, vol.2, pp.1155-1160.

4.Wharton C.B. Proc. of Int. School of Plasma Physics. Societa Italiana di Fisica, 1992, pp. 329-343.

5.Volkov N.I. et.al. Pisma ZhTF (Rus), 1992, vol.18, No.12, pp. 6-10.

DIELECTRIC CHERENKOV MASERS: GENERATION IN THE INTENSE BEAM OPERATION REGIME AND POTENTIAL FOR ULTRAWIDEBAND AMPLIFICATION

A.S.Shlapakovskii
Microwave centre at the Institute of Nuclear Physics,
Tomsk Polytechnical University, Tomsk, Russia

Dielectric Cherenkov masers (DCMs) continue to be of interest as high-power microwave sources. Recently rather successful experiments have been performed with high-current DCMs [1,2]. Both oscillator and amplifier configurations were investigated, and their potential for high-power operation was demonstrated. In this report important features connected with possible future intense DCM development are considered. It consists of two parts regarding high-current DCM as a short wavelength oscillator and as an amplifier with superwide bandwidth.

1 DCM oscillator in the intense beam regime

Simplicity of dielectric slow wave structures is especially attractive for short wavelength range, and investigations of low-power DCMs [3] advanced in this direction. High-current DCM advancement toward millimeter and submillimeter ranges makes the intense beam operation regime [4] (or two-wave coupling regime) inevitable.

In accordance with the classical TWT theory the intense beam

regime takes place when the beam space charge parameter

$$\sigma^2 = \Gamma\left(\frac{\Omega_b}{\alpha^3\omega}\right)^{2/3} \gg 1. \tag{1}$$

Here ω is a frequency, Ω_b, Γ, α^3 are beam plasma frequency, AC space charge depression coefficient, and beam-wave coupling coefficient. The expressions for Γ and α^3 in the case of thin hollow beam in the circular dielectric-lined waveguide were derived in [5]. Ω_b is connected with the current I of such a beam by the formula

$$\Omega_b^2 = \frac{4eI}{\gamma^3 m r_b^2 u}, \tag{2}$$

where r_b, u, γ are beam radius, velocity and Lorentz factor. It follows from (1), (2) that the current value corresponding to $\sigma^2 = 1$, $I^* \propto \gamma^3\alpha^6$. In the experiments [1] the intense beam regime did not take place in spite of 12 kA beam current because of rather high beam energy and long wavelength (strong coupling). But calculations show that $I^* \ll 1$ kA for weak coupling levels when the beam-dielectric gap Δ becomes comparable with the wavelength.

The amplitude condition of generation for DCM oscillator in the intense beam regime may be written as

$$\rho \cosh\left(\frac{L}{u}\sqrt{\frac{\alpha^3\omega\Omega_b}{2\Gamma^{1/2}}}\right) = 1, \tag{3}$$

where ρ and L are reflectivity and length of the dielectric liner. It is very important for start current problem consideration to take into account the dependence of beam-wave coupling on the frequency. Therefore the relation for the frequency at which the peak gain is achieved must be added, and the equation follows

$$\Omega_b = \frac{k_0(\omega)u - \omega}{\Gamma^{1/2}} = \frac{2u^2}{L^2\omega}\frac{\Gamma^{1/2}}{\alpha^3}\operatorname{arccosh}^2\frac{1}{\rho}. \tag{4}$$

Here, $k_0(\omega)$ is the longitudinal wavenumber in the no-beam system. The typical curves for right hand side and left hand side of Eq. (4)

are presented in Fig. 1 (ε is a dielectric constant, r_0 and R are inner and outer radii of the liner, ω_s is the synchronous frequency). Lower intersections of the curves correspond to start current; upper intersections are out of physical sense because a start current must increase with decreasing of liner length. Evidently, there is a limit of start current increasing when the curves touch. Hence, an important conclusion follows: at a certain parameters of the electron beam and the dielectric waveguide, only an amplification but no generation is possible for any howsoever large current value.

Start current values calculated from Eq. (4) are shown vs beam-dielectric gap in Fig. 2 (solid curves). Lowest points of those curves

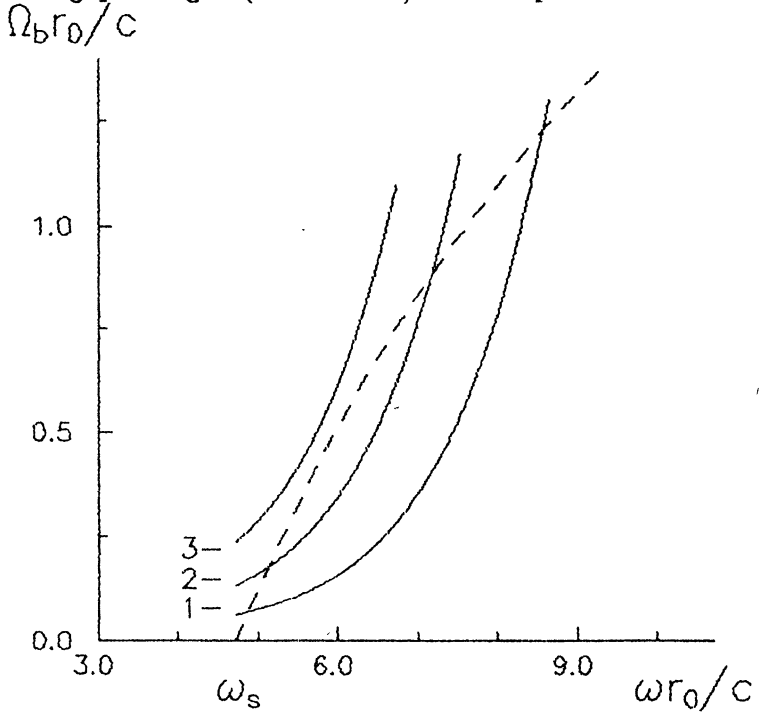

Fig. 1. Plot of left hand side (dashed curves) and right hand side (solid curves) of the Eq. (4). ε = 2.25, R = 2.5 cm, r_0 = 2 cm, ρ = 0.1, γ = 2, r_b = 1.5 cm. L = : 1– 59 cm, 2– 40 cm, 3– 30 cm.

correspond to $\sigma^2 = 1$. At smaller gaps "weak beam regime" takes place, and Eq. (4) becomes incorrect, so that the dashed curves lying under the curve $I = I^*$ may be considered as truthful. Highest points corresponds to the limit of start current rising discussed above. It is significant that this limit lowers with liner length increasing. As a result, it becomes difficult for kiloampere beams to satisfy simultaneously two important requirements: 1) the gap must not be too small, and 2) the operating current must not exceed the start value too much since stohastization of oscillations occurs, and the generation efficiency and signal quality strongly change for the worse.

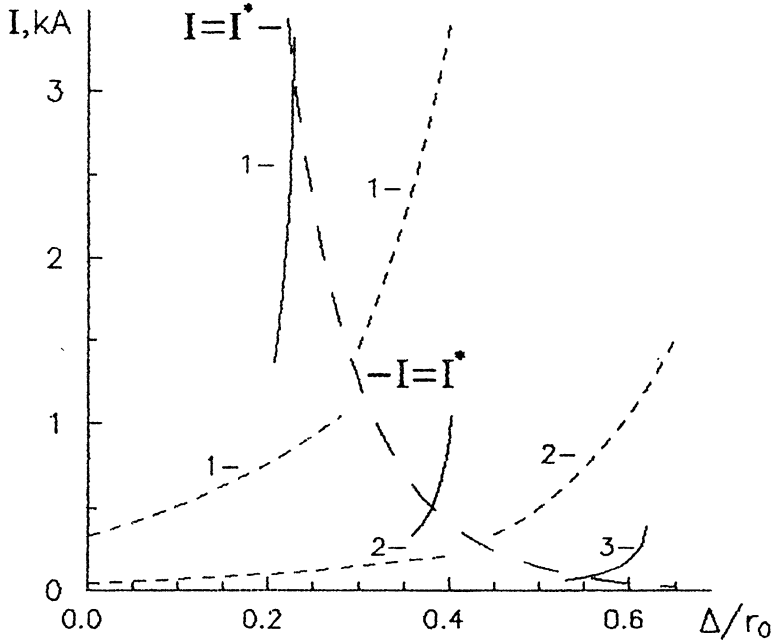

Fig. 2. Start current dependence on the beam – dielectric gap for various liner lengthes. Depression and coupling coefficients' dependences on frequency are taken (solid curves) and not taken (dashed curves) into account. $\varepsilon = 2.25$, $R = 2.5$ cm, $r_0 = 2$ cm, $\gamma = 2$, $\rho = 0.1$. L = : 1– 30 cm, 2– 59 cm, 3– 120 cm. I = I^* is the conditional border current between two–wave and three–wave operation regimes.

2 DCM as ultrawideband amplifier

Perhaps, the place of DCMs among other high-power microwave sources is determined rather by their potential for superwide bandwidth amplifier operation. Really, a dielectric-lined waveguide like a helix in low-voltage traveling wave tube amplifiers is a smooth slow-wave structure and has a weak dispersion over a wide range of operating frequencies, a feature necessary for wide-bandwidth operation. Most previous DCM experiments were carried out with rather thin dielectric liners when the wave field is evanescent, and the beam-wave coupling exponentially decreases as the frequency increases making wide-bandwidth operation impossible. It is, nevertheless, possible in a case, where the dielectric fills a substantial portion of the waveguide cross section, and the transverse size of the vacuum channel is less than the operating wavelength.

Also significant is a proper choice of beam parameters. One can determine how the DCM bandwidth depends on the beam current and energy from the dispersion relation of simplest model of total waveguide filling, both with the dielectric and a cold magnetized beam [6] (k, p are longitudinal and transverse wavenumbers)

$$\omega^2 - \frac{c^2(p^2+k^2)}{\varepsilon} - \frac{\Omega_b^2(\omega^2 - \frac{c^2k^2}{\varepsilon})}{\varepsilon\gamma^3(\omega - ku)^2} = 0. \tag{5}$$

One can derive from Eq. (5) that amplification occurs if the inequality is satisfied

$$\begin{aligned} &\Phi(x>0) < 0, \\ &\Phi = x^3(\tfrac{1}{4} - \zeta) + x^2(1 - 5\zeta + 3\zeta^2) - x(3\zeta^3 + 2\zeta^2) + \zeta^4, \end{aligned} \tag{6}$$

where x and ζ are dimensionless variables

$$x = \frac{\varepsilon\gamma^3(pu)^4}{4\Omega_b^2\omega^2}, \qquad \zeta = \left(\varepsilon\frac{u^2}{c^2} - 1\right)\frac{\varepsilon\gamma^3(pu)^2}{4\Omega_b^2}, \tag{7}$$

and show that the relative bandwidth is maximized at a certain optimum value of ζ, i. e., at the optimal current magnitude for a fixed velocity, and vice versa.

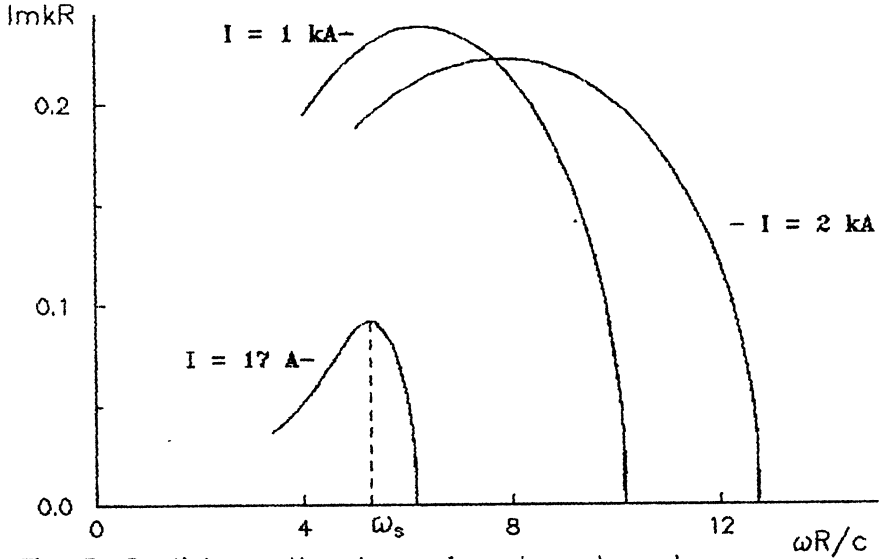

Fig. 3. Spatial growth rate vs frequency dependences for various beam currents.
$\varepsilon = 2$, $r_0/R = 0.5$, $r_b/R = 0.45$, $\gamma = 1.6$.

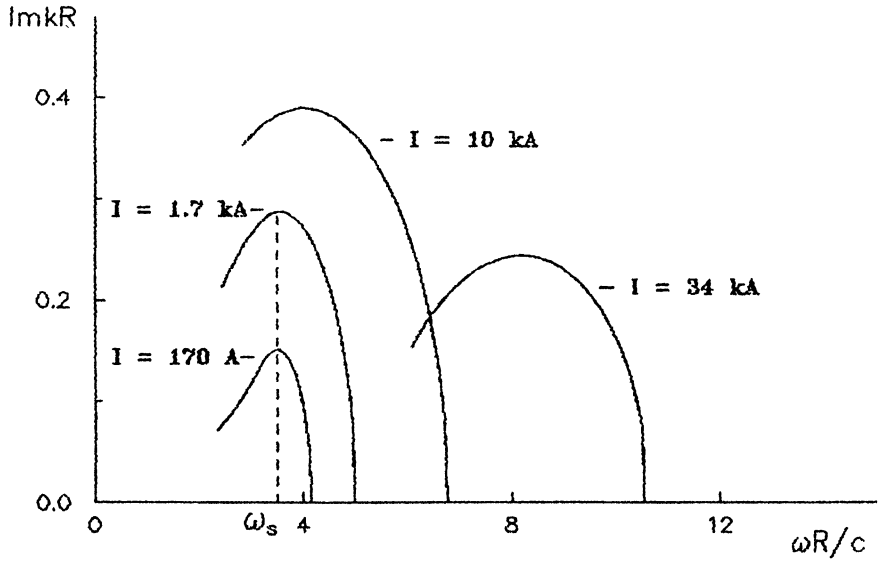

Fig. 4. The same as in Fig. 3. $\gamma = 2.2$, $r_b/R = 0.4$.

The more natural model is necessary to use for the estimation of the bandwidth values achievable in DCMs. In Figs. 3, 4 some results of the numerical solution of the dispersion relation for a thin, hollow beam in a partially-filled waveguide [4] are presented. Actual values of the –3 dB bandwidth depend on the peak gain magnitude and can be determined for large gains by the formula

$$\frac{\delta(\mathrm{Im}k)}{(\mathrm{Im}k)_m} = \frac{10 \ln 2 \lg e}{G(\mathrm{dB}) + C} \approx \frac{3}{G(\mathrm{dB}) + C}, \qquad C \in (6.0, 9.5), \quad (8)$$

where $\delta(\mathrm{Im}k)$ is the difference between the maximum growth rate $(\mathrm{Im}k)_m$, and the value corresponding to –3 dB power level.

The results of calculations illustrate the DCM potential for ultrawideband amplification. For example, for a peak gain of 40 dB and beam current of 2 kA, Eq. (8) and the corresponding curve in Fig. 3 indicate a –3 dB bandwidth of about 50%. At the waveguide radius $R = 4$ cm, we have an amplifier operating in the X-band with a length of 95 cm and a beam-dielectric gap of 2 mm. Among the curves presented in Fig. 4 for a beam of higher energy, the curve with 10 kA current corresponds to the widest bandwidth, 40% at 40 dB peak gain. For an X-band amplifier with $R = 2$ cm, the gap would be 2 mm and the length would be 30 cm.

References

1. Main W., Cherry R., and Garate E., IEEE Trans. Plasma Sci., 1990, **18**, 507.
2. Garate E. et al. In "Intense Microwave and Particle Beams", SPIE Proceedings, Vol.1226 (1990).
3. Walsh J., Cherenkov masers: experiments. In "High Power Microwave Sources", Boston, MA: Artech, 1987, 421.
4. Lemons D. S. and Thode L. E., Phys. Rev. Lett., 1986, **56**, 2684.
5. Karbushev N. I. and Shlapakovskii A. S., Zh. Tekh. Fiz., 1989, **59**(3), 161.
6. Case W., Basic theory of Cherenkov radiators. In "High Power Microwave Sources", Boston, MA: Artech, 1987, 397.

THE REASON FOR THE MICROWAVE RADIATION BREAKDOWN IN A RELATIVISTIC CARSINOTRON

O.T.Loza, P.S.Strelkov, S.N.Voronkov

Institute of General Physics, Moscow, Russia

The problem of secondary effects in vacuum microwave devices became pressing with the development of high-power microwave technology based on relativistic electron beams (REB). The process of microwave radiation terminates usually well before the REB propagation through the generator is completed. The reason for such a behavior of an oscillator is plasma creation in different parts of the setup.

It was shown [1] that the influence of plasma produced in the collector region can be obviated by removing the collector out of the waveguide. It's possible also to stabilize the radius of REB generated by plasma (field-emission) cathode [2], and at the same time to prevent the appearance of plasma at the diaphragm. Creation of plasma in these parts of a microwave device should be taken into account especially if the pulse duration is of the order of microseconds. But only the complete elimination of plasma in all the regions of a vacuum device makes it possible to prevent gradual variations of its properties during the process and by this means to bring the microwave pulse duration to that of the electron beam.

Now it remains to consider the influence of plasma in the slow-wave structure of a microwave device, its origin and the ways of possible preventing of plasma emergence. It was this goal that we pursued in our experimental investigations of microsecond relativistic BWO (carsinotron) in order to obtain the complete utilization of REB pulse duration for microwave radiation in 3 cm wavelength band.

The parameters of the electron beam were: 500 keV, 3.3 kA, 700 ns. The microwave power did not exceed 100 MW, being usually twice less. We got rid of plasma influence on the generator long-term operation in the collector region, on the cathode and the diaphragm using the above mentioned methods. Electrons of the hollow REB $\varnothing$ 40 mm with the thickness of ~ 4 mm propagated along

the lines of a strong magnetic field (~ 1 T) through a rippled waveguide from a diode to a remote collector, keeping their initial radius invariant in 8 mm from the wall. Microwave pulse duration did not exceed 200÷300 ns, and the radiation terminated some hundreds ns before the beam current finished and did not resume.

Electrostatic field on the slow-wave structure walls due to the beam space charge was always more than the electric component of the microwave field, so the field emission of electrons from the walls was prohibited. Our estimations showed, that the space charge of the REB made it impossible for an occasionally (due to photo- or secondary electron emission) born "thermal" electron on the wall to gain excess energy in the microwave field: its flight time was much less than the field period. Hence, for the lack of energy a number of electrons could not be multiplied, e.i. a discharge ignition was impossible. The investigations [3] conducted at our setup showed that a residual gas discharge did not take place in microwave fields of the available magnitude in a time of 1 μs because the pressure was too low: 10^{-4} Tor. For the same reasons the beam relativistic electrons ($\lesssim 3 \cdot 10^{11} cm^{-3}$) could not create a noticeable amount of plasma during the pulse. Besides, the beam propagation itself did not affect the system catastrophically: it was shown [2] that the process of microwave radiation can be turned on as in 100 ns after the onset of the beam current, as in 500 ns. Hence, no plausible reason taken alone was available to conceive creation of plasma.

First, we tried to study, how the bombardment of the structure walls by relativistic electrons influences on the radiation pulse duration. By means of artificial diminishing of the magnetic field only inside the corrugated waveguide we varied the gap between the outer border of REB and the inner radius of the tube. The moment of electron striking was observed by a collimated X-ray receiver (<5 ns) adjusted to a definite zone (6 cm) of the exposed area. The magnetic field having being decreased step by step, the beam radius expanded, and in an appropriate moment electrons touched the wall (Fig.1). The radiation pulse duration having been comparatively large drops simultaneously with the electron impact.

It was known [4] that backscattered electrons can occur on

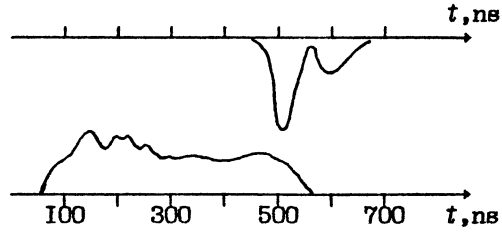

Fig. 1.

the collector. A portion of them possessing the energy of ≥ 100 keV can penetrate into the waveguide, overcoming the potential of the REB. We observed the presence of these electrons inside the device with the help of special sensitive film. The film was pasted to the back side of the anode diaphragm at the entry of the carsinotron and at its exit (being protected from the direct REB).

In the case of axial symmetry the electron beam was wasted in the walls of emitting horn, and the exposed area of the film was ring-shaped, 3÷4 mm thick. If the remote collector was in use the beam had to turn as a whole through ~ 90 degrees, drifting transversely to the plane of bend in the inhomogeneous magnetic field. Note, that the direct and the reverse beams tend to drift in the same direction. Therefore, the position of the backstreaming electron flux (a half-ring in its visible cross section beyond the direct REB) at the exit of the slow-wave structure was observed to be 13 mm displaced with respect to the direct hollow beam. The exposed area of the film at the entry was only 4 mm thick because of comparatively small diameter of the waveguide. This means, that a part of relativistic electrons from the collector (with a current of a few amperes) can not fly unimpeded in the tube and strike ripples of the carsinotron since the beginning of the beam pulse.

Hence, we have proved that electron bombardment of the slow-wave structure suffices to terminate microwave radiation, and then we have elucidated the feasibility of this: back scattering on the collector.

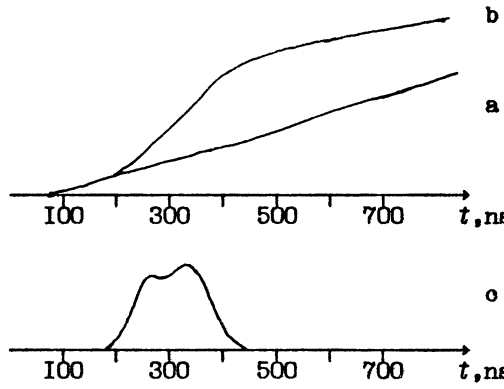

Fig. 2.

An optical system, comprising a lens, a collimator and a photo-electric multiplier, enabled us to determine the position of a glowing object with the accuracy of $\lesssim 20$ cm and, that was more important, it suppressed signals from other light sources. It was urgent, because a powerful light flux from the exploding cathode hindered to reveal glowing in any other region. The signals from the optical receiver, tuned to the center of the slow-wave structure, are shown in Fig.2. The plasma cathode is the only light source if the oscillator is inactive (a): ripples being shunted by a thin tube. With the appearance of microwaves (c) a new light becomes noticeable (b) on the background of that of the cathode, its origin being inside the BWO and the intensity growth fitting the process of the radiation. We attribute this phenomenon to the microwave discharge and the creation of a noticeable amount of plasma in the interior of the rippled waveguide.

So, we consider the scattered electrons from the collector to be the reason for the primary plasma appearance, a comparatively small amount of it, and the further fast accumulation of plasma is due to microwaves.

To diminish the flux of electrons from the collector we applied an additional solenoid that enhanced the magnetic field between the collector and the slow-wave structure twice. A part of electrons with big pitch-angles reflected from such a magnetic

filter, and the total amount of electrons capable to strike the walls diminished. The more limited number of initial plasma spots appeared on the surface of the carsinotron, the more time was it necessary for microwaves to create a sufficient volume of plasma for the premature shortening of the microwave pulse. As a result the radiation pulse duration increased from 200 to 400 ns.

The complete elimination of the scattered electrons in the interaction space of an oscillator can be obtained by a spatial separation of the direct and the backstreaming beams using a particle drift in an inhomogeneous magnetic field. To achieve this it is sufficient to bend the direct beam in the collector chamber. Our estimations and numeric simulations have shown that it is necessary to send the beam into a half-torus with a small (~ 0.1 T) guiding magnetic field.

The above results may be summed up as follows. The electron bombardment of the slow-wave structure by backstreaming electrons causes a microwave discharge in the oscillator. The partial suppressing of this electron flux has culminated in the increase of the radiation pulse duration. Techniques for the complete elimination of the reasons of plasma creation in a vacuum microwave device is proposed.

1. Voronkov S.N., Loza O.T., Strelkov P.S. //Proc. 8 Int. Conf. on High-Power Particle Beams (BEAMS'90), July 2-5, 1990, Novosibirsk, USSR, v.2, p.1147-1152. // Fizika plazmy. 1991. v.17. No.6, p. 751-755.
2. Voronkov S.N., Loza O.T., Strelkov P.S. // Program Abstracts 9 Int. Conf. on High-Power Particle Beams (BEAMS'92), May 25-29, 1992, p.239. // Fizika plazmy. 1993. v.19. No.4, p. 601-605.
3. Tsagareishvili N.S. // Fizika plazmy. 1990. v.16. No.11, p.1389-1391.
4. Aleksandrov A.F., Galuzo S.Yu., Karavichev M.V., Kubarev V.A. // USSR 7 Simp. on High-Current Electronics. Tomsk - 1988. v.2. p. 154-156. (rus.)

STUDIES ON PLASMA WAKE-FIELD EXCITATION USING PULSED RELATIVISTIC E-BEAMS WITH A GREAT NUMBER OF BUNCHES

A.K.Berezin, Ya.B.Fainberg, I.N.Onishchenko,
V.A.Kiselyov, A.F.Linnik, V.V.Uskov,
V.A.Balakirev, G.L.Sidel'nikov, G.V.Sotnikov
Kharkov Institute of Physics & Technology,
310108 Kharkov,Ukraine

The idea of possible use of longitudinal charge density waves ,– the waves excited in plasmas with electron beams or sequence of electron bunches,– for charged particle acceleration was first proposed by Fainberg in 1956 [1]. According to the theory [1–3], the most effective excitation of such waves occurs during collective interactions of monoenergetic, low angular divergence (LADREB) electron beams with plasmas. Our observations at KFTI [4–6] during experiments on the interaction of monoenergetic LADREB with a dense plasma confirmed the generation of ultra high frequency (UHF) electric fields with gradients up to 400 kV/cm, as caused by beam-plasma instability. This instability was discovered by Akhiezer and Fainberg [7]. The use of such fields for particle acceleration to high energy difficult to perform, because during the beam-plasma interaction the wave relativistic factor γ_w decreased to the point of $\gamma_w < \gamma_b$, where γ_b is the beam relativistic factor.

The method of producing plasma excited wake fields for particle acceleration, using a single bunch [8,9] or a train of bunches of relativistic electrons [9–13], remmoved this obstacle, becoming one of

modifications of collective particle acceleration by means of plasma charge density waves. The subsequent theoretical studies [14] indicated that a train of electron bunches could be used to achive high gradient accelerating fields in plasmas. Moreover, the coherent addition of wake fields of single bunches allowed to excite intence plasma waves even with the density of each bunch being rather low.

The first experiments on plasma wake-field excitation with a train of relativistic electron bunches [10–12] were carried out using an experimental set-up which consisted of a linear accelerator, a plasma gun, a interactions chamber, a magnetic analyzer and a diagnostic set. Relativistic electron bunches were produced in the electron linac with the following parameters: beam current I=1 A, beam energy E=2–2.5 MeV, pulse width $\tau = 2\mu s$, frequency modulation f_m=2805 MHz, beam diameter – 1 cm.

In the process of the autophasing the electrons were bunched with length 1,7 cm, number of electrons per bunch $2 \cdot 10^9$, charge 0.32 nC. Frequency repetion was equal to the frequency of modulation. The plasma sourse was a coaxial plasma gun. The inner electrode of the gun was hollow with 2 cm-diameter and used for REB-guiding into the main interactions chamber which was a glass tube 2 m long with 10 cm in diameter, placed in longitudinal homogeneous magnetic field whose strength reached up to 2 kG. The initial pressure was 10^{-6} Torr. The plasma electron density was measured via UHF cut-off frequency signals at the wavelength 10, 3.0 and 0.8 cm and using radiointerferometers at the wavelength 3.0 and 0.8 cm. This set also helped to define the longitudinal plasma density gradient in the interaction chamber. The experiments were carried out with a decreasing density plasma within the limit $10^{13} - 10^{10}$ cm^{-3}. The optimum density of electrons in the plasma was achieved when the electron Langmuir frequency ω_{pe} was equal to the beam modulation frequqncy $\omega_m = 2\pi f_m$ ($\omega_m \approx \omega_{pe}$), $n_{pe} \sim 10^{11} cm^{-3}$. Using longitudinal electric probes, the frequency spectrum measurements were made, as well as those of E_z component of the UHF fields which were excited inside and outside of the plasma via interactions of electron bunch train with plasma.

Experimentally measured was the relationship of beam pulse-averaged energy spectra at the exit from the interaction chamber vs plasma density (Fig.1). Notably, the maximum beam energy losses occured at 200–500 keV ($\sim 12\%$) at the plasma density $n_{pe} \sim 10^{11} cm^{-3}$ when the beam modulation frequency was close the plasma electron Langmuir one ($\omega_m \sim \omega_{pe}$), the longitudinal gradient of plasma density at whole length being ~ 6. The appreciable part of beam electrons was accelerated to 150–200 keV. At a decrease of the gradient of the longitudinal plasma density lowering to 2.5 the range of beam energy losses grew to 300–500 keV. Decreasing of bunch charges (2 times) caused a lowering of the energy loss range to 80–100 keV.

Measurements of the plasma-excited field longitudinal component E_z indicated that amplitude of this component was 10 times smaller on the outside of the interactions chamber than inside at a distance of $r = 2$ cm from the axis. It was found that the maximum frequency spectrum corresponded to the accelerator modulation frequency with the half width of the observable UHF-oscillation spectrum being 10-12 MHz which was not greater than 1.5 times that in vacuum.

In the presence of plasma the field amplitude (Fig.2, 2nd curve) increased linearly in time for $t \sim 1.2 - 1.4 \mu s$. After achieving its maximum the field amplitude fell down sharply, and at this moment the energy spectrum displayed the presence of particle acceleration from the plasma exit port. The same figure shows for comparison the observable variations of field amplitude without plasma.

In our experiments, we registered an increase of the total current I_n as caused by the appearence of plasma current I_p, the direction of beam current I_b ($I_n = I_b + I_p$). The total beam current increase can be calculated from the ratio $I_n/I_b = G = 1 + \gamma_b$ ($\gamma_b \sim 5$). Fig.3 shows the total current variations as a function of plasma density for three different cross sections of the interactions chamber (1 — L=40 cm, 2 — L=80 cm, 3 — L = 120 cm). In our case, the resonant dependence I_n vs n_{pe} is evident. The maximum observable ratio $G \sim 5$ was at $n_{pe} \sim 10^{11} cm^{-3}$.

Similar phenomena were observed during passage of modulated

relativistic electron beames through high density neutral gases (P=1–300 Torr)[15,16]. The created plasma was dissipative and inhomogeneous which, to a considerable degree, hampered the development of unmodulated beam plasma instabilites and decreased beam relaxation.

In our experiments, a train bunches (modulated REB), passing through Ti foil, 30 microns thick, was injected into the interactions chamber filled with neutral gas (hydrogen, air) at pressures P=1–300 Torr. At a distance 25 cm of the foil the foil, plasma density was $n_{pe} \sim 10^{11} - 5 \cdot 10^{11} cm^{-3}$, and therefore $\omega_m \sim \omega_{pe}$. At larger distances, the plasma density became substantially lower. The energy spectra of electron beams which passed through the interactions chamber are shown in Fig.4 for the distances of 2 cm (curve 1), 6 cm (curve 2), 15 cm (curve 3) and 25 cm (curve 4). One can see that near the foil the energy spectrum resembled that in vacuum, and, then, after the bunches had passed through the interaction chamber, it is observed an important change in the spectrum containing groups of accelerated and decelerated electrons. The presence of electron beam energy losses, UHF radiation with a narrow frequency spectrum and radiation in the soft X-ray range, localized within the interactions region, all bore witness to generation in the plasma of high-intensity UHF fields in which beam and plasma electrons can get considerable energy gains. As the preceeding case, we also observed the total current increase but to a lesser degree.

As a result, our experiments confirmed that a train of short electron bunches, upon passing through a plasma, could excite coherent fields that added up to high values. Our results showed that the longitudinal electric wake-fields in plasma increased when the frequency repetition of short relativistic bunches coincided with the plasma frequency ω_{pe}.

We plan to perform the experiments using the same beam, but a different plasma production system which will consist of a 4m-long interactions chamber filled with plasmas in counter-streaming directions to each other to form a plasma column with densities on the order of $10^{10} - 10^{13} cm^{-3}$ and a low plasma density gradient.

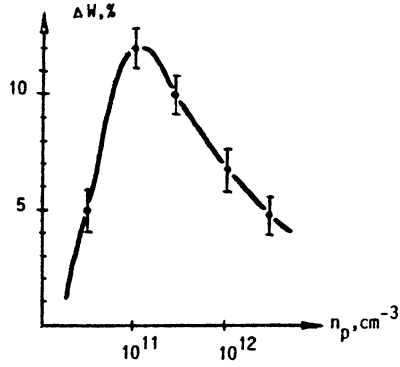

Fig.1

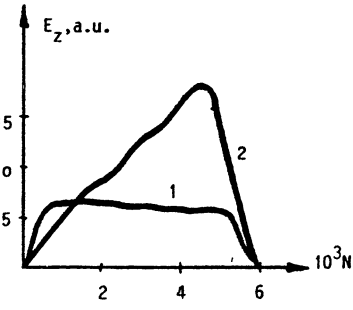

Fig.2

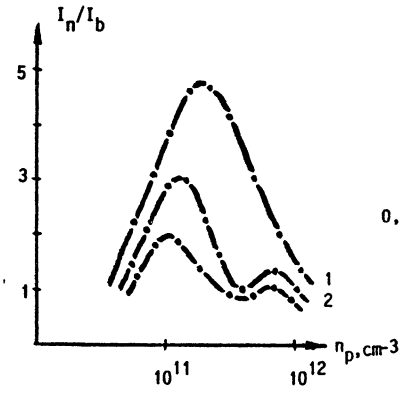

Fig.3

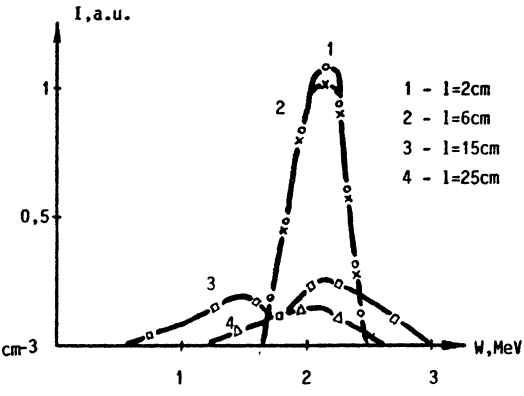

Fig.4.

In this experiment, we shall investigate the parameters of plasma-excited wake-fields as a function of the number of bunches (from 100 to 6000).

In order to study the wake-field generation with more intense bunches, we intend to use an electron linac, already commissioned at KFTI, which has the the following parameters: energy — 15–20 MeV, number of bunches - 10-18, bunch duration $30ps$, number of electrons per bunch $10^{11} - 10^{12}$, current $> 10A$.

This work was supported by the Ukrainian state Commitee of Science and Technology.

References

1. Ya. B. Fainberg. Proc.Symp.on Coll.Acc. CERN, 1956,1,84.
2. Ya. B. Fainberg. Atomnaya energiya, 1961,11,313.
3. Ya. B. Fainberg et al. ZhETF, 1969,**57**,966.
4. V. A. Kisel'ev et al. Pis'ma v ZhETF, 1974,**20**,603.
5. V. A. Kisel'ev et al. ZhETF, 1976,**71**, 193.
6. A. K. Berezin et al. Pis'ma v ZhTF, 1978,4,732.
7. A. I. Akhiezer, Ya. B. Fainberg. DAN SSSR, 1949,**69**,555.
8. P. Chen et.al. Phys. Rev. Lett., 1985,**54**,693.
9. J. B. Rosenzweig et al. Phys.Rev.Lett., 1988,bf 61,98.
10. A. K. Berezin et al. Pis'ma v ZhETF, 1971,**13**,498.
11. A. K. Berezin et al. Preprint KFTI 71-72,1971.
12. A. K. Berezin et al. ZhETF, 1972, **63**,861.
13. K. Nakajama et al. Nucl. Instr. Meth., 1990,**A292**,12.
14. A. K. Berezin et al. Preprint KFTI 93-12,1993.
15. A. K. Berezin et al. Preprint KFTI 90-40,1990.
16. A. K. Berezin et al. Preprint KFTI 91-45,1991.

A CORRUGATED PLASMA WAVEGUIDE AS A SLOWING STRUCTURE FOR POWERFUL MICROWAVE SOURCES

P. I. Markov, I. N. Onishchenko
A. O. Ostrovsky, G. V. Sotnikov
Kharkov Institute of Physics and Technology,
Kharkov, Ukraine

Introduction

There has been a great deal of interest in recent years in the study of slowing structures, where one of the main components is plasma [1,2]. The reason for this interest is the feasibility of constructing powerful amplifiers and generators of SHF oscillations, since in plasma-filled slowing structures there is no restriction on the exciting electron beam power due to the presence of a limiting vacuum current. Furthermore, the presence of the plasma considerably extends the efficiency of SHF devices. A significant growth of generated power in a corrugated slowing structure, filled with the plasma resulting from gas ionization by the beam, has been observed in Refs. [1–6]. The subsequent theoretical works and computer simulation of electrodynamic characteristics of such hybrid plasma-waveguide slowing structures have revealed a number of specific features of these systems. The main of them are:

- increase in the coefficient of the beam coupling with the excited wave and decrease of the starting current, stipulated by volumetricity of the waves in the region filled with a plasma [1-6];
- nonlinear tuning up of synchronism during radiation of the excitated wave and modulation of the plasma in the field of forward

and backward wave, Ref. [8];
- plasma-induced dispersion displacement of the resonance to the region of a more effective beam-wave interaction Ref. [9];
- rise of a "dense" spectrum of self-sustained oscillations of the corrugated waveguide filled with a plasma, Ref. [9].

However it should be noted that by the present time there is no definite clarity in the explanation of the phenomena, which lead to a considerable growth of power in plasma-filled SHF devices.

Statement of the problem. Input equations

In this paper the dispersion characteristics of a corrugated plasma-filled slowing structure are investigated in detail. The equation is derived to describe the characteristics of the electrodynamic system under study. This equation is solved both analytically in the case of small depths of the corrugation for the main radial mode, and numerically for a large number of radial and longitudinal harmonics. It is shown, in particular, that the "dense" spectrum of plasma oscillations is uniformly distributed in the whole interval of low frequencies.

Let us consider an axially-symmetric waveguide with ideally conducting corrugated walls. In the cylindrical coordinate system (r, φ, z) the surface of the waveguide is given by:

$$r(z) = r_0(1 + \alpha \cos k_0 z), \qquad (1)$$

where r_0 is the average radius of the waveguide, $k_0 = 2\pi/D$, D is the spatial period of the structure; $\alpha = \Delta r/r_0 < 1$, Δr is the depth of corrugation. The waveguide is filled with a plasma and is put in a strong longitudinal magnetic field, so, the motion of plasma electrons may be considered as one-dimensional. The contribution of ions to the plasma polarization is neglected. We define the field configuration and the dispersion characteristics of the electrodynamic structure described.

The initial equations of the problem are the Maxwell equations for the material medium, which fall into two subsystems for axially-symmetric fields. This corresponds to the existence of two uncoupled

fields of E -- and H - - type in the plasma waveguide with corrugated walls.

By virtue of spatial periodicity of the corrugated waveguide along the z-axis, let us represent the desired components of the electrical and magnetic field as infinite series of spatial harmonics:

$$F(r,z,t) = \sum_{n=-\infty}^{\infty} a_n F_n(r) \exp(ik_{zn}z - i\omega t), \qquad (2)$$

where $F(r,z,t)$ are the E — type field components, $a_n, F_n(r)$ are, respectively, the amplitude and the distribution function in the cross-sectional plane of the waveguide of the n-th spatial harmonic; $k_{zn} = k_z + k_0 n$ is the longitudinal wave number of the n-th harmonic. Solving the set of Maxwell equations by taking into account (2) and using the boundary condition for the tangential component of the electric field on the lateral surface of the waveguide $E_\tau \Big|_{r=r(z)} = 0$, we shall obtain the dispersion equation of the form:

$$\det \| C_{mn} \| = 0. \qquad (3)$$

where

$$C_{mn} = \left[1 + \frac{\varepsilon_{\|} k_0 k_{zn}(n-m)}{k_{\perp n}^2}\right] \int_{-D/2}^{D/2} J_0[k_{\perp n} r(z)] \exp[ik_0(n-m)z] dz,$$

$k_{\perp n} = \sqrt{\varepsilon_{\|}(\omega^2/c^2 - k_{zn}^2)}$, $\varepsilon_{\|} \equiv 1 - \omega_p^2/\omega^2$, $\omega_p = \left(4\pi n_p e^2/m\right)^{1/2}$, n_p is the plasma density; e, m are the charge and mass of the electron.

Dispersion characteristics of the slowing structure

The formulation of the problem given above is strict, and the solution of the dispersion equation (3) can be obtained only by numerical methods. However, in the case of a small corrugation depth, $\alpha \ll 1$, the dispersion equation is significantly simplified and, as a result of its solution, one can obtain the analytical relation between the frequency and the longitudinal wave number. Such kind of a solution has been given in Ref. [7]. It has been shown that the existence of a small but finite corrugation depth is binding together the spatial

harmonics. A strong interaction between the space harmonics takes place when their phase velocities are close to each other, and the group velocities have opposite ways. This leads to the splitting of the frequency spectrum and to the formation of frequency stop bands. As a result, there exist the frequency intervals $\Delta\omega$, where equation (3) has no solution relative to k_z. For example, near the points $k_z = \pm\pi/D$ the dispersion curve has a break which is equal to $\Delta\omega \sim \alpha\omega$. In order to determine the widths of the frequency stop bands in the regions where the branches with numbers $n \geq 1$ intersect, it is necessary to retain the terms of a higer order relative to the parameter α in the dispersion equation. In this case, the widths of the frequency stop bands decrease with the growth of their number m.

A more detailed analysis of the dispersion characteristics of the plasma structure considered can be performed only by the numerical simulations of the dispersion equation (3). Below the results of numerical simulation are presented for different geometrical parameters of the waveguide and the plasma density. Figs. 1,2 show the dis-

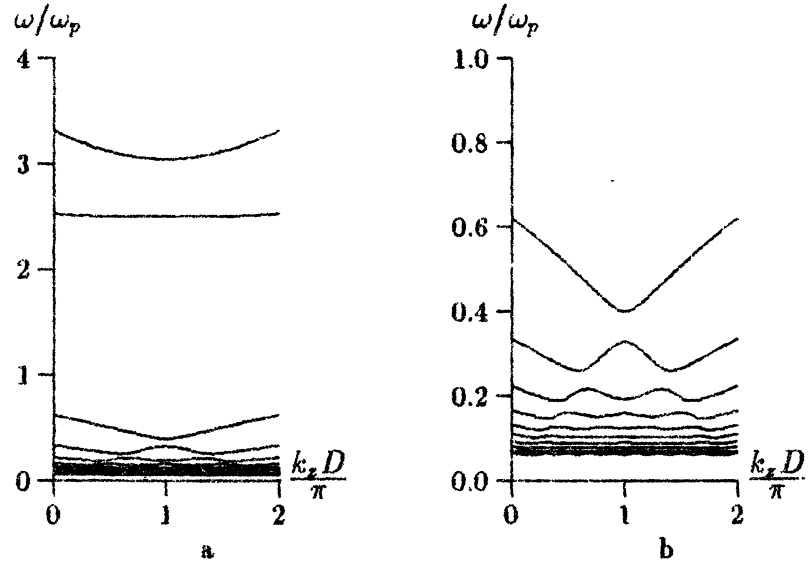

Fig. 1.

persion curves of the plasma waveguide with periodic boundaries for

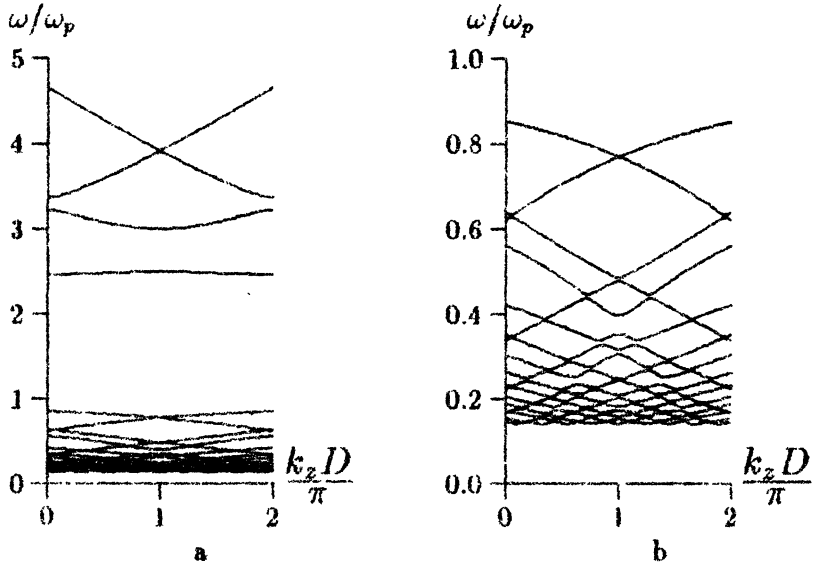

Fig. 2.

the following parameters of the structure: $r_0 = 1$ cm; $k_0 = 2$ cm^{-1}; $\alpha = 0.2$; $n_p = 2.83 \cdot 10^{11}$ cm^{-3} for two $n = 0, -1$ (Fig. 1) and four $n = 0, \pm 1, 2$ (Fig. 2) space harmonics. Note that Figs. a show the complete dispersion patterns of the slow-wave structure, and Figs. b show the dispersion curves only in the low-frequency region.

Basic results. Conclusions

It should be noted that in Ref. [9] the calculations of the dispersion characteristics were made only for the first three radial modes. Our calculations were carried out for an essentially larger number of radial modes. It leads to a qualitatively new behavior of the dispersion curves: in the region $\omega \ll \omega_p$, the thickening of the low-frequency spectrum takes place. This behavior of the dispersion curves is due to a strong relation between the space harmonics which belong to the

radial modes with high numbers $s \gg 1$, and the ones near the region $\omega = 0$.

An infinitely large number of radial and space harmonics give a fundamentally new kind of spectral behavior, i.e., a "dense" spectrum in the whole low-frequency range $0 < \omega < \omega_p$, Ref. [9]. As a result, in the interaction of the electron beam with slow waves of a corrugated waveguide, one should expect the generation of the multimode regime of RF-fields in the low-frequency region.

This work was supported by the Ukrainian State Committee of Science and Technology.

References

1. Fainberg Ya. B. et al, Dokl. Akademii Nauk Ukrainy. Ser. A, 1990, **11**, 55. (In Russ.)

2. Batskikh G. I. et al, Proc. 9ht. Intern. Conf. High-Power Particle Beams. Novosibirsk, 1990, **2**, 1173.

3. Tkach Yu. V. et al, Fizika Plasmy, 1975, **1**, 81. (In Russ.)

4. Tkach Yu. V. et al, Fizika Plasmy, 1979, **5**, 1012. (In Russ.)

5. Minami K. et al, Appl. Phys. Lett., **53**, 559.

6. Carmel Y. et al, Phys. Rev. Lett., 1989, **62**, 2389.

7. Ostrovsky A. O., Ognivenko V. V., Radiotekhnika i Ehlektronika, 1979, **24**, 2470. (In Russ.)

8. Bottom M., Amiram Ron., Phys. Rev. Lett., 1991, **66**, 2468.

9. Lou W. R. et al, Phys. Rev. Lett., 1991, **67**, 2481.

EXCITATION OF MICROWAVE-OSCILLATIONS IN MAGNETICALLY INSULATED SLOW-WAVE TRANSMISSION LINES

V.A.Balakirev, D.Yu.Sidorenko, G.V.Sotnikov
Kharkov Institute of Physics & Technology,
310108 Kharkov,Ukraine

Abstract. The theory of electromagnetic radiation excitation by an electron flow is considered for a flat magnetically insulated transmission line with a comb anode. The dispersion relation describing the excitation of electromagnetic oscillations by the Brillouin flow in the slow-wave structure is derived. The numerical analysis of dispersion equation has shown that in the presence of the slow-wave structure, an essential increase in increments of unstable oscillations takes place. The conditions for optimum generation of microwave power are found. Efficiency estimates are given for the oscillators of the type considered.

Introduction

In magnetically insulated transmission lines the Brillouin electron flow forms[1]. The electrons, emitted from cathode, drifts along the electrodes in crossed self-consistent electrical and magnetic fields.

Being strongly non-equilibrium, such a flow is unstable [2]. In transmission lines with slow waves (coaxial lines, flat lines with a corrugated anode,comb-shaped structures) the synchronism of the Brillouin flow with slow waves of the structure is possible. The instability, arising under these conditions, will lead to the excitation of intense electromagnetic oscillations. The systems of this type can be used as powerful microwave amplifiers and oscillators. In the Magnetically Insulated Line Oscillator(MILO) the electron flow formation and the generation of radiation are combined. For the given geometry of the transmission line, the only external parameter which defines the characteristics of the oscillator is the voltage applied.

Interaction of the electron flow with the slow-wave line

The geometry of the flat slow-wave line is shown in fig.1. The anode has a comb structure. The potential difference applied to the electrodes is sufficient to cause the explosion emission. As a result, the Brillouin flow with thickness x_*, pressed to the cathode, forms in the line. We shall describe the comb using the long-wave approximation

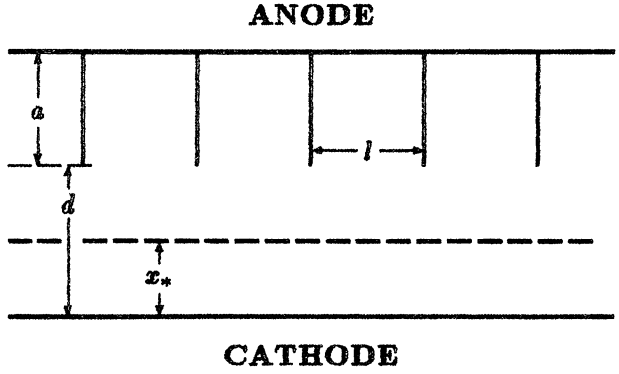

Fig.1. The slow-wave transmission line

$kl \ll 1$,where k is the longitudinal wave number, l is the comb

period. The dispersion equation for TM waves can be obtained by matching the field impedance in the vacuum gap $d > x > x_*$ to the impedances of the comb and the electron flow. As a result, we shall obtain

$$\zeta_b = (\zeta_S - \tanh pB)/(\zeta_S \tanh pB - 1), \qquad (1)$$

where $B = D - X_*$, $D = d\omega_c/c$, $X_* = x_*\omega_c/c$,

$$\zeta_S = (w/p)\tan(wA), \quad \zeta_b = \Gamma\gamma_*^2\Omega_*^2/p(\Delta'_*/2 + \Delta_* F'_*/F_*), \qquad (2)$$

$\zeta_{S,b}$ are the field impedances at the boundaries of the comb $x = d$ and the electron flow $x = x_*$, $p = (K^2 - w^2)^{1/2}$, $w = \omega/\omega_c$, $K = kc/\omega_c$ are the dimensionless frequency and longitudinal wavenumber, c is the speed of light, $\omega_c = eH_c/mc$ is the cyclotron frequency, H_c is the magnetic field on the cathode, $A = a\omega_c/c$, $\Gamma = w^2 - K^2 - 1$, $\Omega_* = w - KV_*$, $V_* = v_*/c$, v_* is the velocity, γ_* is the relativistic factor of electrons at the flow boundary $x = x_*$, $\Delta_* = \gamma_*^2\Omega_*^2 - 1$, $\Delta' = d\Delta/dX\ |_{X=X_*}$, $F = F(X_*)$, $F'_* \equiv dF/dX\ |_{X=X_*}$, $X = x\omega_c/c$, the function $F(X)$ is the solution of the differential equation

$$d^2F/dX^2 + (\Delta'/\Delta)(dF/dX) - p^2F = 0, \qquad (3)$$

$\Delta = \gamma^2\Omega^2 - 1$, $\gamma = \cosh X$, $\Omega = w - KV(X)$, $V(X) = tanhX$. On the cathode, the longitudinal component of electric field goes to zero, therefore, $F(0) = 0$.

Now we shall analyse the Brillouin flow instabilities in the slow-wave structure. In the extreme case of $K \ll 1$, from the dispersion equation (1) we shall obtain the expression for phase velocities of waves

$$V_{ph}^{\pm} = \frac{\sinh X_* cosh X_* \pm [s(s-1) + s\nu(s - \cosh^2 X_*)]^{1/2}}{\sinh^2 X_* + s(1+\nu)}, \qquad (4)$$

where $s = d/x_*$, $\nu = a/d$. If we exclude the electron flow by introducing extreme transition $X_* \to 0$, then from Eq.(4) we shall obtain the expressions for the phase velocities of forward and backward waves of the "cold" structure. The Brillouin flow not produce new branches of oscillations, but it "distorts the "cold" branches.

The LF-instability arises when the discriminant is negative $D = s(s-1) + s\nu(s - \cosh^2 X_*) < 0$. The flow with the minimal current $s = \cosh^2 X_*$ is stable. In this case as in the smooth anode line the phase velocity of the slow wave V_{ph}^- is equal to zero. Phase velocity of the quick wave $V_{ph}^+ = \tanh 2X_*/(1 + \nu \cosh^2 X_*/cosh2X_*)$ is lower than that in the line with smooth electrodes.

The dispersion equation (1) was solved numerically for the minimal current and different slow-wave structure geometries and applied voltage values. The frequency (fig.2a) and the instability growth rate (fig.2b) versus wavenumber were obtained for slow-wave structure with $d/a = 4$ and the applied voltage $U = 0.6$ MV. For small K, in accordance with analytical treatment, the Brillouin flow is stable and two waves propagate in it. The quick wave branch breaks. This feature is also observed for the line with smooth walls[2]. Oscillations grow in the frequency range $W > 1$. The growth rate as a function of the wavenumber has a peak. The gain in the growth rate is due to the wave being in resonance with the slow-waves structure. Outside of the resonance region K, the instability has has shows the same behavior as in the line with smooth walls. Ast the voltage increases, the growth rate peak shifts to the low frequency region, and the increment value at the maximum decreases. For high voltages $U > 2.4$ MV, the resonance instability growth rate is essentially less than the growth rate of magnetron instability [2], which arises in the line with smooth walls. Therefore, in this case, the slow-wave structure will influence weakly the excitation of oscillations in the transmission line. The results of numerical calculations for the slow-wave structure with the parameters $d/a = 2$ and an applied voltage of 1 MV are represented in fig.3. Here the wave with the frequency $W = 0.8$ has the greatest growth rate. And this wave is stable in the transmission line with smooth electrodes. The region $K > 1.8$ corresponds to the magnetron instability, and $1.8 > K > 1.3$ — to the resonance instability.

The maximum dimensionless (a) and dimensional (b) increments vs applied voltage for $d = 2$ cm and a $= 0.5$ cm are represented in fig.4. Similar functions dependencies for $d = 2$ cm and $a = 1$ cm are

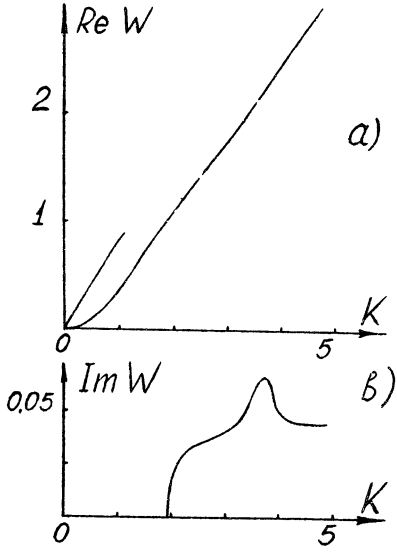

Fig.2

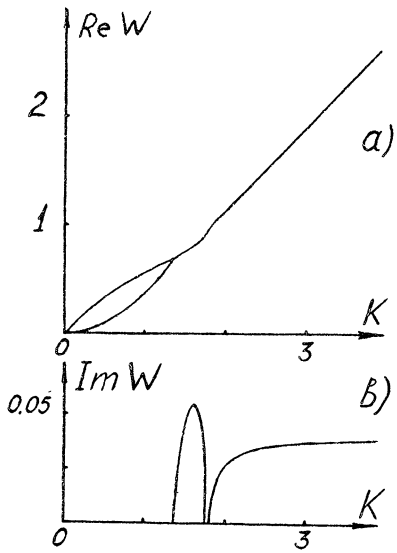

Fig.3

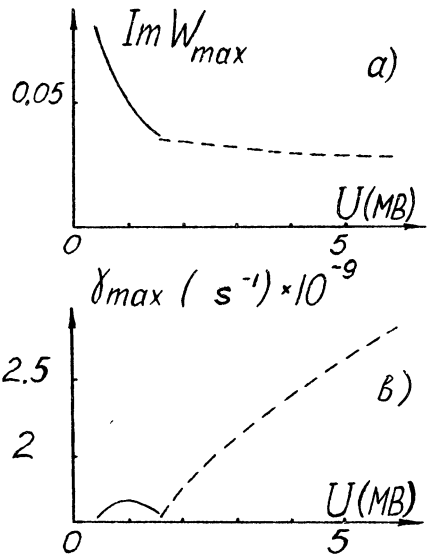

Fig.4

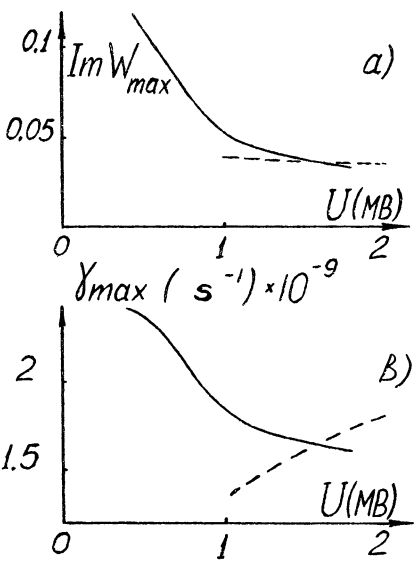

Fig.5

shown in fig.5. The greatest growth rate of resonance instability is depicted by a solid line. The dotted line depicts the gratest growth rate of magnetron instability. As the applied voltage increases, the dimensionless growth rates decrease, and dimensional growth rate behave differently. The resonance instability growth rate decreases and the magnetron one increases. For relatively low voltages the resonance instability is dominating. This instability takes place only in the slow wave structure. For high voltages, the magnetron instability is determining. The frequency of the wave, excited by resonance instability practically does not depend on voltage. The anode efficiency of the oscillator can be determined as

$$\eta = K_i(\gamma - \gamma_*)/(\gamma - 1), \qquad (5)$$

K_i is the ratio of the flow current to the total current in the line, $\gamma = 1 + eU/mc^2$. In particular, for $U = 0.5$ MV we obtain $\eta = 17\%$. Formula (5) must be considered as the top efficiency estimation. In reality the efficiency value will be always lower.

Conclusion

The theoretical analysis has shown MILO to be promising as a superpower microwave oscillator. Under the fixed geometry of the line, the output oscillator parameters, such as microwave power and efficiency, depend only on voltage applied. On the other hand, the generated frequency is practically voltage independent, and this will ensure frequency stability during operation with voltage variations.

References

1. Rudakov L.I., Babykin M.V., Gordeev A.V. et al. *Generation and focusing of high-current relativistic electron beams.* Moscow, Energoatomizdat, 1977.
2. Swegle J., Ott E., Phys.Fluids, 1981,**24**, 1821.
3. Lemke R.W., Clark M.C., J.Appl.Phys., 1987, **62**, 3436.
4. Marder B.M., J.Appl.Phys., 1989, **65**, 1338.

Radiation Field Formation in Open Periodical Structures

V.A. Cherepenin, V.N. Kornienko, V.M. Pikunov
Institute of Radioengineering and Electronics, Moscow, Russia

In our report we should like to present the numeric model for analysing physics processes in limited open periodical structures. We consider this model as the first step in the development of non-stationary theory of high power relativistic oscillators and amplifiers such as multiwave Cerenkov's and diffraction generators with oversized electrodynamic structures [1,2]. For description of these devices, one have to solves the problem of electromagnetic field diffraction on the elements with the dimension about operating wave length. At the same time linear dimension of the electrodynamic structure is approximately equal to its diameter. So the solution of the problem of nonstationary diffraction is one of the basic elements of numerical model.

In case of finite open electrodynamic structures the magnetic field equation is [3]:

$$T\cdot\mathbf{H}(\mathbf{r},t)=\frac{4\pi}{c}\int_V\left(\frac{[\mathbf{J}(\mathbf{r},t'),\mathbf{R}']}{R^3}+[\frac{\partial\mathbf{J}(\mathbf{r}',t')}{\partial t},\mathbf{R}]\frac{1}{cR^2}\right)dV'-$$

$$-\int_S\left(\frac{[[\mathbf{n}_0,\mathbf{H}(\mathbf{r}',t'],\mathbf{R}]}{R^3}+[[\mathbf{n}_0,\frac{\partial\mathbf{H}(\mathbf{r}',t')}{\partial t}],\mathbf{R}]\frac{1}{cR^2}\right)dS'+\mathbf{H}_0(\mathbf{r}',t).$$

Here V - volume loaded by electron beam, S - surface limiting this volume, c - light speed, $\mathbf{R}$ - radius-vector from field source point

to view point, t'- retarded time determined by $t' = t - R/c$ where t - current time, $T = \Omega/4\pi$, Ω - value of space angle of the observation of surface from view point, $\mathbf{n_0}$ - vector of outside surface normal, $\mathbf{H_0}$ - vector of outside magnetic field.

Other components of electromagnetic field are determined by Maxwell equations.

Boundary conditions for E-field correspond to ideal conducting surface. H-field equation was transformed for the case of axial symmetric electrodynamic structures.

The equations of motion of macro particles must be added to field equations for self consistent problem solving. They are:

$$\frac{dP_{zk}(t)}{dt} = q_k(E_z + \frac{1}{c}[\mathbf{v}_k, \mathbf{H_0} + \mathbf{H}]_z),$$

$$P_{zk} = (1 - \frac{v^2}{c^2})^{-1/2} m_k v_{zk},$$

here q_k, m_k, P_{zk}, v_{zk} - charge, mass, impulse, velocity of k-th particle respectively.

Now let us consider some results obtained with our numeric model.

Fig.1 and Fig.2 show the result of the excitation of limited open structure with one and three bulges by the short electron pulse moving in vicinity of the surface.

What is really suprising is that three bulges are enough for excitation of the opposite phase oscillations corresponding to π-mode oscillations in infinite periodical structure.

The result of excitation of limited periodical structure with five bulges are presented on fig.3. The beam current is greater than the starting current. The frequency of generation corresponds to π-mode of oscillations. In noulinear stage of process the radiation spectrum has higher time harmonics (fig.4).

Our numerical model was applied for the analysis of the oscillator excited by the series of short electron bunches . Well studied excitation of FEL and this one are similar but in our case the interaction between beam and field is Cerenkov's one. In this case stable

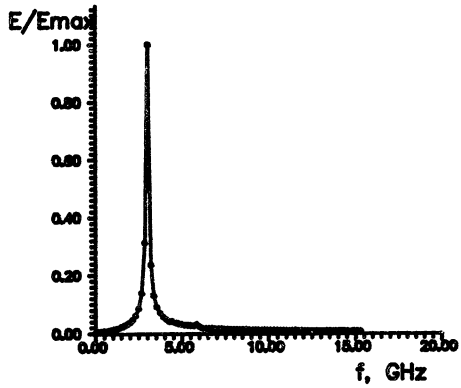

Fig.1. Radiation spectrum. Electrodynamic structure with one bulge excited by short (1ns) electron pulse.

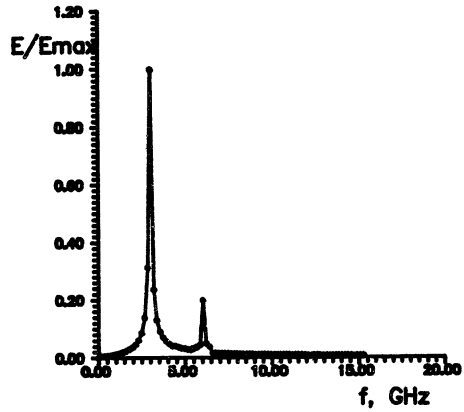

Fig.2. Radiation spectrum. Electrodynamic structure with three bulges excited by short (1ns) electron pulse.

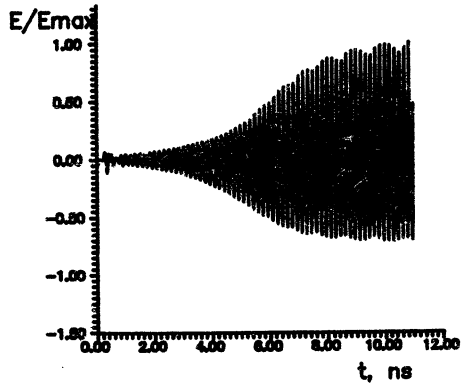

Fig.3. E-field in point of exiting cross section. Beam current is greater than starting one.

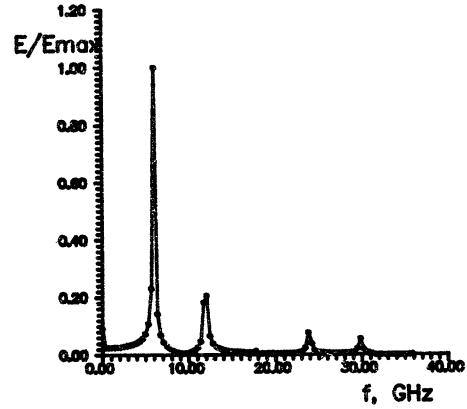

Fig.4. Radiation spectrum in non-linear regime.

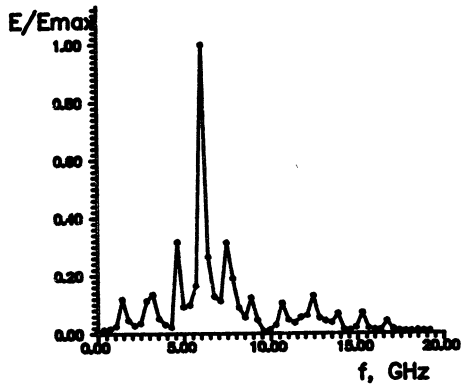

Fig.5. Radiation spectrum in case of 5 bulges structure excited by series of electron bunches.

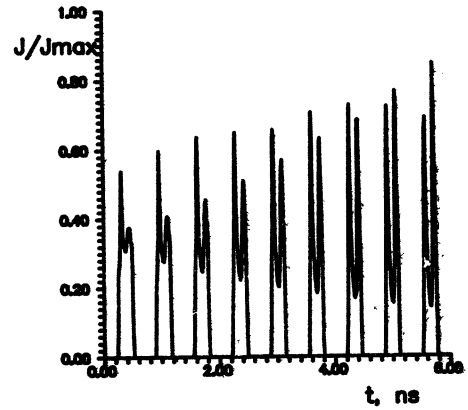

Fig.6. Beam current density in one point.

generation is possible too. The investigation of this process is independent problem. We show only some interesting results. The main frequency of radiation corresponds to the π-mode of oscillations but there are also combination frequencies and their harmonics (fig.5). Since electron bunch is short and has sharp edges two mechanisms of generation interfere. The first one corresponds to the transition radiation, second one - the Cerenkov's radiation. This fact is illustrated by fig.6 which shows the current density in fixed point of beam. The first maximum correspods to the stimulated transition radiation, second one - stimulated Cerenkov's radiation.

These results were obtained by using numerical code FROST. This code can be used even on personal computers.

References

1. Bugaev S.P, Cherepenin V.A., Kanavets V.I. *et al.* IEEE Trans. on Plasma Science, 1990, **18**, No 3, 518.
2. Bugaev S.P, Cherepenin V.A., Kanavets V.I. *et al.* IEEE Trans. on Plasma Science, 1990, **18**, No 3, 525.
3. Bennet C.L., Weeks W.L. IEEE Trans. on Ant. and Prop., 1969, **AP-18**, 627.

INDUSTRIAL GYROTRON DEVELOPMENT IN SALUT

S.D. Bogdanov, V.I. Kurbatov, S.A. Malygin,
V.B. Orlov, E.M.Tai
Research & Production Enterprise "Salut"
N.Novgorod, Russia

Introduction

Progress in gyrotrons development has became possible due to the successes achieved in the electron cyclotron plasma heating experiments. For this application SALUT is producing powerful millimeter wave gyrotrons and superconducting magnets for them during more than 20 years. In 1992 SALUT became one of the founders of GYCOM Ltd. Now SALUT gyrotrons operate not only in Russia (KIAE, GPI and others), but in Germany (IPP), in Japan (NIFS), in Holland (FOM), in China (SWIP) also. Installations in Spain (CIEMAT), in Italy (ENEA) and in Switzerland (EPFL) are in plans.

In Table 1 the last results are presented in comparison with the results shown three years ago at the first workshop "Strong microwave in plasmas".

A lot of new oscillators (28 GHz and 110 GHz) has designed and produced. Output power of the 37.5 GHz gyrotron was increased up to 0.5 MW. Pulse duration of the 140 GHz and 160 GHz tubes was increased up to 1.1 s and 0.7 s respectively.

All gyrotrons include the quasi-optical built-in converter. The microwave power is radiated through the output window in the form of the Gaussian-like beam. The operating efficiency of all tubes is more than 30%. Gyrotrons have no high pressure water cooling system.

Table 1

F(GHz)	1990		1992	
	P(kW)	T(s)	P(kW)	T(s)
28*	—	—	500	0.1
37.5*	250	0.1	500	0.1
54.5*	500	0.1	500	0.1
83	500	1.0	500	1.0
110	—	—	500	0.5
140	500	0.5	500	1.1
160	500	0.1	500	0.7

* Pulse duration of gyrotrons was defined by the customer.

Water pressure is not more than 5 bar for the collector and 3 bar for other systems.

In this report the experimental tests results, the techniques of the pulse duration and output power increasing in the long and short wavelength gyrotrons and the perspectives of the future development will be presented and discussed.

1 Design and experimental study of the long-wavelength gyrotrons

For this class gyrotrons the problem of the mode competition is not so important as for short-wave tubes because it is enough to use relatively low types of modes to ensure the permissible thermal loads.

Problems of the electron gun design correspond to nonadiabatic effects in the cathode region, consequently it is necessary to optimize the gun electrodes configuration.The gun design parameters of the 28 GHz gyrotron are presented in Fig. 1. It is important that the velocity spread minimum takes place near the operating currents 10-20 A.

The calculation of the effective converter of the operating mode to the Gaussian beam is a main problem of long-wave gyrotrons design.

Beam voltage	70 kV
Nominal beam current	20 A
Cathode radius	21.5 mm
Beam radius in cavity	7 mm
Density of emitter current	2.5 A/cm^2
Pitch-factor	1.3
Velocity spread	5%

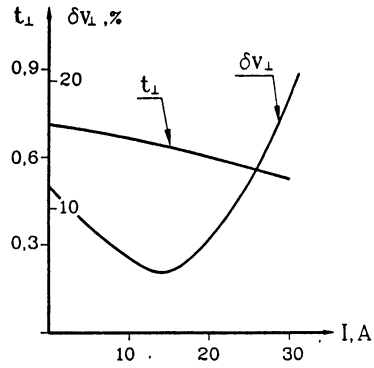

Fig. 1

For example, 37.5 GHz gyrotron has efficiency more than 40% but the Gaussian beam purity is low (about 80%). The transformation efficiency can be increased up to 90% using the mirrors with the most possible size.It is the result of the 28 GHz tube tests. The experimental dependences of the output power and efficiency on the beam current of the 28 GHz gyrotrons are shown in the Fig.2.

In the 53.2 GHz gyrotron the use of the three-electrode electron gun, optimization of the electrodynamic system leads to the following results:

output power	500 kW
beam voltage	80 kV
beam current	15 A
anode voltage	52 kV
efficiency	41.5%
Gaussian beam purity	93%
pulse duration	0.1 s

In principle it is possible to increase the pulse duration for the gyrotrons 28-60 GHz to 0.5-1.0 s by small changes in tubes.

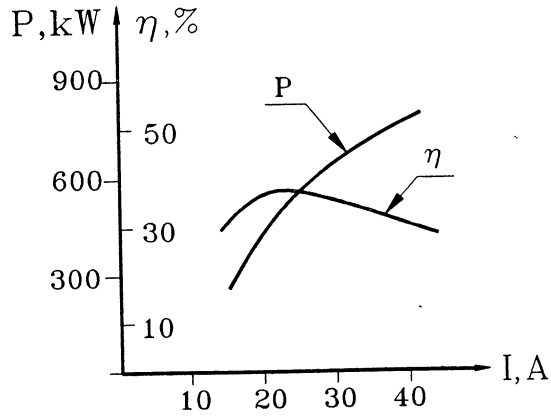

Fig. 2

2 Development of powerful short-wavelength gyrotrons

This year we produced a new 110 GHz gyrotron. Calculations of this oscillator was made in collaboration with the colleagues from the Institute of Applied Physics. The new tape of converter proposed by Dr.Denisov is used in this tube. The experimental tests results are shown in Fig. 3. The Gaussian beam purity at the output window is 98%.

The design and experimental tests of 140 GHz gyrotrons are the most important SALUT achievements. In October 1990 the test of the first long-pulse 140 GHz tube was finished. Output power 0.5 MW at 0.5 s pulse duration was achieved with the efficiency 30%. Pulse duration of the gyrotron was limited by high temperature of the output window.

In the next gyrotron the wave angle 50 in converter, the output window diameter 100 mm and special profile of the last mirror were used to decrease power density at the window. Experiments for application of the magnetic material rings system to decrease the

Operating mode	$TE_{15.4}$
Beam voltage	70 kV
Beam current	22 A
Output power	500 kW
Pulse duration	0.5 s
Gaussian beam purity	98%

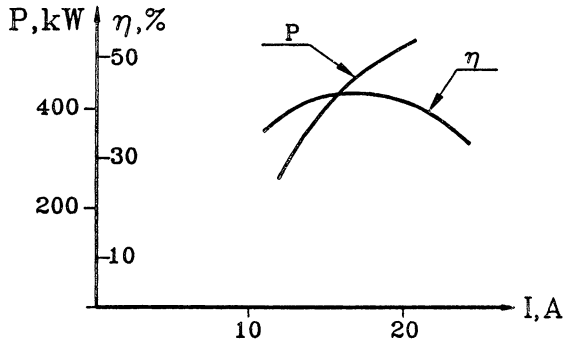

Fig. 3

temperature of the collector and also improvement of the electron gun for beam current in the range 20-30 A were produced. As a result in November 1992 we obtained the following parameters at the experiment:

output power	500 kW
efficiency	35%
Gaussian beam purity	85%
pulse duration	1.1 s

Pulse duration of the tube was limited by the resonator ohmic heating.

It is important that the efficiency is practically independent from current in the 20-40 A range, consequently the 1 MW output power regime of the gyrotron is possible.

After this result the cavity construction was changed to improve the cooling and to decrease the influence of the cavity deformation. In August 1993 pulse duration 2 s with output power 0.5 MW was achieved during the third 140 GHz gyrotron experiments. Results are shown in the Table 2.

Table 2

Operating voltage	70 kW
Operating current	21.5 A
Output power	500 kW
Efficiency	33.2%
Pulse duration	2 s
Gaussian beam purity	85%
Maximum power density in cavity	1.6 kW/cm^2
Maximum power density at collector	1.2 kW/cm^2
Losses in output window	3.28%

3 Future gyrotron development

Recent ECRH experiments have shown that to obtain successful results it is necessary to use the microwave sources with 0.5-1.0 MW power and more than 1 s (better CW) pulse duration. Therefore, to satisfy this requirements now SALUT is executing the additional investigations. In the future the following issues are planned to be developed:

—electron guns operating in the space charge limited current regime for the increase of the electron beam stability and cathode lasting;

—conical cavity for the decrease of the temperature loads at the cavity walls;

—collector with the system of nonadiabatic correction of magnetic field distribution or collector with dynamic spread of the electrons;

—the cryogenic window;

—quasi-uniform electric field distribution at the output window.

Using these methods it will be possible to achieve the following parameters of SALUT millimeter wave gyrotrons in the near future:

—pulse duration 2-3 s at output power 0.5 MW;

—pulse duration 0.5-1.5 s at output power 1 MW.

MAGNETRON-INJECTION GUNS OF GYROTRONS IN SPACE-CHARGE LIMITED CURRENT REGIMES

B. V. Raisky, Sh. E. Tsimring
Institute of Applied Physics RAS, N. Novgorod, Russia
E. A. Solujanova
R & D Company SALUT, N. Novgorod, Russia

Magnetron-injection guns operating in space-charge limited current regime (ρ-regime) are interested from the point of increasing of electron beam stability and improvement of exploitation conditions. Their main advantage over the guns in temperature limited current regime (T-regime) is the absence of current growth in cathode heated by locking electrons as result their reflection from magnetic mirror. That makes easier the application of gyrotrons with high currents and impulse durations up to the continuous generation. Besides, due to the weakening of electric field on cathode the emitter longevity can be increased. The presence of the potential minimum relaxes the influence of the emitter surface roughness on the formed beam parameteries.

The calculation of guns is produced by the combination of synthesis and trajectory analysis methods. It allows to obtain the electrode configuration for forming the electron beam with set current density j_o, radius in resonator r_o, relative transversal energy $t_\perp$ and minimal velocity spread.

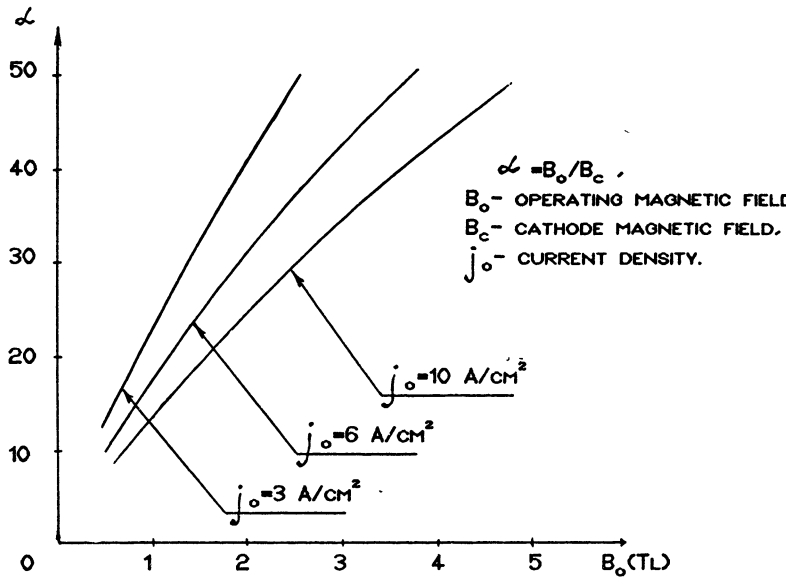

Fig.1. Frequency ranges. $U_o \cong 70$ kV -operating voltage, $\varphi \cong 30^\circ$- angle between emitter surfase and symmetry axis, $\varphi_{ml} \cong 4^\circ$- angle between magnetic flux line and symmetry axis, $r_o = 4 \div 6$ mm -beam radius in resonator, $t_\perp \cong 0.6$ -relative oscillate energy of electrons.

Fig.1 illustrates the ρ-regime guns in different frequency ranges. The dependence of magnetic compression α from operating magnetic field B_o for presented gun parameters is given. It should be noted that in these guns there are more complex connections between parameters of forming system and electron beam than in traditional T-regime guns. As may be shown the electron gyroenergy in operating space is very sensitive to the cathode magnetic field (inversely proportional to B_c^5)and also strongly depends on the emission current density (proportional to j_o^2). It is very important, that

gyroenergy has weak dependence from anode voltage. It allows in principle to change the gyrotron power by the anode voltage without of substantial efficiency change. According to Fig.1 the forming systems in short waves gyrotrons ($\lambda < 3.5$ mm, $B_o > 3$ Tl) need in comparentively high current densities ($j_o > 5$ A/cm^2). The forming systems for $\lambda < 2$ mm ($B_o > 5$ Tl) are not realized practically with ordinary gyrotron cathodes (radius or current density).

At the Fig.2 the examples of possible electrode configurations are given. The cylindricity parameter ν is the main parameter determining the oscillating energy of electrons in the resonator. It is neared to ratio larmore radius to cathode radius on value order. The guns presented at the Fig.2 may be used in gyrotrons suitable both for different versions of plasma heating and for technological purposes.

The gun 3 was investigated experimentally in electron gun analyser in scaling regimes; the high temperature cathode was used. At the Fig.3 the cathode construction is shown. The advantages of graphite as material used for manufacturing of cathode details are the low values of the parasitic thermoelectron emission and the secondary emission coefficient. In inverse case it does no sucsess to get rid of emission from the focusing screens. In this case filament characteristics have view on Fig.4 and ρ-regime is not reached. This fact attracts attention as obviously that mentioned parasitic emission exists and in T-regime guns too. It can cosiderably spoil the beam quality.

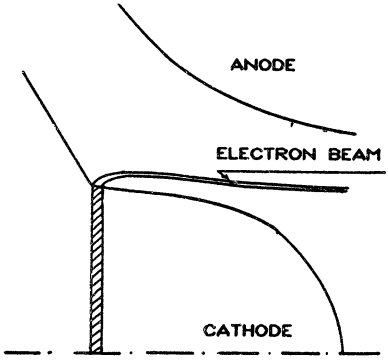

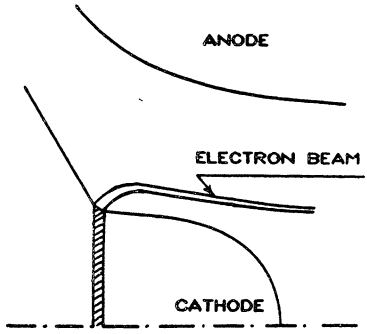

1. B_o=3.5 TL (λ~3MM)
   ν =0.016 - CYLINDRICITY PARAMETER
   j_o=6 A/CM^2 -CURRENT DENSITY
   r_o=5 MM - BEAM RADIUS IN RESONATOR
   r_c=34 MM - CATHODE RADIUS
   α =48 - MAGNETIC COMPRESSION COEFFICIENT

2. B_o=1.5 TL (λ~7MM)
   ν =0.036
   j_o=4 A/CM^2
   r_o=5 MM
   r_c=26 MM
   α =28

U_o=U_a=70 KV - OPERATING AND ANODE VOLTAGES

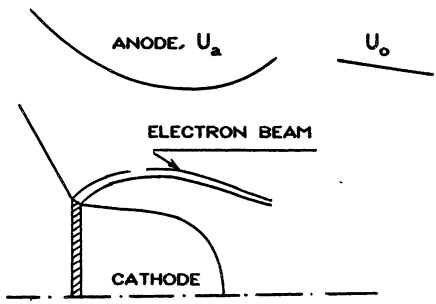

3. B_o=0.57 TL (λ~18MM)
   ν =0.065
   j_o=1.5 A/CM^2
   r_o=4.9 MM
   r_c=20 MM
   α =16.7
   U_o=30 KV
   U_a=23 KV

Fig. 2 $\nu = j_o / \varepsilon_o \eta^2 r_c B_c^3 = j_o \alpha^{2.5} / \varepsilon_o \eta^2 r_o B_o^3$,
ε_o -dielectric permeability of vacuum,
η^o -specific electron charge.

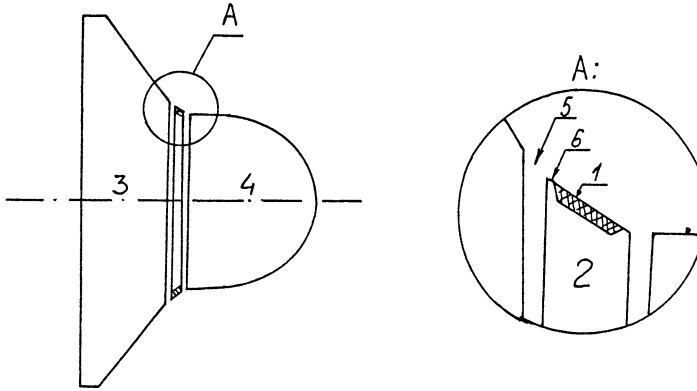

Fig. 3. Cathode construction. 1 -emitter, 2 -graphite or molibden kern, 3,4 - graphite focusing screens, 5 - thermal clearence (~0.4mm), 6 -projection (~0.1mm).

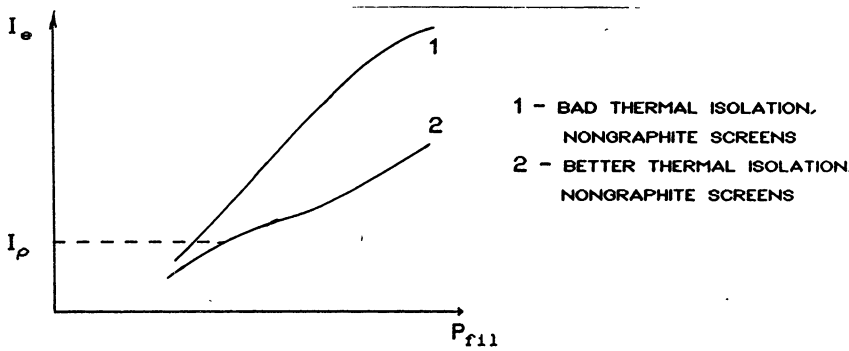

Fig. 4. View of filament characteristics in non-optimum cathode constructions. P_{fil} -filament power, I_e - emission current, I_ρ - current corresponding ρ-regime (calculated).

The emission characteristics shown at Fig.5 were obtained by graphite electrodes using. As seen the clear ρ-regime was achieved. The fact of principal absence of current growth effect was experimentally verified. Moreover, when the strong effect of electron reflection from the magnetic mirror had been realized, it was discovered that trapped electrons were able to reduce essentially the emission in area of full space charge. As may be supposed, it opens for these guns the unigue possibilities of self-adjustment to optimum regime (Fig.6).

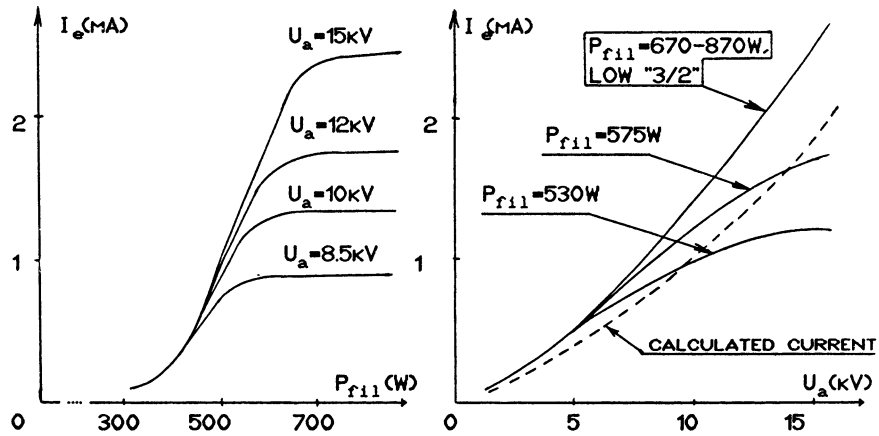

Fig.5. Filament and Volt-Ampere characteristics of gun №3 (scaling regimes).

On finishing the direct current interception regime the anode current decreases to zero and is absent in trap regime. The calculation of electron velocity spread in beam by the anode current cut-off curve gives value $\delta V_{\perp} \sim$ 30%. By the curve of $I_e(B_c)$

dependence the regime with maximum electron energy under little electron reflection may be selected. Also the operating regime with reflected electrons is possible. The power of the device will be less by that, but efficiency will not decrease essentially.

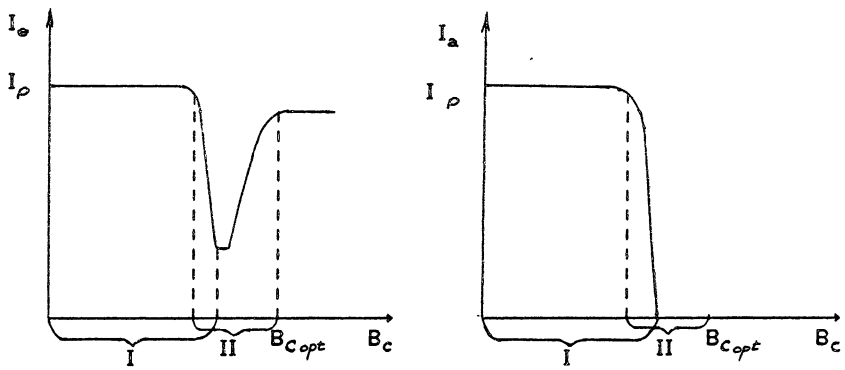

Fig.6. View of emission current dependence from cathode magnetic field and corresponding anode current cut-off curve. I - regime of direct current interception on anode, II - magnetic trap regime, B_{copt} - optimum magnetic field on the cathode.

Thus in present time there are preconditions for creation of gyrotrons with guns working in ρ-regime.

CONTENTS OF VOLUME 2

Nonlinear processes in plasmas (theory and microwave experiment)

Development of high-power microwave sources

«Чувашия». З. К-185. Т. 500 экз.